INFORMATION TO USERS

This material was produced from a microfilm copy of the original document. While the most advanced technological means to photograph and reproduce this document have been used, the quality is heavily dependent upon the quality of the original submitted.

The following explanation of techniques is provided to help you understand markings or patterns which may appear on this reproduction.

1. The sign or "target" for pages apparently lacking from the document photographed is "Missing Page(s)". If it was possible to obtain the missing page(s) or section, they are spliced into the film along with adjacent pages. This may have necessitated cutting thru an image and duplicating adjacent pages to insure you complete continuity.

2. When an image on the film is obliterated with a large round black mark, it is an indication that the photographer suspected that the copy may have moved during exposure and thus cause a blurred image. You will find a good image of the page in the adjacent frame.

3. When a map, drawing or chart, etc., was part of the material being photographed the photographer followed a definite method in "sectioning" the material. It is customary to begin photoing at the upper left hand corner of a large sheet and to continue photoing from left to right in equal sections with a small overlap. If necessary, sectioning is continued again — beginning below the first row and continuing on until complete.

4. The majority of users indicate that the textual content is of greatest value, however, a somewhat higher quality reproduction could be made from "photographs" if essential to the understanding of the dissertation. Silver prints of "photographs" may be ordered at additional charge by writing the Order Department, giving the catalog number, title, author and specific pages you wish reproduced.

5. PLEASE NOTE: Some pages may have indistinct print. Filmed as received.

Xerox University Microfilms
300 North Zeeb Road
Ann Arbor, Michigan 48106

POSITIVE- AND NEGATIVE-ION CHEMISTRY OF THE D-REGION INCORPORATING ENHANCED WATER VAPOR AND SUBMICRON DUST

A

THESIS

Presented to the Faculty of the

University of Alaska in partial fulfillment

of the Requirements

for the Degree of

DOCTOR OF PHILOSOPHY

by

Henry Puryear Cole, Jr., B.A., M.S.

May 1977

POSITIVE- AND NEGATIVE-ION CHEMISTRY OF THE D-REGION

INCORPORATING ENHANCED WATER VAPOR AND SUBMICRON DUST

RECOMMENDED:

Kenneth W. Ratcliffe

Sue Ann Bowhill

Peter Banks

Bernhard Haurwitz

P. Parthasarathy
Chairman, Advisory Committee

T. Neil Davis
Division Head

APPROVED:

Vernon Alexander
Dean of the College of Environmental Sciences

April 29, 1977
Date

K. B. McAfee
Vice Chancellor for Research and Advanced Study

May 2, 1977
Date

ABSTRACT

The major portion of this thesis presents a steady-state ion-kinetic model of D-region chemistry which is devised to explain various experimentally observed chemical features from an altitude of 60 to 90 km in the upper atmosphere. This model uses a set of 23 positive- and 66 negative-ion reactions, enhanced values of water vapor, a flux of submicron dust, neutral profiles suitable for the high-latitude mesosphere in winter and summer and primary production of NO^+, O_2^+, and N_2^+ based upon ionizing radiations of Lyα, Lyβ, CIII, EUV, X and galactic cosmic rays. The computed positive-ion profiles for summer conditions match most principal characteristics of positive-ion profiles derived from rocket-borne sampling. A significant result is the achievement of low values of electron density ($\sim$ 300 cm^{-3}) concurrently with a high ratio of water cluster-ions, $H_3O^+(H_2O)_n$, to nitric oxide cluster-ions, $NO^+(H_2O)_n$, at 80 km. In the case of negative ions, a successful computational scheme is developed to manage the 31 non-linear continuity equations which is shown to be convergent from 80 through 65 km, and possibly lower.

Dust and water vapor play an important role in D-region chemisty. The inclusion of dust in the ion-kinetic calculations as an attachment sink for electrons or positive ions considerably increases the effective recombination coefficient when dust concentrations are high (10-100 cm^{-3}) provided the electron density is low (< 200 cm^{-3}). Furthermore, the coating of the dust particles with ice increases the recombination coefficient by a factor of 100 at the 70-80 km level.

A model of water vapor diffusion in the mesosphere leads to enhanced values when vertical drift of the neutral atmosphere is included. When dust of radius 0.015μ - 0.035μ is allowed to descend through the mesosphere temperature minimum, the growth of visible (> 1300Å) ice particles in a layer ≈ 5 km thick occurs during conditions of polar summer.

ACKNOWLEDGMENTS

My initial debt of gratitude is to Dr. K. B. Mather, Director of the Geophysical Institute and my academic advisor at the time I commenced graduate study. Throughout my tenure he has been most generous in his encouragement of my work and financial support. During a portion of this time I also received support through the State of Alaska Student Loan Program.

The thesis incorporates the labor of several persons. Foremost among them is Professor R. Parthasarathy, chairman of my advisory committee since January 1973. He introduced me to the major topics in the thesis and throughout has provided close guidance and supervision. His professional expertise has been crucial to the work on positive ion-kinetic processes in Chapter 3 and even more so for the detailed formulation of water vapor diffusion in Chapter 4. The most valuable, enduring and enjoyable aspects of my graduate education have derived from my several years of association with him and the exceptional degree of personal and intellectual taste which he maintains.

A considerable portion of the work for the ion-kinetic reactions and water vapor diffusion has required computer programming. Mr. Steve Geller provided much aid in the former problem in adapting the subroutine AL316 to my task. Mr. Tom Wetmore was instrumental in the initial programming of DIFRAD 13 after the original mathematics had been linearized.

It has been my great good fortune in having a most knowledgeable, helpful and fair committee: Dr. Sue Ann Bowling, Professor Bernhard Haurwitz, Dr. Kenelm Philip and Dr. Gunter Weller. Their reading and

pertinent criticism of my thesis has been of the greatest help in transforming it into a coherent and clear statement of work accomplished.

The relentless task of initial typing and retyping of the manuscript was executed with great accuracy by Miss Vicki Wade. The bulk of the final typing was undertaken with great humor and consistency by Mrs. Sandy Moseley to whom I am most grateful. Others who provided aid at crucial moments are Judy Holland, Pat Moore, Fran Pedersen, Marge Howard and Karen Brown.

Judy Mimken contributed to the final product through her accurate proof reading. Miss Hiroko Horiuchi produced drawings with amazing speed and clarity and Frank Danels was tremendously helpful in preparing the necessary photographs. Jim Burton also provided substantial photographic services. To all of the above I am deeply appreciative.

TABLE OF CONTENTS

TABLES

CHAPTER I

GENERAL INTRODUCTION AND OVERVIEW OF THE THESIS

The D-region is a term assigned, rather arbitrarily, to the altitude range of 60 through 90 km of the upper atmosphere where the first appreciable concentration of electrons is encountered. Within this height range lie the pronounced temperature minimum of the mesopause (82 km) and the top of the well-mixed atmosphere. The original deduction of ionized layers aloft was based upon Gugliomo Marconi's long-range radio propagation experiments in 1901. Kennelly and Heaviside interpreted them to imply the existence of ionized reflecting layers although a similar idea had been advanced as early as 1878 by Balfour Stewart who attributed the temporal variations in the earth's magnetic field to electric currents in the upper atmosphere.

In the 1930's and 40's the D-region was explored primarily with the techniques of radio physics, and investigations involved the determinations of parameters such as critical frequencies, virtual heights, radio blackouts (Appleton, Naismith and Builder, 1933) and solar flare radio fadeouts (Dellinger, 1937, Davies, 1969). Evidence from the spectrum of the night sky prompted Kaplan (1939) to postulate the existence of significant quantities of nitric oxide near 80 km. Marcel Nicolet (1945) suggested that the ionization of nitric oxide by the penetrating Lyman α radiation could produce the sharp ledge in electron concentration below the E layer. This possibility provided the basis

for a formal theory of D-region formation proposed by Nicolet and Aiken in 1960. The critical factors were specified to be: a) penetration of X-rays, ultraviolet, Lyman α and galactic cosmic rays to 80 km and below, b) ionization of and absorption by N_2, O_2 and NO, and, in particular, the existence of a "window" in the otherwise continuous absorption by O_2 at the wavelength of Lyman α (1215.7Å), and c) the presence of sufficient quantities of the minor constituent, nitric oxide, to be ionized by Lyα radiation and provide the main source of electrons. In the decade following Nicolet and Aiken's (1960) proposal, investigators measured the strength of solar and galactic cosmic radiation and determined electron density profiles and effective recombination coefficients (Gregory, 1961; Webber, 1962; Piggott and Thrane, 1966; Mitra, 1968). No direct measurements of any minor constituents such as nitric oxide or ionized species were yet feasible at these altitudes. But in spite of these omissions it was presumed that the main characteristics of the D-region could be understood within the Nicolet and Aiken framework.

This happy assumption lasted only until 1965 when R. Narcisi and A. Bailey, using daytime measurements in the mesosphere made by a rocket-borne quadrupole-mass-filter, reported ion-current mass peaks which were identified as H_3O^+, NO^+ and $H_3O^+ \cdot H_2O$. More specifically they found:

1) From 64 to 82.5 km, there were three dominant ion peaks consisting of H_3O^+ (19^+), NO^+ (30^+) and $H_3O^+ \cdot H_2O$ (37^+), with the latter numbering about 500 to 1000 cm^{-3} and possessing a very sharp ceiling at 82.5 km.

2) Above the ceiling at 82.5 km, NO^+ (30^+) and O_2^+ (32^+) became predominant and increased in abundance with height.

These results were surprising for various reasons: (1) The presence of water cluster ions implied that water vapor had a critical role in a complex ion-chemistry which, nevertheless, had to originate with the primary production of N_2^+, O_2^+ and NO^+. (2) Nicolet and Aiken had predicted the existence of only the positive ions NO^+, O_2^+ and N_2^+ which, in fact, were found to be only 16% of the total number observed. (3) The observed electron density profile showed a sharp and unexplained ledge which required, somehow, a major change in the effective recombination coefficient within 2 km. Some investigators believed that this could be explained by the change from a large cluster-ion population (with recombination coefficients of $\lesssim 10^{-5}$ cm^3 sec^{-1}) below the ledge to a population of NO^+ and O_2^+ above (with recombination coefficients of $\lesssim 3 \times 10^{-7}$ cm^3 sec^{-1}) (Reid, 1971). Others proposed that aerosols or dust in layers could act as attachment sinks to remove electrons below 80 km which would result in an increase in the effective recombination coefficient.

Other unusual phenomena associated with the upper mesosphere have been the existence of high-level cloud layers, so-called noctilucent clouds, which were observed first in 1885 in Europe (see Fogle and Haurwitz (1966) for a review). Early morphological studies seemed to indicate a summer occurrence at high latitudes with heights measured to be around 82 km. More recent in situ sampling in these layers with rockets (Hemenway et al., 1964, and others) has been

inconclusive in establishing the composition of the cloud particles, but a prevalent belief is that they are composed of ice-coated dust although the origin of the dust is unclear. At this time, however, no satisfactory formulation has been devised to explain the existence of the clouds or the formation of these (supposed) ice crystals.

Since all the phenomena discussed above relate to the upper mesosphere and are the result of chemical interactions which include water vapor and possibly also dust or aerosols, it may be possible to investigate some of these relationships through a suitable ion-kinetic reaction scheme which also includes input from independently formulated water vapor profiles and a flux of descending dust particles. Deficiencies in current ion-kinetic reaction schemes which have not included dust or extreme concentrations of water vapor suggest a reconsideration of the role of these factors. In addition, a new formulation would provide an opportunity to attempt to model the growth of ice crystals upon mesospheric dust particles under conditions characteristic of a high latitude summer.

In particular, the tasks to be undertaken are the following:

1) Reassess the state of D-region observational studies and ion-kinetic modeling schemes, particularly those which produce cluster ions.

2) Derive an H_2O profile which incorporates all transport and loss processes of importance and then inserted it into a 'complete' chemical D-region model for the computation of positive and negative ions.

3) Examine whether the dust particles have a direct role of importance in the ion-kinetic calculations.

4) As a by-product of (2), re-examine quantitatively the formation of noctilucent clouds in the temperature regime of high latitude summer by utilizing the enhanced water vapor profile and a plausible flux of descending extra-terrestrial dust.

Chapter II provides a review of limitations of in situ sampling and a synopsis of previous observational studies. In Chapter III the ion-kinetic calculations leading to positive-ion profiles are presented using water vapor profiles obtained from Chapter IV. Previous problems in devising successful chemical reaction schemes, experimental observations of dust aloft and dust attachment theory are also reviewed in Chapter III. In Chapter IV a rather complete derivation and calculation of the water vapor profile and the growth of ice crystals on submicron dust is presented. Key parameters controlling crystal growth will be fully discussed. Chapter V presents the non-linear computational scheme used to solve for negative ions, and results are presented for levels of 65 through 80 km. Chapter VI is a summary of results, overall conclusions and directions for future research.

CHAPTER II

CLUSTER IONS IN THE D-REGION: MEASUREMENT, OBSERVATION AND THEORY

INTRODUCTION

In situ sampling of ions or the measurement of electron density from 60 through 100 km in the upper atmosphere is difficult owing to the fact that this is a region of rapid transition in certain atmospheric parameters (e.g., Debye Length) which affect measurement techniques. These and other problems in sampling will be discussed in the first section of this chapter. Current results of positive-ion sampling in the D-region will then be presented and organized with respect to season, location, time and solar zenith angle. The commonly observed features of positive-ion profiles will be identified since they must be reproduced by any successful ion-kinetic reaction scheme. The chapter concludes with a review of the existing ion-kinetic reaction sequences which have been proposed for the D-region.

LIST OF SYMBOLS

e	charge on an electron
m	mass (gm)
τ_c	chemical reaction time (sec)
τ_R	rocket length/velocity of rocket (sec)
λ_D	Debye Length (cm)
T	absolute temperature (°K)

N_e	number density of electrons (cm^{-3})
N^+	number density of positive ions (cm^{-3})
$[N_i]$	square brackets indicate number density of constituent N_i (cm^{-3})
j_i or J_m	ion current (amperes)
Z_i	charge on a sampled particle i
ρ_{STD}	neutral gas density at STP (cm^{-3})
ρ_∞	free stream particle density (cm^{-3})
$n_{i\infty}$	number density of charged particles in the laminar region (cm^{-3})
K_i^o	reduced mobility of positive ions (cm^2 $volt^{-1}$ sec^{-1})
D_{12}	molecular diffusion coefficient (cm^2 sec^{-1})
k	Boltzmann's constant (=1.38 x 10^{-16} erg/deg)
χ	solar zenith angle (degrees)
$\bar{c}$	mean molecular velocity (cm sec^{-1})
α	angle of attack of rocket (degrees)
W_R	speed of the rocket (cm sec^{-1} or Mach number)
V_c	potential of rocket collector plate (Volts)
ν	collision frequency of particles (sec^{-1})
MFP	mean free path (cm)
$H_3O^+(H_2O)_n$	general designation for the hydrated hydronium ion or
$NO^+(H_2O)_n$	hydrated nitric oxide ion which will be referred to as water cluster-ions or nitric oxide cluster-ions, respectively.

1. Problems of Measurement in the D-Region

A. Mass Filter Design

The instruments used for measurements of positive ions in the mesosphere are strictly designated as mass-filters ("massenfilter" after Paul et al., 1958) as opposed to mass spectrometers, names which have been used interchangeably in the literature. A mass spectrometer produces a spatial dispersion of a stream of charged particles according to their e/m ratio. A mass-filter, on the other hand, has a single target point (collector) bombarded by particles of a narrow mass range which is fixed beforehand by the RF and DC magnitudes of the electric field.

The mass filters used in these experiments are almost identical and are reviewed to some extent in each paper, but more detailed (and roughly similar) descriptions are found in: Narcisi (1966), Narcisi (1970a), Narcisi and Roth (1970), and Narcisi and Bailey (1965). This design of a quadrupole mass filter originated with Paul et al. (1958) and was adopted because of its 1) low weight (it has no magnet) and compact size, 2) ability to operate at high ambient pressures, and 3) linear mass scale due to a linear voltage sweep. The operation and design of the instrument are as follows (Narcisi, 1970a).

Positive ions outside the rocket are accelerated to the top surface of the quadrupole vacuum envelope collection plate by a bias of -10 v with respect to the rocket skin. Through the opening of diameter .03", the ions pass into the top of the filter (see Fig. II-1) and are accelerated towards the quadrupole rod system by a bias voltage of -50 v with respect to the quadrupole vacuum envelope system. Superimposed RF and DC voltages provide the magnetic and electric fields which are

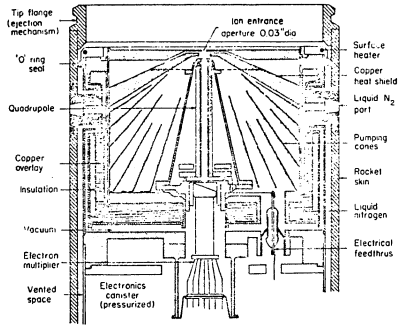

Figure II-1.

Diagram of construction of the popular quadrupole mass filter, originally designed by Paul et al. (1958) and adapted by Narcisi (1970a) and others.

adjusted (scanned) so that only those ions with a specific charge-to-mass ratio will have the exact bounded oscillatory trajectories suitable to traverse the length of the rods and strike the electron multiplier. All other ions of unsuitable e/m ratio will oscillate in unstable trajectories and impact upon the rods or outer envelope of the vacuum system. The ion current for a specific e/m ratio is amplified by a factor of 10^4 by the multiplier and sensed by a logarithmic electrometer with a current range of 10^{-12} to 3 x 10^{-7} amp which corresponds to a range in ion densities of 1 to 10^5 cm^{-3}. Scanning is achieved by varying the RF and DC voltages as a function of time while holding their ratio constant. 2 sec are required to scan over the full mass range (12 to 46 amu in this case), and the electrometer is calibrated each 10 sec. To identify the mass number the RF sweep voltage is monitored on another continuous channel previously calibrated with known gases and an ion source in the laboratory.

Critical design and operating parameters of this instrument are (Narcisi, 1970a):

Rod radius	0.1905 cm
Field radius	0.164 cm
Length of field	7.62 cm
RF frequency	4 to 6 MHz (held at a fixed frequency in this range)
Mass range	1 to greater than 100 amu
Resolution m/Δm	Set at 16 (Δm taken at 10% peak amplitude)
Multiplier gain	10^4 (adjustable)
Sensitivity range	1 to 10^5 ions cm^{-3} (adjustable.)

During sampling the ambient pressure drops from .06 to 10^{-3} torr (1 torr = 1 mm Hg) in about 2 min as a Mach 2 rocket travels from 60 km to 90 km. Because the spectrometer collection plate is at the "stagnation point" behind the bow shock, the pressure at the orifice may be higher by a factor of three at steep angles of attack. These high ambient pressures require a high capacity pump to maintain the mass filter within its operating pressure range of $< 5 \times 10^{-5}$ torr. To prevent collisional effects and multipler voltage breakdown this low pressure is satisfactorily maintained by a nitrogen-cooled zeolite-absorption pump (Narcisi's shots) or a titanium sublimation pump (e.g., Goldberg and Blumle, 1970).

The following estimates of error pertain to measurements with this system:

1. Altitude: $\pm$ .01 km with radar tracking;
2. Mass number: $\pm$ 3% of magnitude of mass number;
3. Ion density: $\pm$ 200% based upon the measurement of peak current.

B. Sampling Theory

Fundamental difficulties with accurate ion measurements in the altitude range of 50 to 100 km take three forms: (a) those which derive from the dimension of the sampling instrument relative to the Debye length and the mean free path within the ambient plasma, (b) those which relate to the effects of shock waves from the supersonic rocket upon the cluster ions to be sampled and c) contamination of the spectrometer. Narcisi (1966, 1970a), Goldberg and Aiken (1971), Goldberg and Blumle (1970) and Johannessen and Krankowsky (1972) all discuss the credibility

of measurement of water cluster ions, particularly with respect to possible contamination by the rocket exhaust. Only Sonin (1967) and Sayers (1970), however, try to formulate, mathematically, the criteria for predictable measurement of charged ionic species based upon the physical parameters of the region. For their purpose, the D-region is divided into three sampling layers: 45-70, 70-90 and 90 km and above.

a. 45 to 70 km:

Sonin's treatment originates by considering the diffusion of a charged species through a weak plasma stressed by an electrostatic field (provided by the mass-filter collector plate). With a supersonic rocket passing from 45 to 70 km, the following assumptions apply to his formulation.

a) Compressible Boundary flow or $R_e >> 1$: This means that the flow field at the blunt rocket nose separates into an outer inviscid flow region and an inner turbulent boundary layer of higher temperature and pressure (called the stagnation point if directly before the rocket) across which the sampled particles must diffuse.

b) Chemically Frozen Flow: If the chemical reaction time within the plasma is τ_c and rocket length/velocity is τ_R, then $\tau_c > \tau_R$ or the chemical reactions will need more time to react than the transit time from bow shock to collector orifice. For example,

If the rocket velocity is:	then τ_R (ℓ = 5 x 10^2 cm) is:
Mach 1 = 2.94 x 10^4 cm sec^{-1}	1.70 x 10^{-2} sec
Mach 2 = 5.88 x 10^4 cm sec^{-1}	.85 x 10^{-2} sec
Mach 3 = 8.83 x 10^4 cm sec^{-1}	.57 x 10^{-2} sec

For the reaction: $e + 2O_2 \rightarrow O_2^- + O_2$, $\tau_c = 2 \times 10^{-3}$s at 50 km and .3s

at 70 km. Thus this reaction is not frozen at lower altitudes and the measurement of O_2^- would be too high.

c) Ionic number density is low enough so that the space charge field is exceeded by the applied field of the spectrometer plate.

d) The Debye length, λ_D (= 6.9 $(T/N_e)^{1/2}$) exceeds the thickness of the turbulent layer produced in the bow shock. This is achieved by 50 km where $\lambda_D \cong 30$ cm.

e) The ambient atmosphere is a weak plasma in thermal equilibrium with the neutral gas.

These conditions are satisfied from 45-70 km where the mean free path of the ions is small (=0.66 cm at 80 km) and the electrostatic potential (-10v on most flights) of the collector plate extends sufficiently far out to attract charged particles and over-ride flow effects at the rocket surface. (This is the strong field case of Sonin, 1967, which is identical with the Hoult (1965) strong field case used with a sub-sonic balloon-borne blunt probe.) Species current entering the mass-filter orifice will depend only upon the mobility of the ion and be independent of flow effects or angle of attack. An upper limit of -10v on the magnitude of the collector plate bias voltage is necessary due to the possibility of secondary ionization. The relation between the ion current, j_i, captured by the collection plate and the ambient charged particle density is given by Sonin (1967) equation (29):

$$j_i = -e\, Z_i^2\, n_{i\infty} \left(\frac{\rho_{STD}}{\rho_\infty}\right) \chi_i^o (T_o) V_c \qquad (2\text{-}1)$$

Ion mobility is the only term in this expression with a mass dependence, but this dependence is weak. Indeed, according to experiments

by Chanin and Biondi (1957) mobility drops by a factor of 2 from 10 to 40 amu and decreases only slightly at higher mass numbers. Therefore, the lighter ions hitting the collector plate and passing to the interior of the mass filter will be somewhat more numerous because of their higher mobility. E/P, the ratio which expresses the relative magnitude of the field energy of the ion to its thermal energy and the tendency of the applied electric field to move the ion, increases with altitude due to the decrease in pressure and is a critical parameter in the formulation at 70 km. (See Table I.)

On the other hand, with increasing altitude the Debye length shrinks and the electric field of the collector is confined close to the rocket surface. This means that the mass dependence of the collected current is diminished above 70 km and the ion current, j_i, which is measured becomes identical to the value, $eZ_i n_i \alpha V_c$, which is "swept out" geometrically by the rocket collector plate. Hoult (1965) has made experimental verification of this latter expression in experiments with ion capture by blunt probes at the 70-80 km altitude level.

b. 90 km and Above:

At high altitudes Debye lengths are less than 1 cm, and the collector plate electric field is confined close to the rocket surface. The Maxwellian distribution of velocities controls the ion current and the rocket effectively scoops up the sample. The critical parameter, S, which expresses speed of the rocket relative to mean molecular velocity,

TABLE I

CRITICAL PARAMETERS AFFECTING MEASUREMENT IN THE MESOSPHERE

ALTITUDE (km)	NUMBER DENSITY (cm^{-3})	TEMP (°K)	PRESSURE (Torr)	N_e (cm^{-3})	ν (s^{-1})	$\bar{c}$ (cms^{-1}) ($x10^5$)	MFP (cm)	λ_D (cm)
100	$9.2x10^{12}$	190	$.26x10^{-3}$	10^5	10^5	3.31	10	.3
90	$7.2x10^{13}$	160	$.204x10^{-2}$	10^4	$3x10^5$	3.02	2	1.
80	$5.3x10^{14}$	170	.0149	$3x10^2$	$6x10^5$	3.12	.66	3.2
70	$2.3x10^{15}$	215	.067	10^2	$4x10^6$	3.5	.032	10
60	$7.9x10^{15}$	262	.224	50	$2x10^7$	3.86	.0021	15
50	$2.6x10^{16}$	277	.76	10	10^8	3.99	$6.1x10^{-3}$	30

$\bar{c}$ (Narcisi, 1970a), is used in the following fashion.

If $$S = \frac{W_R \cos\alpha}{\bar{c}}$$ which expresses the ratio of vehicle speed to $\bar{c}$. (2-2)

$$\bar{c} = \left(\frac{8kT}{\pi m}\right)^{1/2} = 3.1 \times 10^4 \text{ cm sec}^{-1} \quad (2\text{-}3)$$

and $$F(s) = \exp(-S^2) + S\sqrt{\pi}\,[1 + \text{erf}(s)] \quad (2\text{-}4)$$

where N(m) - ionic number density with mass m.

Then $$J(m) = \frac{-N(m)\, e\, \bar{c}\, F(s)}{2\sqrt{\pi}}. \quad (2\text{-}5)$$

For $S \gg 1$, for a high Mach number rocket, $J(m) = N(m)eW_R$ which means no mass dependence exists for current entering the mass-filter and the current density of two species will be proportional to their ambient number densities. When $S \ll 1$ which is the case in the upper mesosphere if the rocket slows to velocities below Mach 1,

$$\frac{J(m_1)}{J(m_2)} = \frac{N(m_1)}{N(m_2)} \cdot \left(\frac{m_2}{m_1}\right)^{1/2}, \quad (2\text{-}6)$$

so that at these altitudes and rocket velocities the current density is proportional to the number density for a particular mass. In this case the mass dependence enters weakly through the mean velocity of the molecule, $(8\ kT/\pi m)^{1/2}$, rather than through the mobility, but only if the rocket speed $\lesssim \bar{c}$. Variations of temperature will have an effect counter to that of mass, particularly in the region of considerable temperature increase from the mesopause and up. If, however, temperature is neglected, the skewing of the populations of high and low mass hitting the

collector plate will be in the same sense as that produced by mobility dependence at levels below 70 km (ion currents for lighter masses will be greater). By the use of inflight calibrations, it has been possible to derive absolute ion densities within a factor of two (Narcisi, 1970a) although a lingering problem has been multiplier gain drifts.

c. 70 to 90 km

Since this altitude range is a transition region between molecular boundary flow above and continuum flow below, no precise analytic theory exists to deal with it, and relative temporal variations at a given altitude are the most reliable measurements to attempt (Sonin, 1967 and Narcisi, 1970). What is normally done is to extend the previous analysis downward from 90 km and rely upon various types of in situ calibrations to fix the absolute values for the number densities. This is a region of significant changes in chemistry and composition, however, which makes a successful measurement more important scientifically.

Because of their importance as in-flight calibration devices it is pertinent to briefly describe Langmuir probes and Gerdien condensers which both measure total positive ion current and the Faraday rotation method of determining electron density.

C. Langmuir Probe

A Langmuir probe is a rhodium plated steel wire metal cylinder about 10 cm by .05 cm in diameter (Bowling et al., 1967) mounted perpendicular to the side of a rocket and biased a few volts negative to repel electrons and collect a positive ion current. The condition that the ion current is absolutely proportional to the ion density is best

fulfilled at heights where the mean free path of the ions exceeds the probe dimensions (such as, above 100 km, where the mean free path, λ, is greater than 10 cm). From 60 to 80 km where the mean free path is comparable with probe dimensions it is possible only to measure relative temporal variations of the positive ion current such as those occurring during solar eclipse passage. At these heights space charge effects are obviated by a large Debye length. Bowling et al. (1967) is careful to use the probe only to detect temporal variations at altitudes below 90 km because of complexities in flow and the opportunity to neglect the motion of the supersonic rocket. Photoelectric effects due to sunlight are relieved by the spinning of the rocket which places the probe in shadow.

Many investigators have used the probe as a calibration device to normalize the total positive ion density from 60 to 90 km (Pedersen et al., 1970; Mechtly, Sechrist and Smith, 1972; Mechtly and Smith, 1968). For reasons mentioned earlier it also serves best as a calibration tool for total positive ion current above 90 km.

D. Gerdien Condenser

Another possibility for measurement and calibration is provided by the Gerdien condenser, an open ended cylinder mounted on the rocket nose facing in the forward direction which contains a small cylindrical concentric probe recessed inside and biased a few volts negative (Bourdeau et al., 1966). At D-region altitudes the collector current is a function of mobility, and at a critical threshold potential all ions entering the

instrument are collected, resulting in a saturation current value dependent only upon the ambient ion density.

$$I_c = N_+ e W_R A \cos\theta \qquad (2\text{-}7)$$

where θ = angle of attack of the rocket.

The analysis of this technique provided by Bourdeau et al. (1966) neglects consideration of the problems due to shock wave effects at the condenser orifice or problems related to the overlap of regimes where the short Debye length limits or high mobility control the ion current. Furthermore, evidence cited by Bauer et al. (1964) with a radio propagation experiment invalidates the Bourdeau et al. (1966) expression for ion current and casts doubt upon the use of the Gerdien condenser as a calibration tool for D-region measurements.

E. Faraday Rotation Method

Aside from the use of probes which suffer from the same aerodynamic complexities of sampling in a plasma as those of the forward collection plate of a rocket-mounted mass filter, the Faraday rotation method of determining electron density was frequently applied as useful ancilliary calibration. The basis of this method is well reviewed in many volumes: Whitten and Popoff (1971), Banks and Kockarts (1974) and Davies (1973).

If a plane polarized electromagnetic wave propagates through an ionized medium which is in a magnetic field, the plane of polarization of the electromagnetic wave will be rotated through an angle which depends upon the strength of the applied field and the dielectric constant of the medium. In representing linearly polarized electromagnetic radia-

tion by two circularly polarized components rotating in opposite directions, the influence of the applied field renders the medium anisotropic such that the phase velocity of the one (extraordinary) wave will be retarded with respect to that of the other (ordinary) wave. After passing a distance through the medium the resultant plane of polarization of the $\bar{E}$ vector will have been rotated through an angle ϕ, the magnitude of which depends upon the magnetic field aloft (the value of which is known or at least assumed) and the local electron density. This Faraday rotation is the basis of a method of determining the columnar and consequently volume electron density in the ionosphere. With a suitable ground station sending up a signal to the rocket this is the most accurate method for the measurement of electron density.

With the preceeding discussion serving as descriptive background, the existing mass-filter observations of ions in the D-Region will now be discussed.

2. Positive-Ion Mass Filter Observations

Currently there exist 20 profiles of positive ions in the D region based upon mass-filter measurements made from rockets. The profiles have been made under geophysically quiet and disturbed conditions, such as auroral, polar cap absorption and sporadic E events, and cover a wide range of latitudes and seasons as well as a variety of local times and solar zenith angles. Appendix I lists the investigator, reference, resume of apparatus, peripheral experiments and principal results of these shots. Table II presents a synopsis of this appendix: times, dates, locations and results of these same shots. In all cases, the

TABLE II

COMPILATION OF POSITIVE ION MASS FILTER OBSERVATIONS IN THE D-REGION

MID AND HIGH LATITUDE SEASON	DAYTIME DATE	DAYTIME TIME	DAYTIME χ	DAYTIME REF.	NIGHTTIME DATE	NIGHTTIME TIME	NIGHTTIME I.D.#	NIGHTTIME χ	NIGHTTIME REF.	LOCATION	GEOPHYSICAL CONDITIONS
SUMMER	August 8, 1971	1211	55°	14						Andoya (69°17')	Quiet
	July 23, 1970		38°	22						Sardinia (39.6°N)	Quiet
					August 10, 1970	0039	C58/2	95°	12	Kiruna 67°54')	Sporadic E and NLC
FALL	October 31, 1963	1200 AC6.341	44°	1,3						Eglin AFB	Quiet
	November 3, 1969	1120 CST AH7.886	74°	9,7						Ft. Churchill	PCA
	November 16, 1965	1222 LT AE6.379	49°	3,5						Eglin AFB	Leonid Meteor Shower
					November 3, 1969	0130	AG7.882	133°	9	Ft. Churchill	PCA
					November 4, 1969	1650 LT	AH7,893	94.6°	9,7	Ft. Churchill	PCA
					November 17, 1969	2320 LT	AE6.382	?	3,5	Eglin AFB	Sporadic E and Meteor Shower
					November 26, 1969	0138	F21 N-C	128.8°	12	*Andoya* (69°17')	*Slight Absorbtion*
SPRING	March 11, 1964	1200 AC6.342		2						Eglin AFB	Quiet - Bad Data
	March 15, 1968	1415 NASA 18.10	49°	10						Wallops Is.	Quiet
					March 23, 1970	2358	F22 N-C	109°	12	Andoya (69°17')	Weak Absorbtion
					April 9, 1969	2138	F20 N-A	97°	12	Andoya (69°17')	Weak Absorbtion
					April 12, 1967	1849	N-I	99°	5	Eglin AFB	?
LOW LATITUDE	March 19, 1970	0827 N-A14.425	53°	11						Thumba, India	Quiet
	March 19, 1970	1017 N-A14.424	28°	11						*Thumba, India*	Quiet
ECLIPSE	November 5, 1966	1355 N-H CERT		4						Cassino, Brazil (32°S)	Certification
	November 12, 1966	1354 N-H D-4		4						Cassino, Brazil (32°S)	80% Obscured
	November 12, 1966	1408:37 N-H D-11		4						Cassino, Brazil (32°S)	Totality

positive-ion detection systems were basically identical: quadrupole-mass-filters evacuated by cryogenically-cooled pumping systems or titanium-getter pumps, the principal choice during sampling being the range of atomic mass over which the filter could register.

Examination of profiles (#3, #9, #12 in Appendix I) shows a variation in $[O_2^+]$ and $[NO^+]$ which is due to solar zenith angle control and geophysical activity, particularly above 95 km. Lack of accompanying radiation and particle flux data precludes any quantitative analysis of these profiles. Only six measurements were made under geophysically quiet conditions by day: #1, 4, 10, 11, 14, 22, of Appendix I, and these will form the representative sample for the forthcoming analysis. It is not possible to unambiguously assert that the variations between the profiles are due to the effects of either season or location. Profiles #1 and 14 from Narcisi and Bailey (1965) and Johannessen and Krankowsky (1972), (Fig. II-2a,b) show most clearly the main features of the vertical distribution of water and nitric oxide clusters which dominate the positive ion group. The common features are as follows:

1. All cluster ions have a sharp ceiling (decrease) at 84 $\pm$ 2 km.
2. The altitude of the ceiling corresponds with the position of the ledge in electron density. Electron density concentrations at 80 km are $\simeq$ 500 cm^{-3}.
3. Below the ceiling, the sum of the water clusters, $\sum_{n=0}^{\infty} H_3O^+.(H_2O)n$ is over an order of magnitude larger than the sum of the nitric oxide clusters, $\sum_{n=1}^{\infty} NO^+.(H_2O)n$.

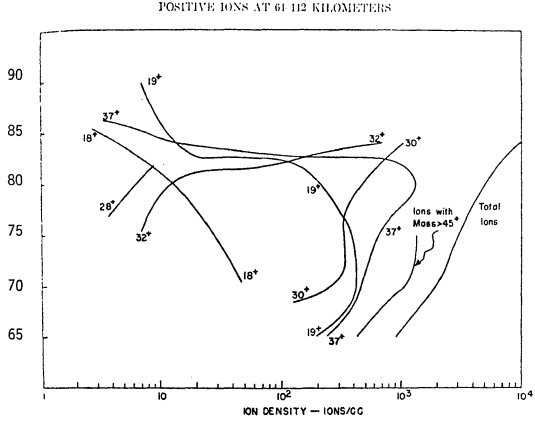

Figure II-2a

Figure II-2 a, b

Profiles of positive ions in the D-region obtained by rocket-borne mass-filters of Narcisi and Bailey (1965), a, and Johanssen and Krankowsky (1972),b. These profiles are chosen from the set of all rocket measurements (Appendix I) as most representative of quiet time D-region daytime conditions. Figure a, incidentally, was the first observation of positive ions in the D-region.

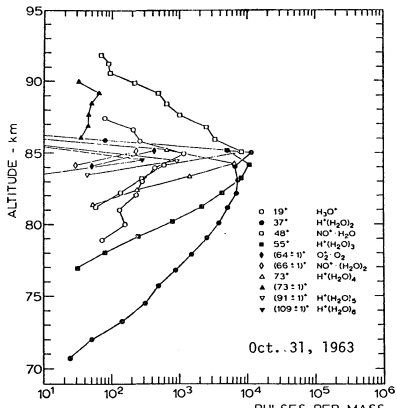

Normalized counts per mass peak for cluster ions obtained on the upleg.

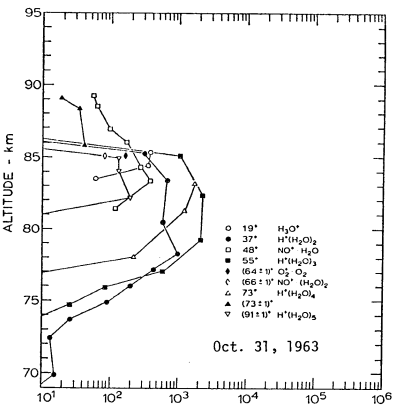

Normalized counts per mass peak for cluster ions obtained on the down leg.

Figure II-2b

4. Among the water clusters, $H_3O^+.(H_2O)_2$, (55^+) and $H_3O^+.H_2O$, (37^+) are dominant.
5. Among the nitric oxide clusters, only $NO^+.H_2O$, (48^+) has been identified.
6. Molecular ions NO^+ and O_2^+ are relatively negligible below the ceiling, but dominant immediately above.

More detailed (if less reproducible) features within the cluster ions may be seen by studying Fig. II-2a, one of the two polar summer profiles. Cluster ion $H_3O^+(19^+)$ forms a minor part of the total population and occupies a thin wedge (5 km) within the upper portion of the cluster $H_5O_2^+(55^+)$ profile. Clusters 37^+ and 55^+ have generally similar vertical distributions in a layer 15 km thick but 37^+ is less plentiful in the upper portion. It is almost as if there are successive altitudes where a particular order cluster becomes the dominant species, but the observational record is too sparse to isolate precise patterns. 55^+ has not been observed on all rocket flights.

It will be noticed by the reader that these D-region features are couched descriptively rather than in terms of precise number densities. There is greater reliability in comparing relative magnitudes of the ion currents due to various atomic masses in the mass-filter than in translating these measurements into the actual in situ number densities. Furthermore, certain profiles are reported only in terms of ion current (i.e., b of Figure II-2).

3. Supersonic Bow Shock Effects, Decomposition of Cluster Ions and Exhaust Gas Contamination

Although the problems of determining the true number density of various cluster-ionic species are considerable, a number of authors have pointed out the possibility of decomposition of the large and weakly bonded cluster ions within the bow shock of the rocket or the possibility of contamination by rocket exhaust. Narcisi and Bailey (1965) discuss this latter possibility, but it seems impossible that exhaust from a 30' long supersonic rocket could travel up to the nose and be sampled by the mass filter.

From a review of data from Mach 2 and Mach 4 rocket sampling, Narcisi (1970c) inferred that the reduction in $[H_3O^+(H_2O)_2]$ measured by the higher speed rocket is due to shock heating decomposition. Also, in-flight variations of draw-in potential to an excess of -10v apparently caused cluster fragmentation. Decomposition due to heat is supported theoretically by the extreme temperature dependence of the equilibrium constants K for the hydration reactions (Kebarle et al., 1970; Niles et al., 1972; and Narcisi and Roth, 1970). The effective lifetimes of $H_3O^+(H_2O)_2$, (73^+), near 75 km for T = 370°, 600°, 900°K which correspond to shock stagnation temperatures for velocities of Mach 2, 3, and 4 are 0.3, 10^{-6} and 10^{-9} sec, respectively. Since the time necessary for a cluster to travel the 9 cm from the shock front to the spectrometer orifice is about 10^{-4} sec, $H_3O^+(H_2O)_2$ could decompose as it is sampled by a Mach 3 rocket due to temperature alone. But no laboratory test of this argument has yet been possible under simulated D-region conditions although Narcisi and Roth (1970) incorrectly ascribe one to Burke (1970).

An additional factor is the orientation of the rocket: frequently the descent shows higher numbers of high hydrates since then the spectrometer orifice is pointed away from the shock front of the falling rocket. Profiles which demonstrate the above effects have been made by Goldberg and Aiken (1971), shots 14.425 and 14.424 upleg and downleg. On the other hand, Johannessen and Krankowsky (1972), (Figure II-2b), do not support this conjecture as a higher order cluster $H_3O^+(H_2O)_5$, 109^+ was detected on the upleg as opposed to $H_3O^+(H_2O)_4$, 91^+ on the downleg. They say that with an angle of attack of $> 90^0$, he velocities (proportional to $1/\sqrt{m}$) are less for heavier rather than lighter masses. Actually, using the rocket velocity profile in Figure II-3 of Goldberg and Aiken (1971), if the rocket is pointed upward on descent the mean speed $\bar{c}$ in the molecular flow field area (> 90 km) is insufficient (particularly with heavy ions) to catch up with the falling rocket and hence downward samples are suspect. The shot by Goldberg and Blumle (1970) was ambiguous in this regard.

In summary, the sampling problems associated with cluster decomposition, rocket orientation, contamination, change of Debye length, mean free path and sampling regime are considerable but not sufficient to cast doubt on the existence of water cluster ions at 80 km or dispose of the broad patterns of positive-ion profiles which were depicted in the last section. The conclusions that one must draw from this discussion are that (a) for any given D-region altitude there exists no hard theory to relate a particular ion curent to a precise ambient number density and (b) a variation of a few kilometers of height changes

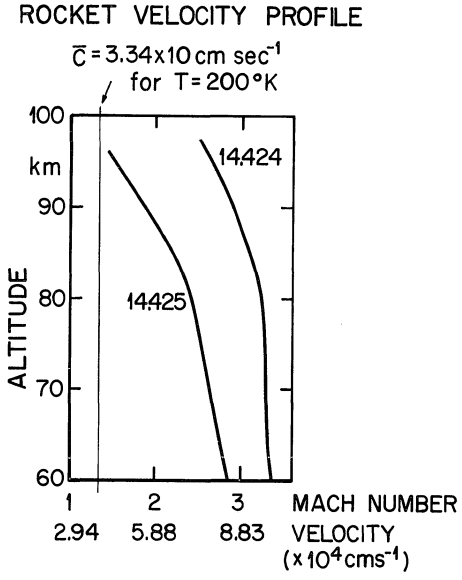

Figure II-3.

A velocity vs. height profile for the upleg and downleg of a D-region sampling rocket of Goldberg and Aiken (1971).

the sampling environment so drastically that comparisons between heights must not be made. Even the observed dominance of $H_3O^+ \cdot 2H_2O(55^+)$, $H_3O^+ \cdot H_2O(37^+)$, and $H_3O^+(19^+)$ at successive altitudes has to be due in large part to geophysical changes modifying the collected ion current. In-flight calibration can provide some measure of total positive ion and electron densities, but it cannot lead to a quantitative sorting out of true relative abundances of various ions at an altitude. Rockets fired in quick succession, such as at an eclipse (Narcisi et al., 1972), could successfully establish temporal variations as the eclipse evolves. For example, the observed upward migration of the transition level between cluster ions and NO^+ and O_2^+ during the course of the eclipse is probably real.

4. Studies of Water Vapor Phase Chemistry

A. Basic Reactions

Prior to 1965, the D-region was not considered a problem area since the early formulation of Nicolet and Aiken (1960) was believed to describe the existing features. Early effort concentrated on verifying this formulation, and theoretical analyses focused upon determining rates of ionization (Webber, 1962; Smith, 1966), the concentration of nitric oxide (Nicolet, 1965) and the achievement of values of the effective recombination coefficients to account for the electron density ledge. Mitra (1968) thoroughly reviews these approaches. More comprehensive composition studies were undertaken by Keneshea (1963) who attempted to model neutral species profiles and reactions leading to cluster ions in the range 20 to 150 km by computer in a careful computational effort

which suffered, however, from the lack of key reactions and accurate rate constants.

The discovery of cluster ions in 1965, however, caused D-region processes to be regarded as something of an enigma. Reviews of initial water vapor phase chemistry may be found in Ferguson (1971b), Fehsenfeld and Ferguson (1969), Narcisi and Roth (1970), Narcisi (1970a), and Sechrist (1969). Briefly, the problem of the chemistry of cluster ions may be outlined as follows.

Cluster ions, $H_2^+(H_2O)_n$ n = 1, 2, ... N, had been produced since 1962 in the laboratory by electron beam irradiation of an atmosphere of moist oxygen and detected by mass spectrometry (Good et al., 1970b):

$$H_2O^+ + H_2O \longrightarrow H_3O^+ + OH, \qquad (2\text{-}8)$$

with a rate constant of $k \simeq 10^{-9}$ cm^3 sec^{-1}. However, the following reaction also occurs,

$$H_2O^+ + O_2 \longrightarrow O_2^+ + H_2O,$$

$$k = 2 \times 10^{-10} \text{ cm}^3 \text{ sec}^{-1}. \qquad (2\text{-}9)$$

with the results that the high O_2/H_2O ratio in the D-region favors the latter reaction (2-9) and the production of O_2^+ instead of H_3O^+ (Fehsenfeld and Ferguson, 1969).

This problem was solved by Ferguson (1971b), Sechrist (1969) and Good et al. (1970a) by the announcement that such a direct hydration chain was unnecessary. NO^+ and O_2^+ may hydrate directly:

$$NO^+ + H_2O + M \longrightarrow NO^+ \cdot H_2O + M \qquad (2\text{-}10)$$

$$O_2 + H_2O + M \longrightarrow O_2^+ \cdot H_2O + M. \qquad (2\text{-}11)$$

Thereupon, the hydrates are built by an alternate path,

$$P^+(H_2O)_n + H_2O \longrightarrow H_3O^+(H_2O)_{n-1} + P + OH, \qquad (2\text{-}12)$$

where for $P = O_2$ and $n = 1$ or $P = NO$ and $n = 3$ this reaction becomes exothermic. Verification of the reaction and values of the rate constants is substantial: Ferguson (1971b), Lineburger and Puckett (1969), Puckett and Teague (1971), Howard et al. (1971) in addition to previously mentioned sources. Since primary ionization in the D-region is NO^+, N_2^+ and O_2^+, through a fast charge exchange

$$N_2^+ + O_2 \longrightarrow O_2^+ + N_2, \qquad (2\text{-}13)$$

and the main primary ions become NO^+ and O_2^+ from which clusters would have to grow.

If NO^+ is the primary ion,

$$NO^+(H_2O)_n + H_2O + M \longrightarrow NO^+(H_2O)_{n+1} + M. \qquad (2\text{-}14)$$

When $n = 3$, the conversion to water clusters occurs:

$$NO^+(H_2O)_3 + H_2O \longrightarrow H_3O^+(H_2O)_2 + HNO_2, \quad (55^+). \qquad (2\text{-}15)$$

The clustering scheme originating with O_2^+ is:

$$O_2^+ + O_2 + M \longrightarrow O_4^+ + M \qquad (2\text{-}16)$$

$$O_4^+ + H_2O \longrightarrow O_2^+(H_2O) + O_2 \qquad (2\text{-}17)$$

$$O_2^+(H_2O) + H_2O \longrightarrow H_3O^+(OH) + O_2 \qquad (2\text{-}18a)$$

$$\longrightarrow H_3O^+ + OH + O_2, \ (19^+) \qquad (2\text{-}18b)$$

$$H_3O^+(OH) + H_2O \longrightarrow H_3O^+(H_2O) + OH, \ (37^+) \qquad (2\text{-}19)$$

$$H_3O^+(H_2O) + H_2O + H_2O + M \longrightarrow H_3O^+ (H_2O)_2 + M, \ (55^+) \quad (2\text{-}20)$$

Ferguson and Fehsenfeld (1969) computed water cluster concentrations based upon primary production of O_2^+ and NO^+ and achieved an order of magnitude agreement with the results of Narcisi and Bailey (1965). In addition to x-rays and galactic cosmic rays (GCR), they included ionization due to the reaction

$$O_2(^1\Delta g) + h\nu \longrightarrow O_2^+ + e \qquad \text{Hunten and McElroy (1968)} \quad (2\text{-}21)$$

since the path starting with O_2^+ is apparently more efficient than that with NO^+ (due to having only one 3-body reaction and that with major constituents). However, calculations of the absorption of Lyβ (1027Å) and CIII (977Å) (the ionizating wavelengths for $O_2(^1\Delta g)$) by CO_2 indicate that Hunten and McElroy's $q(O_2^+)$ should be reduced and, therefore, the O_2^+ route for formation of cluster ions would not be possible (Huffman et al., 1971). This weakening of the O_2^+ chain as a source of hydrates prompted scrutiny of NO^+, but the NO^+ pathway leads to several problems. Foremost is the fact that if primary ionization of NO by Lyα produces the high concentrations of electrons observed by rocket sampling at 80 km, then some compound with a very high recombination coefficient must exist to remove electrons and produce the sharp ledge at 82 km. Reid (1971), in particular, using a set of 22 ion-kinetic reactions, examined the relative advantages of variations in $q(O_2^+)$ and $q(NO^+)$ only to reach this impasse. The second problem is that the NO^+ pathway leads directly to water cluster 55^+ whereas observations show $H_3O^+(19^+)$ and $H_3O^+ \cdot H_2O(37^+)$ to be more plentiful.

B. Backward Reactions

Some help may be achieved on answering the question of generating smaller clusters since the act of sampling by a supersonic rocket may cause clusters to decompose in the shock front (Narcisi, 1971; Narcisi and Roth, 1970) as discussed previously. Also, studies by Kebarle et al. (1967) and Leu et al. (1973) indicate that a class of back reactions from larger to smaller order clusters exists where the backward rate constants are dependent upon temperature and pressure.

To investigate the potential usefulness of this possibility we calculated the backward rate constants as a function of temperatures and pressures appropriate to the D-region. In particular, rates for forward and backward hydration for this set:

$$H_3O^+(H_2O)_n + H_2O + M + M \underset{k_b}{\overset{k_f}{\rightleftharpoons}} H_3O^+(H_2O)_{n+1} + M \qquad (2\text{-}22)$$

for n = 0 to n = 5 were computed. The more clustered the ion, the greater the backward velocity. Figures II-4,a,b show plots of the resultant relative composition in the atmosphere of multiply hydrated water clusters as a function of temperature and pressure and the shift from one preferred cluster species to another due to a change in altitude (pressure) or temperature. For D-region conditions (temperature T = 240^0 for winter and water vapor partial pressure of 10^{-8} Torr), the dominant equilibrium cluster ions are $H_3O^+ \cdot 2H_2O$ (73^+) and $H_3O^+ \cdot H_2O$ (37^+). Temperatures of 140^0K, common to the high latitude summer mesopause, force the equilibrium toward clusters of n = 6 or mass number 127^+.

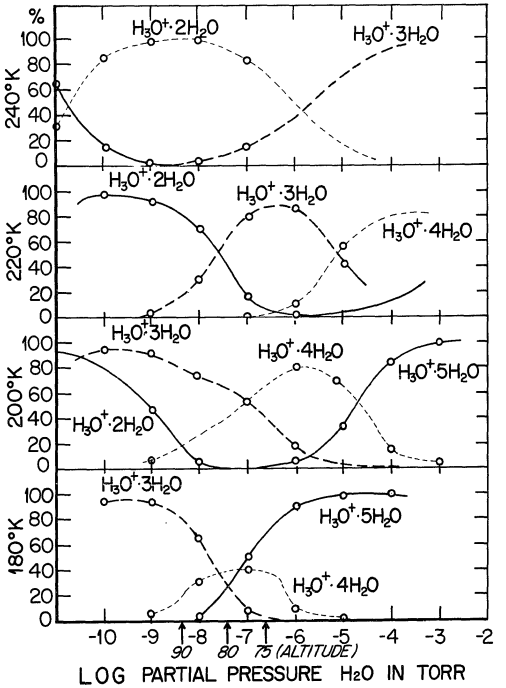

Figure II-4a.

The set of reactions:

$$H_3O^+ \cdot (H_2O)_n + H_2O + M \underset{k_b}{\overset{k_f}{\rightleftharpoons}} H_3O^+ \cdot (H_2O)_{n+1} + M$$

for n = 0 to n = 1, when solved as a set, will equilibrate with a specific hydrate being the preferred species for a given temperature and pressure. This figure plots the percentages of hydrates obtained for temperatures of 240°K, 220°K, 200°K and 180°K and a range of D-region pressures.

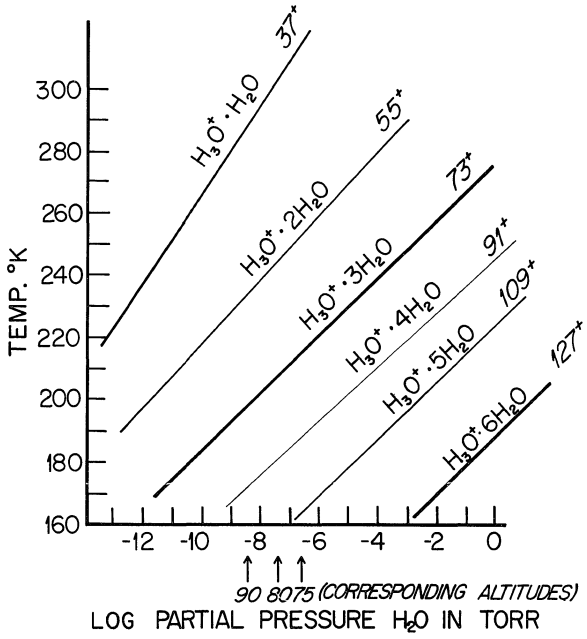

Figure II-4b.

This plot is based upon Figure 4a. For a given order hydrate, n, the temperatures and pressures at which it is the dominant species is plotted along with the sets of temperature and pressure producing 100% in other hydrates. By examining this family of curves the control of temperature and vapor pressure (altitude) upon this isolated set of compounds is apparent. Reduction to low temperatures forces the equilibrium in the direction of heavier clusters. Low pressures (greater altitude) favor smaller clusters.

Such high order hydrates have indeed been observed by Johanssen and Krankowsky (1972) on a daytime shot from Andoya, Norway. Additional evidence by Narcisi and Roth (1970) proves that there is a reaction path from higher to lower order clusters which has been observed in the laboratory. Furthermore, Brown (1970) reports that electron precipitation can shift the center of hydrated cluster population from n = 3 or 4 to 1 or 2, a fact of significance at subauroral heights. Hence, depending on conditions and altitude, a wide range of clusters may exist with various distributions characterized by a preferred cluster species which may also decompose easily to clusters of a lower molecular mass.

C. Less Important Crossover Reactions to Build Hydrated Clusters from the NO Pathway

Due to the impasse with the direct approach, other methods of crossing over from the NO^+ chain to O_2^+ chain were suggested:

1. Since there is ample atomic hydrogen in the D-region (Hesstvedt, 1968; Anderson, 1971) a crossover reaction could be

$$NO^+ \cdot H_2O + H \longrightarrow H_3O^+ + NO + 22 \text{ ev (Burke, 1970)}, \quad (2\text{-}23)$$

a reaction which would produce lower order hydrates. Although the reaction is exothermic, Ferguson (1971) discounts this possibility since the reaction does not readily occur in his laboratory.

2. Heimerl and Vanderhoff (1971) suggest

$$NO^+ + N_2 + M \longrightarrow NO^+ \cdot N_2 + M \qquad M = N_2$$
$$k = 2\text{x}10^{-31} \text{ cm}^6 \text{ sec}^{-1} \quad (2\text{-}24)$$

which then hydrates to $NO^+ \cdot H_2O$ (Dunkin et al., 1971). This reaction is directly discounted by more recent studies (Biondi, 1974b).

3. Hunt (1971a) attempts to use $NO^+ \cdot O_2$ and $H_3O^+ \cdot O_2$ as intermediates for cluster ions, but this is highly speculative since the reaction has not been observed in the laboratory and he must guess at the rate constants.

4. Snider (1970) suggested that ionization of methane by Lyα to produce CH_3^+ could then react

$$CH_3^+ + H_2O \longrightarrow H_3O^+ + CH_2. \qquad (2\text{-}25)$$

Unfortunately, the reaction is endothermic.

5. There are a set of 'shuffling' reactions (Ferguson and Fehsenfeld, 1969) which can increase the number of cluster ions:

$$H_3O^+ \cdot OH + H_2O \longrightarrow H_3O^+ \cdot H_2O + OH \qquad (2\text{-}26)$$

$$H_3O^+ \cdot OH + O_2 + M \longrightarrow H_3O^+ \cdot OH \cdot O_2 + M \qquad (2\text{-}27)$$

$$H_3O^+ \cdot OH \cdot O_2 + H_2O \longrightarrow H_3O^+ \cdot OH \cdot H_2O + O_2 \qquad (2\text{-}28)$$

$$H_3O^+ \cdot OH \cdot H_2O + H_2O \longrightarrow H_3O^+ \cdot (H_2O)_2 + OH \qquad (2\text{-}29)$$

but aside from the first reaction which turns out to be quite important, these are not very efficient.

As an additional detail to the positive ion chemistry, the decrease of numbers of cluster ions at 82 km may be accomplished by the reaction

$$O_4^+ + O \longrightarrow O_2^+ + O_3 \qquad \text{Fehsenfeld (1971)} \qquad (2\text{-}30)$$

which is fast and could successfully interrupt the clustering sequence starting with O_2^+, particularly above 85 km where there is ample atomic oxygen.

It turns out that most of the current solutions to D-region chemistry which remain within the limits of purely vapor phase chemistry and the standard number densities of the neutral atmosphere are unable to enhance the population of water clusters to match observation while simultaneously preserving high electron density. Even if one is suspicious of the absolute number densities recorded on the various rocket shots, one may probably assume that for a given altitude the ratio of the ion currents for water cluster-ions to nitric oxide clusters represents an observed ratio of those positive ions at a given altitude. Reid (1971) believed that if enough hydrated water clusters could be produced, then their large recombination coefficients (of up to 2×10^{-3} cm^3 sec^{-1}) in comparison with those of nitric oxide clusters might provide the much needed sink for electrons in spite of a high primary production of NO^+. As will be seen in the next chapter, the problem need not be solved in exactly that manner.

In summary, previous formulations have been somewhat unsuccessful in matching D-region features. The normal production of NO^+ by Lyα yields excessive electron densities and nitric oxide clusters, thus violating items 2 and 3 in Section 2 of this chapter. It follows that items 4 and 5 are not matched either. Cross over reactions do not alleviate the problem. Item 1, the existence of a ceiling, is not met, and only item 6 is satisfactory.

CHAPTER III

ION-KINETIC REACTIONS

INTRODUCTION

The discussion in the last chapter focused upon the inadequacies of current positive-ion reaction schemes in accounting for observed D-region features. Part of the apparent mismatch was shown to be due to the extreme difficulty of making accurate concentration measurements from 70 to 90 km. The governing philosophy of investigators seems to have been to uncover "key" chemical reactions which could produce hydrated water cluster-ions and lead to a match between theory and observation. It is equally possible, though less spectacular, that the gradual improvement in several of the already existing partial solutions to the problem may be sufficient. With this in mind, a review is made in this report of all of the elements bearing on D-region photochemistry and, if necessary, they are recomputed from fundamental data.

Specifically, our approach to matching the observed D-region features requires a) a unique set of ion-kinetic chemical reactions which include the dominant positive-ion species, b) model atmospheres and temperature profiles for summer and winter, c) nitric oxide profiles for summer and winter temperatures, d) primary product ion rates of N_2^+, NO^+ and O_2^+ due to X-rays (< 10Å), UV and EUV (1000Å - 10Å), Lyα (1215.6Å), Lyβ (1027.5Å), CIII (977Å), and ionization of $O_2(^1\Delta g)$, e) water vapor profiles computed from diffusion and vertical drift of the neutral atmosphere (Chapter IV), and f) downward flux of dust (.015 - .035μ) to serve as a sink for positive ions and free electrons.

LIST OF SYMBOLS

N_e = electron density (cm^{-3})

N_i^+ = positive-ion number density (cm^{-3})

N_j^- = negative-ion number density (cm^{-3})

α_i = ion-ion recombination coefficient ($cm^3\ sec^{-1}$)

α = recombination coefficient of positive ions and electrons ($cm^3\ sec^{-1}$)

α_D = recombination coefficient of dust to electrons or positive ions ($cm^3\ sec^{-1}$)

D = dust attachment coefficient ($cm^3\ sec^{-1}$)

n_D = dust concentration (cm^{-3})

ν_z^- and ν_z^+, capture rates of electrons and positive ions by dust particles (sec^{-1})

k_f = forward rate constant ($cm^3\ sec^{-1}$ for 2-body, $cm^6\ sec^{-1}$ for 3-body)

k_b = backward rate constant ($cm^3\ sec^{-1}$for 2-body, $cm^6\ sec^{-1}$ for 3-body)

$q(N_i^+)$ = primary production rate of positive ion N_i^+ (sec^{-1})

λ = wavelength ($\mathring{A}$)

χ = solar zenith angle (degrees)

σ_λ^T = total absorption cross section (cm^2)

σ_λ^i = photoionization cross section (cm^2). This $\sigma_\lambda^i = \eta \cdot \sigma_\lambda^T$ where

η = ionization efficiency $\equiv$ number of electrons produced/impact photon. Efficiency equals 1 when radiation is much more energetic than the ionization potential of the species. Frequently, (e.g., Banks and Kockarts, 1973, Vol. A, Table

7.7, p. 148), the ionization rate constant, IRC, is tabulated instead. IRC $\equiv I_\infty \equiv \phi_\infty \cdot \eta \cdot \sigma_\lambda^T$ where ϕ_∞ is the flux of photons/wavelength band at the top of the atmosphere. In that case the primary production rate q is given by $q \equiv I_\infty \cdot e^{-\tau} [N_i]$ where $\tau \equiv$ optical depth $= \sigma_\lambda^T(i) [N_i] \cdot H_i$

H_i = scale height of constituent i (cm). This will be taken equal to the scale height H, of the neutral atmosphere.

r_D = radius of dust (cm)

ϕ_D = flux of dust (cm^{-2} sec^{-1})

W_D = Stokes fall velocity of dust particle (cm sec^{-1})

W_o and W = Neutral atmosphere vertical velocity (cm sec^{-1})

1. Ion-Kinetic Formulation

A. Continuity and Charge Balance Equations

The basic scheme for the calculation of the equilibrium (i.e., steady state) concentrations employs the continuity equation for each constituent and the condition of charge neutrality applied to all constituents. If N_i^+ is any positive ion:

$$\frac{d(N_i^+)}{dt} = q(N_i^+) - \alpha N_i^+ N_e - \alpha_D N_i^+ - \alpha_i N_i^+ \cdot \Sigma N_j^- \qquad (3\text{-}1)$$

+ other gain reactions - other loss reactions. (Table IIIa)

and $$\frac{dN_i^+}{dt} \equiv 0 \text{ for steady state conditions.} \qquad (3\text{-}2)$$

Negative ions are not important at altitudes of above 65 km, and they are excluded in the positive-ion computations presented in this chapter.

Hence the ion-ion recombination term, $\alpha_i N_i^+ \cdot \Sigma \; N_j^-$ is not included in computations. We ignore the negative molecular ions, $\Sigma \; N_j^-$, and the small quantity of negative charges on the dust particles, $n_D N_e$ and thus the statement of charge neutrality between positive ions and electrons in the daytime D-region is;

$$\sum_{i=1}^{16} N_i^+ = N_e. \qquad (3\text{-}3)$$

17 equations, 16 continuity equations (one for each positive ion in the reaction set, see Table IIIb) plus the charge neutrality condition are solved as a linear set with the potentially non-linear term for each positive ion, $\alpha_i N_i^+ N_e$, being made linear through an initial guess of electron density. In the computer program POSCHEM or DUSTCHEM, the positive-ion densities are calculated and summed, and a new electron density value is determined. This value is reinserted in the set to solve for positive ions and this iteration continues until convergence within 1% occurs, which is normally after about 7 iterations. The POSCHEM and DUSTCHEM computer programs are listed with explanations in Appendix VI.

B. Ion-Kinetic Reaction Set

The positive-ion reactions which will be used are listed in Tables IIIa,b,c with rate constants and recombination coefficients taken from the compilation in the Defense Nuclear Agency (DNA) (1972) Reaction Rate Handbook and recent literature. Twenty-two of the positive-ion reactions are common to Reid (1971a) and are considered fundamental in the literature. This set includes most reactions which had

TABLE IIIa

D-REGION POSITIVE-ION REACTIONS AND ASSOCIATED FORWARD RATE CONSTANTS (after DNA, 1972)

($cm^3\ sec^{-1}$ for 2-body or $cm^6\ sec^{-1}$ for 3-body)

	POSITIVE ION REACTIONS	RATE CONSTANTS
1.	$N_2^+ + O \rightarrow NO^+ + N$	2.5×10^{-10}
2.	$N_2^+ + O_2 \rightarrow O_2^+ + N_2$	6.0×10^{-11}
3.	$O_2^+ + NO \rightarrow NO^+ + O_2$	6.3×10^{-10}
4.	$N_2^+ + NO \rightarrow NO^+ + N_2$	3.3×10^{-10}
5.	$NO^+ + H_2O + M \rightarrow NO^+ \cdot H_2O + M$	1.6×10^{-28}
6.	$NO^+ \cdot H_2O + H_2O + M \rightarrow NO^+ \cdot (H_2O)_2 + M$	1.1×10^{-27}
7.	$NO^+ \cdot (H_2O)_2 + H_2O + M \rightarrow NO^+ \cdot (H_2O)_3 + M$	2.0×10^{-27}
8.	$NO^+ \cdot (H_2O)_3 + H_2O \rightarrow H_3O \cdot (H_2O)_2 + HNO_2$	8.0×10^{-11}
9.	$O_2^+ + O_2 + M \rightarrow O_4^+ + M$	2.8×10^{-30}
10.	$O_4^+ + H_2O \rightarrow O_2^+ \cdot H_2O + O_2$	2.2×10^{-9}
11.	$O_2^+ \cdot H_2O + H_2O \rightarrow H_3O^+ + OH + O_2$	3.0×10^{-10}
12.	$\rightarrow H_3O^+ \cdot OH + O_2$	1.9×10^{-9}
13.	$H_3O^+ \cdot OH + H_2O \rightarrow H_3O^+ \cdot H_2O + OH$	3.2×10^{-9}
14.	$H_3O^+ \cdot OH + O_2 + M \rightarrow H_3O^+ \cdot OH \cdot O_2 + M$	1.0×10^{-29}
15.	$H_3O^+ \cdot OH \cdot O_2 + H_2O \rightarrow H_3O^+ \cdot OH \cdot H_2O + O_2$	1.0×10^{-9}
16.	$H_3O^+ \cdot OH \cdot H_2O + H_2O \rightarrow H_3O^+ \cdot (H_2O)_2 + OH$	1.0×10^{-9}
17.	$H_3O^+ + H_2O + M \rightarrow H_3O^+ \cdot H_2O + M$	3.4×10^{-27}
18.	$H_3O^+ \cdot H_2O + H_2O + M \rightarrow H_3O^+ \cdot (H_2O)_2 + M$	2.3×10^{-27}
19.	$H_3O^+ \cdot (H_2O)_2 + H_2O + M \rightarrow H_3O^+ \cdot (H_2O)_3 + M$	2.4×10^{-27}
20.	$NO^+ + CO_2 + M \rightarrow NO^+ \cdot CO_2 + M$	3.0×10^{-29}

TABLE IIIa (Cont'd)

21.	$NO^+ \cdot CO_2 + H_2O \rightarrow NO^+ \cdot H_2O + CO_2$	1.0×10^{9}
22.	$O_2^+ + H_2O + M \rightarrow O_2^+ \cdot H_2O + M$	1.9×10^{28}
23.	$O_4^+ + O \rightarrow O_2^+ + O_3$	3.0×10^{10}

TABLE IIIb

VALUES OF DECOMPOSITIONAL (BACKWARD) RATE CONSTANTS ($cm^6\ sec^{-1}$)

FOR T = 130°K

	POSITIVE-ION REACTION	RATE CONSTANT
17.	$H_3O^+ + H_2O + M \leftarrow H_3O^+ \cdot H_2O + M$	10^{-59}
18.	$H_3O^+ \cdot H_2O + H_2O + M \leftarrow H_3O^+ \cdot (H_2O)_2 + M$	10^{-39}
19.	$H_3O^+ \cdot (H_2O)_2 + H_2O + M \leftarrow H_3O^+ \cdot (H_2O)_3 + M$	10^{-30}

TABLE IIIc

POSITIVE-ION SPECIES AND VALUES OF THEIR RECOMBINATION COEFFICIENTS (after DNA, 1972, and Leu, 1973)

	IONIC SPECIES	DISSOCIATIVE RECOMBINATION COEFFICIENTS (cm^3 sec^{-1})	
1.	N_2^+	3.0×10^{-7}	
2.	NO^+	7.5×10^{-7}	
3.	O_2^+	3.5×10^{-7}	
4.	O_4^+	2.0×10^{-6}	
5.	$O_2^+ \cdot H_2O$	5.0×10^{-6}	
6.	$NO^+ \cdot H_2O$	5.0×10^{-6}	
7.	$NO^+ \cdot (H_2O)_2$	7.0×10^{-6}	
8.	$NO^+ \cdot (H_2O)_3$	1.0×10^{-5}	
9.	$NO^+ \cdot CO_2$	1.0×10^{-5}	
10.	H_3O^+	1.6×10^{-6}	Leu (1973)
11.	$H_3O^+ \cdot H_2O$	2.2×10^{-6}	Leu (1973)
12.	$H_3O^+ \cdot (H_2O)_2$	3.8×10^{-6}	Leu (1973)
13.	$H_3O^+ \cdot (H_2O)_3$	4.9×10^{-6}	Leu (1973)
14.	$H_3O^+ \cdot OH$	8.0×10^{-6}	
15.	$H_3O^+ \cdot OH \cdot H_2O$	1.0×10^{-5}	
16.	$H_3O^+ \cdot OH \cdot O_2$	1.0×10^{-5}	

been assembled by Good et al. (1971) and Fehsenfeld and Ferguson (1969) but omits those of uncertain validity such as cross over reactions between the O_2^+ and NO^+ pathways (see Chapter II, Sec. 4c). Included also are the set of four decompositional ('backward') reactions from higher to lower order water clusters of the form:

$$H_3O^+(H_2O)_n + H_2O + M \underset{k_b}{\overset{k_f}{\rightleftharpoons}} H_3O^+(H_2O)_{n+1} + M \text{ for } n = 0\text{-}3. \tag{3-4}$$

with temperature sensitive rate constants, k_b, with values from Kebarle et al. (1967) which are also in agreement with Niles et al. (1972). Included also is the reaction

$$O_4^+ + O \longrightarrow O_2^+ + O_3, \tag{3-5}$$

because it interrupts the bottom pathway at $\sim$ 90 km due to plentiful atomic oxygen (Fehsenfeld and Ferguson, 1972).

2. Model Atmospheres

The neutral atmosphere used in this study is taken from the United States Standard Atmosphere Supplements (USSAS) (1966), for January and July at 60°N. Appendix IIa,b,c lists the concentrations of O_2, $O_2 + N_2$ and temperature for both seasons, minor constituents, the eddy diffusion coefficents, K, and the photodissociation coefficient, J. Due to the temperature dependence of some of the rate constants and also of concentrations of minor constituents, Figure III-1 depicts comparative temperature profiles from various sources. The temperature profile from the USSAS (1966) corresponded more closely than did the COSPAR International Reference Atmosphere (CIRA) (1965)

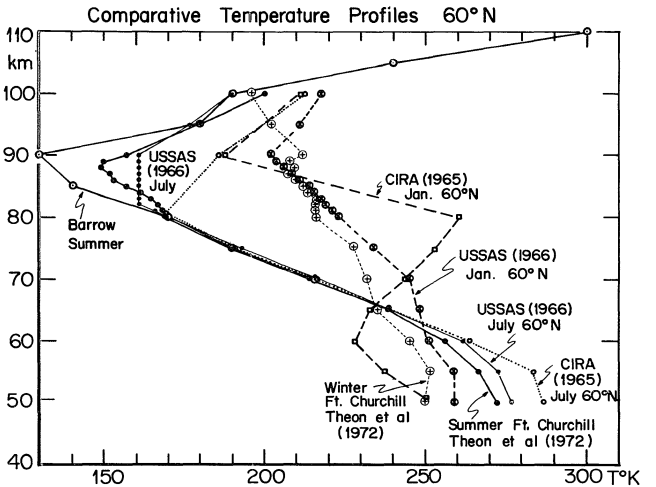

Figure III-1.

Plot of temperature profiles from:

a) USSA Supplement (1966) mean winter 60°N and summer 60°N.
b) CIRA (1965) mean January 60°N and July 60°N.
c) Pt. Barrow summer obtained from rocket grenade soundings (Theon et al., 1972).

with recent rocket grenade soundings for summer and winter made at Ft. Churchill by Theon et al. (1972). Included also is a Pt. Barrow August temperature sounding (Theon et al., 1972) showing the very cold summer mesopause and a hypothetical temperature profile with a minimum set at 145°K, a value half way between that of the Barrow minimum and mean summer minimum (USSAS, 1966).

Aside from H_2O, which is calculated in Chapter IV from the diffusion equation, and nitric oxide which will be discussed immediately, most minor constituents are taken from the literature. $O_2(^1\Delta g)$ is taken from Paulsen et al. (1972), since it is a more realistic profile than that of Huffman et al. (1971). CO_2 is held to its generally accepted mixing ratio of 3×10^4 ppm, and ground state $O(^3P)$ is the high latitude summer value from Crutzen (1971).

3. Production and Loss of Nitric Oxide

The low ionization potential of nitric oxide, 9.25 ev, permits ionization by Lyα radiation, 1215.7Å (10.2 ev) and as a result nitric oxide is the most important ionizable species of the daytime D-region. Hence, the proper choice of nitric oxide profiles for use in ion-kinetic calculations is as important as proper solar flux values. Unfortunately, as will be demonstrated in the ensuing discussion, the choice of this profile is difficult.

Originally, a purely photochemical model of nitric oxide had been proposed (Nicolet, 1960 and Barth, 1961) which had as key reactions

$$N(^4S) + O_2 \longrightarrow NO + O \qquad (3\text{-}6)$$

$$k = 1.2 \times 10^{-11} T^{1/2} e^{-3600/T}$$

(and when $T = 180°K$, $k = 3.32 \times 10^{-19}$ cm^3 sec^{-1})

and $N(^4S) + NO \longrightarrow N_2 + O \qquad k = 3 \times 10^{-11}\ cm^3 sec^{-1}.$ (3-7)

It will be noticed that atomic nitrogen reacts from the ground state, (^4S), in these reactions. Barth's (1964) airglow measurement (see Figure III-2) exceeded this photochemical model prediction by two orders of magnitude and stimulated the next proposal: that atomic nitrogen in its first excited metastable state $N(^2D)$ could be used in

$$N(^2D) + O_2 \xrightarrow{k} NO + O \quad \text{where } k = 5 \times 10^{-12}\ cm^3 sec^{-1} \qquad (3\text{-}8)$$

which is a substantial increase in rate constant. $N(^2D)$ could be reproduced in significant quantities by dissociative recombination of NO^+ if

$$NO^+ + e \longrightarrow N(^2D) + O \text{ occurred more frequently than} \qquad (3\text{-}9)$$

$$NO^+ + e \longrightarrow N(^4S) + O. \qquad (3\text{-}10)$$

Meanwhile, the destruction of NO is unchanged and occurs via

$$N(^4S) + NO \xrightarrow{k} N_2 + O \qquad (3\text{-}11)$$

and $$O_2^+ + NO \xrightarrow{\gamma_1} NO^+ + O_2. \qquad (3\text{-}12)$$

In Meira's (1971) report on his rocket observation of NO (Figure III-2) and in his discussion, which relies heavily upon the analysis of Norton and Barth (1970), a theoretical NO profile from 70 to 100 km is computed using a fractional production of $N(^2D)$ of .87 by dissociative recombination of NO. This fraction was set at .87 since that led to the necessary amount of NO required to match Meira's (1971) observed concentration of NO at 105 km. Meira then calculated a

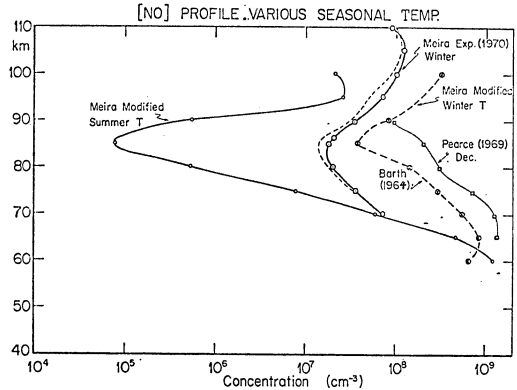

Figure III-2.

Plot of various nitric oxide profiles: a) Meira (1970) experimental measurements of January 31 and February 1, 1969. b) Meira (1970) experimental profile scaled for USSAS (1966) winter temperatures through the expression: $[NO] = .4 \exp(\frac{-3700}{T})[O_2] + 5 \times 10^{-7}[O]$. c) Meira (1970) experimental profile scaled for USSAS (1966) summer temperatures. d) Experimental determinations of Barth (1964), and Pearce (1969).

profile of NO downward from 105 km to 90 km, the destruction below 100 km being due to a reaction with the gas N_2O which had diffused upward from the troposphere.

Strobel, in a series of articles (Strobel et al., 1970 and Strobel, 1971a) introduces two new factors: (1) energetic photoelectron (> 90 ev) dissociation of N_2^+ which could lead to $N(^2D)$, $N(^2P)$ or $N(^4S)$, and, (2) an eddy diffusive model for NO flux based upon that of Colegrove et al. (1966). Here again, however, the relative proportion of atomic nitrogen in the excited or ground states is still unknown so the reactions may only be written:

$$N_2^+ + e \xrightarrow{k} N(^4S) + N(^4S) + 5.82 \text{ ev} \quad (3\text{-}13)$$

$$\longrightarrow N(^4S) + N(^2D) + 3.44 \text{ ev} \quad (3\text{-}14)$$

$$\longrightarrow N(^4S) + N(^2P) + 2.26 \text{ ev} \quad (3\text{-}15)$$

$$\longrightarrow N(^2D) + N(^2D) + 1.06 \text{ ev}, \quad (3\text{-}16)$$

where the gross recombination coefficient, $\alpha = 2.9 \times 10^{-7}$ cm^3 sec^{-1} (Banks and Kockarts, 1973).

Strobel et al. (1970) assumes that all the N atoms produced in the above reactions are in the ground state, $N(^4S)$, and may serve as major daytime destroyers of NO which produce the sink of NO at 80 km. On the other hand, his use of an eddy diffusion formulation clarified what Norton and Barth (1970) had asserted through time constant arguments, namely, that NO is well mixed up to 80 km and that transport instead of photochemistry controls the concentration.

Strobel (1972) presents an excellent review of this literature and the fate of odd nitrogen.

At lower levels of the mesosphere and upper stratosphere, NO reacts with O_3 and O to interconvert to NO_2, primarily at night:

$$NO + O_3 \longrightarrow NO_2 + O_2 \qquad (3\text{-}17)$$

$$NO + O + M \longrightarrow NO_2 + M \qquad (3\text{-}18)$$

$$NO + O \longrightarrow NO_2 + h\nu \qquad (3\text{-}19)$$

$$NO_2 + h\nu \longrightarrow NO + O \qquad (3\text{-}20)$$

$$NO_2 + O \longrightarrow NO + O_2. \qquad (3\text{-}21)$$

Geistler and Dickenson (1968) and Geistler (1969) amended these formulations by including a neutral atmosphere drift for the purpose of further concentrating NO in winter. Their constant value with height of the upward drift of NO is perhaps somewhat unrealistic, but the inclusion at all is a useful step.

However, aside from transport problems, the key photochemical problem lies with determining the amount of $N(^2D)$ produced. Two recent articles on the chemistry of odd nitrogen in the thermosphere, Oran et al. (1975) and Strobel et al. (1976), give a slightly firmer grasp upon the exact sources of $N(^2D)$ which may exist in the thermosphere. But confusion still exists due to the choice of model atmospheres used for the theoretical profiles. Currently, the situation with regard to "credibility" of reactions to produce $N(^2D)$ is:

$$e(\text{fast}) + N_2 \longrightarrow N(^2D) + N(^4S): \qquad \text{Assumption} \qquad (3\text{-}22)$$

$N_2 + h\nu(800\text{-}1000\text{Å}) \longrightarrow N(^2D) + N(^4S)$: Theoretical with support based on predissociation of N_2. (3-23)

$N_2^+ + O \longrightarrow NO^+ + N(^2D)$: Experimentally Observed (3-24)

$NO^+ + h\nu \longrightarrow N(^2D) + O$: Theoretical based upon matching points with observations. (3-25)

$\longrightarrow N(^4S) + O$ (3-26)

For the last reaction the fraction of $N(^2D)$ produced is between 0.5 and 1.0 which brackets the value of .87 which Meira required. It is important to realize, therefore, that the use of $N(^2D)$ to solve NO photochemistry does not introduce new and independent information since:

(a) the branching ratio to produce $N(^2D)$ from the dissociative recombination of NO^+ is unknown;

(b) $N(^2D)$ is metastable (lifetime $\cong$ 26 hrs.) and before reacting to form NO it could be quenched by either of these reactions

$$N(^2D) + O_2(X^3\Sigma_g^-) \longrightarrow N(^4S) + O_2(^1\Delta \text{ or } ^1\Sigma_g) \quad (3\text{-}27)$$

or $$N(^2D) + O_2(X^2\Sigma_g^-) \longrightarrow NO + O, \quad (3\text{-}28)$$

the former being more likely (Wallace and McElroy, 1966),

(c) NO theoretical profiles have not been modeled from first principles but have always required an anchor point with observation to set the branching ratio of $N(^2D)$ and $N(^4S)$.

(d) Transport control of NO is a critical factor in the upper mesosphere and is incompletely understood.

Hence, only a very general understanding of nitric oxide behavior exists at present, and in the upper mesosphere it is still very much an open question. Other more recent measurements of NO with ultraviolet spectrometers and photometers have been made in the mesosphere by Baker et al. (1975) and by means of a chemiluminescent detector by Mason and Horwath (1976), Rusch (1973), and Tisone (1973). Nevertheless, these are not particularly helpful as data to elucidate the photochemistry.

In spite of the dominance of eddy transport control of NO some evidence exists for a temperature control through temperature dependent rate constants. A series of D-region electron density profiles made by the partial reflection method (Gregory, 1965) during a June stratospheric warming in New Zealand shows an increase in electron density of 500 to 2000 cm^{-3} (a factor of 4) (Fig. III-3a) associated with a temperature increase of 10°K at 25 km (Fig. III-3b). It was found by studies conducted by Labitzke (1972) on the temperature changes from 20 km to 90 km during the course of stratospheric warmings at Barrow and Ft. Churchill (Figure III-3c) that a ΔT of +15°K at 25 km was simultaneous with a ΔT = -15°K at 80 km. Mitra's (1968) temperature dependent photochemical expression for the equilibrium concentration of nitric oxide is:

$$[NO] = .4 \exp(\frac{-3700}{T})[O_2] + 5 \times 10^{-7}[O] \qquad (3\text{-}29)$$

since $$N + O_2 \xrightarrow{k_1} NO + O \qquad k_1 = 1.4 \times 10^{-11} (\frac{T}{300}) e^{-3600/T} \qquad (3\text{-}30)$$

and $$N + NO \xrightarrow{k_2} N_2 + O \qquad k_2 = 2.2 \times 10^{-11} \frac{T}{300} . \qquad (3\text{-}31)$$

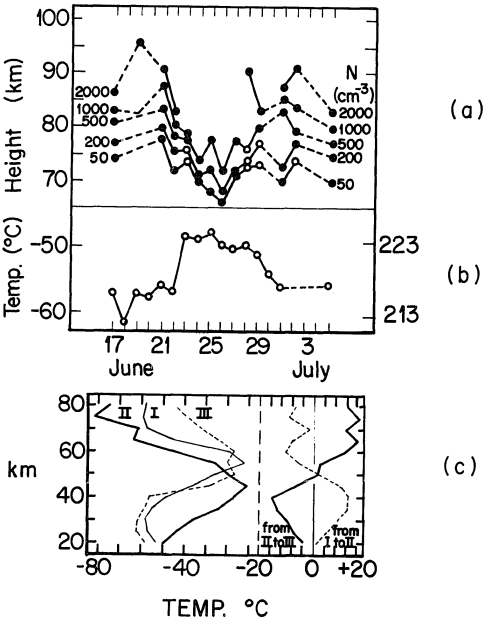

Figure III-3a,b,c.

D-region changes during a winter stratospheric warming in June 1963 at Christchurch (Gregory, 1965). a) Noon electron concentrations obtained by the partial reflection method, b) stratospheric temperature at the 25 km altitude, c) temperature profiles of the stratosphere and mesosphere, before (I), during (II), and after (III) a stratospheric warming (Labityke, 1972).

$$[NO]\Big|_{T=198} = [NO]\Big|_{T=213} \frac{.4 \exp\left(\frac{-3700}{198}\right)[O_2] + 5 \times 10^{-7}[10"]}{.4 \exp\left(\frac{-3700}{213}\right)[O_2] + 5 \times 10^{-7}[10"]}, \tag{3-32}$$

so that $[NO]\Big|_{T=198} = [NO]\Big|_{T=213} \times .3$ or, low temperature reduces the concentration of nitric oxide. It may be shown by means of ion-kinetic calculations of electron density while varying the nitric oxide concentration (Figure III-8) that the change in electron density is 28% of the change in nitric oxide. So, a change in [NO] of factor of 3.66 would result in a ΔN_e of a factor 3.66 x .287 = 1.05 which is a change from 500 cm^{-3} to 1025 cm^{-3} concentration of electrons due to a temperature change of 15°K.

Such a computation is, of course, limited, but it argues for some degree of temperature dependence of nitric oxide concentration and tempers the assertion of total control of NO by transport processes in the mesosphere. Consequently, for the purposes of this thesis, the following curves of NO will be used as inputs into the ion-kinetic formulations (see Table IV):

a) Meira's (1971) observational profile of nitric oxide.

b) Photochemical scaling of Meira's observation to winter values based on a mean winter temperature profile (USSAS, 1966).

TABLE IV

PROFILES OF NITRIC OXIDE USED IN ION-KINETIC CALCULATIONS

ALTITUDE (km)	EXPERIMENTAL MEIRA [NO](cm^{-3})	MEIRA - MODIFIED SUMMER [NO](cm^{-3})	MEIRA - MODIFIED WINTER [NO](cm^{-3})
50		(3.5×10^9)	(1.8×10^9)
55		(2.3×10^9)	(10^9)
60		(1.24×10^9)	6.3×10^8
65		(4.64×10^8)	8.5×10^8
70	7×10^7	5.9×10^7	5.3×10^8
75	3.5×10^7	7.8×10^6	2.96×10^8
80	2×10^7	5.3×10^5	1.42×10^8
85	1.5×10^7	7.9×10^4	3.74×10^7
90	3×10^7	5.4×10^5	8.41×10^7
95	6×10^7	(2.53×10^7)	(9.67×10^8)
100	10^8	(2.14×10^7)	(3.19×10^8)

c) Photochemical scaling of Meira's observation for summer values based upon summer temperature profiles (USSAS, 1966).

4. Primary Production of O_2^+, N_2^+ and NO^+

Calculations of primary ionization have been made in the usual manner (Whitten and Poppoff, 1971, Nicolet and Aiken, 1960) for summer and winter 60°N atmospheres (USSAS, 1966) and solar zenith angles of 0, 20, 40, 60, 80° with a 'quiet sun'. Nitrogen ionization is computed using fluxes of x-rays (1-8Å) and galactic cosmic rays (GCR). Oxygen ionization includes those wavelengths plus Lyβ (1027Å), CIII (977Å) and the ionization of $O_2(^1\Delta g)$ by 1027-1118Å (SiIII at 1108Å) using an $O_2(^1\Delta g)$ profile of Paulsen et al. (1972) with the O_2 densities taken from high latitude summer or winter. Absorption by CO_2 is taken into account in producing the following expression for O_2^+ production:

$$q(O_2^+) = [O_2(^1\Delta g)]\ .549 \times 10^{-9} \exp(-2.406 \times 10^{-20}[O_2]\cdot H) + 2.614 \times 10^{-9} \exp(-8.508 \times 10^{-20}[O_2]\cdot H). \quad (3\text{-}33)$$

As pointed out by Reid (1971), the knowledge of the degree of the ionization of O_2 relative to that of NO is crucial to the solution of D-region chemistry even more than knowledge of correct water vapor distribution. Consequently, the whole UV spectrum from Lyβ (1025.7Å) to x-rays was checked for further contributions to primary production for O_2 and N_2. Aside from Lyβ (1027Å) and CIII(977Å) there was no appreciable contribution from 910-1000Å (UV) or the extreme ultraviolet

(EUV) range of 100-30Å. Lyα (1215.7Å) and x-ray fluxes (2,4,8Å), absorption and photoionization cross sections (DNA, 1972, Swider, 1969, Nicolet and Aiken, 1960) are tabulated in Appendix III and graphed to compare dependence on solar activity. The quiet solar flux of 3×10^{11} photon cm^{-2} sec^{-1} at zero optical depth corresponds to a radiant energy of 5.17 ergs cm^{-2} sec^{-1} and an ionization rate coefficient of 6×10^{-7} sec^{-1} for Lyα. In Appendix III are listed flux, energy, absorption cross section, ionization efficiency, and photoionization cross section for CIII(977Å) and Lyβ (1025.7Å) based upon DNA (1972) and Yonezawa (1966). Calculation of ionization due to galactic cosmic rays (GCR) is based directly upon an ionization rate coefficient (IRC) = 1.7×10^{-17} sec^{-1} (Nicolet and Aiken, 1960) with no absorption or solar zenith angle dependence.

Primary production values which are presented in Appendix III and graphed in Figure III-4a,b are entered directly into ion-kinetic calculations of the computer programs POSCHEM and DUSTCHEM.

Formulation:

$$q(NO^+) = \phi_{Ly\alpha} \cdot \sigma^i_{Ly\alpha}(NO)[NO]\exp\left(-\tau_{Ly\alpha} \mathrm{Sec}\chi \right) + \sigma^i_{GCR}[NO] \tag{3-34}$$

$$q(O_2^+) = \phi_{2\text{Å}} \cdot \sigma^i_{2\text{Å}}(O_2)[O_2]\exp\left(-\tau_{2\text{Å}} \mathrm{Sec}\chi \right)$$

$$+ \phi_{4\text{Å}} \cdot \sigma^i_{4\text{Å}}(O_2)[O_2]\exp\left(-\tau_{4\text{Å}} \mathrm{Sec}\chi \right)$$

$$+ \phi_{6\text{Å}} \cdot \sigma^i_{6\text{Å}}(O_2)[O_2]\exp\left(-\tau_{6\text{Å}} \mathrm{Sec}\chi \right)$$

$$+ \phi_{977\text{Å}} \cdot \sigma^i_{977\text{Å}}(O_2)[O_2]\exp\left(-\tau_{977\text{Å}} \mathrm{Sec}\chi \right)$$

$$+ \phi_{1025\mathring{A}} \cdot \sigma^{i}_{1025.7\mathring{A}} (O_2)[O_2]\exp\left(-\tau_{1025.7\mathring{A}} \mathrm{Sec}\chi\right)$$

$$+ \phi_{GCR} \cdot \sigma^{i}_{GCR} (O_2)[O_2]$$

$$+ [O_2(^1\Delta g)] \times .549 \times 10^{-9} \exp[-2.406 \times 10^{-20}[O_2]\cdot H]$$

$$+ 2.614 \times 10^{9} \exp[-8.508 \times 10^{-20}[O_2]\cdot H] \qquad (3\text{-}35)$$

$$q(N_2^+) = \phi_{2\mathring{A}} \cdot \sigma^{i}_{2\mathring{A}} (N_2)[N_2]\exp\left(-\tau_{2\mathring{A}} \mathrm{Sec}\chi\right)$$

$$+ \phi_{4\mathring{A}} \cdot \sigma^{i}_{4\mathring{A}} (N_2)[N_2]\exp\left(-\tau_{4\mathring{A}} \mathrm{Sec}\chi\right)$$

$$+ \phi_{6\mathring{A}} \cdot \sigma^{i}_{6\mathring{A}} (N_2)[N_2]\exp\left(-\tau_{6\mathring{A}} \mathrm{Sec}\chi\right)$$

$$+ \phi_{GCR} \cdot \sigma^{i}_{GCR} (N_2)[N_2]. \qquad (3\text{-}36)$$

5. Dust and Dust Attachment

Sampling experiments by Hemenway, Soberman and Witt (1964), Witt et al. (1963), and Soberman et al., (1964) in noctilucent clouds (NLC) strongly suggest, but do not prove, the existence of micrometeorites capable of serving as ice condensation nuclei (Reiter, 1971). Optical radar measurements by Fiocco and Gramms (1969) indicated scattering layers around 80 km. More recently, Donahue (1972), by means of OGO-6 satellites, has observed a large "polar cap" of scatterers in the mesopause which reach a maximum concentration at very high latitudes during summer, a characteristic similar to the observed distribution of noctilucent clouds. He rules out pure sodium or oxygen airglow as the

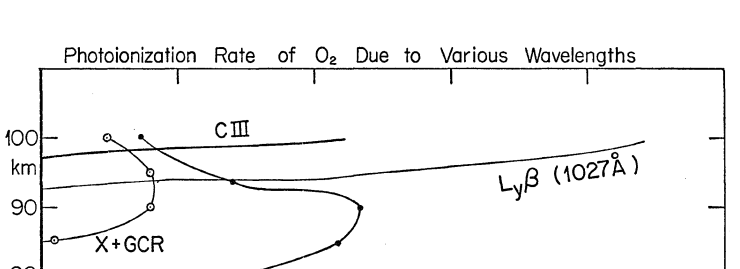

Figure III-4a.

Photoionization Rate of O_2^+ derived from various radiations: Lyβ (1027A) and CIII (977A) and Ionization of $O_2(^1\Delta g)$ via Paulson et al. (1972).

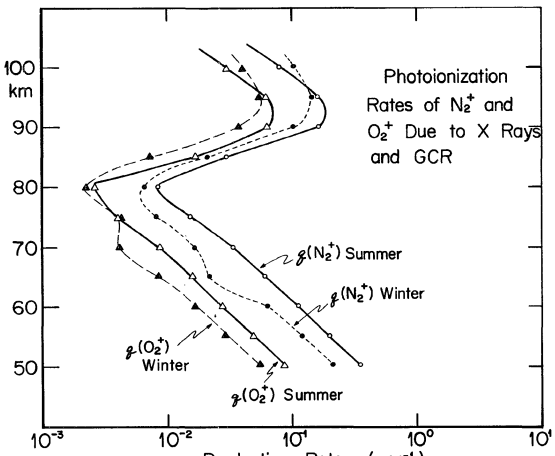

Figure III-4b.

Plot of Photoionization Rates of N_2^+ and O_2^+ due to standard radiations: X-rays, and galactic cosmic rays for solar zenith angles of 0° and 60° for summer and winter atmospheres.

source and believes that the layer consists of particulate scatterers. However, no positive identification as particulates is possible by this method. Photometric measurements of scattering at .57μ in the twilight sky by Divari (1964) lead to a determination of the concentrations and height distributions of the scatterers from 40-135 km. As in the reduction of other scattering measurements, an assumption must be made of scattering cross-section and scattering coefficient. Comparison of the intensity of dust and air molecule scattering at 40-60 km permits an estimation of absolute concentrations and size distribution to be made with the following result:

$$N(a)da = 1.3 \times 10^{-7} a^{-3} \cdot da \quad \text{for } a > .05\mu \tag{3-38}$$

$$= 10.4 \times 10^{-4} da \quad \text{for } a < .05\mu \tag{3-39}$$

in the altitude range of 40-135 km. Whipple (1961) believes the dust source is interplanetary and is the same as that which causes the zodiacal light. On the other hand there is no data which rules out the possibility of a terrestrial source such as volcanic eruptions. Further reviews of these topics may be found in Reiter (1971).

One possible effect of a flux of dust is that it serves as a sink for electrons. In partial reflection radio studies of mesospheric electron density, attachment to dust has been invoked to provide requisite high values of the effective recombination coefficient, α_{eff} (see Mitra, 1968, for a review). The same effect has been attributed to ice particulates by some (Chesworth and Hale, 1974) in order to ex-

plain the high statistical correlation between positive conductivity and temperature.

Since 1965, ion-kinetic models of the D-region which have included attachment of electrons or positive ions to mesospheric dust have not been reported in the literature. The charging of small dust particles had been explored, however, by Natanson (1960) who derived analytic expressions for the rate of capture of ions and electrons. Ionospheric dust particles, mostly of interstellar origin, are generally negatively charged. The capture of positive ions occurs through direct Coulomb attraction, and the capture cross section of positive ions should exceed geometric cross section. Electrons and negative ions have a reverse problem: In order to be captured they must possess sufficient thermal energy to advance to within a distance where the positive (attractive) image potential will begin to exceed the repulsive Coulomb potential. Parthasarathy and Rai (1966) extended Natanson's (1960) formulation to derive a coefficient for ion-dust attachment. Their original treatment is amended by Parthasarathy (1976) who reformulates the problem in terms of a) a probability distribution of the number of charges expected on dust particles at certain ambient electron densities and b) formal incorporation of electron release by photoelectric emission. The net result of this calculation is that the presence of dust (1-10 cm^{-3}, $r_D \approx .01\mu$) is estimated to decrease the degree of ionization at the mesopause at low electron densities ($N_e < 200\ cm^{-3}$). The specific capture rates of electrons or positive ions, ν_z^- and ν_z^+, for given

ambient electron densities are depicted in Figure III-5a, b (Partha-sarathy's (1976) Figure 5 and 6). The attachment coefficients, D, are computed with the aid of Figure 5 and the formula,

$$D = \frac{\nu_z^+}{N_i^+} = \frac{\nu_z^- - \nu_p}{N_e} \quad \text{and Figure 6.} \tag{3-39}$$

A plot of D vs. particle size for electron density $N_e = 200\ cm^{-3}$ is given in Figure III-6. For ion-kinetic computations, a value of $D = 2 \times 10^{-6}\ cm^3\ sec^{-1}$ was used which corresponds with a dust radius of $\sim$ .015μ. Formal inclusion of dust attachment is through the term

$$-\left[\int_0^\infty N_D(a)\ D\ da\right]\left[xy^+\right] \text{ for positive ions } xy^+ \tag{3-40}$$

and

$$-\left[\int_0^\infty N_D(a) \cdot D \cdot da\right]\left[N_e\right] \text{ for electrons, } N_e. \tag{3-41}$$

Since the value of the integral of the size distribution function for dust will be dominated by the very much larger dust population at the lower limit (smaller radius), for use in calculations it is permissable to replace the integral by the number density of the dust of the size of the lower radius limit. This is equivalent to a flux, ϕ_D, of $10\ cm^{-2}\ sec^{-1}$ for dust of radius .01μ (Parthasarathy, 1976).

In each run of the DUSTCHEM computer program values of the downward flux of dust will be used as the primary entry, namely:

$$0,\ 1.0, \text{ and } 10.0\ cm^{-2}\ sec^{-1}.$$

Each of these flux values must be converted into a dust concentration,

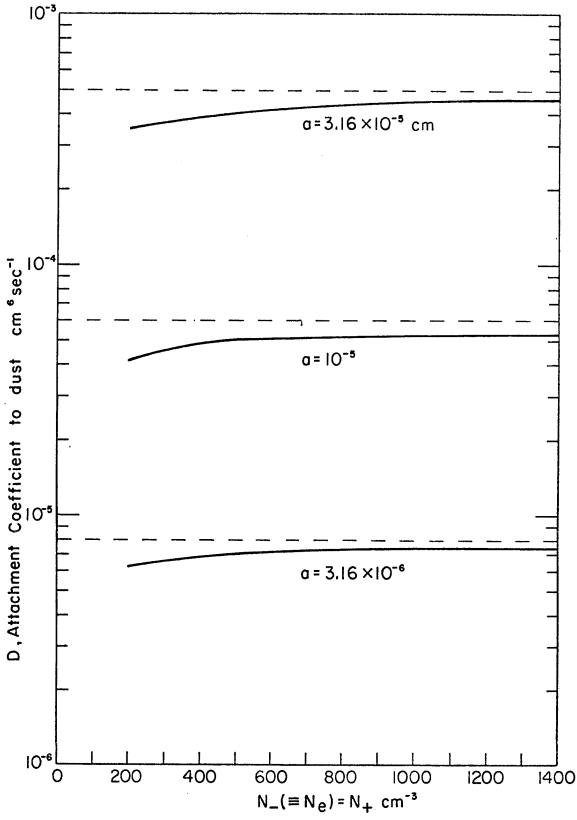

Figure III-5a.

The coefficient D of attachment to dust ((cm^6 sec^{-1}) continuous curves). The dashed lines represent the limiting values of D when photoelectric emission is neglected.

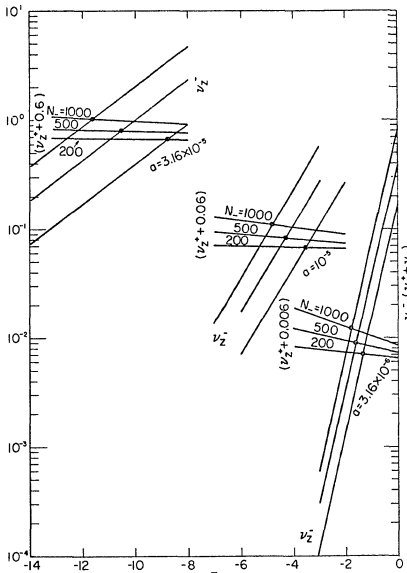

Figure III-5b.

A formulation for the calculation of the D coefficients, essentially that of Parthasarathy and Rai (1965). Three sets of lines, for $a = 3.16 \times 10^{-5}$, $a = 10^{-5}$, and $a = 3.16 \times 10^{-6}$ cm, may be recognized. For each set, three electron densities are considered, N = 200,500, and 1000 cm^{-3}. The approximately horizontal lines in each set depict $(\nu_z^+ + \nu_0)$ (i.e., the rate at which a dust particle is driven less negative), and the slanted lines depict ν_v^- (i.e., the rate at which it is driven more negative by electron capture). The intersection points in each set, shown as filled circles, represent the equilibrium values of $(\nu_z^+ + \nu_p)$ and ν_z^-, from which the D coefficients may be derived through $D = \nu_z^+/N_+ = \nu_z^+/N_-$.

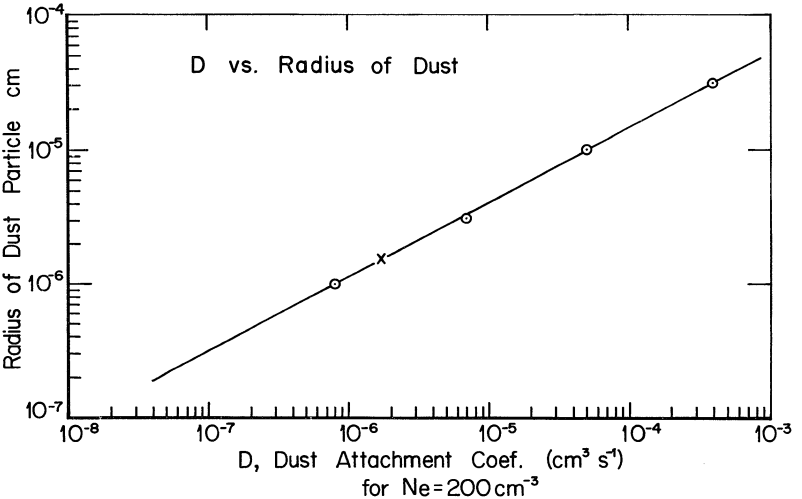

Figure III-6.

Plot of dust attachment coefficient, D, against radius of dust particles.

n_D, at each height level.

$$n_D = \frac{\phi_D}{W_D} \cdot \tag{3-42}$$

The Stokes fall velocity, W_D, of a particle is given by

$$W_D = \frac{-rd\beta}{[N_2]} , \tag{3-43}$$

where d = dust density ($\sim$ 3 gm cm^{-3}) ,

$[N_2]$ = ambient number density,

$\beta = 6.01 \times 10^{20}$.

Only .015μ dust will be used in DUSTCHEM since this matches the calculations in Chapter IV. For this radius D = 2×10^{-6} cm^3 sec^{-1} from Figure III-6. Hence, the specific entry at each level will be

$-n_D \cdot 2 \times 10^{-6} \cdot [xy^+]$ for positive ion xy^+

or

$-n_D \cdot 2 \times 10^{-6} \cdot [N_e]$ for electron attachment.

6. POSCHEM and DUSTCHEM Computations

A. Characteristics of the Model

In order to test the sensitivity and become familiar with the behavior of this ion-kinetic reaction set, various input parameters to the model were varied and the resulting changes in electron density noted:

a) Temperature Sensitivity. Without changing the number density of NO (whose production rate is temperature sensitive) the rate constants for the positive-ion reactions were allowed to vary according to their

temperature dependence. The minor result is shown in Figure III-7, and, hence, temperature is considered a negligible factor.

b) Nitric Oxide Sensitivity. Meira's (1971) experimental value was changed by a factor of 10, and the resulting change in electron density is graphed in Figure III-8. The drastic degree of control of NO concentration upon electron density is apparent. Variations in NO of a factor of 10 produce changes in Ne of 2.87. The actual NO profiles used were discussed earlier in this chapter.

c) Lyα Flux Sensitivity. A variation of Lyα flux between 3 and 6 ergs cm^{-2} sec^{-1} produces a change in electron density of 45% at the 80 km level. The control works via the ionization of NO, the principle electron donor. A value of Lyα of 5.17 ergs cm^{-2} sec^{-1} is used in subsequent calculations in this report (Figure III-9).

d) Solar Zenith Angle Sensitivity. The large control of solar zenith angle, χ, due to a change in atmospheric attenuation for Lyα is shown for $\chi = 0°$ to $\chi = 75°$ in Figure III-10. To more or less match parameters in existing rocket shots and fit high latitude conditions a constant solar zenith angle of 60° will be used in calculations.

B. Water Vapor Profiles

A full discussion of water vapor observations, photochemistry and diffusion profiles will be presented in Chapter IV. For the present purpose of making ion-kinetic calculations the profiles so derived will be presented without explanation (see Figure III-11). Table Va,b lists these concentrations for vertical drifts of W_o = 0, +1, +2.5 +5 cm sec^{-1} for summer and W_o = 0, -1, -2.5 cm sec^{-1} for winter. The drift

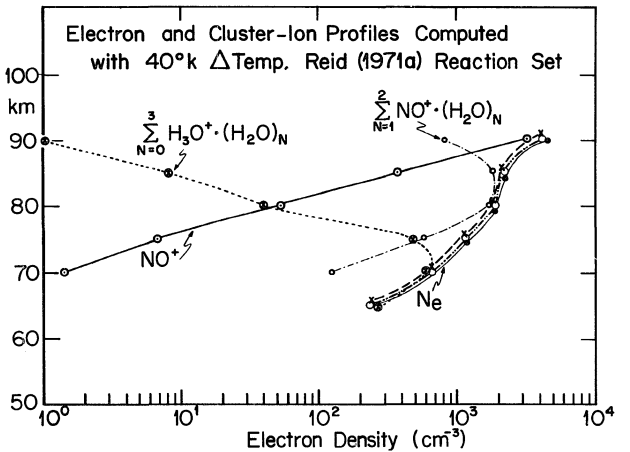

Figure III-7.

Profiles of total electron density computed from the ion-kinetic reaction set under conditions of a 40° variation in temperature. Backward reactions and changes in NO concentrations due to neutral chemical reactions are not included. It is apparent that the temperature variation in the forward rate constants are negligible.

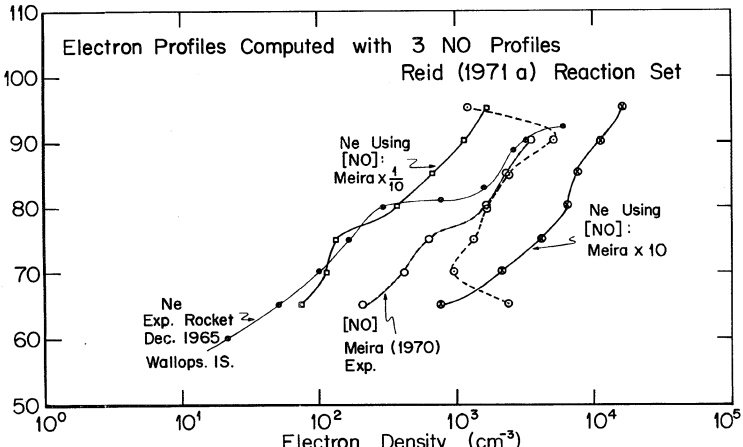

Figure III-8.

Meira's (1970) experimental NO profile was varied up and down by a factor of 10 and the results used as input to the ion-kinetic computations. The sensitivity to this change is extreme and variations of a factor of 10 in NO modify the electron concentration profile by a factor of 2.87.

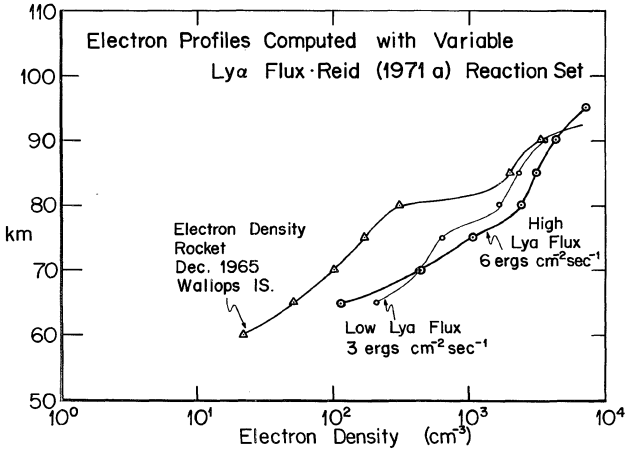

Figure III-9.

Lya incident flux is varied from 3 to 6 ergs cm^{-2} sec^{-1}, a range which brackets commonly accepted values. An increase of flux by a factor of 2 increases the electron density by a factor of .45 at 80 km.

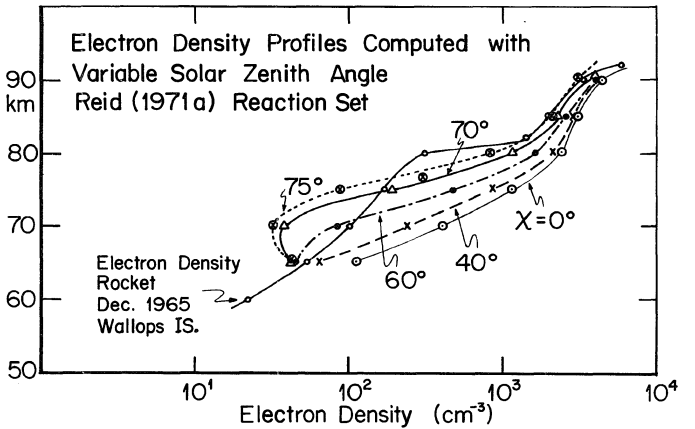

Figure III-10.

Solar zenith angle control of electron density. Variations in electron concentration profiles are extreme with change of a factor of .15 for each 10° change in χ. For ion-kinetic calculations at high latitudes a χ of 60° is appropriate.

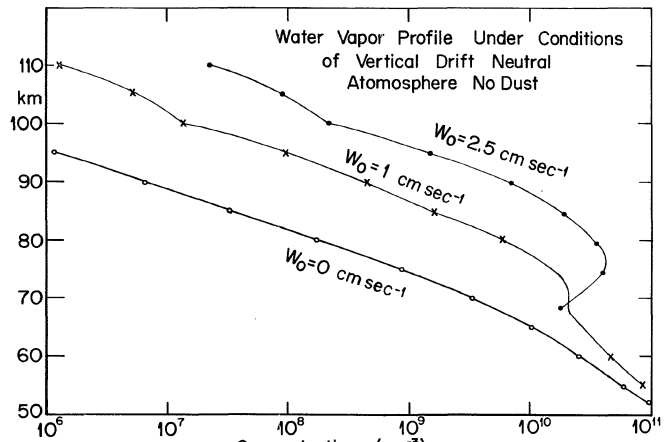

Figure III-11.

Water vapor profiles at mesospheric altitudes computed under the action of upward diffusion and a drift of the neutral atmosphere $W_o = 0, 1, 2.5$ cm sec^{-1}. The designated drift has a peak value set at 70 km altitude tapering off to 0 at 120 km.

TABLE Va

NUMBER DENSITIES (cm^{-3}) AND MIXING RATIOS (MR) OF WATER VAPOR

UNDER CONDITIONS OF VERTICAL DRIFT OF NEUTRAL ATMOSPHERE, SUMMER 60° N

DATE OF RUN:	9/29/76		9/9/76 TS		9/9/76 TS		9/26/76 T2	
Vertical Drift of Neutral Atmosphere ($cm\ sec^{-1}$)	0		+1		+2.5		+5	
Altitude (km)		MR ppm		MR ppm		MR ppm		MR ppm
100	$1.56x10^{5}$	.02	$1.36x10^{7}$	1.47	$2.22x10^{8}$	24.14	$3.48x10^{9}$	378.4
95	$1.14x10^{6}$	.04	$9.74x10^{7}$	3.78	$1.52x10^{9}$	58.88	$2.22x10^{10}$	864.3
90	$6.51x10^{6}$	.09	$4.52x10^{8}$	6.28	$7.00x10^{9}$	97.19	$6.82x10^{10}$	947.3
85	$3.31x10^{7}$	.17	$1.65x10^{9}$	8.46	$1.76x10^{10}$	90.13	$7.58x10^{10}$	387.8
80	$1.73x10^{8}$	.33	$5.94x10^{9}$	11.21	$3.21x10^{10}$	60.62	$5.03x10^{10}$	94.88
75	$8.71x10^{8}$	.77	$1.58x10^{10}$	13.98	$3.62x10^{10}$	32.06	$2.83x10^{10}$	25.06
70	$3.35x10^{9}$	1.40	$2.08x10^{10}$	8.66	$1.83x10^{10}$	7.63	$1.48x10^{10}$	6.16
65	$1.02x10^{10}$	2.33	$2.67x10^{10}$	6.12	$2.60x10^{10}$	5.96	$2.46x10^{10}$	5.64
60	$2.58x10^{10}$	3.27	$4.66x10^{10}$	5.90	$4.57x10^{10}$	5.79	$4.28x10^{10}$	5.42
55	$5.96x10^{10}$	4.16	$8.46x10^{10}$	5.90	$8.12x10^{10}$	5.66	$7.44x10^{10}$	5.19
50	$1.30x10^{11}$	4.98	$1.54x10^{11}$	5.91	$1.43x10^{11}$	5.49	$1.29x10^{11}$	4.97
45	$2.73x10^{11}$	5.11	$2.92x10^{11}$	5.46	$2.74x10^{11}$	5.13	$2.56x10^{11}$	4.78
40	$5.68x10^{11}$	5.16	$5.81x10^{11}$	5.28	$5.57x10^{12}$	5.06	$5.24x10^{11}$	4.77
35	$1.20x10^{12}$	5.44	$1.19x10^{12}$	5.43	$1.15x10^{12}$	5.23	$1.08x10^{12}$	4.89
30	$2.53x10^{12}$	5.76	$2.47x10^{12}$	5.61	$2.36x10^{12}$	5.37	$2.18x10^{12}$	4.95

TABLE Vb

NUMBER DENSITIES (cm^{-3}) AND MIXING RATIOS (MR) OF WATER VAPOR

UNDER CONDITIONS OF VERTICAL DRIFT OF THE NEUTRAL ATMOSPHERE. WINTER 60°N

DATE OF RUN: Vertical Drift of Neutral Atmosphere ($cm\ sec^{-1}$)	9/29/76 TW 0		9/29/76 TW -1		9/29/76 TW -2.5	
Altitude (km)		MR ppm		MR ppm		MR ppm
100	1.65×10^{6}	.12	3.07×10^{3}	.00	.483	.00
95	5.86×10^{6}	.18	1.13×10^{4}	.00	1.87	.00
90	2.05×10^{7}	.28	4.26×10^{4}	.00	7.91	.00
85	6.77×10^{7}	.45	1.63×10^{5}	.00	3.75×10	.00
80	2.43×10^{8}	.78	7.42×10^{5}	.00	2.39×10^{2}	.00
75	8.80×10^{8}	1.44	3.95×10^{6}	.01	2.17×10^{3}	.00
70	2.78×10^{9}	2.32	2.40×10^{7}	.02	3.12×10^{4}	.00
65	7.5×10^{9}	3.23	2.49×10^{8}	.11	1.58×10^{6}	.00
60	1.82×10^{10}	4.02	1.60×10^{9}	.36	3.82×10^{7}	.01
55	3.97×10^{10}	4.68	7.42×10^{9}	.87	5.23×10^{8}	.06
50	8.32×10^{10}	5.2	2.78×10^{10}	1.73	4.68×10^{9}	.29
45	1.76×10^{11}	5.49	8.98×10^{10}	2.81	2.95×10^{10}	.92
40	3.74×10^{11}	5.85	2.59×10^{11}	4.04	1.39×10^{11}	2.17
35	8.00×10^{11}	6.33	6.87×10^{11}	5.43	5.27×10^{11}	4.17
30	1.70×10^{12}	6.81	1.71×10^{12}	6.84	1.71×10^{12}	6.84

maximizes at 70 km and decreases linearly to 0 by 120 km and decreases exponentially below.

C. Positive-Ion and Electron Density Profiles

Ion-kinetic calculations of positive-ion densities utilizing the water vapor concentrations from Table Va,b will be presented in this section.

a) W_o = 0, cm sec^{-1} Winter (#106) and Summer (#109). X = 60° (Figures III-12,13)

The effect of enhanced water vapor on the positive-ion concentrations is presented in curves #106 and #109 (Figures III-12, III-13). Included in the primary production is the contribution to $q(O_2^+)$ by Lyβ and CIII and the ionization of $O_2(^1\Delta g)$ (Huffman et al., 1971). The winter profiles (Figure III-12) are considerably different from experimental observations: Hydrated water clusters are almost non-existent and are clearly outnumbered by $NO^+ \cdot H_2O$; electron density at 80 km is 3000 cm^{-3} which is more than ten times the summer values. The main ledge in electron density occurs at the altitude of about 73 km, almost 10 km lower than the ledge altitude for summer. These high electron densities are due to the high concentration of NO obtained in winter as a result of scaling Meira's (1971) experimental NO value upward for the higher temperature. Primary production of NO^+ is increased proportionately with a resulting increase of $NO^+ \cdot H_2O$. In addition, insufficient water exists to bleed this off and establish a pathway to hydrated water clusters. The sharp dip of O_2^+ at 95 km to values of less than 10 cm^{-3} is a common feature of these profiles in

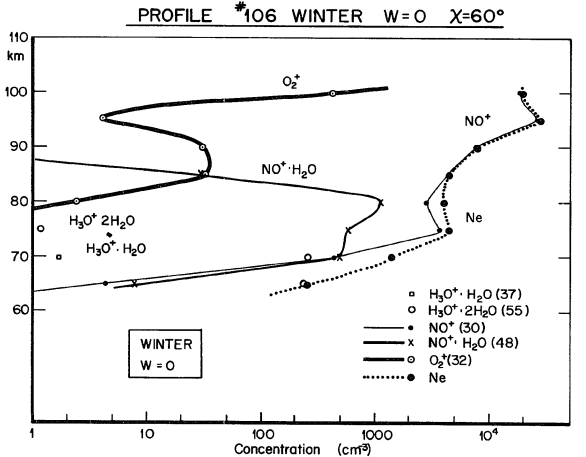

Figure III-12.

Profile #106. Plot of profile of the main positive-ion species and electron density for winter and under conditions of no updraft W = 0 cm sec^{-1}. NO^+ and N_e are excessive and the ceiling is low due to a high NO concentration. Primary production of O_2^+ includes contributions from Lyβ, CIII, X and GCR.

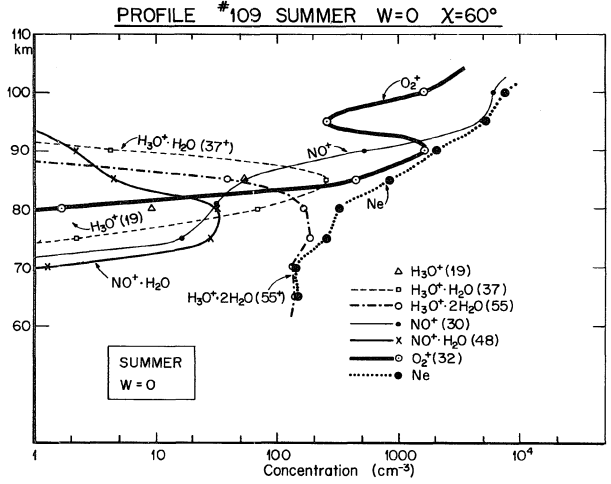

Figure III-13.

Profile #109. Same basic input as Figure III-12 but summer 60°N atmosphere and NO modified for temperature. Updraft W_o = 0 cm sec^{-1}.

both seasons and has been experimentally observed in a number of rocket shots (Appendix I, Reference 3).

The relative abundance of positive ions under summer conditions with no drift (#109) is remarkable in that a large population of hydrated water cluster-ions are present and dominate nitric oxide clusters. It should be noted, however, that no clearly defined ceiling on cluster-ions exists. $H_3O^+ \cdot H_2O$ (37^+) has a ceiling at 87 km and $H_3O^+ \cdot 2H_2O$ (55^+) has a ceiling some 4 km lower at 83 km. The electron density has dropped to an experimentally observed value of a few hundred per cm^3 at 80 km with the ledge present at 80 km. The drop in concentration of O_2^+ at 95 km is again present and would not vary using the Paulson et al. (1972) expression for $q(O_2^+)$ which is derived from $O_2(^1\Delta g)$ ionization.

b) W_o = 1 cm sec^{-1} Summer (#111). Figure III-14

This ion profile, with an updraft of the neutral atmosphere of W_o = 1 cm sec^{-1}, is not too different from that due to W_o = 0 cm sec^{-1} case for summer, (#109), Figure III-13. The same predominance of hydrated water clusters over nitric oxide clusters holds with a broad high ceiling at 88 km. The increase of water vapor at 80 km from $[H_2O]$ = 2 x 10^9 cm^{-3} to 3.5 x 10^{10} cm^{-3}, a factor of 17, does not appreciably affect the overall pattern of the ion profiles. The predominance of water clusters is due, therefore, primarily to the low values of NO^+ primary production: This depletes the NO^+ clustering to form hydrates and may be considered a tradeoff influence with that of water. The details of this type of cross control will be investigated

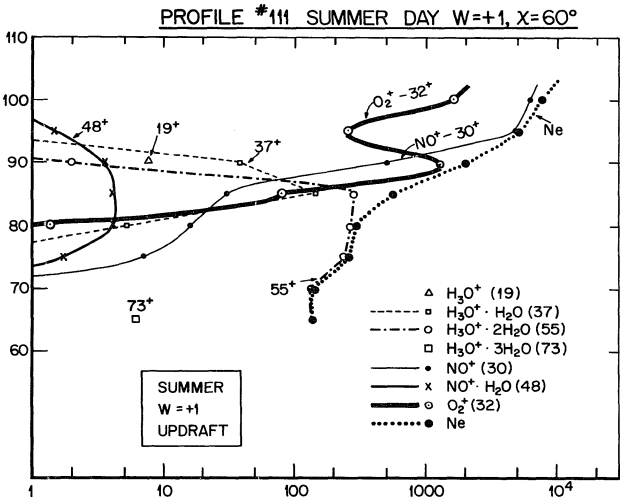

Figure III-14.

Profile #111. Same basic input as Figures III-12 and III-13 but with an upward drift W_o = 1 cm sec^{-1} into a summer 60°N mesosphere.

in the next section by means of the Flow Rate Diagrams (FRD).

c) W_o = 1 cm sec^{-1} Summer (#121). Figure III-15

In this profile all parameters are identical to those in #111 with the exception of the use of a contribution to $q(O_2^+)$ from a modified value of $O_2(^1\Delta g)$ from Paulson et al., (1972). The net result of this change is to increase the electron density slightly at 85 km from 567 cm^{-3} to 1112 cm^{-3} due to the doubling of $q(O_2^+)_{85}$ from .81 sec^{-1} to 1.6 sec^{-1} and increase $[H_3O^+ \cdot H_2O]$ from 141 to 389 cm^{-3}. All other features are very similar to profile #111, and electron density at 80 km has a computed value of a few hundred cm^{-3}.

In general, these profiles, #109, 111, 121, successfully match those determined experimentally by in situ observations. That is:

1) Hydrated water cluster ions outnumber nitric oxide hydrated clusters below the electron density ledge.

2) $H_3O^+ \cdot H_2O$ (37^+) and $H_3O^+ \cdot 2H_2O$ (55^+) are the most numerous of the water cluster ions.

3) O_2^+ and NO^+ achieve dominance only above the ledge.

4) Electron density values at 80 km are about 300 cm^{-3}.

The fact that the no drift (W_o=0) situation produced an acceptable ratio of $\Sigma H_3O^+ \cdot (H_2O)_n / \Sigma NO^+ \cdot (H_2O)_n$ (Profile #109 in Fig. 13) is due to the strong control of a high $q(O_2^+)/q(NO^+)$ ratio on the chemistry. That is, a large amount of O_2^+ leads directly to the formation of hydrated water cluster-ions. When, however, primary production of O_2^+ is reduced relative to primary production of NO^+, then greater amounts of water vapor become necessary to form water

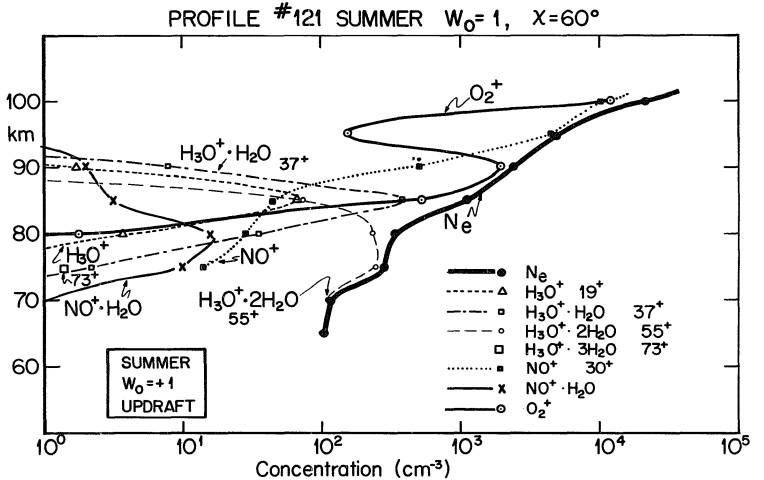

Figure III-15.

Profile #121. Same basic input as Figures III-12, III-13 and III-14 but with an upward drift of W_0 = 1 cm sec^{-1} in summer and an addition to the primary production of O_2 from the Paulson et al. (1972) ionization of $O_2(^1\Delta g)$.

cluster-ions through the route starting with NO^+.

The main deficiency of the results of these calculations is that the cluster ion ceiling is not sharp and lies around 88-90 km, a level $\sim$ 6 km higher than rocket observations have indicated. A sharper and lower ceiling for the cluster ions could be most efficiently achieved by an increase in the photodissociation rate coefficient for water, J_{H_2O}, or a sharp increase in atomic oxygen concentration. Alternate J profiles were not included in this present set of calculations, but enough uncertainty exists in the reported values in the literature to judge it a parameter which may be adjusted. J values higher by at least an order of magnitude would be required at 85-90 km in order to match in situ observations.

6D. Flow Rate Diagrams (FRD)

The purpose of a flow rate diagram (FRD) for this ion-kinetic reaction set is to examine, at a particular altitude, the strength and importance of various reactions in producing and depleting positive-ions.

The FRD depends upon data from the computer program FLOPOS: If we are interested in the behavior of the constituent A in the coupled reactions $A + B \xrightarrow{k_1} C + D$ and $E + F \xrightarrow{k_2} A + B$, then the rate of growth of A, $G = k_2[E][F]$ and the rate of loss, $L = k_1[A][B]$ may be computed for the steady state. These terms, representing net gain and loss rates and concentrations, are tabulated for a specific level of the atmosphere by the computer program FLOPOS. In the literature, flow diagrams have often been used, but only in a qualitative or

diagrammatic sense (e.g., Thomas et al., 1973, Ferguson, 1971b). Arguments about the efficiencies of various reactions have been based upon the comparative values of competing rate constants and rarely have included concentrations and third bodies in a quantatitive manner. Application of FRD at successive altitudes is an effective quantitative diagnostic tool. Not included in our diagrams is a depiction of the recombination of each positive ion with electrons.

Profile #121 Summer W_0 = 1 cm sec^{-1} Updraft
[NO] Adjusted for Temperature

1.	75 km	Fig. III-16
2.	80 km	Fig. III-17
3.	90 km	Fig. III-18

From examination of the FRD at levels of 75, 80 and 90 km certain observations about the ion-kinetics may be made which are similar.

1. The pathway through O_2^+ for the formation of H_2O hydrates is more effective than the route through nitric oxide. At 80 km the formation rate of $H_3O^+ \cdot 2H_2O$ from $NO^+ \cdot 2H_2O$ is .0419 cm^{-3} sec^{-1} while the flow from $H_3O^+ \cdot H_2O$ is .257 cm^{-3} sec^{-1}. On the other hand, at 75 km, Figure III-16 illustrates that the major water cluster producing route is via NO^+.

2. The reaction route through $H_3O^+ \cdot OH \cdot O_2$ proposed by Ferguson and Fehsenfeld (1969) may be eliminated as it never carries more than 4% of the flow.

3. Charge exchange reactions from N_2^+ to O_2^+ and O_2^+ to NO^+ are of negligible consequence.

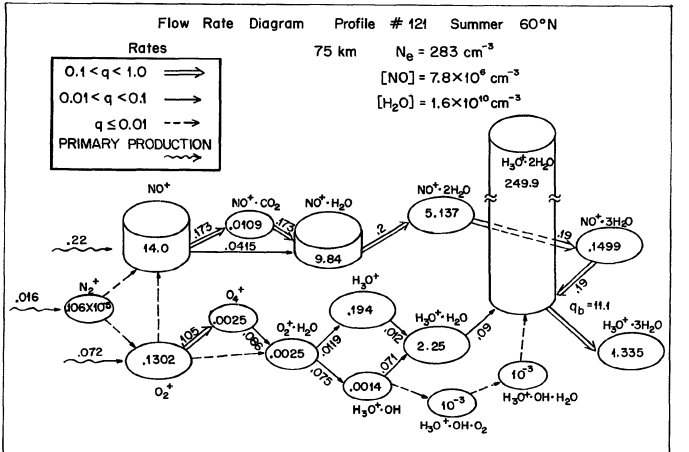

Figure III-16.

Flow rate diagram (FRD) in which the steady state concentrations are presented pictorially by a "drum" and the strength of each connecting reaction by the thickness of the arrow. This figure presents steady state results for 75 km, summer 60°N and a H_2O profile due to our updraft of +1 cm sec^{-1} based upon Profile #121.

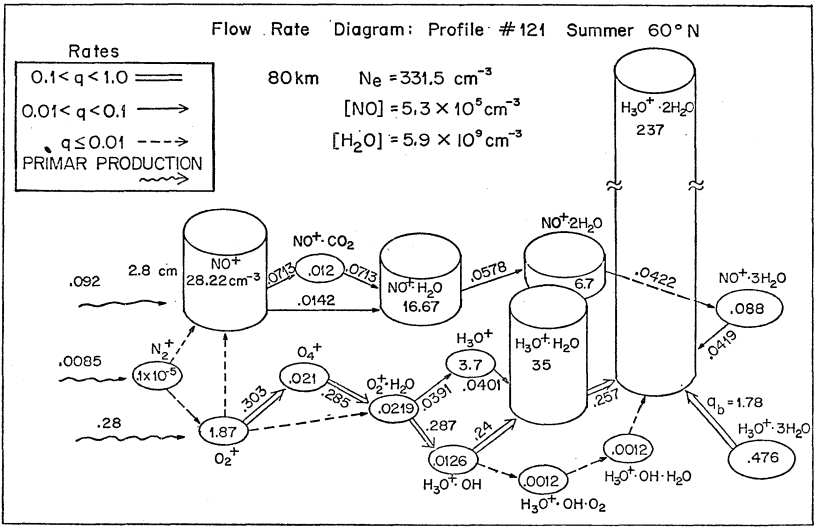

Figure III-17. Flow Rate Diagram based upon profile #121 at the 80 km level.

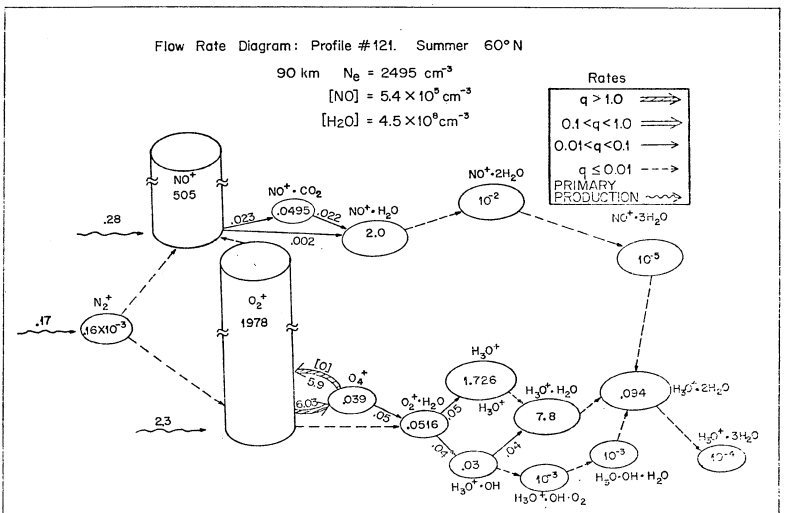

Figure III-18. Flow Rate Diagram based upon profile #121 at the 90 km level.

4. The reaction route to build $H_3O^+ \cdot H_2O$ is stronger by a factor of ten when going via $H_3O^+ \cdot OH$ than a direct hydration of H_3O^+. There is some uncertainty in the literature about the value of the rate constants for these important bottom pathway reactions since the current range of values could permit a shift in the concentration of hydrated clusters by a factor of ten. Variations in the values of these critical rate constants are as follows: For the reaction $O_2^+ \cdot H_2O + H_2O \rightarrow H_3O^+ + OH + O_2$, the rate constants range among: 3×10^{-10} cm^3 sec^{-1}, Kebarle (1970) and Fehsenfeld (1971); 1.2×10^{-10} cm^3 sec^{-1}, Ferguson (1970); and 1.9×10^{-9} cm^3 sec^{-1}, Reid (1971). For the branch reaction $O_2^+ \cdot H_2O + H_2O \rightarrow H_3O^+ \cdot OH + O_2$, the rate constants range among: 9×10^{-10}, Kebarle (1970); 1.9×10^{-9} Fehsenfeld (1971); and $1.2 - 3.0 \times 10^{-9}$, Ferguson (1970).

5. The reaction route to hydrated clusters via O_4^+ to $O_2^+ \cdot H_2O$ is 300 times stronger at 80 km than direct hydration of O_2^+.

6. The back reactions (eg. $H_3O^+ \cdot 3H_2O$ reverting to $H_3O^+ \cdot 2H_2O$) are a significant (and temperature dependent) factor in building lower order clusters at the expense of higher ones.

Comparisons of FRD's at 75, 80 and 90 km show the control which water vapor has in bleeding off the O_2^+ on the bottom pathway. $[O_2^+] = 1978$ cm^{-3} at 90 km since the key ingredient required further along the bottom pathway (which is lacking) is water. At 90 km, the existence of appreciable atomic oxygen reconverts O_4^+ to O_2^+ and successfully

truncates the lower chain. This is in accord with the suggestion of Fehsenfeld and Ferguson (1972). At 90 km NO^+ is plentiful since the chain effectively terminates at that point due to a lack of water.

7. The Effect of Dust

A. Programming Procedure

For each run of the program DUSTCHEM three flux values of .015μ dust were entered: 0, 1.2 and 12 cm^2 sec^{-1}. The number density, n_D, of dust was computed for each level:

$$n_D = \frac{\phi_D}{W_D - W} \tag{3-47}$$

where W_D = descent speed of dust relative to the earth's surface, W is neutral atmosphere updraft and ϕ_D is the flux of dust. The dust recombination coefficient, α_D, was given by

$$\alpha_D = (.2 \times 10^{-5}) \cdot n_D, \tag{3-48}$$

where $.2 \times 10^{-5}$ is the recombination coefficient from Parthasarathy (1976) for .015μ dust at electron densities of less than $\approx$ 200 cm^{-3}. For each altitude in the DUSTCHEM program the three successive values of dust flux (concentrations) are entered and the corresponding values of positive ions computed. The electron densities with or without dust are listed in the next three tables along with the percent change in the effective recombination coefficient, α_{eff}, caused by the inclusion of the dust. Limitations upon the choice of minimum dust radius and

TABLE VIa

RESULTS OF ION-KINETIC CALCULATIONS INCLUSING A FLUX OF DUST

Profile #109: Summer 60°N $W_o = 0$

Downward Flux of Dust = 1.2 (cm^2 sec^{-1})
Radius of Dust = .015μ
Single Dust Attachment Coefficient = .2 x 10^{-5}(cm^3 sec^{-1})

Z	$n_D(cm^{-3})$	$N_e(cm^{-3})$	α_D	α_{eff}	$\%\Delta\alpha_{eff}$
65	0	141.1	0	$.3804x10^{-5}$	
	1.98	140.0	$.3958x10^{-5}$	$.3804x10^{-5}$	
	19.79	135.7	$.3958x10^{-4}$	$.4080x10^{-5}$	7%
70	0	140.0	0	$.3807x10^{-5}$	
	1.05	139.5	$.2094x10^{-5}$	$.3807x10^{-5}$	
	10.47	137.3	$.2094x10^{-4}$	$.3956x10^{-5}$	4%
75	0	247.9	0	$.3887x10^{-5}$	
	.52	247.6	$.1038x10^{-5}$	$.3887x10^{-5}$	
	5.19	247.1	$.1038x10^{-4}$	$.3946x10^{-5}$	1.5%
80	0	314.0	0	$.3271x10^{-5}$	
	.24	313.9	$.4703x10^{-6}$	$.3271x10^{-5}$	
	2.35	312.8	$.4703x10^{-5}$	$.3271x10^{-5}$	
85	0	856.3	0	$.1193x10^{-5}$	
	.09	856.2	$.1793x10^{-6}$	$.1193x10^{-5}$	
	.90	855.1	$.1793x10^{-5}$	$.1193x10^{-5}$	
90	0	2129.0	0	$.4561x10^{-6}$	
	.03	2129.0	$.6398x10^{-7}$	$.4561x10^{-6}$	
	.32	2128.0	$.6398x10^{-6}$	$.4561x10^{-6}$	
95	0	5113.0	0	$.7306x10^{-6}$	
	.01	5113.0	$.2227x10^{-7}$	$.7306x10^{-6}$	
	.11	5113.0	$.2227x10^{-6}$	$.7306x10^{-6}$	
100	0	7687.0	0	$.6647x10^{-6}$	
	0	7687.0	$.8182x10^{-8}$	$.6647x10^{-6}$	
	.04	7687.0	$.8182x10^{-7}$	$.6647x10^{-6}$	

TABLE VIb

RESULTS OF ION-KINETIC CALCULATIONS INCLUDING A FLUX OF DUST

Profile #111: Summer 60°N, W_o = +1 cm sec^{-1}

Downward Flux of Dust = 1.2 cm^2 sec^{-1}
Radius of Dust = .015μ
Single Dust Attachment Coefficient = .2 x $10^{-5}cm^3$ sec^{-1}

Z	$n_D(cm^{-3})$	$N_e(cm^{-3})$	α_D	α_{eff}	$\%\Delta\alpha_{eff}$
65	0	139.5	0	$.3814x10^{-5}$	
	17.57	135.5	$.3515x10^{-4}$	$.4097x10^{-5}$	7%
	175.7	101.5	$.3515x10^{-3}$	$.7225x10^{-5}$	89%
70	0	139.2	0	$.3829x10^{-5}$	
	9.3	137.0	$.1860x10^{-4}$	$.3973x10^{-5}$	4%
	93.0	116.9	$.1860x10^{-3}$	$.5373x10^{-5}$	40%
75	0	252.2	0	$.3744x10^{-5}$	
	.85	251.7	$.1700x10^{-5}$	$.3744x10^{-5}$	
	8.5	250.6	$.1700x10^{-4}$	$.3832x10^{-5}$	2.3%
80	0	297.7	0	$.3635x10^{-5}$	
	.278	297.5	$.5578x10^{-6}$	$.3635x10^{-5}$	
	2.78	296.2	$.5578x10^{-5}$	$.3635x10^{-5}$	
85	0	567.4	0	$.2695x10^{-5}$	
	.0945	567.4	$.1891x10^{-6}$	$.2695x10^{-5}$	
	.945	567.7	$.1891x10^{-5}$	$.2707x10^{-5}$	
90	0	2032.	0	$.5017x10^{-6}$	
	.0325	2031.	$.6502x10^{-7}$	$.5017x10^{-6}$	
	.325	2030.0	$.6502x10^{-6}$	$.5017x10^{-6}$	
95	0	5114.-	0	$.7310x10^{-6}$	
	.0119	5114.-	$.2238x10^{-7}$	$.7310x10^{-6}$	
	.119	5114	$.2238x10^{-6}$	$.7310x10^{-6}$	
100	0	7693.	0	$.6645x10^{-6}$	
	.004	7693.	$.8193x10^{-8}$	$.6645x10^{-6}$	
	.0409	7693.	$.8193x10^{-7}$	$.6645x10^{-6}$	

TABLE VIc

RESULTS OF ION-KINETIC CALCULATIONS INCLUDING A FLUX OF DUST

Profile #106: Winter 60°N $W_o = 0$

Downward Flux of Dust = 1.2 cm^2 sec^{-1}
Radius of Dust = .015μ
Single Dust Attachment Coefficient = .2 x 10^{-5} cm^3 sec^{-1}

Z	$n_D(cm^{-3})$	$N_e(cm^{-3})$	α_D	α_{eff}	$\%\Delta\alpha_{eff}$
65	0	255.5	0	$.3814x10^{-5}$	
	1.02	256.1	$.2041x10^{-5}$	$.3848x10^{-5}$	< 1%
	10.21	253.7	$.2041x10^{-4}$	$.3920x10^{-5}$	3%
70	0	1349.	0	$.3564x10^{-5}$	
	.52	1349.	$.1047x10^{-5}$	$.3564x10^{-5}$	
	5.24	1348.	$.1047x10^{-4}$	$.3574x10^{-5}$	< 1%
75	0	4350.	0	$.1353x10^{-5}$	
	.27	4350.	$.5484x10^{-6}$	$.1353x10^{-5}$	
	2.74	4348.	$.5484x10^{-5}$	$.1355x10^{-5}$	
80	0	4045.	0	$.2067x10^{-5}$	
	.14	4045.	$.2769x10^{-6}$	$.2068x10^{-5}$	
	1.38	4045.	$.2769x10^{-5}$	$.2068x10^{-5}$	
85	0	4429.	0	$.7884x10^{-6}$	
	.07	4429.	$.1358x10^{-6}$	$.7884x10^{-6}$	
	.68	4428.	$.1358x10^{-5}$	$.7888x10^{-6}$	
90	0	7608.	0	. x10^{-}	
	.03	7607.	$.6425x10^{-7}$	$.7540x10^{-6}$	
	.32	7607.	$.6425x10^{-6}$	$.7540x10^{-6}$	
95	0	$.2682x10^{5}$	0	$.7502x10^{-6}$	
	.01	$.2682x10^{5}$	$.2786x10^{-7}$	$.7502x10^{-6}$	
	.14	$.2682x10^{5}$	$.2786x10^{-6}$	$.7502x10^{-6}$	
100	0	$.1920x10^{5}$	0	$.7413x10^{-6}$	
	.01	$.1920x10^{5}$	$.1216x10^{-7}$	$.7413x10^{-6}$	
	.06	$.1920x10^{5}$	$.1216x10^{-6}$	$.7413x10^{-6}$	

the relationship to neutral atmosphere updraft are discussed in Chapter IV, Section 8.

B. Calculations and Results

The profiles, #109: summer W_o = 0, #111: summer W_o = 1 and #106: winter W_o = 0, are sufficient to indicate the effect of dust (Table VIa,b,c).

The effect of dust in changing the electron density is dependent largely upon the dust concentration at the level in question and is inversely proportional to electron density. The clearest demonstration of this is found in Profile #111 (Table VIb) where the effective fall velocity of the dust is reduced due to the atmosphere updraft of 1 cm sec^{-1}, so that at 65 and 70 km the dust concentrations are calculated to be 17.57 cm^{-3}, 175.7 cm^{-3}, 9.3 cm^{-3} and 93 cm^{-3}, respectively. At 65 km, the high dust concentration of 175.7 cm^{-3} increases the effective recombination coefficient by 89% and decreases the electron density from 135 to 101 cm^{-3}, a 25% decrease. Parthasarathy (1976) and Parthasarathy and Rai (1966) state that the influence of dust is greatest at low electron densities. This occurs because at higher electron densities the recombination of positive ions, $\alpha\ N_i^+ N_e$, becomes competitive with and overrides dust attachment of positive ions. Using a reasonable range of flux values, 1.2 and 12 $cm^2\ sec^{-1}$, for .015μ dust, effects are greater than a few percent only when a vertical updraft is included. In this model the level of significant concentration of dust (> 50 cm^{-3}) lies at 65-70 km, and, hence, uncoated dust itself does not seem likely to be the agent with the necessary high recombination coefficient which

has been postulated to produce the ledge in electron density at 80 or 82 km (Reid, 1971, Ferguson and Fehsenfeld, 1969, etc.).

The dominant positive ion combining with dust is $H_3O^+ \cdot 2H_2O$ with a mass of 55. There will be no shift in the above results since the D values from Parthasarathy (1976) were devised for positive ions with a mass of 50. A reduction of these calculated values in the dust recombination coefficient by $\sim$ 30% in the real atmosphere could be expected due to photoelectric emission.

If, in the upper mesosphere, the dust could acquire an ice coating to grow to a total radius of about $\sim 10^{-5}$ cm, α_D would become 100 times greater than the α_D of uncoated dust (i.e., 10^{-4}, Figure III-6). Then the increased electron attachment to the ice crystal would considerably increase the effective recombination coefficient to values higher than those in Table VI, particularly with high dust concentration such as found in Profile #111, Table VIb. The result would be to accentuate the ledge in electron density at 80 km since this is about the level at which the ice coating would occur. As an additional factor, photoelectric emission from an ice surface is less than from dust composed of nickel or iron. Consequently, in the case of ice particles at 80 km, photoelectric reduction of the effective recombination coefficient would be minor (Parthasarathy and Rai, 1966).

In conclusion, a closer match of the model calculations with summer positive-ion profiles could be achieved through variation of some of the uncertain parameters (i.e., J and K). Furthermore, the trade-off in influence on cluster ion population of the $q(O_2^+)/q(NO^+)$

ratio with water vapor mixing ratio should be investigated for an additional set of nitric oxide profiles. Since the in situ observations of cluster profiles show similar patterns in winter and summer, if our present chemical model is correct and water vapor is correctly incorporated, then these facts suggest that a revision of our understanding of the nature of the wintertime mesosphere may be required, and that water vapor is enhanced somehow even in winter, possibly by a shallow circulation cell in the upper mesosphere which maintains an upward vertical drift at the mesopause.

Finally, the inclusion of dust layers into the ion-kinetic calculations significantly modifies the effective recombination coefficient in the 60-85 km altitudes, particularly when the dust is concentrated by a vertical updraft of the neutral atmosphere. It is highly possible that the proper dust profile could account for the sharp ledge in electron density at 80 km particularly if ice coated.

CHAPTER IV

MESOSPHERIC WATER VAPOR AND ICE CRYSTAL GROWTH

INTRODUCTION

The formulation of mesospheric water vapor in this chapter includes an upward flux of water vapor due to eddy and molecular diffusion, a vertical drift of the neutral atmosphere and ice formation upon dust particles. The observational record of water vapor will be reviewed in order to provide the basis for boundary conditions chosen in the model. The resulting water vapor profiles are used as inputs for the ion-kinetic calculations of Chapter III. Part of the discussion of this chapter concerns the interaction of water vapor and dust at the mesopause and a stipulation of the conditions under which the growth of ice crystals could be expected. In the latter sections of the chapter the observational record of noctilucent clouds and the neutral chemistry of water vapor are reviewed along with a discussion of the possibility that the circulation of the mesosphere may contain vertical components (upwelling or downwelling) located at the mesopause.

LIST OF SYMBOLS

z = vertical dimension or altitude above the surface of the earth (km)

n_v = number density of water vapor (cm^{-3})

n_s = saturated water vapor number density (cm^{-3})

n_D = dust concentration (cm^{-3})

n_i = number density of water molecules in the ice phase (either per ice crystal or per cm^3)

P = pressure (dynes cm^{-2} or Torr (=1 mm Hg))

T = Temperature (°K)

$\bar{c}$ = mean molecular velocity (cm sec^{-1})

MFP = mean free path (cm)

Δ = Fuchs Interface Distance (cm)

r = radius of ice coated dust particle (cm)

r_D = radius of dust particle (cm)

m = mass (gm)

D_v = coefficient of molecular diffusion of water vapor (cm^2 sec^{-1})

K = coefficient of eddy diffusion (cm^2 sec^{-1})

K_T = combined diffusion parameter (cm^2 sec^{-1}), ($\equiv K + D_v$)

H_v = scale height of water vapor (cm)

H = scale height of neutral atmosphere (cm)

ϕ_{V_T} = flux of vapor (cm^{-2} sec^{-1}), $= \phi_D + \phi_B$

ϕ_D = flux of vapor under action of diffusion (cm^{-2} sec^{-1}), $\phi_D = \phi_E + \phi_M$

ϕ_B = flux of vapor due to bulk drift of neutral atmosphere,

ϕ_E = flux of vapor due to eddy diffusion (cm^{-2} sec^{-1})

ϕ_M = flux of vapor due to molecular diffusion (cm^{-2} sec^{-1})

Q_v = chemical gain term for water vapor

L_v = chemical loss term for water vapor

W = velocity of the neutral atmosphere in the z-direction. Upward is positive. (cm sec^{-1})

W_v = velocity of water vapor in the z-direction (cm sec^{-1})

W_i or W_D = descent rate of ice crystal or dust (cm sec^{-1})

ρ_d = density of dust ($\equiv$ 3 gm cm^{-3})

ρ_i = density of ice ($\equiv$ 1 gm cm^{-3})

d = net density of the ice coated dust particle (gm cm^{-3})

$\mathcal{Q}$ = evaporative loss rate of water molecules from crystal

$\mathcal{Q}_s$ = evaporative loss rate of water molecules from crystal under saturated conditions

R_w = gas constant for water (= 4.646 x 10^6 erg $mole^{-1}(°K)^{-1}$)

C = "shape" factor (= 2r)

k = Boltzman's Constant (1.38 x 10^{-16} erg deg^{-1})

L = latent heat of sublimation (2834 x 10^7 erg g^{-1})

e_∞ = ambient vapor pressure (dynes cm^{-2})

e_s = saturation vapor pressure over ice at ambient temperature (dynes cm^{-2})

g = acceleration of gravity (=980 cm sec^{-2})

β = a constant ($= \frac{g}{2}\left(\frac{\pi}{2kmT}\right)^{1/2}$ = 6.01 x 10^{20} cm^2 sec^{-3})

η = a constant equal to the number of water molecules in one gm of ice (= 3.3 x 10^{22})

α_s = sticking coefficient of water molecules to a nucleus (= 1.0)

τ_c = photochemical lifetime

τ_D = diffusive-transport lifetime

1. Water Vapor Diffusion Model

A. Introduction

In this section shall be presented the basic assumptions, flux equations and boundary conditions governing the ascent of water vapor from 30 to 300 km and the formation of ice crystals. The formulation is essentially that of Parthasarathy (1974, 1975) and incorporates a variety of processes: (a) upward transport from 30 km of vapor by eddy diffusion, bulk updraft and molecular diffusion; (b) photo-dissociation of H_2O at altitudes above 60 km; (c) sublimation of the water vapor onto the descending sub-micron dust particles at the mesopause when it is cold enough, and (d) subsequent release of the vapor from the crystals as they descend into warm regions below the mesopause. The computer program is written to iterate between the processes of upward diffusion of water and ice crystal formation until a steady-state water vapor and ice crystal radius profile is achieved. Motions, forces and gradients are taken to be in the vertical direction only. Other chemical gain and loss reactions for H_2O which involve CH_4, H, H_2, OH are of second order importance to the present problem and are not included in the present formulation. An outline of the appropriate additions is assembled in Appendix V in the form in which they should be inserted into the diffusion equation.

B. Derivation of the Diffusion Equation

The continuity equation applied to a volume at a level z is

$$\frac{\partial n_v}{\partial t} + \bar{\nabla} \cdot \bar{\phi}_{v_T} = \text{source terms} \tag{4-1}$$

where $\bar{\phi}_{v_T} = \bar{\phi}_D + \bar{\phi}_B$, the total flux of water vapor, (4-2)

and where $\bar{\phi}_D = \bar{\phi}_E + \bar{\phi}_M$ is the flux of vapor due to eddy and molecular diffusion. Since we are considering transport only in the vertical direction, these vector quantities are changed to the corresponding scalar quantities. $\phi_B = n_v W$ is the flux due to the vertical component of the bulk drift of the neutral atmosphere and Q_v and L_v are chemical gain and loss terms.

For the steady-state, $\frac{\partial n_v}{\partial t} = 0$, (4-3)

and considering the Z direction only,

$$\frac{d}{dz}[\phi_D + n_v W] + Q_v - L_v = 0 \tag{4-4}$$

$$-\frac{d}{dz} \cdot \phi_D - n_v \frac{d}{dz} W - W \frac{d}{dz} n_v + Q_v - L_v = 0 \tag{4-5}$$

The diffusive flux of water vapor, under the influence of both eddy and molecular processes, is expressed as follows:

$$\phi_E = -K\left(\frac{dn_v}{dz} + \frac{n_v}{H} + \frac{n_v}{T}\frac{dT}{dz}\right) \quad \text{(Colegrove } \underline{\text{et al.}}\text{, 1965)(4-6)}$$

$$\phi_M = -D_v\left(\frac{dn_v}{dz} + \frac{n_v}{H_v} + \frac{n_v}{T}\frac{dT}{dz}\right) \text{(Chapman and Cowling, 1952) (4-7)}$$

where the terms express diffusive, hydrostatic and thermal gradient flow.

Combining,

$$\phi_E + \phi_M = \frac{dn_v}{dz}\ (-K - D_v) + \frac{n_v}{T}\frac{dT}{dz}\ (-K - D_v) + n_v\left(\frac{-K}{H} - \frac{D_v}{H_v}\right), \quad (4\text{-}8)$$

differentiating and setting $K + D_v = K_T$,

$$\frac{d}{dz}\ (\phi_E + \phi_M) = \frac{d^2 n_v}{dz^2}\ (-K_T) + \frac{dn_v}{dz}\ \frac{d}{dz}\ (-K_T) + \frac{dn_v}{dz} \cdot \frac{1}{T}\frac{dT}{dz}\ (-K_T)$$

$$+ n_v \frac{dT}{dz}\ (-K_T) \cdot \frac{-1}{T^2}\left(\frac{dT}{dz}\right) + \frac{n_v}{T}\frac{d^2T}{dz^2}\ (-K_T) + \frac{n_v}{T}\frac{dT}{dz}\frac{d}{dz}\ (-K_T)$$

$$+ \frac{dn_v}{dz}\left(\frac{-K}{H} - \frac{D_v}{H_v}\right) + n_v\ \frac{d}{dz}\ \left(\frac{-K}{H} - \frac{D_v}{H_v}\right). \quad (4\text{-}9)$$

Rearranging and setting $n_v' = \frac{dn_v}{dz}$ and $n_v'' = \frac{d^2 n_v}{dz^2}$,

$$\frac{\frac{d}{dz}\ (\phi_E + \phi_M)}{-K_T} = n_v'' + \frac{n_v'}{K_T}\left\{\frac{dK_T}{dz} + \frac{K_T}{T}\frac{dT}{dz} + \frac{K}{H} + \frac{D_v}{H_v}\right\}$$

$$+ \frac{n_v}{K_T}\left\{\frac{-K_T}{T^2}\left(\frac{dT}{dz}\right)^2 + \frac{K_T}{T}\frac{d^2T}{dz^2} + \frac{1}{T}\frac{dT}{dz}\frac{dK_T}{dz}\right.$$

$$\left. + \frac{d}{dz}\left[\frac{K}{H} + \frac{D_v}{H_v}\right]\right\}. \quad (4\text{-}10)$$

$\frac{d^2T}{dz^2} \approx 0$ since the vertical gradients of scale height and temperature change slowly with height.

$$\frac{1}{-K_T}\frac{d}{dz}(\phi_E + \phi_M) = n_v'' + n_v' \quad \frac{1}{K_T}\frac{dK_T}{dz} + \frac{1}{T}\frac{dT}{dz} + \frac{K}{K_T H} + \frac{D_v}{K_T H_v}$$

$$+ n_v \quad \frac{-1}{T^2}\left(\frac{dT}{dz}\right)^2 + \frac{1}{K_T T}\frac{dT}{dz} \cdot \frac{dK_T}{dz} + \frac{1}{K_T}\frac{d}{dz}\left[\frac{K}{H} + \frac{D_v}{H_v}\right] \qquad (4\text{-}11)$$

For convenience, let

$$a = \frac{1}{K_T}\frac{dK_T}{dz} + \frac{1}{T}\frac{dT}{dz} + \frac{1}{K_T}\left(\frac{K}{H} + \frac{D_v}{H_v}\right) \qquad (4\text{-}12)$$

$$b = -\frac{1}{T^2}\left(\frac{dT}{dz}\right)^2 + \frac{1}{K_T T}\frac{dT}{dz} \cdot \frac{dK_T}{dz} + \frac{1}{K_T}\frac{d}{dz}\left[\frac{K}{H} + \frac{D_v}{H_v}\right] \qquad (4\text{-}13)$$

Then $$-\frac{d}{dz}(\phi_E + \phi_M) = K_T(n_v'' + n_v' \cdot a + n_v \cdot b) \qquad (4\text{-}14)$$

Inserting 4-14 into 4-5 and dividing by K_T with $\phi_D = \phi_E + \phi_M$,

$$n_v'' + n_v' \cdot a + n_v \cdot b + \frac{1}{K_T}(Q_v - L_v) - \frac{W}{K_T} n_v' - \frac{n_v}{K_T} W' = 0 \qquad (4\text{-}15)$$

All that remains to bring this equation into final form is to insert the appropriate expressions for gain, Q_v, and loss, L_v, of water vapor due to condensation upon and evaporation from ice crystals and also photodissociation. The digression into the physics of growth of ice crystals follows at this point.

C. Physics of Growth of Ice Crystals

The growth of ice crystals occurs through collision and attachment of water molecules to a nucleus. In the troposphere the mean free path (MFP) of a molecule is of the order of 6×10^{-6} cm, about 16 times smaller than the dimension of a micron size nucleus particle. Any molecule moving toward the nucleus particle from a distance less than or equal to the mean free path will attach itself to the particle (assuming sticking coefficients of 1.0) and due to the existence of this attachment "sink" for water vapor molecules the number density of molecules will approach zero in the layer infinitesmally close to the surface of the nucleus. (In this discussion the loss of molecules by evaporation from the surface is ignored.) Molecules at distances greater than 1 MFP would not be able to reach the ice particle within 1 collision, and the number density at a MFP distance away would be equal to the ambient number density. Consequently, a density gradient adjacent to the particle surface would be established, and the attachment rate of vapor molecules would be governed by their diffusion down this gradient. In the mesosphere where the particle radius is far smaller than the mean free path an attachment sink cannot exist, the H_2O gradient cannot be sustained, and growth would depend only upon the ambient flux of vapor molecules times the surface area of the particle, i.e., $\frac{1}{4}[H_2O]\bar{c} \times 4\pi r^2$, and the rate of removal of latent heat.

Troposphere: MFP $<<$ r

(a) Diffusion limited growth

(b) Thermal conduction of latent heat away from the particle.

Mesosphere: MFP >> r

(a) Collisional attachment.

(b) Removal of heat by radiation (Stefan-Boltzman) and collisional "thermalization".

A detailed analysis and derivation of diffusion limited and nondiffusion limited growth is given by Wright (1961) who expresses the size of discontinuities in diffusion phenomena in terms of an interface distance Δ, of the order of the MFP, previously introduced by Fuchs (1934). Through a consideration of the rate of evaporation of molecules across an interface Δ from a water drop of radius r, he obtains expressions for the two limiting cases of evaporative loss rate, Q, of water molecules from a crystal.

When $\Delta << r$ (troposphere)

$$Q = 4\pi r D_v n_s \tag{4-16}$$

and when $\Delta >> r$ (mesosphere)

$$Q = \pi r^2 \alpha_s \bar{c} n_s \tag{4-17}$$

where D_v is the diffusion coefficient of vapor molecules through N_2 and O_2.

The net rate of growth of a crystal is equal to the rate of addition of H_2O molecules minus the loss through evaporation. By the definition of saturation vapor pressure, the rate at which molecules are lost by evaporation is exactly equal to the rate at which they are added under saturated conditions, i.e., when $n_v = n_s$: $Q_s = \pi r^2 \alpha_s \bar{c} n_s$. So net rate of growth in the mesosphere is $\pi r^2 \alpha_s \bar{c}(n_v - n_s)$ and in the troposphere

it is $4\pi r D_v(n_v - n_s)$. For the case r >> MFP, the troposphere, the expressions may be shown to be identical with those developed by Fleagle and Businger (1963) and Latham (1969) for use in standard tropospheric applications:

$$\frac{dm}{dt} = \frac{4\pi C\, D_v\, kR_w T^2 (e_\infty - e_s)}{L^2 e_s\, D_v + R_w^2\, T^2\, k} \quad \text{Fleagle and Businger (1963).} \tag{4-18}$$

In some formulations, an "analogy" of diffusive growth with electrostatic phenomena (Fleagle and Businger, 1963 and MacDonald, 1963) has been invoked to support the possibility that ice crystals may grow in diverse shapes: needles, flakes, etc. This analogy was applied primarily in the troposphere but an assumed similarity with the physics of growth of crystals for the mesosphere had led some to the (unfounded) hope of growing needle shapes in the mesosphere so that one large and visible dimension ($\gtrsim$ 1300Å) could be produced at the cost of but little ambient vapor or so that a slower rate of fall of a needle would occur (Reid, 1974). Unfortunately, it may be shown that with collisional growth a needle shaped nucleus will end up more or less 'spherical' (length = diameter) (Parthasarathy, 1976, private communication).

The geometry of the ice crystal formed upon a dust core is shown below.

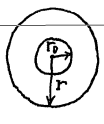

The net density of the ice crystal, d, is given by:

$$d = \frac{\frac{4}{3}\pi r_D^3 \cdot 3 + \frac{4}{3}\pi(r^3 - r_D^3) \cdot 1}{\frac{4}{3}\pi r^3} = 1 + \frac{2r_D^3}{r^3} . \qquad (4\text{-}19)$$

The descent rate (Stokes) of crystals or dust is expressed as

$$W_D = \frac{grd}{2[N_2]} \left(\frac{\pi}{2km_2\bar{r}}\right)^{1/2} \qquad (4\text{-}20)$$

$$= \frac{rd}{[N_2]} \beta \text{ where } \beta \equiv \frac{g}{2} \left(\frac{\pi}{2km_2\bar{r}}\right)^{1/2} = 6.01 \times 10^{20} \text{ gm}^{-1} \text{ sec}^{-1}$$

or $$W_D = \frac{r\beta}{[N_2]} \left(1 + \frac{2r_D^3}{r^3}\right). \qquad (4\text{-}21)$$

Since the accessible quantity in the literature is the flux of dust rather than the concentration, a conversion should be available, namely,

$$\phi_D = n_D \cdot W_D \qquad (4\text{-}22)$$

or $n_D = \frac{\phi_D}{W_D}$ where n_D really refers now both to dust or ice coated dust. The change in descent rate as the dust becomes ice coated is managed through a change in the value of d, the net density.

The rate of loss of water vapor from the environment to a single ice crystal is

$$\left.\frac{dn}{dt}\right|_{\substack{\text{single} \\ \text{crystal}}} = \pi r^2 \alpha_s \bar{c}(n_s - n_v). \qquad (4\text{-}23)$$

If η_D is the volume concentration of dust particles,

$$\left.\frac{dn}{dt}\right|_{\substack{\text{volume}\\(cm^{-3})}} = \pi r^2 \alpha_s \bar{c}\, n_D(n_s - n_v). \tag{4-24}$$

$$= \pi r^2 \alpha_s \bar{c}\, \frac{\phi_D}{W_D}(n_s - n_v). \tag{4-25}$$

$$= \frac{\pi r\, \alpha_s \bar{c} \phi_D (n_s - n_v)[N_2]}{\beta \cdot d}. \tag{4-26}$$

This expression is to be inserted into the diffusion equation for water vapor as the gain /loss term due to ice crystal growth.

The number of water molecules on an ice crystal is:

$$n_i = \frac{4}{3}\pi (r^3 - r_D^3)\rho_i \cdot \eta, \tag{4-27}$$

Differentiating with respect to time,

$$\left.\frac{dn_i}{dt}\right|_{\substack{\text{single}\\\text{particle}}} = 4\pi r^2 \rho_i \cdot \eta \frac{dr}{dt}. \tag{4-28}$$

But since r = r(z), z = z(t) and r = r(z(t)),

$$\frac{dr}{dt} = \frac{dr}{dz} \cdot \frac{dz}{dt} = \frac{dr}{dz} \cdot W_D. \tag{4-29}$$

So $$\frac{dn_i}{dt} = 4\pi r^2 \rho_i \cdot n \frac{dr}{dz} \cdot W_D \cdot \tag{4-30}$$

But from the earlier discussion the net rate of gain or loss of water molecules upon a crystal is

$$\left.\frac{dn_i}{dt}\right|_{\substack{\text{single}\\ \text{particle}}} = \pi r^2 \alpha_s \bar{c}(n_v - n_s) \cdot \tag{4-31}$$

Equating these last two expressions and rearranging,

$$W_D \cdot \frac{dr}{dz} = \frac{\alpha_s \bar{c}(n_v - n_s)}{4 \cdot \rho_i \cdot n} , \tag{4-32}$$

$$\frac{dr}{dz} = \frac{\alpha_s \bar{c}(n_v - n_s)}{4\eta\rho_i} \cdot \frac{-[N_2]}{rd\beta} , \tag{4-33}$$

$$r \frac{dr}{dz} = \frac{\alpha_s \bar{c}(n_v - n_s)}{4\eta\rho_i} \cdot \frac{-[N_2]}{d\beta} , \tag{4-34}$$

Considering that crystal growth starts at a level z_0 with a radius r_0,

$$\int_{r_0}^{r} r\, dr = \int_{z_0}^{z} \frac{-\alpha_s \bar{c}(n_v - n_s)}{4\eta\rho_i \beta d} [N_2] dz \tag{4-35}$$

and $$r^2 - r_0^2 = \frac{-\alpha_s \bar{c}(n_v - n_s)}{4\eta\rho_i \beta d} [N_2(z)](z - z_0). \tag{4-36}$$

In the computer program, DIFRAD 13, this expression is evaluated downward in steps of 1 km from an initial level z_0 thus allowing density d and $N_2(z)$ to be treated as a constant at each step, taking the value at z_0. Since the change of radius is computed from a higher (z_0) to lower (z) altitude, $z - z_0 < 0$ so $z - z_0 = -\Delta z$.

$$r^2 = r_0^2 + \frac{\alpha_s \bar{c}(n_v - n_s)}{4\eta\rho_i \beta d} N_2(z_0)\Delta z. \tag{4-37}$$

If

$$A \equiv \frac{\alpha_s \bar{c}(n_v - n_s)N_2(z_0)\Delta z}{2\beta\eta\rho_i} \tag{4-38}$$

and $\rho_i = 1$

$$r^2 = r_0^2 + \frac{A}{2(1 + \frac{2r_D^3}{r_0^3})} . \tag{4-39}$$

This reckons the stepwise increase or decrease of the radius of the ice crystal r(z) at a level z referent to its value r_0 at the level Δz above and is the expression used to compute the radius profile.

D. Inclusion of Ice Crystal Gain and Loss Terms into the Diffusion Equations

Q_v: Rate of increase of ambient vapor by evaporation from crystals:

$\pi r^2 \alpha_s \bar{c} n_D n_s$

L_v: a) Rate of loss of ambient water molecules through condensation:

$\pi r^2 \alpha_s \bar{c} n_D n_v$

b) Rate of loss of ambient water molecules due to photodissociation:

$J n_v$

$$\text{Net gain } Q_v = \pi r^2 \alpha_s \bar{c}\, n_D n_s \tag{4-40}$$

$$\text{Net loss } L_v = \pi r^2 \alpha_s \bar{c} n_D n_v + J n_v . \tag{4-41}$$

Inserting into Eqn. 4.15, and rearranging,

$$n_v'' + n_v'(a - \frac{W}{K_T}) + n_v \left(b - \frac{\pi r^2 \alpha_s \bar{c} n_D + J + \frac{dW}{dz}}{K_T} \right) + \frac{\pi r^2 \alpha_s \bar{c} n_D n_s}{K_T} = 0 \tag{4-42}$$

This is the fundamental equation for water vapor diffusion which, after it is put in finite difference form, must be coupled with equation 4-39 through the r^2 term. For flexibility in inputs to the computer program the dust concentration, n_D, has not been expressed in terms of flux, ϕ_D. This expression may be abbreviated with further substitutions.

$$\ell = \frac{J + \pi r^2 \alpha_s \bar{c}\, n_D + dW/dz}{K_T} \tag{4-43}$$

$$c = \frac{\pi r^2 \alpha_s \bar{c}\, n_D n_s}{K_T} \quad . \tag{4-44}$$

The final expression is:

$$n_v'' + n_v' (a - \frac{W}{K_T}) + n_v(b - \ell) = -c . \tag{4-45}$$

E. Linearization Procedure

The finite difference expressions for n_v'' and n_v' may be written:

$$n_v' \Big|_m = \frac{n_{m+1} - n_m}{\Delta z} \tag{4-46}$$

$$n_v'' \Big|_m = \frac{n_{m-1} - 2n_m + n_{m+1}}{(\Delta z)^2} \tag{4-47}$$

The finite difference form of the diffusion equation, (4-45) is:

$$\frac{n_{m-1} - 2n_m + n_{m+1}}{(\Delta z)^2} + \frac{(n_{m+1} - n_m)}{\Delta z}\left(a - \frac{W}{K_T}\right) + n_m(b - \ell) = -c, \tag{4-48}$$

which simplifies to

$$n_{m-1} + n_m\left[(b-\ell)(\Delta z)^2 - \Delta z\left(a - \frac{W}{K_T}\right) - 2\right] + n_{m+1}\left[1 + \left(a - \frac{W}{K_T}\right)\Delta z\right] = -c(\Delta z)^2 \tag{4-49}$$

which is the fundamental recurrent relationship.

This expands as a linear array

m = 0

$$n_{-1} + n_o\left[(b-\ell)(\Delta z)^2 - \Delta z\left(a - \frac{W}{K_T}\right) - 2\right] + n_1\left[1 + \left(a - \frac{W}{K_T}\right)\Delta z\right] = -c(\Delta z)^2 \tag{4-50}$$

m=1

$$n_o + n_1\left[(b-\ell)(\Delta z)^2 - \Delta z\left(a - \frac{W}{K_T}\right) - 2\right] + n_2\left[1 + \left(a - \frac{W}{K_T}\right)\Delta z\right] = -c(\Delta z)^2 \tag{4-51}$$

$m = 2$

$$n_1 + n_2[(b-\ell)(\Delta z)^2 - \Delta z(a - \frac{W}{K_T}) - 2] + n_3[1 + (a - \frac{W}{K_T})\Delta z] = -c(\Delta z)^2 \tag{4-52}$$

$m = M-1$

$$n_{M-2} + n_{M-1}[(b-\ell)(\Delta z)^2 - \Delta z(a - \frac{W}{K_T}) - 2] + n_M[1 + (a - \frac{W}{K_T})\Delta z] = -c(\Delta z)^2 \tag{4-53}$$

$m = M$

$$n_{M-1} + n_M[(b-\ell)(\Delta z)^2 - \Delta z(a - \frac{W}{K_T}) - 2] + n_{M+1}[1 + (a - \frac{W}{K_T})\Delta z] = -c(\Delta z)^2. \tag{4-54}$$

For the solution of the equations from level $m = 0$ through $m = M$, number density boundary values would be applied at levels Δz above the level $m = 0$ and Δz below the level $m = M$. Specifically, the upper boundary condition number density is assigned to n_{-1}, the lower boundary condition number density is assigned to n_{M+1}, and these values are entered directly at the start of running the program.

To allow for a flux boundary condition to be applied at a level Δz above $m = 0$ we have:

$$\text{Total Flux, } \phi_{V_T} = n_v W_v + n_v W = -K_T \frac{dn_v}{dz} + n_v W \tag{4-55}$$

$$\text{At level m: } \phi_m = -K_T \left[\frac{n_m - n_{m-1}}{\Delta z}\right] + n_m \cdot W_m \tag{4-56}$$

$$\frac{-\phi_m(\Delta z)}{K_T} = n_m - n_{m-1} + \frac{n_m \cdot W_m(\Delta z)}{K_T} \tag{4-57}$$

For level m = 0 $\frac{-\phi_o(\Delta z)}{K_T} = n_o - n_{-1} + \frac{n_o \cdot W_o}{K_T}(\Delta z)$ (4-58)

$= n_o[1 + \frac{W_o}{K_T}(\Delta z)] - n_{-1}$ (4-59)

Outward flux ϕ_o is (+) if dn_v/dz is (-) or $n_o - n_{-1} < 0$

K_T and $z_m - z_{m-1} = \Delta z$ are always (+). $n_o < n_{-1}$.

or $n_{-1} = n_o[\frac{W}{K_T}(\Delta z) + 1] + \frac{\phi_o \Delta z}{K_T}$ (4-60)

Only the first equation of the array is modified to eliminate n_{-1} and it becomes:

$$n_o[\frac{W}{K_T}(\Delta z) + 1] + \frac{\phi_o \Delta z}{K_T} + n_o[(b-\ell)(\Delta z)^2 - \Delta z(a \frac{W}{K_T}) - 2] + n_1[1 + (a - \frac{W}{K_T})\Delta z] = -c(\Delta z)^2 \quad (4\text{-}61)$$

or

m = 0

$$n_o[(b-\ell)(\Delta z)^2 - \Delta z(a - \frac{2W}{K_T}) - 1] + n_1[1 + (a - \frac{W}{K_T})\Delta z] = -c(\Delta z)^2 - \frac{\phi_o \Delta z}{K_T} \quad (4\text{-}62)$$

Subsequent terms are the same as before:

m = 1

$$n_o + n_1[(b-\ell)(\Delta z)^2 - \Delta z(a - \frac{W}{K_T}) - 2] + n_2[1 + (a - \frac{W}{K_T})\Delta z) = -c(\Delta z)^2 \quad (4\text{-}63)$$

F. Minimum Step Size in the Linearization Procedure

The question which must be considered here is: What is the maximum allowable step size, Δz, for accurate results? Since the finite difference expressions are representations of a Taylor expansion of the derivatives, n" and n', the remainder of a Taylor expansion is:

$$\text{Taylor Expansion } n'' = \text{Finite Diff Form} + \frac{h^2}{12} n'''' \tag{4-64}$$

where $\frac{h^2}{12} \frac{d^4 n_v}{dz^4} \equiv$ error of the method (Kantorovich and Krylov, 1964), p. 202).

In the D-region n_v is a slowly varying function of z:

$$n_v = n_{v_o} e^{-\alpha z} \tag{4-65}$$

$$\frac{d^4 n_v}{dz^4} = n_{v_o} \alpha^4 e^{-\alpha z} \tag{4-66}$$

With a nominal scale height of H = 5 x 10^5 cm

$$\frac{d^4 n_v}{dz^4} = \frac{n_{v_o}}{125 \times 5 \times 10^{20}} e^{-\alpha z} \tag{4-67}$$

when Δz = 1 km = 10^5 cm.

$$\text{Error} \leq \frac{10^{10}}{12} \cdot \frac{n_{v_o}}{625 \times 10^{20}} = 1.33 \times 10^{-14} n_v. \tag{4-68}$$

But $n_v \cong 10^9$ cm^{-3} at 80 km so the error of this linearization for a step size of 1 km is 1.33 x 10^{-5}.

An acceptable criterion for use of this procedure would be that the error is one percent of n_y'' or less, so that

$$\frac{\text{Error}}{\frac{d^2 n_y}{dz^2}} = .01, \tag{4-69}$$

$$= \frac{\alpha^2 h^2}{12} = \frac{1}{H^2} \frac{(\Delta z)^2}{12}, \tag{4-70}$$

$$\Delta z = \left(\frac{H^2}{100} \cdot 12\right)^{1/2} = \frac{H}{10}\sqrt{12}, \tag{4-71}$$

or $\Delta z = .346H.$

Hence, to have an error of less than 1% of the expansion of the 2nd derivative of the finite difference equation the maximum step size should not exceed about one-third of the scale height. The Runge-Kutta method which is frequently used has the advantage that the step size may be changed at any level in the calculation and, hence, conserves computer time and money. The problem with the present linearization procedure is that step size must be fixed beforehand. If the step size halves, the time and cost quadruple. It turned out that in some runs where a very sharp ledge of water vapor was found and the scale height H_y was << 1 km, the programming financial budget restricted step sizes to large increments which blurred the features. In actual practice, Δz was set = 1 km which satisfied the above criterion and revealed most of the major diffusion features. On some runs a Δz = .3 km was used.

G. DIFRAD 13 Computer Program

The linearized equation for upward diffusion of water vapor and radius growth is solved by program DIFRAD 13 in the following manner:

A simple diffusion profile for water vapor, $n_v(z)$, is first obtained by means of a subroutine SIMQ (see Appendix VI) which solves the matrix formed from the linearized 2nd order diffusion equation for water vapor, equations (4-61) through (4-63). Based upon the input temperature profile the saturated water vapor number density, $n_s(z)$, is computed for each altitude step. Values from this pair of profiles are entered into the radius equation, (4-39), at each altitude. If $n_s < n_v$ (supersaturation) an increment of growth takes place on the ice particle, and the total radius increment is computed by starting at the upper altitude and summing downward as the ice crystal descends. Simultaneously, local ambient water vapor number density is depleted. When $n_s > n_v$ at the low altitude edge of the supersaturated region, the ice crystal will evaporate at a rate proportional to $n_s - n_v$ and enrich the local atmosphere in water vapor. These stepwise increments in the number of water molecules due to condensation or evaporation from ice crystals are entered next as gain or loss terms for a second solving of the diffusion equation. From this a second pair of n_v and n_s profiles is computed as input into the radius growth expression to perturb the first radius growth profile. This modified radius growth profile is then the basis for the next local depletion and enrichment terms for water vapor. This exchange occurs up to the maximum number of iterations which is set beforehand. It is possible to follow the convergence

process by plotting the successive water vapor and radius profiles. In most cases, around 6 iterations are satisfactory for each profile to converge for a step size Δz = 1 km.

The program, DIFRAD 13, is executed from any remote console tied into the University of Alaska Honeywell 60/6000 computer system. The remote consoles are interactive so that all boundary parameters of the problem are entered each time DIFRAD 13 is run. They are the following:

SEASONAL ATMOSPHERE AND TEMPERATURE PROFILE
UPPER BOUNDARY ALTITUDE
LOWER BOUNDARY ALTITUDE
STEP SIZE IN KILOMETERS
DOWNWARD FLUX OF DUST
AVERAGE DUST CORE RADIUS IN MICRONS
STICKING COEFFICIENT
VERTICAL DRIFT AT 70 KM OF NEUTRAL ATMOSPHERE
UPPER BOUNDARY CONDITION: FLUX OF WATER VAPOR
LOWER BOUNDARY CONDITION: NUMBER DENSITY OF WATER VAPOR
MAXIMUM NUMBER OF ITERATIONS

2. Inputs to the Model.

A. Boundary Conditions

a). Review of Water Vapor Observations in the Mesosphere and Stratosphere.

Direct measurements of water vapor at altitudes in and above the stratosphere are rare. Currently, the most extensive and reliable series of high altitude measurements (100 mb) are those of Mastenbrook (1968) who finds a "dry" stratosphere with average mixing ratios of 2-3 ppm (part per million). These data are generally more reasonable and

reproduceable than those of Sissenwine et al. (1968) reporting 17 ppm at 25 km, an altitude at which nacreous clouds are encountered, or Gutnick (1962) whose abnormally high values of 100 ppm at 30 km may be due to balloon outgassing. Reiter (1971) presents detailed reviews of most observations. A seasonal variation is manifested by lowest mixing ratios in late winter and spring and highest values in summer (Masterbrook, 1968).

In the mesosphere two direct measurements exist: The first is that of Fedynski (1966) who measures a mixing ratio of 31 ppm at 79 km in August by means of a pair of rocket-mounted heat recorders. Fogle and Haurwitz (1966) suggest caution in accepting this measurement since it took place at the limits of sensitivity of the instrument. In the second, Byuro and Martynkevich (1973) measured the relative ion current of H_2O^+/N_2^+ by rocket-borne spectrometer flown from Hayes Is., Volgagrad and the Sahara. They found ratios of 100 ppm to 2000 ppm in winter and 200 ppm in summer and more water vapor in the Arctic than in temperate latitudes. Their results may be grossly erroneous since, as they admit, contamination through possible chemical reactions between O, H, H_2 and OH within the chamber of the mass spectrometer was a serious problem.

b). Lower Boundary Conditions (LBC)

This boundary condition will be taken as a fixed water vapor number density equal to 5 ppm at 30 km which averages values from Mastenbrook (1968) and Sissenwine (1960). On calculations using a lower boundary set at 50 km, the boundary number density used at 50 km is merely the value at 30 km exponentially reduced.

c). Upper Boundary Conditions (UBC)

This boundary condition is a flux boundary condition which is physically more sensible than a number density condition: $\phi_v = 0$. At 120 km and above (in the thermosphere) H_2O and H_2 are controlled only by transport processes and are not in photochemical equilibrium, $\tau_c > \tau_D$.

B. Drift of the Neutral Atmosphere

On the basis of the data and inferences of Murgatroyd and Singleton (1961), Leovy (1964), Hesstvedt (1971), Young and Epstein (1962) and Tohmatsu and Nagata (1963), a neutral atmosphere drift profile has been chosen of the following form:

$$W = 0 \qquad z > 120 \text{ km} \tag{4.72}$$

$$W = W_0\left(\frac{120-z}{50}\right) \qquad 70 \leq z \leq 120 \text{ km} \tag{4.73}$$

where z is in km.

$$W = W_0\, e^{\frac{-(70-z)}{H}} \qquad z \leq 70 \text{ km}. \tag{4.74}$$

A full discussion and justification of this profile will be left until Section 5 of this chapter.

C. Saturated Vapor Pressure and Number Density, n_s

The value of the saturation vapor pressure over ice is taken from the Smithsonian Meteorological Tables (1963).

Where e_i = saturated vapor pressure over ice (mb)

n_s = saturated vapor number density over ice (cm^{-3})

T = ambient temperature (°K)

T_0 = 273°K

$$\text{Log } e_i = -9.097.8 \left(\frac{T_o}{T} - 1\right) - 3.56654 \log_{10}\left(\frac{T_o}{T}\right)$$

$$+.\ 876793 \left(1 - \frac{T}{T_o}\right) + \log_{10}(6.1071) \quad . \qquad (4\text{-}75)$$

$$n_s = e_i\ (mb)/T.(1.38 \times 10^{-19}).$$

The saturated number densities and pressures in mb are listed in Appendix IV and plotted in Figure IV-1.

Figures IV-2 shows the saturated water vapor number density profiles corresponding to temperature profiles for: A) summer, extreme cold mesopause at Pt. Barrow (Theon et al., 1969), B) midway between Barrow temp and mean summer, C) Mean Summer 60°N, USSAS (1966) and water vapor profiles computed for various values of upward drift, W_o. The condition of supersaturation in the mesopause requires the intersection of one each from these two sets of curves.

D. Photodissociation and Eddy Diffusion Coefficients

Photodissociation rates for water vapor are taken from Nicolet (1971) p. 29, Figure 13. The values used as input to compute diffusion of water vapor (program DIFRAD 13) are listed in Appendix II. The eddy diffusion coefficient, K, is from Shimayaki and Liard (1972).

3. Test Runs

Initial runs of DIFRAD 13 were limited to computations of diffusion only. No neutral atmospheric drift or flux of dust was entered. The following four model parameters were varied widely in order to test the

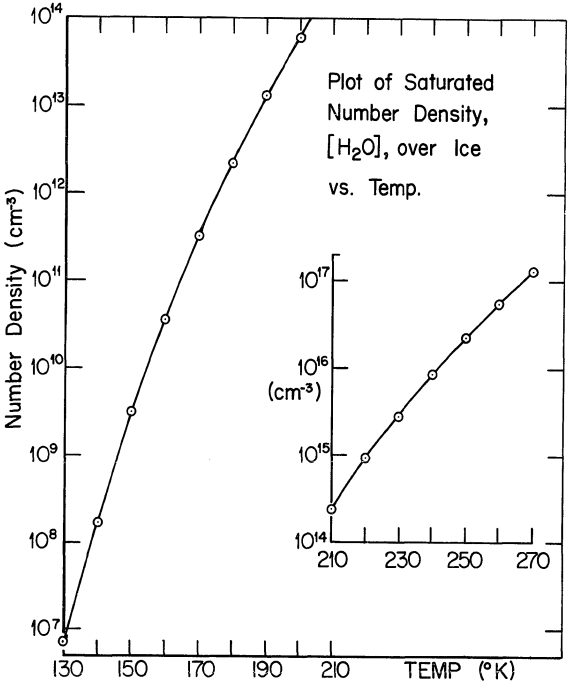

Figure IV-1

Plot of saturated number density of $H_2O(cm^{-3})$ over ice vs. absolute temperature.

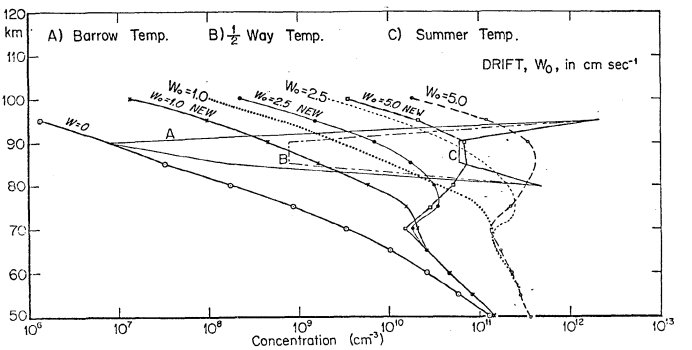

Figure IV-2

Water vapor profiles produced by diffusion and updrafts of 0, 1, and 2.5 cm sec^{-1} of the neutral atmosphere superimposed upon saturated water vapor number densities for three mesospheric temperature profiles: A) Summer: Extreme Cold mesopause of Pt. Barrow (Theon et al., 1972); B) A midway temperature profile with a minimum set to 145°K; C) Mean summer 60°N (USSAS, 1966). The profile marked "NEW" are computed with the dW/dz divergence term included in order to assess its influence by contrast with the other curves.

stability of the model and discover, if possible, shortcuts to the calculations:

a) Altitude of Upper Boundary: The flux boundary condition $\phi_v = 0$ was varied in altitude: 120, 150, 200, 250, 300 km with a fixed lower boundary condition at 30 km of $[H_2O] = 2.4 \times 10^{12}$ cm^{-3}. Figure IV-3 shows the variability of the diffusion profile plotted over the most critical range: 40-90 km. The variation is a factor of 3 which is minor.

b) Range of Both Boundaries: Sets of upper and lower bounds: 110-62, 110-30, 300-30, were applied and the results are plotted in Figure IV-4. No appreciable effect is noticeable. The curves group within 50% of each other and match closely the value of water vapor computed by Hesstvedt (1968). The purpose of this check is to estimate how close together the upper and lower bounds may be set since it would be efficient to reduce step size and focus on a particular layer without increasing cost.

c) Lower Boundary Condition Number Density Variations: On Figure IV-5 is plotted the diffusion profile with 2.4×10^{12}, 10^{13}, and 3×10^{13} cm^{-3} as number densities for the LBC at 30 km. It is obvious that the concentrations at any altitude increase and decrease in direct proportion to the lower number density. This is to be expected since at the bottom boundary is the source function for the upward diffusion of water vapor.

d) Upper Boundary Condition Flux Variations: Figure IV-6 shows the extreme control which the upper flux condition at 300 km exerts on

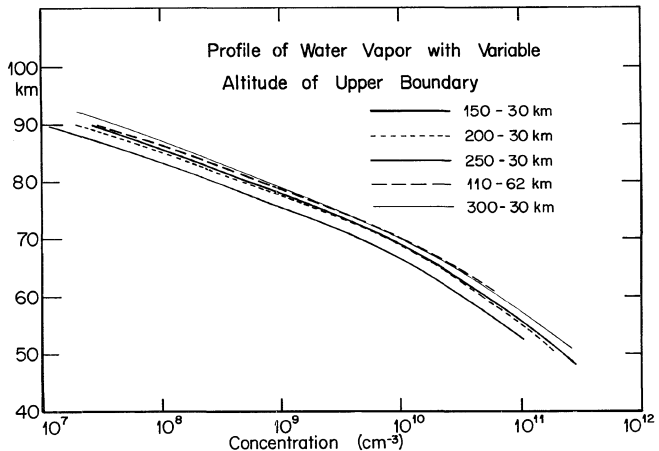

Figure IV-3

Profiles of water vapor with no neutral vertical drift or dust but with the upper flux boundary condition $\phi_i = 0$ sec at altitudes: 120, 150, 200, 250 and 300 km. Variation in the resultant profile is a minor factor of three within the critical range of 40-90 km.

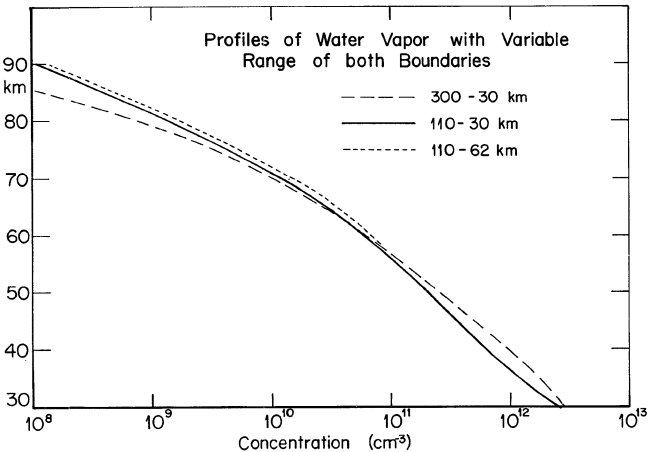

Figure IV-4

Profiles of water vapor with no neutral vertical drift or dust but with the altitudes of both boundaries varied: 110-62, 110-30, and 300-30. The curves group within 50% of each other and match the value of water vapor computed by Hesstvedt (1968).

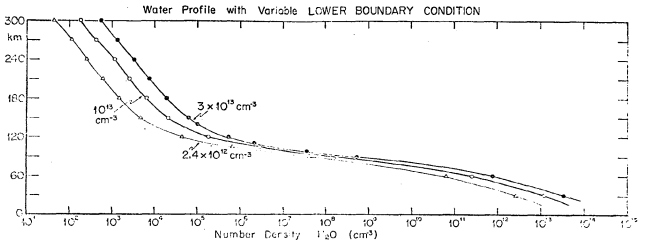

Figure IV-5

Profiles of water vapor with no neutral vertical drift or dust but with the number density (cm^{-3}) lower boundary condition varied: 2.4×10^{12}, 10^{13}, $3 \times 10^{13} cm^{-3}$. The profiles scale proportional to the lower boundary condition.

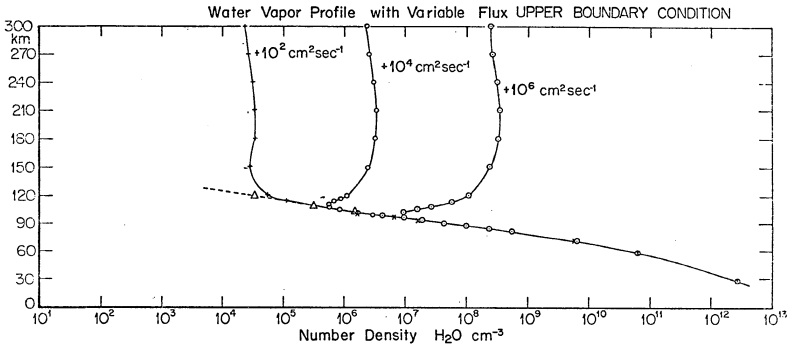

Figure IV-6

Profiles of water vapor with no neutral vertical drift or dust with the flux value of the upper boundary condition varied: 10^6, 10^4, 10^2, -10^6, -10^4, -10^2 cm^2 sec^{-1}. Control is exerted only as far down as the homopause (110 km).

the diffusion profile down to the altitude of the homopause. Flux values of $+10^6$, $+10^4$ and $+10^2$ cm^2 sec^{-1} cause the number density at 200 km to vary each by 2 orders of magnitude. Negative values of flux: -10^6, -10^4, -10^2 cm^2 sec^{-1}, which represent a downward flux of water vapor, cause the computation to fail and "blow up" because of the lack of a loss function for water. The important fact, however, is that the particular choice of a mathematically reasonable (yet possibly physically strange) upper flux condition does not vary the density profile below 100 km.

4. DIFRAD 13: Production Runs

In this section shall be presented the main results of the formulation of water vapor diffusion and coalescence upon dust. The first topic will deal with the computation of the water vapor concentration profile under various conditions of updraft of the neutral atmosphere. Second, a flux of dust will be introduced as a gain and loss term for water vapor concentration with the emphasis being placed upon the resulting perturbation of the water vapor profile. Thirdly, the characteristics of growth of the ice crystal will be examined, particularly with respect to the features of noctilucent clouds as they are presented in the literature.

A. Vapor Profiles with Variable Updraft of Neutral Atmosphere and No Dust

DIFRAD 13 was run using summer and winter 60°N latitude atmospheres and 60°N temperature profiles with neutral atmosphere drifts centered at 70 km and decreasing linearly to zero at 120 km. For each run, the following conditions applied:

Range: 110-30 km

Step Size: 1 km

Upper BC: $\phi_{H_2O} = 0$

Lower BC: $[H_2O] = 2.4 \times 10^{12}$ cm^{-3}

Iterations: 1 (since no dust is included)

Drift, W_o: 0, +1, +2.5, +5 cm sec^{-1} for summer; 0, +1, +2.5 cm sec^{-1} for winter.

The water vapor concentration for w = 0 cm sec^{-1} summer atmosphere matches the Hesstvedt (1968) profile. The results for other drifts are listed below in terms of mixing ratio in Table Va, b and graphed in Figure IV-7.

The majority of vapor profiles computed are "wetter" than previous (and untested) calculations which had served as inputs to models of neutral and positive-ion chemistry and noctilucent clouds. This unusual result requires additional verification and supporting evidence. The extreme difficulty of direct water vapor measurement raises the interesting question of whether in situ sampling of positive ions and the success of NLC models could themselves indicate the true water vapor

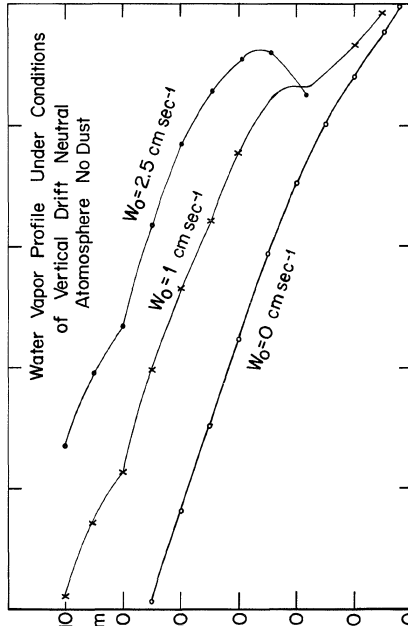

Figure IV - 7

Water vapor profiles at mesospheric altitudes computed under the action of upward diffusion and drift in the neutral atmosphere for g_1. 2.5 cm sec^{-1}. The designated drift has a peak value set at 70 km altitude tapering off to 0 at 120 km.

concentration in the mesosphere. The choice of 1 to 2.5 cm sec^{-1} vertical drifts with maxima near 70 km is favored by other studies in the literature (Murgatroyd and Singleton, 1961). Further indication of the vapor profiles could derive from successful modeling of positive cluster ions or noctilucent clouds.

The summer w = 0, 1, 2.5 cm sec^{-1} and winter w = 0 cm sec^{-1} profiles were used as inputs in Chapter III for determining the positive-ion chemistry. In particular, w = 1 cm sec^{-1} and 2.5 cm sec^{-1}, summer, led to values and profiles for hydrated cluster ions which satisfy these positive-ion chemistry features: (a) above 86 km NO^+ and O_2^+ are dominant ions, (b) below 86 km cluster ions dominate, (c) among the cluster ions $\Sigma\ H_3O^+(H_2O)_n > \Sigma\ NO^+(H_2O)_n$. The only fault was that the computed "ceiling" in cluster ion population at 86 km is not as sharp as the experimentally observed ceiling.

The fact that profiles computed using an updraft successfully match rocket observations of positive ions and is indirectly verified in other ways leads to one of three conclusions: (a) Since the features of mesospheric chemistry noted above have been observed in most seasons and worldwide, the consequence of the updraft in this formulation is merely fortuitous and a critical omission has been made in the chemical reaction set. (b) The upper mesosphere in the zones of rocket sampling always has an updraft and somewhere a downdraft of this "cell" must exist. The extent of the cell could be hemispheric since there is

already some evidence for a worldwide circulation pattern in the mesosphere and stratosphere (Murgatroyd and Singleton, 1961). (c) Some other mechanism is transporting water into the upper mesosphere. Of these three conclusions the second or third is more likely. The extensive previous investigations on the formulation of a suitable chemical reaction set for the D-region probably insures that no reactions are missing and although the concentration of nitric oxide is uncertain we are left with the strong possibility that water vapor must exist in a mixing ratio of at least 12 ppm at 80 km which would have to be due to a transport process of some sort.

B. Vapor Profiles with Downward Flux of Dust

The incorporation of dust into the diffusion equation and the subsequent perturbation of the water vapor profile will be considered in this section. A range of dust sizes considered match the few existing observations of dust in the upper mesosphere, (which have been discussed in Chapter III), but suffer from a restriction inherent in the computation.

The magnitude of the water vapor loss term, L_v, in the diffusion formulation depends upon the photodissociation coefficient, J, and the rate of condensation on dust particles to form ice. Dust particles are entered into the program DIFRAD 13 via the flux of dust, ϕ_D, but within the program the number density of dust (cm^{-3}) must be computed:

$$n_D = \phi_D/(W_D-W)$$

If the upward neutral drift velocity equals or exceeds fall velocity of dust reckoned with respect to a still atmosphere, then n_D will approach infinity and produce a singularity in the equation. This must be avoided by the choice of a sufficiently large initial dust radius to keep the fall velocity high. Maximum upward drift occurs at 70 km and since the supersaturated region in this model lies some 10 km higher, only uncoated dust will exist at 70 km so that the density of the falling particle will be 3 gm cm^{-3}. The restriction could therefore be formulated as follows:

Fall Speed $W_D = \frac{-rd\beta}{[N_2]} >$ Updraft, where W_o, peak updraft, is fixed at 70 km.

$$\frac{-rd\beta}{[N_2]} > W_o \cdot$$

or $$r > \frac{[N_2]}{d \cdot \beta}$$

or $r > W_o \cdot (.0133)$ in microns.

W_o	r(N)	DIFRAD 13 Values Used (microns)
1	.0133	.015
2.5	.033	.035
5.0	.066	.07

This data is graphed on Figure IV-8. The restriction is mild at W_o= 1 cm sec^{-1} since observations of dust radius distribution (Divari, 1963) take .01μ as a lower limit on size.

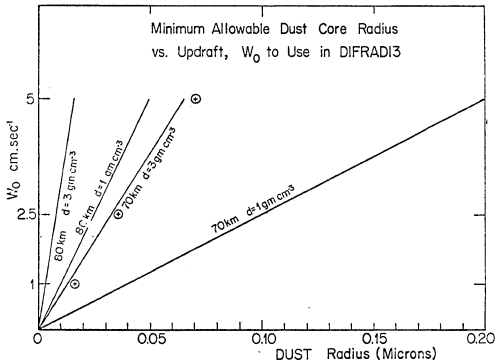

Figure IV-8

Plot of minimum permissable dust core radius in order to prevent a mathematical singularity in the DIFRAD 13 computer program vs. magnitude of updraft.

The following runs were made with dust:

TABLE VII

INPUT TO DIFRAD 13 AND RESULTANT ICE-CRYSTAL GROWTH.

Temp Profile	Drift W_o (cm sec^{-1})	Flux of Dust	Core Radius (μ)	Max Radius (μ)	Date
TEMP 2	1	2	.015	.0332	12/8/76
TEMP 2	1	10	.015	.0332	12/8/76
BARROW	1	10	.015	.0627	12/8/76
TEMP 2	2.5	2.0	.035	.2627	12/8/76
BARROW	2.5	2	.035	.2938	12/8/76

The relation between the vapor number density profile n_v and the saturated vapor number density n_s for three temperatures: (A) Barrow, (C) Mean Summer, (B) the average profile of A and C (TEMP 2), is given in Figure IV-2. The horizontal distance between these curves govern the degree of supersaturation and the maximum growth to be expected from a given profile and initial dust core.

With low (and experimentally observed) values of dust flux such as 2 and 10 cm^2 sec^{-1}, the depletion of ambient water vapor is negligible and the existing vapor profile does not change to any visible extent. This would not necessarily be the case with a higher degree of supersaturation ($n_v >> n_s$) and a higher flux of dust, (eg. W_o = 2.5 cm sec^{-1} and ϕ_D = 10 cm^2 sec^{-1}). In these extreme cases it may be shown that the increased dust flux may indeed lead to a significant depletion of the total population of ambient water molecules and, in reducing the

vapor concentration reduce the saturated layer thickness and the maximum radius to be expected. Furthermore, a thin (< 5 km) spike of a vapor layer may be shown to form below the supersaturated region as the previously trapped water vapor is released to the air. In very extreme cases high flux values forced the computation with DIFARD 13 to "blow up" since large ice crystals (> 2μ) removed all available water (down to saturation) and the resulting perturbation to the iterated n_v curve was too severe to permit further iterations to be convergent. Such a computational dilemma could be avoided by reducing the sticking coefficient to a small value, say 0.2, and gradually increasing it as the program is run.

Dust has been brought into the above formulation as an additional gain or loss mechanism for water vapor profile used in the ion-kinetic calculation. The perturbation was not extreme under conditions of nominal updraft ($\sim$ 1 cm sec^{-1}) and flux (1-10 cm^2 sec^{-1}). Under the conditions where a spike of enhanced water vapor could be produced, ion-kinetic calculations were not made with this profile since the effect would be buried in the gross 5 km steps of the DUSTCHEM and POSCHEM programs. It may easily be argued, however, that the effect of a "spike" of enhanced water vapor would be to provide a "spike" in hydrated water cluster ions of masses 37^+ and 55^+ with an extremely sharp ceiling which would be located a few kilometers below the mesopause temperature minimum.

C. Growth of Ice Crystals

It is necessary now to focus upon the behavior and growth of the ice crystals themselves in order to investigate whether a formulation of

noctilucent clouds might be possible. To provide a matching point with observation, some of the observational details of noctilucent clouds will be considered.

a) Noctilucent Clouds: Observed Characteristics

Noctilucent clouds (NLC) have been observed since 1885 in summer in both hemispheres. Early effort centered on collating the variety of observations throughout the Northern Hemisphere (Vestine, 1934), in Scotland (Paton, 1964), Sweden (Ludlam, 1957) and the USSR (Willman, 1967) with considerable attention paid to quantitative aspects of formation, nucleus material, temporal variations and so on. More recently, Fogle (1966a, b, 1972), Fogle and Haurwitz (1966) and Reiter (1971) have reexamined the geographical characteristics and succinctly codified known features. Also, the proceedings of two conferences: "The Physics of Mesospheric (Noctilucent) Clouds" in Riga, November, 1968, and "Noctilucent Clouds" in Tollin, 1966, present a wealth of ground-based observations, over Russia particularly, with the first report investigating the physics of formation.

NLC have been triangulated to lie from 74 to 92 km with a mean altitude of 82 km and a thickness of 5 km. Most sightings peak in frequency in July and August, although the maximum temporal range recorded is April 28 to September 28 in North America (Fogle and Haurwitz, 1966) and early March to November in the Soviet Union (Willman, 1967). It should be noted that the maxima of NLC in summer could be fortuitous because of the peculiar observing conditions necessary, namely, a solar depression angle of 6° to 12°. Additional uncertainty may be due to

confusion with other objects, obscuration of the sky and the fact that the numbers and geographic extent of observations reported depend upon reports from untrained observers. In any case, the apparent maximum in July has been linked to the well-established cold summer mesopause temperature which suggests a supersaturated condition of the atmosphere at 80 km. However, even temperature data obtained during a NLC display at Barrow (Theon et al., 1966) are insufficient evidence in demonstrating that cold temperatures ($\sim$ 150°K) alone are the critical influence.

The detailed review by Fogle and Haurwitz (1966) of the various in situ sampling experiments in Volume 16 of Tellus (Hemenway, Soberman and Witt, 1964, and Hemenway et al., 1964), Soberman et al. (1964) and Witt et al. (1964)) yields the following information on the composition, size and number of ice crystals:

(a) NLC nuclei are of extraterrestrial origin;

(b) Their integral size distribution is of the form

$$N(r) = \text{const.}(2r)^{-P} \qquad 3 < P < 4$$

(see Chapter III for a similar result in the distribution of dust by Divari (1963));

(c) The size distribution has a lower limit at 1500Å and an upper limit of 5000Å for uncoated dust. This fact, however, could depend upon the sensitivity of the method used; polarization measurements of Witt (1966) lead to a cloud particle radius of 1000-1800Å with an upper limit of 2400Å.

(d) Particle concentration in the sampled layer (75-98 km) is 10^3 times greater in the presence of clouds than at other times;

(e) The column density through a NLC equals 8×10^6 particles cm^{-2}. For a cloud 5 km thick this is equivalent to a volume concentration of $8 \times 10^6/5 \times 10^5 = 80/5 = 16$ particles cm^{-3}.

More recent measurements of the resonance scatter from Na(5893Å) by the OGO-6 satellite (Donahue et al., 1972) reveal a dense aerosol scattering layer centered at 85 km which is most pronounced in summer and high latitudes. Analysis of received radiation and optical depths places the size of the scattering particles at 1300Å. Fogle and Rees (1972) made spectral intensity measurements of radiation scattered off of NLC displays above Fort Nelson, B.C., in July. By assuming Witt's (1963) effective radius of 1300Å and a layer thickness of .75 km, and using Mie Scattering Theory they obtained a number density of 1 cm^{-3}.

Although the results of these investigations are not in conflict, neither are they unanimous in their specification of NLC properties. However, as a working set of common features, we postulate that any model of NLC formation should at least duplicate the following properties.

(a) Altitude range: 75-85 km.

(b) Range of ice crystal radii: 1000-2400Å.

(c) Concentration: 1-10 cm^{-3}.

It is to match these properties that the subsequent formulations are made. Other properties of NLC such as spatial extent, lifetime, drift direction and wave motion have been intentionally neglected.

b. Model Calculation of Ice Crystal Growth

The results of this section have been tabulated in Table VII and are displayed in Figure IV-9. The neutral atmosphere drifts closest to literature values are those for W_o = 1 and 2.5 cm sec^{-1} and a summer temperature with a minimum equal to 145°K (TEMP 2). The dust flux of 10 cm^{-2} sec^{-1} and a core size of .015μ are the most likely values to be found at 90 km. In these cases the maximum growth of the ice crystal was to .0332μ and .2627μ, respectively, the first crystal not being large enough to be visible by the scattering experiments of Donahue (1971) which require a r > .13μ. From Figure IV-2 it may be seen that the appropriate saturated number density curve is Curve "B" which is intersected by W_o = 1 cm sec^{-1} (#2) only over one corner and this accounts for the small growth. On the other hand, the W_o = 2.5 cm sec^{-1} curve (#4) represents a high degree of supersaturation in its intersection with temperature curve "B" and the ice particle grows to a visible size of .2627μ. The important point for the ice particle growth is that $n_v \geq 10\ n_s$ for most of the altitude range through which the curves intersect which means that the rate of addition of water molecules is at least ten times as rapid as the rate of loss from the crystal. Comparisons of growth with an identical water vapor profile with W_o = 1 cm sec^{-1} (curve #2 on Figure IV-2) and a dust flux of 10 cm^2 sec^{-1}, but with two different temperature profiles: Barrow Extreme Cold (Curve A) and Mid Range Temp (Curve B), result in crystals of .0627μ and .0332μ, respectively. This result and those of earlier test runs concur in indicating that the maximum radius achieved for a given vapor profile and dust core radius is closely proportional to the vertical thickness

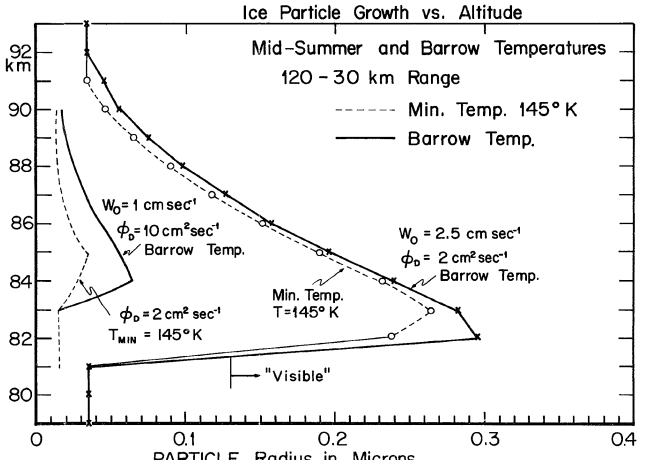

Figure IV-9

Plot of size of ice crystal grown under conditions of updraft of W_o = 1 cm sec^{-1} and W_o = 2.5 cm sec^{-1}. If 1300A is taken to be the lower cutoff of visibility, then a crystal of that size is possible only with an updraft of W_o = 2.5 cm sec^{-1}.

of the saturated layer and not to any other parameter such as the enclosed area or the log of the enclosed area between the n_s and n_v curves. In the case of an updraft of W_o = 2.5 cm sec^{-1} (Curve #4) and the temperature profiles for Barrow (Curve A) and the midrange temperature (Curve B) the same holds true with the maximum radii being .2938μ and .2627μ, respectively. Maximum growth is greater here, of course, since n_v is larger than the previously discussed case by about an order of magnitude.

Although the precise radius profile to be expected from a given core radius must be solved for by means of the full iterative computation, examination of a n_v - n_s plot such as depicted on Figure IV-2 enables one to determine:

a) Whether any growth is possible at all,

b) The altitudes over which growth will occur,

c) The relative size of crystals to be expected if the vapor profile (n_v) curve is fixed and the temperature (n_s) curve is varied.

It turns out, therefore, that with modest values of neutral atmosphere drift and dust flux that this formulation is capable of producing a 5 km layer of visible ice crystals (> 1500Å) located at and below the mesospause. Dust of an initial radius .01μ is required and any smaller size would be incapable of growing to a visible dimension under the conditions of polar summer atmosphere and temperature. Gross characteristics of noctilucent clouds are thereby matched.

5. Summary, Comparison with Previous Work and Conclusion

A. Previous Mathematical Models

The purpose of this chapter has been to investigate the behavior of water vapor in the mesosphere under the influence of a) eddy and molecular diffusion, b) a drift of the neutral atmosphere, c) photodissociation, d) sublimation of the ascending vapor upon a flux of descending dust particles and release in unsaturated regions. In the course of carrying out this task it has also been possible to a) compute a series of water vapor profiles for use in the ion-kinetic calculations of Chapter III, b) show the conditions under which crystals of ice could grow to a visible dimension on descending dust.

This present diffusive and photochemical model has its origins in that of Hesstvedt (1968) who produced the first steady state H_2O profiles with diffusion in an oxygen hydrogen atmosphere. This and other early formulations (eg. Bowman et al., 1970) derive ultimately from Colegrove et al. (1965) in their mathematical formulation and Chapman and Cowling (1923) in their expressions for eddy and molecular diffusion fluxes. Many of these investigations included considerable neutral chemistry, the formulations were time dependent and the steady state was approached more or less by permitting the model to run to "infinity." Bowman et al. (1970) developed a model giving considerable physical insight with respect to the role of solar flux, eddy coefficients and successfully achieved a true steady state. This is more than can be said for either Shimayaki (1967), Shimayaki and Liard (1970, 1972) or Hunt (1971b, 1973).

The full review of many of these early works and others on minor neutral constituents is given by Strobel (1972) who focuses particular attention upon boundary conditions. In addition, his discussion of the Jean's escape of atomic hydrogen (Hunten and Strobel, 1974) as being the ultimate fate of hydrogen compounds on earth gives probably the most comprehensive insight into all aspects of atmospheric water vapor and "odd hydrogen." Liu and Donahue (1974), using similar chemistry and diffusion formulations which were embedded in a very turgid analysis, reached the same conclusions.

The boundary conditions we have used: UBC - Flux of H_2O = 0; LBC - a number density of H_2O, reflect the physics of the behavior of water vapor. Since no sampling of H_2O has ever been made at the range of 120 km, exact concentrations there are unknown. It is certain that at some altitude above 120 km water vapor ceases to exist, and the flux will go to zero. As was shown in the tests of this present model and the variation in the profiles below 100 km, it doesn't really matter at which level this occurs, only that it is above the homopause. The formulation is shown to be quite insensitive to various perturbations of the upper boundary condition. The choice of a measured number density instead of photochemical equilibrium (n_i = P/L) at the lower boundary condition was due to the availability of existing measurements at $\approx$ 30 km. These boundary conditions were both physically meaningful and computationally easy to apply to our formulation. This latter consideration has not always been possible with previous models of minor constituents and the casting of the boundary conditions has been confusing in some cases.

For example, Wofsy et al. (1972) use a complicated set of boundaries in modeling CH_4, CO, CO_2 and seems to use a Runge-Kutta method. The Runge-Kutta method has advantages since it is self starting, stable and permits one to change the step size whenever the variable changes rapidly. Also computer and numerical techniques are well developed for Runge-Kutta (Kreysig, 1972, and Romanelli, 1960). Strictly speaking, however, use of Runge-Kutta changes the computation into an initial value problem because the Runge-Kutta method is an algorithm to compute the Taylor expansion of a function about a boundary (initial point). What frequently happens (Wofsy et al., 1972; Reid, 1974) is that if, by starting at one (say, the upper) boundary with a guessed number density and slope, the resultant density at the other boundary does not match observations or inferences, the computation is rerun using a different initial value or slope in order to match an acceptable criterion at the other boundary. Boundary conditions are thereby "approached" iteratively rather than applied directly and casting the problem in this manner lacks precision. The computation is stopped when it all "looks about right." Wofsy et al. (1972), for the sake of computational economy, added confusion to his treatment of CO by splitting the computation into three adjoining altitude ranges and the use of a number density and flux for internal boundaries effectively predetermined the resulting profile.

The most instructive procedure in being straightforward, physically insightful and unambiguous in the treatment of boundary conditions is that of Strobel et al. (1970), Strobel (1972) and Hunten and Strobel (1974) since they transform the original differential equation into a set of linear non-homogeneous algebraic equations with lower photo-

chemical equilibrium boundary conditions ($n_i = P_i/L_i$) and flux upper boundary conditions.

B. Drift of the Neutral Atmosphere

The inclusion of an updraft of the neutral atmosphere had been invoked several times previously on a qualitative basis, particularly for a formulation of noctilucent clouds; e.g., Chapman and Kendall (1965), Charlson (1965), and Fiocco and Gramms (1971). However, it also had been inferred based upon more comprehensive studies of the general circulation.

The existence of high winter and low summer mesopause temperatures (230°K and 150°K) (Theon et al., 1972) which could not be explained by solar heating and radiative processes alone (Murgatroyd and Goody, 1958) led Murgatroyd and Singleton (1961) to start with the existing temperature fields in the stratosphere and mesosphere and derive the meridional and vertical motions of the neutral atmosphere necessary to provide dynamic cooling and heating to fit the observed temperature profiles. Figure IV-10 presents the vertical contours based on these calculations. Their updraft has a maximum at 70 km. Leovy (1964) also computes models of thermally driven mesospheric circulation which result in summer updrafts of 2.8 cm sec^{-1} and .16 cm sec^{-1} and winter downdrafts of -2.8 cm sec^{-1} and -.16 cm sec^{-1}. His peak value lies at 60-80 km which is also the level of the maximum of the meridional flow. Hesstvedt (1971), using an oxygen-hydrogen photochemical model with temperature, computes summer updraft values of 4 cm sec^{-1} at 80 km and winter downdrafts of -1 cm sec^{-1}.

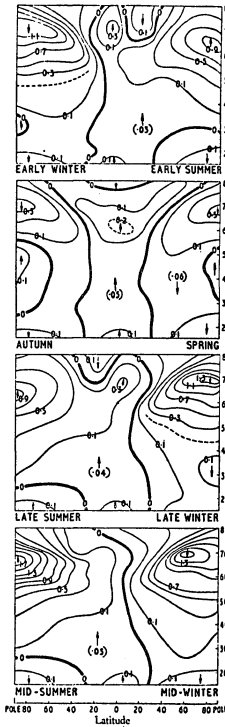

Figure IV-10

Vertical drifts of the neutral atmosphere in a vertical meridional section pole to pole computed by Murgatroyd and Singleton (1961) from radiative balancing.

Additional sources of evidence exist. $O + O + M \rightarrow O_2^* + M +$ 5.2 eV is an exothermic reaction resulting in the emission by oxygen atoms at 5577Å. Young and Epstein (1962) and Tohmatsu and Nagata (1963) found the peak altitude and intensity of this emission to be dependent upon vertical drift of the neutral atmosphere. The intensity of 5577Å increases with downward drift since flow is from a region more rich in atomic oxygen; low levels of emission are associated with updrafts. Figure IV-11a illustrates the relation between the shift in height and vertical transport of -1, 0, +1 cm sec^{-1}. The composite of these two effects is interpreted in terms of the upper atmospheric circulation pattern pictured in Fig. IV-11b. Dachs (1969) deduces vertical velocities of the order of 1 cm sec^{-1} from comparisons of the height of 5577Å emissions with the height of sporadic E layers.

A limitation to this formulation lies in the fact that with a one dimensional (vertical) flow, conservation of mass cannot be maintained. Our particular vertical velocity profile for the drift of the neutral atmosphere results in a negative divergence from 70 to 120 km which accounts for the bulge in water vapor at these levels. If the formulation were three dimensional, then the horizontal components of flow would provide the necessary positive divergence of water vapor which would reduce the size of the bulge. By way of providing horizontal divergence, Leovy's (1964) results show a maxima in meridional flow at the altitude of maxima in vertical velocity. Also, tidal winds whose meridional and zonal components are of the order of 10^4 cm sec^{-1} at around 100 km associated with the Sq current system have been observed (Volland, 1971).

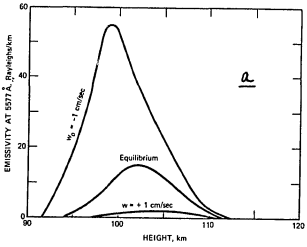

Fig. 5.3 Altitude distributions of the 5577 Å radiation emissivity at different vertical transport velocities (w). [From T. Tohmatsu and T. Nagata, *Planetary and Space Science*, 10:108 (1963).]

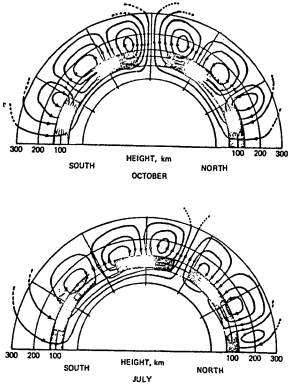

Fig. 5.8 Model of the upper atmospheric circulations as inferred from airglow distributions, the latter indicated schematically by hatched regions. [From T. Tohmatsu and T. Nagata, *Planetary and Space Science*, 10:113 (1963).]

Figure IV-11

a) Altitude of maximum of 5577Å emission under action of neutral atmosphere drifts of -1, 0, +1 cm sec^{-1} (Tohmatsu and Nagata, 1963).
b) Hemispheric circulation pattern of vertical drift from 0-300 km (Dachs, 1969).

The precise vertical placement of the drift profile was not critical since test runs with other drift formulations used in the diffusion equations (Figure IV-5, 6, 7) demonstrated the following features: (a) A variation from 100 to 200 km of the upper altitude where the drift, W, becomes equal to zero resulted in a shift in the altitude of the maximum of the vapor profile from 80 to 90 km. Hence, the position of the 'bulge' is not terribly sensitive to the variations on the upper end of the drift profile. Since the turbopause is experimentally observed to be at 105 km, the current choice of the 'zero point' for the drift was set toward the lower end at 120 km. (b) The position of the altitude of maximum drift sets the altitude of the minimum in the vapor profile curves.

The ultimate decrease in concentration with height is due to increasing photodissociation at 90 km.

C. Neutral Chemistry of H_2O

Contrary to the requirements of many studies of minor constituents in the upper atmosphere, extensive chemistry has not been needed in this present treatment. The dominating loss process in the mesosphere is photodissociation by sunlight in the Schumann-Runge bands and Lyα. Chemical reactions occur, but at altitudes lower than the mesosphere, as the following description will justify.

The chemistry of H_2O is normally formulated in terms of an oxygen hydrogen atmosphere with a tropospheric source of H_2O and other hydrogen compounds which diffuse upward to the mesopause. In the troposphere hydrogen is apportioned between the forms of H_2O, CH_4, and H_2, which all

diffuse upward. CH_4 may convert to odd hydrogen (OH, HO_2, H, H_2O_2) in the stratosphere as the concentration of $O(^1D)$ increases through the reactions:

$$O(^1D) + CH_4 \rightarrow OH + CH_3 \quad (4\text{-}79)$$

$$O(^1D) + H_2 \rightarrow H + OH \quad (4\text{-}80)$$

H_2O is recycled via:

$$H + O_2 + M \rightarrow HO_2 + M \quad (4\text{-}81)$$

$$OH + HO_2 \rightarrow H_2O + O_2 \quad (4\text{-}82)$$

Since the stratosphere is optically too thick for the penetration of Lyα or the Schummann-Runge bands (SRB), the principal destruction of H_2O in that region is chemical:

$$O(^1D) + H_2O \rightarrow OH + OH \quad (4\text{-}83)$$

but H_2O is again rapidly recycled via the reaction (4-82) above. Hence, the increase in H_2O mixing ratio from 2-3 ppm in the stratosphere (Mastenbrook, 1968) to 10 ppm at 42-66 km measured by Scholtz et al. (1970) could be at the expense of CH_4 although this possibility is discounted by Reiter (1971) through a calculation of the oxidation of methane.

Above the stratopause H_2O is mixed upward by eddy diffusion against the photodissociation by Lyα (1215Å) and the SRB (1759-1930Å).

$$H_2O + h\nu \xrightarrow{Ly\alpha} H + OH \quad 75\% \quad J = 4.7 \times 10^{-6}\ sec^{-1} \quad (4\text{-}84)$$

$$H_2O + h\nu \longrightarrow H_2 + O \quad 25\% \quad J = 6.1 \times 10^{-7}\ sec^{-1} \quad (4\text{-}85)$$

(Hunten and Strobel, 1974)

In the mesosphere the odd hydrogen compounds quickly equilibrate chemically with one another (see Eqns. 8, 9, 10, p. 308, Hunten and Strobel, 1974) whereas H_2 and H_2O concentrations are principally controlled by transport processes. Photodissociative loss for H_2O has a long lifetime, $\tau_{ph} = 1/4.7 \times 10^{-6} \cong 2.1$ days, compared with a diffusion lifetime of $\tau_D = H^2/D = (3 \times 10^5)^2/10^6 \cong 1.0$ days, so that the important control over H_2O in this region is through diffusive transport, and not chemical processes. It is this fact which allows our diffusive model to be viable. The net result is that towards the top of the mesosphere H_2O is converted to the more rapidly diffusing molecule H_2 which moves upward and downward, and H_2O is not strongly reformed since reaction (4-82) is minor above 70 km. Further aloft, at higher thermospheric temperatures, the following reactions become exothermic

$$H_2 + O \rightarrow OH + H \qquad (4\text{-}86)$$

$$OH + O_2 \rightarrow O_2 + H \qquad (4\text{-}87)$$

producing H atoms which evaporate into interplanetary space.

D. Ice Crystal Growth Models

The formulation of the growth of a visible ice crystal falls out, as it were, from the normal course of water vapor interacting with dust in a super-saturated atmosphere. Ice crystals are shown to grow when the neutral atmosphere updraft is 1 cm sec^{-1} but they do not become "visible" (> 1300Å) until the updraft is increased to about 2.5 cm sec^{-1}, a concentration of about 1.7×10^{10} cm^{-3}, which is a mixing ratio of 90

ppm at $\approx$ 80 km. Existing uncertainties in the important parameters, J, the photodissociation coefficient, and K, the eddy diffusion coefficient could lead to variations in the above results such as a reduction in updraft required for visible crystals. Previous authors investigating NLC had recognized the need for supersaturated conditions (produced by sufficiently cold temperatures) (McDonald, 1964 and Schilling, 1964), but Hesstvedt was the first to attempt an analytic treatment though he used an erroneous ice crystal growth expression. Charlson (1964) used the correct collisional growth expression for ice particles but did not link upward diffusion of vapor analytically with descending dust. He finally just postulated updrafts of 1 to 20 cm sec^{-1} to resupply water to the dried out layer, but these values are clearly extreme in the light of other investigations of drift.

Chapman and Kendall (1965) carefully formulated the downward diffusion of extraterrestrial dust which achieved an exponential distribution with a base at an altitude set by the upward drift of the neutral atmosphere. The actual growth rate of crystals, supersaturation and diffusion of water vapor was not explicitly worked out although NLC were "suggested" to form when (a) the base of the dust layer descends into the mesopause, (b) convection transports sufficient water aloft. Fogle and Haurwitz (1964), in a study of the temporal correlation between major volcanic eruptions and NLC displays, suggest that the injection of water into the stratosphere could provide the necessary enhanced concentrations which would diffuse upward to provide the supersaturation aloft. Fiocco and Gramms (1971) incorporated Chapman and Kendall's dust sedimentation

and Murgatroyd and Singleton's (1961) mesopheric circulation patterns to derive a meriodional dust flow trajectory which produces the required high dust concentration at 80 km. Updrafts and eddy mixing of the neutral atmosphere are omitted but the authors produce ice crystals of radius 1000Å in a .3 km thick layer.

After the start of this present investigation a formulation of vapor diffusion and ice crystal growth by Reid (1974) was brought to the attention of the author. The formulation is roughly similar, but certain differences exist. Reid (1974) postulates sublimation nuclei of radius 10Å ($10^{3}\mu$) which he states may be composed of about 140 multiply hydrated cluster-ions but does not describe how the normal hydrated cluster-ion of 3 or 4 molecules becomes an aggregate of 140 molecules. In fact, based upon the data of Kebarle et al. (1967) discussed in Chapter II Figure III-4b, for D-region temperature and pressure it seems that there would be a distinct inhibition to the growth of clusters greater than n=6 by virtue of the increasingly strong backward reactions, even with an increase of ambient vapor concentration by a factor of 100. Based on this nucleus his calculations lead to a total growth of only 630Å which is below the visible threshold.

CHAPTER V

NEGATIVE IONS IN THE D-REGION OBSERVATIONS AND MODEL CALCULATIONS

INTRODUCTION

This chapter presents a short review of D-region negative-ion observations and previous theoretical work. A computation of the steady-state concentration of the major negative-ion species at 80, 75 and 65 km is described which extends the computational technique described in Chapter III by including the 66 most important negative ion-kinetic reactions taken from the literature. Negative ions are considered in relatively less detail in this chapter than the positive ions had been, because, as will be demonstrated, negative ions are not populous at 80 km by day and, are not apt to be involved with dust attachment or the formulation of water vapor profiles.

1. Theory of Negative-Ion Formation

In the D-region the production of NO^+ and O_2^+ is the original photochemical process which initiates the pathways producing all positive ionic species and cluster ions. The free electrons so released by day readily attach themselves to O_2 at night according to the reaction

$$e + 2O_2 \longrightarrow O_2^- + O_2 \qquad k = 1.89 \times 10^{-30} \qquad (5\text{-}1)$$

(Chanin et al., 1962),

and thus O_2^- becomes the primary source for a series of charge exchange reactions which lead ultimately to the negative ions O_3^-, O_4^-, CO_2^-, CO_3^-, NO_2^- and NO_3^-, and their hydrates. The radiative attachment reaction

$$e + O_2 \rightarrow O_2^- + h\nu, \quad k = 2 \times 10^{-19}, \text{ DNA (1972)} \qquad (5\text{-}2)$$

is not as important. Above 85 km the reaction

$$e + O \longrightarrow O^- + h\nu \qquad (5\text{-}3)$$

$$k \overset{\sim}{=} 10^{-19} \quad \text{Phelps (1969)},$$

may be important as a source of O^- due to the presence of considerable atomic oxygen at these levels and, thus, O^- becomes an alternate electron donor for the sequence of charge exchange reactions (Branscomb, 1964). The O_2^- chain is inoperative by day due to electron release through solar photodetachment,

$$O_2^- + h\nu \longrightarrow O_2 + e \qquad (5\text{-}4)$$

$$\rho = 0.4 \text{ sec}^{-1} \text{ LeLevier and Branscomb (1968)}$$

or the reaction,

$$O + O_2^- \longrightarrow O_3 + e \quad \text{(Branscomb, 1964)}, \qquad (5\text{-}5)$$

$$k = 3.3 \times 10^{-10} \text{ cm}^3 \text{ sec}^{-1}$$

which is more rapid than the first reaction by a factor of 100 due to the high daytime abundance of atomic oxygen. The release of electrons through the reaction with atomic oxygen becomes increasingly ineffective on larger negative ions since their electronegativity increases. Examples are: O^-, 1.47 ev; O_2^-, .43 ev; $O_2^-(H_2O)$, 1.2 ev; $O_2^-(H_2O_2)_2$, 1.95 ev; $O_2^-(H_2O)_3$, 2.6 ev; $O_2^-(H_2O)_4$, 3.2 ev; CO_4^-, 1.2 ev; NO_2^-, 2.5 ev;

NO_3^-, 3.6 ev; (DNA, 1972). Therefore CO_2^-, CO_3^-, NO_2^-, NO_3^-, and hydrates, the so-called "terminating" ions, are increasingly immune to attack by atomic oxygen and are most stable.

Peterson and Moseley (1974) state that the photodissociation of CO_3^- and its hydrate,

$$CO_3^- \cdot H_2O + h\nu \longrightarrow CO_3^- + H_2O \qquad k \cong .5 \text{ sec}^{-1}, \text{ at zero optical depth} \tag{5-6}$$

$$CO_3^- + h\nu \longrightarrow CO_2 + O^- \qquad k \cong .2 \text{ sec}^{-1}, \text{ at zero optical depth} \tag{5-7}$$

may be quite rapid at sunrise in producing O^- whose photodetachment rate of 1.4 sec^{-1} is more than 100 times faster than the photodetachment rates of the stable complex ions (such as $O_2^- \cdot H_2O$) which normally dominate the D-region at night. Therefore this CO_3^- photodetachment reaction is an important time dependent process which may lead to the sharp maxima in D-region electron densities observed at sunrise (Turco and Sechrist, 1972a,b).

Since the daytime ratio of negative ions to electrons is large only at altitudes below 75 km, negative ion chemistry may be formulated quite independently of positive ion chemistry of the daytime D-region. Since pathways for charge exchange are straightforward the main problem in investigating negative ions has been the establishment of correct values of photodetachment and rate constants.

The formulation of negative-ion reaction schemes began prior to rocket observations of negative ions in the mesosphere. The fundamental approach was introduced with significant insight by Lelevier and Branscomb (1968) and reviewed later by Ferguson (1971b). Fehsenfeld and Ferguson (1974) discussed critical details of the thermodynamics, rate and equilibrium constants for various types of bonds and interactions with trace constituents. They pointed out that rate constants for the exothermic reactions are insensitive to the degree of hydration: e.g., $k = 3.1 \times 10^{-10}$ cm^{-3} sec^{-1} for either

$$O_2^-(H_2O) + O_3 \longrightarrow O_3^-(H_2O) + O_2 \qquad (5\text{-}8)$$

or

$$\longrightarrow O_3^- + H_2O + O_2. \qquad (5\text{-}9)$$

This insensitivity applies also to O_3^- atom interchange with CO_2, and CO_3^- reactions with NO and NO_2 and is important since it permits an inference of the rate constants leading to other hydrated species in the chemical scheme. Thomas et al. (1973) present a vaguely formulated steady state model including photodetachment of CO_3^-, NO_2^- and NO_3^- and suggest that photodetachment from NO_3^- is the main source of free electrons below 70 km. Reid (1971b) models negative-ion species under Polar Cap Absorption (PCA) conditions and explores the relationship to effective recombination coefficient (Reid, 1970). In most of these reports, however, lack either of accurate knowledge of trace constituents or of a rigorous mathematical treatment limit results to qualitative discussions instead of the more quantitative investigations such as those associated with positive-ion chemistry. The principal

initial source of information on recent laboratory measurements of rates is provided by Reaction Rate Handbook DNA (1972), and its occasional supplements.

2. Observations of Negative Ions

Actual observations of negative ions are limited to Arnold et al., (1971), Narcisi et al. (1971), in situ sampling during an eclipse (Narcisi et al., 1972). Arnold et al. (1971), and measurements conducted at night from Andoya, Norway (see Appendix I, Profile #13), found the negative ions: O_2^-, Cl^-, CO_3^- and HCO_3^- with CO_3^- dominant below 78 km. Their mass filter was sensitive from 2-134 amu, a sufficiently broad range to detect multiple hydrates if they were there. Narcisi et al., (1971) (Profile #6) recorded signals corresponding to the light ions, O^- and NO_2^-, negative ions of mass in excess of 54 amu from 80-90 km, and a sharp ceiling on their concentration at 90 km. Furthermore, a sequence of heavy ions differing in mass by 18 amu were detected along with 61 $\pm$ 1 and 63 $\pm$ 1 amu, identified as either CO_3^-, NO_3^-, or CO_4^-. Narcisi et al., (1972) (Profile #8) in August, October and November flights from Fort Churchill found large numbers of negative ions, $NO_3^-(H_2O)_n$ where n = 0-5 with a sharp ceiling from 90 to 92 km. One of these November flights was under PCA conditions yet significant numbers of negative ions were measured. As discussed by Reid (1971b), the result of a PCA would be merely to eliminate higher members of the chain due to ion-ion recombination. Negative clusters were detected in a daytime sample during an eclipse at 97% obscuration from Wallops Is. (Narcisi et al., 1972) (Profile #4) and their presence implied a rapid

attachment process to account for the electron decrease. The point of these data is to document the existence of negative ions in the nighttime D-region and in eclipse conditions during the day. As was the case with an analysis of positive-ion shots no conclusions may be drawn concerning seasonal or geographic variability. In negative-ion sampling the measurement problems (discussed in Chapter II) are compounded since the positively charged collector plate of the mass filter also attracts electrons causing high levels of background signal in the mass-filter.

3. Negative Ion-Kinetic Calculations and Convergence Problems

The steady-state computation of daytime negative ion concentration required the input of 66 separate reactions in addition to the 23 necessary for positive ions. A complete set of our reactions is listed by reaction category in Table IXa, along with the rate coefficient taken from the DNA (1972) compilation.

The steady-state formulation used in this case is an expansion of the positive-ion computation scheme. Continuity equations are written for 16 positive and 15 negative ions and include a) all gain and loss reactions, b) ion-ion recombinations, only for negative ions, N_j^-, which are expressed as,

$$(1.0 \times 10^{-7}) \cdot N_j^- \cdot \sum_{i=1}^{16} N_i^+, \qquad (5\text{-}9)$$

and c) positive-ion electron recombination. The summation in the above expression occurs because all positive ions contribute equally to and are combined in the ion-ion recombination term. These continuity equations are solved as a set of 31 equations. The solution of

these equations is managed by the computer program HCO29 which starts with an initial guess for the electron density and inserts it into the subroutine AL316 (Brown, 1967) which solves the set of 31 equations. In each of the 31 continuity equations the positive-ion electron recombination term, $\alpha N_i^+ \cdot N_e$, and ion-ion recombination term, are nonlinear.

Although the estimate of electron density removes the nonlinearity of the positive-ion recombination term, and AL316 is able to solve the remaining nonlinear set by a method described below. The resultant positive and negative ions are summed and a new electron density is computed in the main program via the charge neutrality condition:

$$N_e = \sum_{i=1}^{16} N_i^+ - \sum_{j=1}^{15} N_j^- \qquad (5\text{-}10)$$

The new electron density, Ne, so produced is compared with the old and, after a short computation, a revised guess is fed back into AL316.

This scheme has been successfully run at 65, 75 and 80 km with the (necessary) criteria of $\Sigma N_i^+ > \Sigma N_j^-$ from the output of AL316 at 65 km easily satisfied. It seems as if this set of reactions is well behaved at least to this altitude. The procedure is straightforward and values of the initial guess of electron density, the computed value of electron density, and sums of positive and negative ions are printed after each computation by AL316. Input data and calculated values are listed in Table VIII b,c.

A detailed description of AL316 may be found in Brown (1966). Basically, the method described by Brown (1967), is as follows: Initial guesses for the concentration of each ion must first be made. Generally these were set between 1 cm^{-3} and 100 cm^{-3} according to indications in the literature. In particular, at an altitude of 65 km, all negative ion concentrations were set at 1 cm^{-3}. The first continuity equation is expanded as a Taylor series about the starting guess for the ion, thereupon retaining only linear terms, equating to zero and solving for one variable as a linear combination of the remaining n-1 variables. In the second continuity equation, the first variable is replaced by its linear representation, the second variable is now expanded about its starting guess, equated to zero and solved for in terms of the now remaining n-2 variables. One continues in this fashion eliminating one variable per equation until the last equation is an equation with one unknown. A Newton iteration is performed, followed by back substitution within the triangularized linear system. A pivoting effect is achieved by choosing for elimination at any step that variable whose partial derivative has the largest absolute value.

An effort to reduce computation time failed when AL316 was reprogrammed by incorporating the charge neutrality condition inside it as a 32nd equation instead of leaving the charge neutrality condition in the main program. This was a key discovery, since the presence of electron density as the 32nd unknown within AL316 increased the degree of nonlinearity to where it was unmanageable by AL316 and the system could not be solved. Except at altitudes of 75 km and

above, where the sum of the negative ions was small and AL316 was effectively solving almost a pure positive-ion set, AL316 did not work and consistently produced some negative roots in the answers. Procedures such as removing all the negative-ion hydrating reactions or "fast" reactions did not alleviate the problem.

In the literature no broadly successful negative-ion computational scheme exists. Although Thomas et al. (1973) formulate a model their procedure is not specified. Reid (1971b) uses a 3 way iterative procedure in his PCA model so that only linear steps occur. 1) guess an electron density, 2) compute positive ions, 3) compute negative ions. The model is limited, however, to 8 negative ions, nighttime, and altitudes of 70-90 km. More recently, Reid (1975, personal communication) attempted to model a set of positive- and negative-ion reactions, and since he had encountered convergence problems at $z \leq$ 65 km, he dispensed with the negative ions altogether. Also Niles (1975a, 1975b, personal communication) using a time dependent formulation found difficulty with time steps which were excessive such that reactions which were "stiff" (had high rate constants) converged with difficulty. In all likelihood, however, a time dependent formulation with small steps is likely to produce a valid computation since a steady state is naturally achieved by allowing the model to run to infinity.

The atmosphere used was the United States Standard Atmosphere Supplements (1966) mean winter mesosphere, with nitric oxide modified for temperature and the water vapor corresponding to the no-drift case (Chapter IV). Primary production is the same as previously

except for the omission of flux due to Lyβ, and C(III). $O_2(^1\Delta g)$ ionization is given by Huffman et al. (1969). This is all of little consequence, however, since only Galactic Cosmic Rays are significant ionizers below 65 km. These data are listed on Table VIII.

4. Results, Comparisons with Observations, and Conclusions

The results of the negative-ion calculations are reasonable and generally match both the predicted concentrations made by other investigators and data from the few rocket measurements. O_2^-, the primary compound in the electron attachment chain has a measurable concentration of 2.17, 1.13 and 1.8 cm^{-3} at 65, 75 and 80 km, respectively. The most plentiful negative ions are the hydrates of NO_3^-, namely $NO_3^- \cdot H_2O$ (=1.2 cm^{-3}) and $NO_3^- \cdot 2H_2O$ (=113 cm^{-3}) particularly at 65 km. Reid (1971b) finds a high proportion of NO_3^- at 70 km, but this is probably due to his not including hydrating reactions in his set. Differences in ion concentration with altitude are due to the reduction with height of NO_2 from a value of .2 x 10^5 cm^{-3} to .1 x 10^2 cm^{-3} through destruction by atomic oxygen. This reduction in NO_2 cuts the pathway forming the NO_3^- clusters. CO_3^- exists as one of the terminal species. The nitric oxide clusters exceed the concentration of hydrated water clusters at 75 km, a fact due to the low values of primary production of O_2^+ used here. Nevertheless, the negative-ion results as described here are valid, and one result of the computations is to verify that, indeed, the principal charged species above 70 km are only positive ions and electrons, and negative ions are negligible by day above altitudes of 70 km.

The description in this chapter of a computational method which solves the nonlinear negative ion-kinetic system is an important result in view of the serious difficulties which other investigators have had. In the present case computer expense to investigate the convergence at other altitudes and conditions was excessive, and it was not possible to investigate negative ions as thoroughly as in the case of the pure positive-ion set. Hence, no variations in the input of neutral constituents or radiation levels were attempted, and only profiles under the most standard conditions were made from 80 km to 65 km. The next step would be to test this procedure and rate of convergence at lower altitudes and include the ion-ion recombination term for positive ions. This term would become increasingly important at lower altitudes, particularly for terminal species. Non-linearity would not necessarily become a problem since as the ion-ion recombination term increased, the positive ion-electron recombination term would decrease. Furthermore, the Flow Rate Diagram Program, FLONEG, is available to use as a diagnostic tool to investigate the strengths of various reactions in the negative ion-kinetics.

TABLE VIIIa

NEGATIVE ION REACTIONS

DNA Handbook (1972)

(Rate Constants $cm^3\ sec^{-1}$ for 2 body and $cm^6\ sec^{-1}$ for 3 body)

ELECTRON ATTACHMENT REACTIONS

Reaction Numbers		
1	$e + O \longrightarrow O^- + h\nu$	1.3×10^{-15}
38	$e + O + M \longrightarrow O^- + M$	6.5×10^{-29}
65	$e + O_2 \longrightarrow O_2^- + h\nu$	2×10^{-18}
17	$e + O_2 + N_2 \longrightarrow O_2^- + N_2$	1×10^{-31}
16	$e + O_2 + O_2 \longrightarrow O_2^- + O_2$	1.52×10^{-30}
32	$e + O_2 + H_2O \longrightarrow O_2^- + H_2O$	1.4×10^{-29}
33	$e + O_2 \longrightarrow O^- + O$	1.0×10^{-16}
3	$e + O_3 \longrightarrow O^- + O_2$	1.0×10^{-11}
51	$e + NO_2 + M \longrightarrow NO_2^- + M$	1.0×10^{-29}

PHOTODETACHMENT

4	$O^- + h\nu \longrightarrow O + e$	1.44
22	$O_2^- + h\nu \longrightarrow O_2 + e + .33$ ev	.33
30	$O_3^- + h\nu \longrightarrow O_3 + e$	.2
56	$NO_2^- + h\nu \longrightarrow NO_2 + e$	.04
61	$NO_3^- + h\nu \longrightarrow NO_3 + e$	.03
46	$CO_3^- + h\nu \longrightarrow CO_3 + 3$	.2
34	$CO_3^- \cdot H_2O + h\nu \longrightarrow CO_3^- + H_2O$	.5

TABLE VIIIa, (cont'd)

COLLISIONAL DETACHMENT

7	$O^- + O \longrightarrow O_2 + e + 3.6$ ev	2.0×10^{-10}
35	$O^- + O_2 \longrightarrow O_3 + e$	5.0×10^{-15}
37	$O^- + O_2(^1\Delta g) \longrightarrow O_3 + e$	3.0×10^{-10}
6	$O^- + N_2 \longrightarrow N_2O + e$	1.0×10^{-12}
8	$O^- + H_2 \longrightarrow H_2O + e + 3.5$ ev	6.0×10^{-10}
10	$O^- + NO \longrightarrow NO_2 + e + 1.6$ ev	5.0×10^{-10}
5	$O^- + CO \longrightarrow CO_2 + e$	6×10^{-10}
42	$O^- + N \longrightarrow NO + e + 5.1$ ev	2.2×10^{-10}
24	$O_2^- + O \longrightarrow O_2 + O + e$	2.1×10^{-18}
23	$O_2^- + O \longrightarrow O_3 + e + .6$ ev	3.0×10^{-10}
72	$O_2^- + O_2(^1\Delta g) \longrightarrow 2O_2 + e$	2.0×10^{-10}
52	$O_2^- + O_2 \longrightarrow 2O_2 + e$	1.6×10^{-22}
54	$O_2^- + N \longrightarrow NO_2 + e + 4.1$ ev	5×10^{-10}

CHARGE EXCHANGE AND REARRANGEMENT

11	$O^- + O_2 + O_2 \longrightarrow O_3^- + O_2$	1.2×10^{-30}
9	$O^- + O_3 \longrightarrow O_3^- + O$	5.66×10^{-10}
13	$O^- + NO + M \longrightarrow NO_2^- + M$	1.0×10^{-29}
55	$O^- + NO_2 \longrightarrow NO_2^- + O$	1.2×10^{-9}
12	$O^- + CO_2 + M \longrightarrow CO_3^- + M$	9.0×10^{-29}
2	$O_2^- + O \longrightarrow O_2(^1\Delta g) + O^-$	3.28×10^{-10}

TABLE VIIIa, (cont'd)

CHARGE EXCHANGE AND REARRANGEMENT (cont'd)

25	$O_2^- + O_2 + M \longrightarrow O_4^- + M$	4.0×10^{-31}
26	$O_2^- + O_3 \longrightarrow O_3^- + O_2$	2.17×10^{-10}
27	$O_2^- + CO_2 + O_2 \longrightarrow CO_4^- + O_2$	2.0×10^{-29}
28	$O_2^- + CO_2 + CO_2 \longrightarrow CO_4^- + CO_2$	9.0×10^{-30}
15	$O_2^- + NO_2 \longrightarrow NO_2^- + O_2$	8.0×10^{-10}
19	$O_3^- + O \longrightarrow O_2^- + O_2$	1.0×10^{-10}
36	$O_3^- + NO \longrightarrow NO_2^- + O_2$	1.0×10^{-11}
40	$O_3^- + NO \longrightarrow NO_3^- + O_2$	2.0×10^{-10}
39	$O_3^- + NO_2 \longrightarrow O_3 + NO_2^-$	1.9×10^{-11}
31	$O_3^- + CO_2 \longrightarrow CO_3^- + O_2$	4.0×10^{-10}
29	$O_4^- + O \longrightarrow O_3^- + O_2$	4.0×10^{-10}
18	$O_4^- + M \longrightarrow O_2^- + O_2 + M$	1.7×10^{-14}
44	$O_4^- + NO \longrightarrow NO_3^- + O_2$	2.5×10^{-10}
43	$O_4^- + CO_2 \longrightarrow CO_4^- + O_2$	4.3×10^{-10}
21	$CO_3^- + O \longrightarrow O_2^- + CO_2$	8.0×10^{-11}
47	$CO_3^- + NO \longrightarrow NO_2^- + CO_2$	9.0×10^{-12}
48	$CO_3^- + NO_2 \longrightarrow NO_3^- + CO_2$	8.0×10^{-11}
45	$CO_3^- + O \longrightarrow CO_3^- + O_2$	1.5×10^{-10}
41	$CO_4^- + O_2 \longrightarrow O_4^- + CO_2$	2.0×10^{-14}
62	$CO_4^- + O_3 \longrightarrow O_3^- + O_2 + CO_2$	1.3×10^{-10}
60	$CO_4^- + NO \longrightarrow NO_3^- + CO_2$	4.8×10^{-11}
20	$NO^- + O_2 \longrightarrow NO + O_2^-$	5.0×10^{-10}
59	$NO_2^- + O_3 \longrightarrow NO_3^- + O_2$	1.8×10^{-11}

TABLE VIII,a (cont'd)

CHARGE EXCHANGE AND REARRANGEMENT (cont'd)

63	$NO_2^- + NO_2 \longrightarrow NO_3^- + NO$	4×10^{-12}
49	$O_2^-\cdot H_2O + CO_2 \longrightarrow CO_4^- + H_2O$	5.8×10^{-10}
67	$X^- + YZ^+ \longrightarrow X + ZY$	1×10^{-7}
66	$YZ^+ + e \longrightarrow Y + Z$	1×10^{-5}
50	$O^- + N_2O \longrightarrow NO^- + NO$	1×10^{-10}

HYDRATIONS

14	$O_2^- + H_2O + M \longrightarrow O_2^-\cdot H_2O + M$	2.2×10^{-28}
69	$O_2^-\cdot H_2O + H_2O + M \longrightarrow O_2^-\cdot (H_2O)_2 + M$	5.4×10^{-28}
68	$O_4^- + H_2O \longrightarrow O_2^-\cdot H_2O + O_2$	1.4×10^{-9}
57	$NO_2^- + H_2O + M \longrightarrow NO_2^-\cdot H_2O + M$	1.6×10^{-28}
64	$NO_2^-\cdot H_2O + H_2O + O_2 \longrightarrow NO_2^-(H_2O)_2 + O_2$	3.8×10^{-29}
70	$NO_3^- + H_2O + M \longrightarrow NO_3^-\cdot H_2O + M$	7.5×10^{-29}
71	$NO_3^-\cdot H_2O + H_2O + M \longrightarrow NO_3^-\cdot (H_2O)_2 + M$	3.4×10^{-29}

TABLE VIIIb

PRIMARY PRODUCTION AND INPUT CONCENTRATIONS FOR NEGATIVE-ION COMPUTATIONS

	65 km	75 km	80 km
$q(N_2^+)$ (sec^{-1})	.02	.015	.0068
$q(NO^+)$	.22	5.3	34
$q(O_2^+)$	.0082	.004	.0022
O (cm^{-3})	$.23 \times 10^{11}$	$.36 \times 10^{11}$	$.26 \times 10^{11}$
O_2	$.48 \times 10^{15}$	$.2 \times 10^{15}$	$.65 \times 10^{4}$
NO	$.85 \times 10^{9}$	$.3 \times 10^{8}$	$.14 \times 10^{9}$
H_2O	$.25 \times 10^{11}$	$.7 \times 10^{10}$	$.2 \times 10^{10}$
$M(=O_2+N_2)$	$.23 \times 10^{16}$	$.1 \times 10^{16}$	$.31 \times 10^{15}$
CO_2	$.69 \times 10^{12}$	$.3 \times 10^{12}$	$.94 \times 10^{12}$
N	$.30 \times 10^{6}$	$.1 \times 10^{10}$	$.50 \times 10^{6}$
$O_2(^1\Delta g)$	$.20 \times 10^{11}$	$.4 \times 10^{2}$	$.7 \times 10^{10}$
O_3	$.6 \times 10^{10}$	$.32 \times 10^{9}$	$.9 \times 10^{8}$
NO_2	$.2 \times 10^{5}$	$.1 \times 10^{2}$	$.1 \times 10^{2}$
N_2	$.18 \times 10^{16}$	$.69 \times 10^{15}$	$.24 \times 10^{15}$
OH	$.25 \times 10^{6}$	$.6 \times 10^{7}$	$.18 \times 10^{6}$
HO_2	$.3 \times 10^{6}$	$.4 \times 10^{8}$	$.3 \times 10^{6}$
N_2O	$.10 \times 10^{10}$	$.85 \times 10^{8}$	$.1 \times 10^{9}$
CO	$.23 \times 10^{9}$	$.3 \times 10^{11}$	$.94 \times 10^{9}$
H_2	$.7 \times 10^{6}$	$.2 \times 10^{9}$	$.2 \times 10^{7}$
H	$.2 \times 10^{7}$	$.6 \times 10^{8}$	$.5 \times 10^{8}$

TABLE VIIIc

COMPUTED CONCENTRATIONS OF POSITIVE AND

NEGATIVE IONS AT 65, 75, and 80 KM.

Positive ions

	65 km	75 km	80 km
N_e	93	1113	4034
λ	1.28	.002	.001
N_2^+	$.828 \times 10^{-6}$	$.246 \times 10^{-5}$	$.2 \times 10^{-5}$
NO^+	4.018	485.4	2828
O_2^+	$.8507 \times 10^{-2}$	$.537 \times 10^{-1}$	.08
O_4^+	$.427 \times 10^{-3}$	$.114 \times 10^{-2}$	$.37 \times 10^{-3}$
$O_2^+(H_2O)$	$.430 \times 10^{-3}$	$.114 \times 10^{-2}$	$.37 \times 10^{-3}$
$NO^+(H_2O)$	3.583	369.6	1156
$NO^+(H_2O)_2$	1.959	130.5	26.9
$NO^+(H_2O)_3$	.1126	3.199	.167
$NO^+(CO_2)$	$.153 \times 10^{-1}$	.6231	28.8
H_3O^+	$.1710 \times 10^{-1}$	.5541	.013
$H_3O^+(H_2O)$	.3435	.8502	.042
$H_3O^+(H_2O)_2$	201.8	123.5	.5126
$H_3O^+(H_2O)_3$	1.705	.2909	$.32 \times 10^{-3}$
$H_3O^+ \cdot OH$	$.223 \times 10^{-3}$	$.988 \times 10^{-4}$	$.216 \times 10^{-3}$
$H_3O^+ \cdot OH \cdot H_2O$	$.9961 \times 10^{-4}$	$.2814 \times 10^{-4}$	$.21 \times 10^{-4}$
$H_3O^+ \cdot OH \cdot O_2$	$.9961 \times 10^{-4}$	$.2814 \times 10^{-4}$	$.21 \times 10^{-4}$

TABLE VIII c, (cont'd)

Negative Ions

	65 km	75 km	80 km
O^-	$.148 \times 10^{-1}$	$.5694 \times 10^{-2}$	.19
O_2^-	2.171	1.134	.1.8
O_3^-	$.1115 \times 10^{-1}$	$.1604 \times 10^{-1}$	$.126 \times 10^{-3}$
O_4^-	$.8201 \times 10^{-2}$	.1366	$.49 \times 10^{-4}$
NO^-	6127×10^{-8}	$.4840 \times 10^{-9}$	$.58 \times 10^{-7}$
NO_2^-	$.9016 \times 10^{-1}$	$.1962 \times 10^{-1}$	$.91 \times 10^{-3}$
NO_3^-	.5682	$.1726 \times 10^{-1}$	$.106 \times 10^{-2}$
CO_3^-	1.886	.6599	$.3 \times 10^{-1}$
CO_4^-	.1967	$.4404 \times 10^{-3}$	$.42 \times 10^{-2}$
$O_2^- \cdot H_2O$	$.7317 \times 10^{-3}$	$.7694 \times 10^{-2}$	$.35 \times 10^{-6}$
$O_2^- \cdot (H_2O)_2$	.2234	$.3866 \times 10^{-1}$	$.61 \times 10^{-7}$
$NO_2^-(H_2O)$	$.6384 \times 10^{-6}$	$.3725 \times 10^{-8}$	$.1 \times 10^{-9}$
$NO_2^-(H_2O)_2$	$.1372 \times 10^{-4}$	-	-
$NO_3^- H_2O$	1.24	$.6657 \times 10^{-2}$	$.11 \times 10^{-3}$
$NO_3^-(H_2O)_2$	113.5	$.4181 \times 10^{-2}$	$.62 \times 10^{-5}$

CHAPTER VI

SUMMARY AND FINAL CONCLUSIONS

The intent of this work has been to produce an improved formulation of the ion chemistry in the D-region, which is based upon a careful reworking of the input parameters and a new computational scheme for non-linear ion-kinetic equations. This task has required a review of the observational evidence, existing ion-kinetic reactions, and the theory of mesospheric nitric oxide, and has led to a formulation of water vapor transport which incorporated neutral atmospheric motions and ice crystal growth.

The main experimental reference points are the ion profiles measured on rocket flights and the characteristics of noctilucent clouds. The improvement in the modeling of positive-ion chemistry has been derived from the realization that currently accepted positive ion-kinetic reactions formed a more or less satisfactory set, and that, hence, only minor revisions of each component part would be necessary. Consequently, this has led to the use of a) all ionizing radiations which penetrate to below 90 km, b) atmospheric models for high latitudes and specific seasons, c) revised nitric oxide profiles, d) current values for rate constants and recombination coefficients, e) an inclusion of temperature sensitive "backward" reactions among cluster ions, f) dust as an attachment sink for electrons and positive ions, and g) a modified water vapor profile.

The modified water vapor profile is obtained from a computation of water vapor diffusion up from the mid-stratosphere where reliable number density measurements exist. A downward flux of dust and a vertical neutral atmosphere drift were the hitherto foreign elements incorporated in the formulation. A flux of dust is certainly valid considering the number of observations of dust made in the mesosphere and higher. A vertical drift of the neutral atmosphere is perhaps the most ad hoc of the inclusions, but it is strongly inferred by several studies and is not at variance with any experimental data.

The net result of these revisions has been a) to offer substantial improvements in matching the various elements of D-region ion-kinetics with rocket measurements, b) to formulate analytically the growth of a "visible" ice crystal on dust falling through the supersaturated summer mesopause, c) and to successfully compute the non-linear negative-ion reaction set without convergence problems. Detailed results have already been enumerated in the appropriate chapters.

Among these, a significant achievement was the matching of observed electron densities ($\sim$ 300 cm^{-3}) at 80 km while concurrently maintaining a high water cluster-ion to nitric oxide cluster ratio. Previously these two items had been mutually exclusive and success here is due to a) an increase of the ionization of O_2 relative to NO due to the use of CIII and Lyβ radiation, b) somewhat lower NO concentrations and c) high values of water vapor. Many detailed profiles of the concentrations of particular hydrated water clusters were computed and are shown to be highly dependent upon a) the

profiles of neutral constitutents used, b) the nitric oxide concentrations, c) the concentration of atomic oxygen in its ground state which determines the cluster-ion ceiling height, and d) values of the photodissociation constant and eddy diffusion coefficient which strongly influence water vapor. Observed values of ion profiles could be matched more closely by including various sets of J, and profiles of $O(^4S)$, and using those which provided a ceiling height at 84 km since current values of J and $[O(^4S)]$ are probably too small at 84 km.

The inclusion of dust as an attachment sink for positive ions and electrons (even within the limits of a steady-state formulation) has been shown to greatly modify the effective recombination coefficient under certain conditions. The dust flux and size used could be further adjusted to provide a closer fit with observation and refine the model results.

A key result of the use of our particular dust sizes and concentrations has been the achievement of the growth of visible ice crystals at the mesopause. The model results demonstrate a seasonal dependence and a match with the observed features of noctilucent clouds. Further progress would require a) greater verification of dust concentrations and sizes aloft, b) a considerable improvement in our understanding of the general circulation in the mesosphere, and c) knowledge of the source function for water vapor at the base of the stratosphere.

The solution of the negative-ion kinetics is based upon the ability to manage the inherent non-linearity of the continuity

equations by means of a subroutine, AL316. The key to this success was to keep the electron density within the main program as the iterated variable. At altitudes of 65 km convergence was no problem with the complete set of 89 positive- and negative-ion reactions, which includes all principal reaction categories. This computational achievement is a useful contribution to negative ion-kinetics.

Modifications and improvements of the present work are suggested in four areas which would serve as follow-on investigations to the present one.

1. As discussed in section 4 of Chapter IV the concentration of dust approaches infinity when the Stokes velocity equals neutral updraft velocity. This means that the dust could increase to an infinite concentration in a layer with an infinite concentration gradient above and below it. A formulation which incorporates a term for the diffusive flux of dust would result in a more blunt layer and avoid the problem of the mathematical singularity.

2. A more complete formulation of drift of the neutral atmosphere should be made which would require the inclusion of horizontal components on a global scope instead of one dimensional vertical drift.

3. A second order adjustment of the H_2O profile may be provided by including neutral chemistry of H_2O in the mesosphere, particularly the reactions with CH_4. A possible formulation is offered in Appendix VI.

4. The potential for use of this negative-ion computational scheme is considerable. It should be investigated and exploited by being extended to lower altitudes and by the inclusion of the best current data to investigate the D-region under geophysically quiet and disturbed conditions.

LIST OF APPENDICES

Appendix I

Included herein are mass-filter ion profiles and a shorthand tabulation of the parameters pertinent to these measurements. The data is by no means complete but merely serves to identify the main features of the experiment and geophysical conditions.

CHECK LIST - 1

1. Author and Ref: R. S. Narcisi and A. D. Bailey, "Mass Spectrometer Measurements of Positive-Ions at Altitudes from 64 to 112 km." JGR 70, 3687, 1965.

2. Purpose of Investigation: 1 (+) ion profile. Test spectrometer.

3. Equipment Flown:

   (a) Quadrupole mass spectrometer. Liquid N chilled Zeolite pump

4. Date, Time. Launch Site, Latitude, Rocket Equipment:

   (a) Oct. 31, 1963 1200 LT Eglin, AFB Florida
   AFCRL #AC 6.341 Day X=44° Range 1-46 amu Apogee 111.7 km.

5. Geophysical Conditions: Quiet.

6. Scientific Results:

   (a) Ceiling at 83 km: NO^+, O_2^+ dominate above. 19^+ and 37^+ dominate below.

   (b) Metalic ion layers found at 95 km and above 105 km. 2 graphs for results: 65-82 km; 82-120 km.

   (c) No electron profile.

7. Interpretation of Results? No.

8. Literature and theory discussed? No.

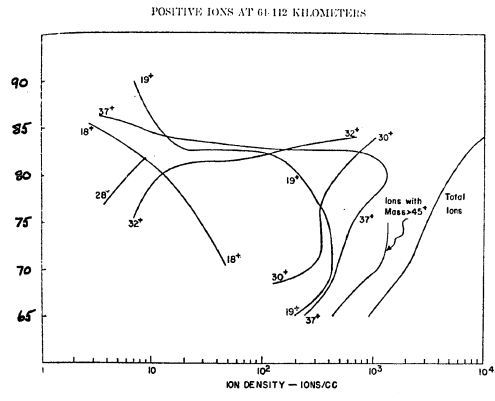

Profile 1a

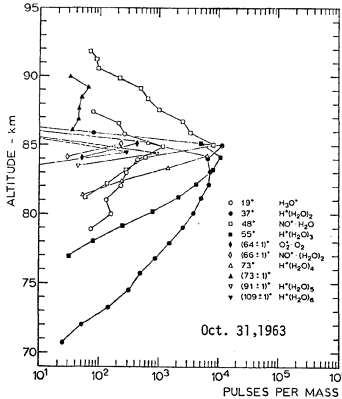

Normalized counts per mass peak for cluster ions obtained on the upleg.

Profile 1b

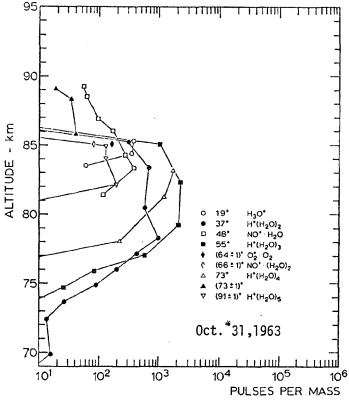

Normalized counts per mass peak for cluster ions obtained on the down leg.

Profile 1c

CHECK LIST - 2

1. Author and Ref: R. S. Narcisi, "Ion composition measurements and related ionospheric processes in the D and lower E regions." Ann. Geophys., 22, 224, 1966.

2. Purpose of Investigation: Positive-ion measurement.

3. Equipment Flown:

   (a) Quadrupole Mass Spectrometer.

4. Date, Time, Launch Site, Latitude. Rocket Equipment:

   (a) Mar. 11, 1964 1200 LT Eglin, Florida
   AC6.342 Pump failed; DC connector broke;
   NIKE-CAJUN could measure total current made above 34 mau. Mass spec unsuccessful.

   (b) Oct. 31, 1963 1200 LT Eglin, Florida Good (+) ion profile
   AC6.341

   (c) Mar. 6, 1965 0132 LT Ft. Churchill No profile. AD3.613

5. Geophysical Conditions: See Narcisi (1966b).

6. Scientific Results: None from the one original rocket shot Mar. 11, 1975.

   (a) Metallic-ion layers. No good profiles showing both.

   (b) Cluster-ions and metallic-ion layers and transition.

7. Interpretation of Results? No.

8. Literature and theory discussed? Yes. Chapman and Kendall Water and dust clusters also.

CHECK LIST - 3

1. Author and Ref: R. S. Narcisi, "Ion composition of the mesophere" Space Res. V11, 186, 1966.

2. Purpose of Investigation: (+) ion shots.

3. Equipment Flown:

   (a) Quadrupole mass spectrometer.

4. Date, Time, Launch Site, Latitude, Rocket Equipment:

   (a) Oct, 31, 1963 1200 LT Eglin, Florida X=44°
   AC6.341 Day Apogee = 111.7 km.
   NIKE-CAJUN 1-45 amu.

   (b) Mar. 6, 1965 0132 Ft. Churchill Apogee = 192.5 km
   AD3.613 No profile
   AEROBEE HI Night

   (c) Nov. 17, 1965 1222 CST Eglin, Florida X=49°
   AE6.379 Day Apogee 112.9 km
   NIKE-CAJUN

   (d) Nov. 17, 1965 2320 CST Eglin, Florida Apogee 115.8 km
   AE6.382 Night
   NIKE-CAJUN

5. Geophysical Conditions: Quiet: aurora: meteor shower: E_s.

6. Scientific Results: Good profiles for all but Mar. 6, 1965 which was not profiled.

   (a) No^+ and O_2^+ above ledge, cluster ions below.

   (B) Metallic ions ledges at 95 km and 115 km. No metallic transition graphed.

7. Interpretation of Results? No.

8. Literature and theory discussed? No.

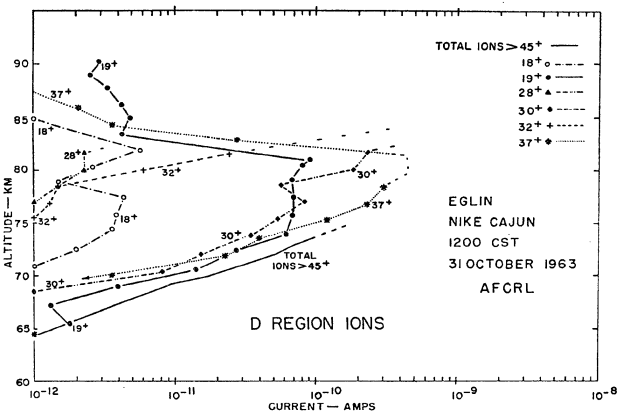

Positive ion composition of the daytime D region measured by a quadrupole mass spectrometer on rocket ascent.

Profile 3a

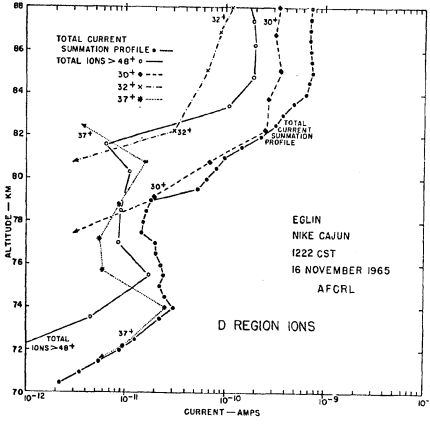

Profile 3b

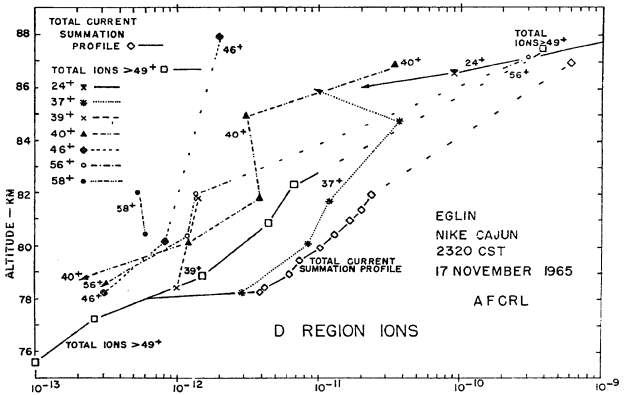

Positive ion composition of the nighttime D region measured by a quadrupole mass spectrometer on rocket ascent. The ions 56^+, 24^+ and 40^+ increase rapidly to form a sporadic E layer at 89 km. Arrows indicate the limits of detectability at the designated altitudes.

Profile 3c

CHECK LIST - 4

1. Author and Ref: R. S. Narcisi, A. D. Bailey, L. E. Wlodyka and C. R. Philbrick, "Ion Composition Measurements in the lower ionosphere during Nov. 1966 and March 1970 solar eclipse", JATP, 34, 647-658, 1972.

2. Purpose of Investigation: (+) measurements in D and E regions (Nov). during eclipse. (-) measurements at March 1970 eclipse.

3. Equipment Flown:

   (a) Quadrupole mass spec. 10-64 amu mass range
   Retarding potential analyzer: (+) ion conc. to 86 km. Electron to 64 km. Impedance Probe

   (b) Langmuir probe
   Spherical ion trap
   X-ray detector
   Lyα detector

   (c) (-) ion mass spec: pulse counting detection system.

4. Date, Time, Launch Site, Latitude, Rocket Equipment:

(a) Nov. 5, 1966	1355:21 GMT	Cassino, Brazil 32°S	
(+) ion		Apogee 106.2 only ascent good.	
NIKE-HYDAC CERTIFICATION		Payload failed to separate from motor. Severe coning.	
(b) Nov. 12, 1966	1354 GMT	80% obscured	Cassino
+) ion D-4	low altitude	300% above 90, 20%	
		Apogee 107 km. Descent measurements only.	
(c) Nov. 13, 1966	1408:37	Totality	Cassino
(+) D-11	low altitude	300% above 90,20%	
		Apogee 95 km. Ascent and descent within 50% of each other.	
(d) Mar. 7, 1970	1839:30	99.2-96.5%	Wallops Is.
(+) NIKE-IROQUOIS		obscuration	
A07.902-5		Apogee 111 km. 14-170 amu	

5. Geophysical Conditions: Eclipse Nov. 12, 1966, Mar. 7,1970

6. Scientific Results:

   (a) (+) ions, NO^+ decreases in totality and clusters build up

   (b) Normal metallic ions at 105 km in E region

7. Interpretation of Results: Fast conversion of NO^+ requires conglomerates of water-ice. (-) ion clusters imply large conglomerates. Fast attachment process required to provide rapid decrease in electron density. E region results during eclipse are standard and explainable.

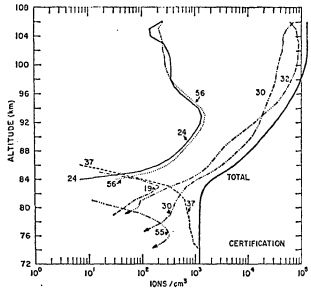

Major positive ions in the D- and E-regions for a full sun at about 20° solar zenith angle.

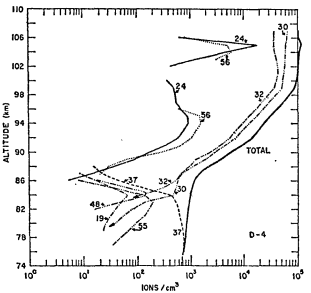

Profile 4a

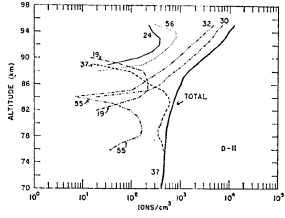

Profile 4b

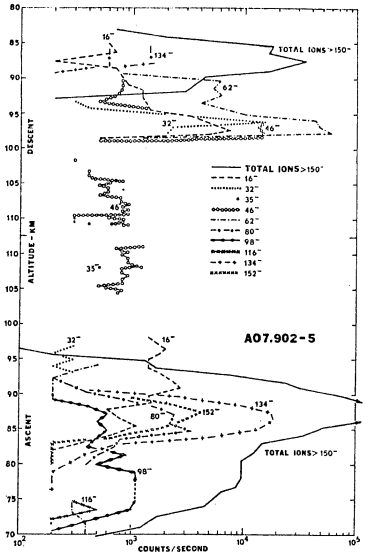

Negative ion composition measurements shortly following totality. The solar obscuration was 99·1–99·2 per cent in the 70–111 km upleg region and 97·8–96·6 per cent in the 111–82 km downleg region. The vehicle angle of attack was between 0 and 12° from 70–90 km on upleg and decreased uniformly from 32 to 6° on descent from 100–82 km.

Profile 4c

CHECK LIST - 5

1. Author and Ref: R. S. Narcisi, "Processes associated with metal-ion layers in the E-region of the ionosphere" Space Res. VIII, 360, 1967.

2. Purpose of Investigation: Relationship of Metallic-ion to molecular Layering on the E-Region.

3. Equipment Flown:

   (a) Quadrupole Mass Spectrometer.

4. Date, Time, Launch Site, Latitude, Rocket Equipment:

   (a) April 12, 1967 1849 CST X=98.6° Eglin AFB
   NIKE-IROQUOIS

   (b) Nov. 16, 1967 1222 CST Eglin AFB Apogee 112.9 km.
   AE 6.379 Day
   NIKE-CAJUN

5. Geophysical Conditions: Leonid meteor shower (Nov. 16, 1965 shot).

6. Scientific Results: Profiles of relative percentages of NO^+, O_2^+ and metallic ions 80-120 km.

   (a) A minimum in NO^+ and O_2^+ occurs at maximum in metallic-ions.

   (b) Nov. 16, 1965 shot analyzed for cluster ions also. Narcisi (1966).

7. Interpretation of Results: Charge exchange $NO^+ + M \rightarrow M^+ + NO$ explains the minimum, O_2^+ is not as quick with charge exchange.

8. Literature and theory dicsussed? Yes.

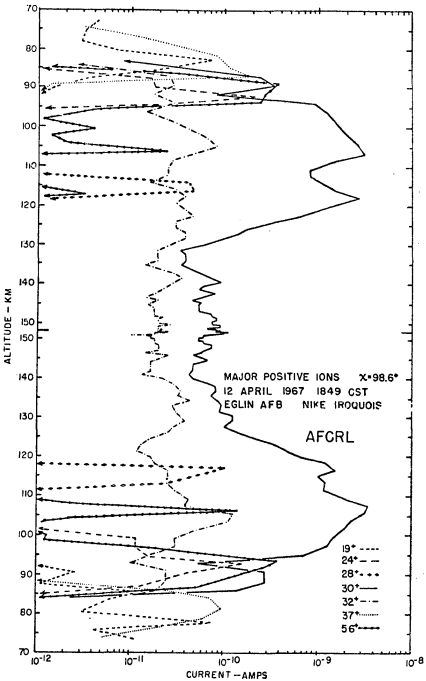

The positive ion composition of the D and E regions shortly after sunset.

Profile 5a

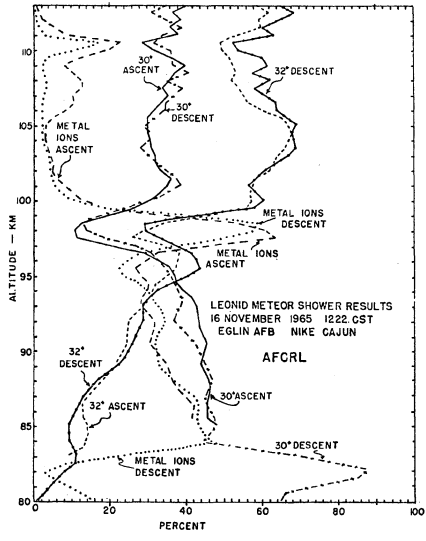

Profile 5b

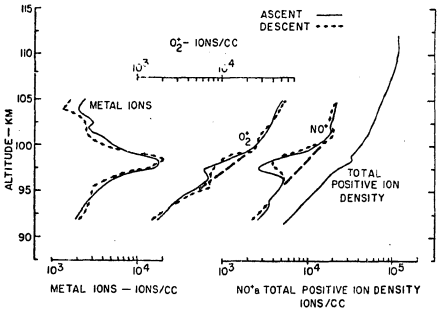

LEONID METEOR SHOWER RESULTS
16 NOVEMBER 1965 1222 CST
EGLIN AFB NIKE CAJUN

AFCRL

Profile 5c

CHECK LIST - 8

1. Author and Ref: Narcisi, R. S., C. Sherman, C. R. Philbrick, D. M. Thomas, A. D. Bailey, L. E. Wlodyka, R. A. Wlodyka, D. Baker and G. Federico, Negative ion composition of the D & E regions during a PCA, in Proc. COSPAR Symposium of Solar Particle Event of November 1969, AFCRL, 411, 1972.

2. Purpose of Investigation: (-) ion composition measurements.

3. Equipment Flown:

   (a) Cryopumped quadrupole mass spectrometers with pulse counting detection system. (Potential of +10v will gather negative ions above 90 km in E-region) (Potential of more than 10v necessary in D-region)

   (b) Collector plate biased to +40v in Nov. shots

4. Date, Time, Launch Site, Latitude, Rocket, Equipment:

   (a) Aug. 13, 1969 0423 GMT 12-79 amu Ft. Churchill
   Night
   Sample plate bias = +20v or 0 to 20v in steps. 79-90 cut off below 80 km

   (b) Oct. 11, 1969 0200 GMT 162 amu. Mass resolution low
   Heavy ion run Night

   (c) Nov. 3, 1969 0629 GMT X=136° Ft. Churchill
   Night pump failed and heavy ions appear only on downleg scan.

   (d) Nov. 3, 1969 1749 GMT X=73.9° "
   Day

5. Geophysical Conditions: Aug. and Oct. Flights, quiescent
   Nov. flights PCA conditions.

6. Scientific Results:

   (a) Mass peaks Aug. night: 32, 35, 37, 61, 63, 76 amu
   High decrease neg. ions from 90 to 92 km

   (b) Oct: Peaks at 62, 80, 98, 116, 134, 152 amu. $NO_3(H_2O)_n$ n = 0-5 Nov: PCA: 16, 32, 62, 98, 116, 134 amu

(c) Nov. Daytime 32-between 76 and 94, 76 amu = CO_4 below 77

7. Interpretation of Results: No.

8. Literature and theory discussed? No.

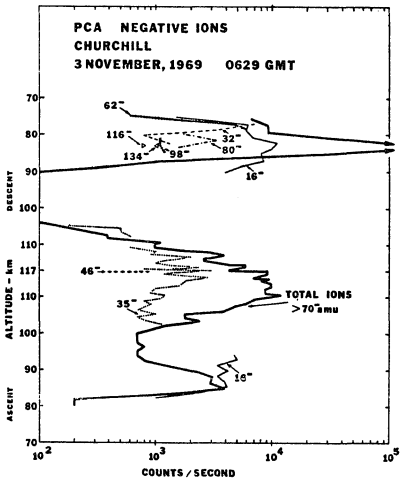

Nighttime Negative Ion Composition Measurements in the D and E Regions During a PCA

Profile 8a

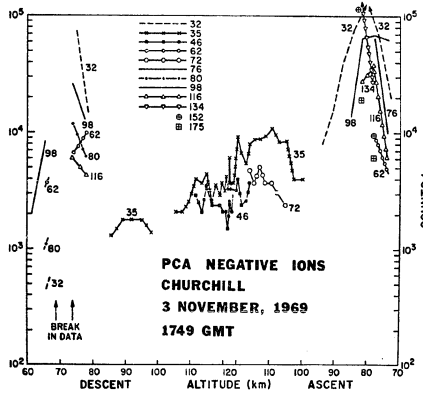

Daytime Negative Ion Composition Measurements in the D and E Regions During a PCA

Profile 8b

CHECK LIST - 9

1. Author and Ref: Narcisi, R. S., C. R. Philbrick, D. M. Thomas, A. D. Bailey, L. E. Wlodyka, D. Baker, G. Federico, R. Wlodyka and M E. Gardener, Positive ion composition of the D & E regions during a PCA in Proc. COSPAR Symposium on Solar Particle Event of November 1969, AFCRL, 421, 1972.

2. Purpose of Investigation: (+) ion profiles to compare to mid-latitude quiescent conditions.

3. Equipment Flown:

   (a) Cryopumped positive-ion mass spectrometer
   Cylindrical Langmuir probe

4. Date, Time, Launch Site, Latitude, Rocket Equipment:

   (a) Nov. 3, 1969 0130 CST X=133°, 13.5-108.5 amu
   #AG7.882 Ft. Churchill all shots 72-139 km.

   (b) Nov. 3, 1969 1130 CST X=74 , 9.5-7.15 amu Success
   AH7.886 73-144 km Daytime

   (c) Nov. 4, 1969 1650 CST X=94.6°, 12.5-67.0 amu Success
   AH7.893 78-144 km Sunset

5. Geophysical Conditions: Nov. 2-4, 1969, PCA

   AG7.882 Riometer Absorption - .4 dB
   AH7.886 Riometer Absorption - 3 dB
   AH7.893 Riometer Absorption - .7 dB

6. Scientific Results:

   (a) Water cluster ceiling about 80 $H_5O_2^+$, H_3O^+ dominate below 77 during PCA at $10^4(cm^{-3})$ conc. nighttime high conc.

   (b) Cluster conc. = $10^3(cm^{-3})$ by daytime and ceiling at 82 km. Similar to mid-latitude conditions.

   (c) Cluster conc. = $10^2(cm^{-3})$ at Sunset.

7. Interpretation of Results. No

8. Literature and theory discussed? No

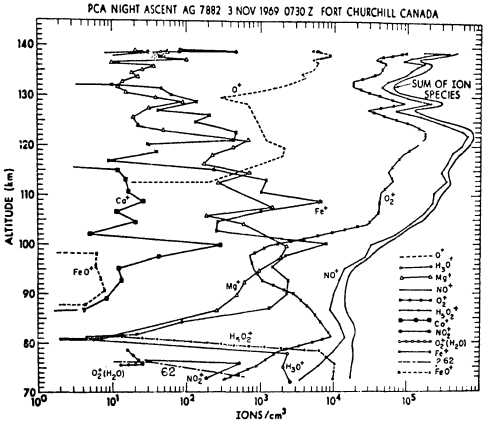

The Positive Ion Composition in the Nighttime D and E Regions During a Simultaneous PCA Event and Auroral Event

Profile 9a

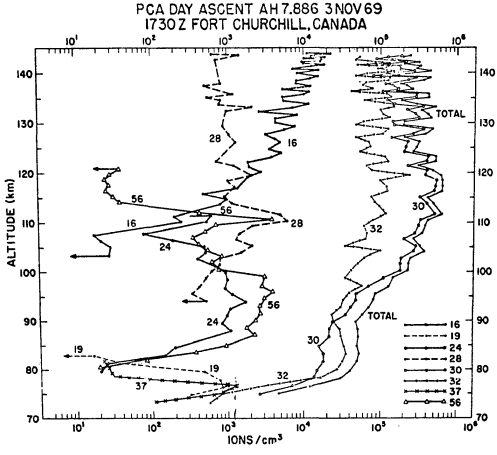

Daytime Positive Ion Composition of the D and E Regions During a PCA

Profile 9b

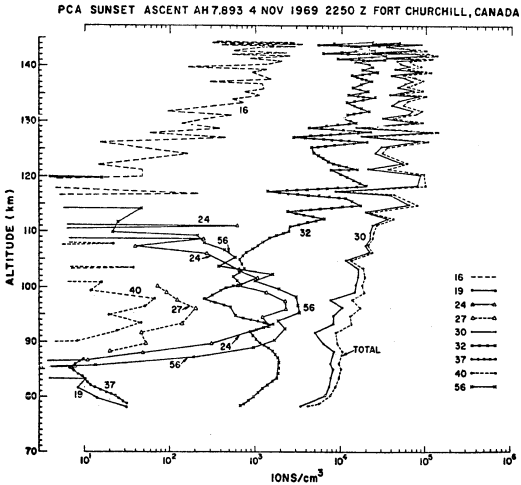

Sunset Positive Ion Composition of the D and E Regions During a PCA

Profile 9c

CHECK LIST - 10

1. Author and Ref: R. A. Goldberg and L. J. Blumle, "Positive-ions composition from a rocket-borne mass spectrometer," JGR, 75, 133, 1970.

2. Purpose of Investigation: (+) ion measurement. Test new Ti pump.

3. Equipment Flown:

   (a) Quadrupole mass spec. Titanium getter pump. Range 13 to 49 amu. CW radio propagation Exp: 73.6 and 24.53 Mhz for absolute calibration.

   (b) Ground based ionosonde.

4. Date, Time, Launch Site, Rocket Equipment:

   (a) Mar. 15, 1968 1415 LT Wallops Is. X=48.8°
   NASA #18.10 Day
   Upleg: Measured 98 303 km.
   Downleg: Measured 303 to 68 km. 13 to 49 amu.

5. Geophysical Conditions: Quiet.

6. Scientific Results:

   (a) 30^+ and 32^+ with $NO^+ > O_2^+$ dominate above 100 km.

   (b) 19^+ and 37^+ appear below 85.

7. Interpretation of Results: Where are metallic ions? Na 23^+, 24^+, 25^+, 26^+ - Mg and Ca^+, 40^+?

8. Literature and theory discussed? Some.

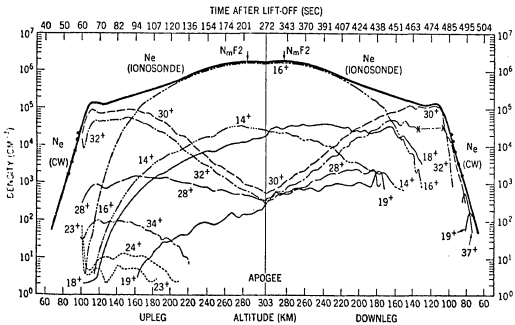

Positive ion composition measured by NASA 18.10. Up- and downleg results are shown as a function of altitude and time. The electron concentration profile used for normalization is also illustrated.

Profile 10

CHECK LIST - 11

1. Author and Ref: R. A. Goldberg and A. C. Aiken, "Studies of positive ion composition in the equatorial D-region ionosphere," JGR 76, 8352, 1971.

2. Purpose of Investigation: (+) ion in situ measurement.

3. Equipment Flown:

   (a) Quadrupole Mass Spectrometers Ti getter pumps. Improvements from Goldberg and Brumle, JGR 75, 133. Monitor for Lyα, X-rays 2A-8A.

   (b) Gerdien Condenser.

4. Date, Time, Launch Site, Latitude, Rocket, Equipment:

   (a) Mar. 19, 1970 0827 LT Z=53.2° Thumba, India
   NASA 14.425 Day Data on up and down
   NIKE-APACHE Apogee 100 km.

   (b) Mar. 19, 1970 1071 LT Z=27.8° Thumba, India
   NIKE 14.424 Day Data up and down
   NIKE-APACHE Apogee 122 km.

5. Geophysical Conditions: Quiet.

6. Scientific Results:

   (a) Cluster ions belwo 86, NO^+, and O_2^+ above.

   (b) Large difference in up and down leg data. Shock decomposition on up leg of large clusters into smaller clusters. Wake composition more reliable.

   (c) 55^+ clusters peak at Lyα peak indicating a formation from NO^+. 37^+ clusters dominates for X=27 and not for X=53 indicating X-ray control through O_2^+.

7. Interpretation of Results: By means of vapor phase reactions through O_2^+ to generate clusters. Burke H reaction. Gets a reasonable cluster profile.

8. Literature and theory discussed? Yes.

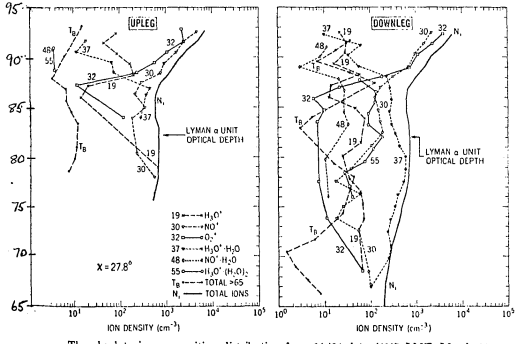

The absolute ion-composition distribution from 14.424 data (1017 LMT, March 19, 1970).

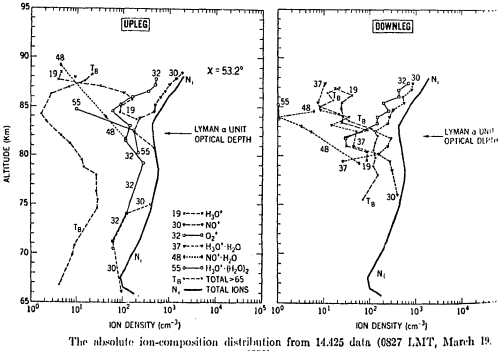

The absolute ion-composition distribution from 14.425 data (0827 LMT, March 19, 1970).

Profile 11

CHECK LIST - 12

1. Author and Ref: D. Krankowsky, F. Arnold, H. Wider, J. Kissel, J. Zahringer, "Positive-ion composition in the lower ionosphere," Radio Sci. 7, 93-98, 1972.

2. Purpose of Investigation: (+) ion composition high latitudes.

3. Equipment Flown:

   (a) Quadrupole mass spectrometer, cryogenically pumped He.

4. Date, Time, Launch Site, Latitude, Rocket, Equipment:

   (a) March 23, 1970 0039 LT X=95.5° Andoya Sporadic E
   C58/a Centaur and NLC

   (b) April 9, 1969 2138 LT X=96.9° Andoya
   F20 NIKE-APACHE

   (c) Aug. 10, 1970 0039 LT
   C58/2

   (d) Nov. 26, 1969 0138 LT X=128.8° Anodya
   F21 NIKE-CAJUN

5. Geophysical Conditions: Low absorbtion, E_s, NLC

6. Scientific Results: Riometer = 1.6-3.; 1.4; .2; Es and NLC

   (a) More hydrated clusters on downleg: reduced shade conditions

   (b) NO^+ and O_2^+ increase above ceiling: $NO^+ > O_2^+$ below; $NO^+ < O_2^+$ above

   (c) Generally cluster ions dominate below ceiling but more overlap is in these shots than others

   (d) Summer shot has higher numbers of highly hydrated clusters. $H_3O^+(H_2O)_4$ first time

7. Interpretation of Results: Cluster formation proceeds through O_2^+ sequence. Upleg and downleg differ based upon shocks.

8. Literature and theory discussed? Yes.

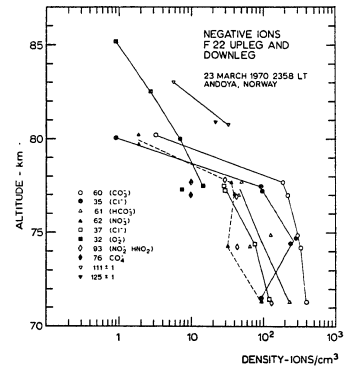

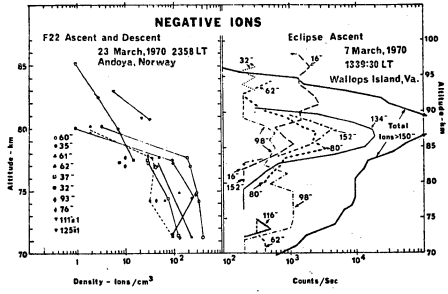

Negative ion composition measurements in the *D* region. Left panel from Arnold *et al.* (1971). Right panel from Narcisi *et al.* (1972a).

Profile 12a

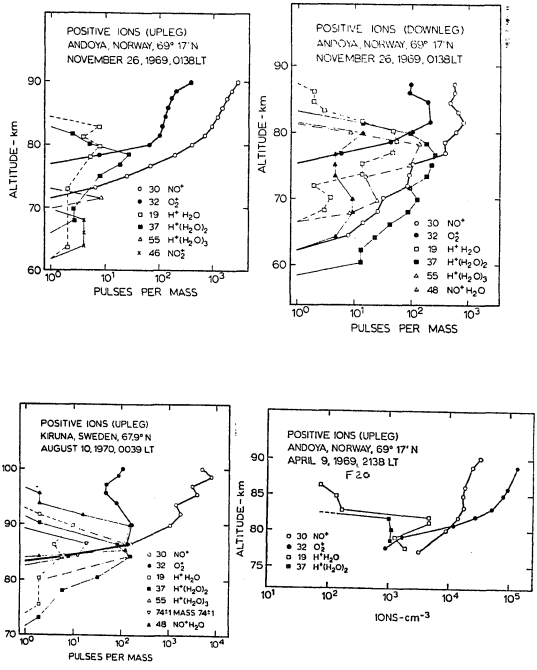

Profile 12b

CHECK LIST - 13

1. Author and Ref: F. Aronold, J. Kissel, D. Krankowsky, H. Wieder and J. Zahringer, "Negative ions in the lower ionsphere: a mass-spectrometric measurement," JATP 33, 1169-1174, 1971.

2. Purpose of Investigation: Measure (-) ions, Nighttime D-Region.

3. Equipment Flown:

   (a) Quadrupole Mass spectrometer. Liquid He cryogenic system. 2-134 amu range. Faraday rotation.

   (b) (+) and (-) ion electrostatic detector. Langmuir probe.

4. Date, Time, Launch Site, Latitude, Rocket Equipment:

   (a) Mar. 23, 1970 2358 LT Andoya, Norway
   F22 NIKE-CAJUN Night .2-134 amu 71-85 km upleg data best.

   (b) Data every 2-1/2 km.

5. Geophysical Conditions: Night - enhanced ionization in weak aurora.

6. Scientific Results:

   (a) (-) ions: O_2, Cl, CO_3, HCO_3, NO hydrates of NO_2 and NO_3 as found by Narcisi.

   (b) Rapid decrease of negative ions above 78 km (night).

   (c) Below 78 km CO_3 dominates (68) followed by Cl($\sim 10^2$).

7. Interpretation of Results? No.

8. Literature and theory discussed? No.

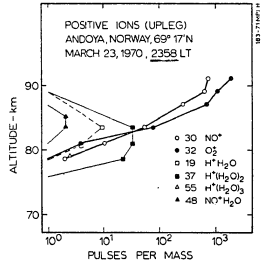

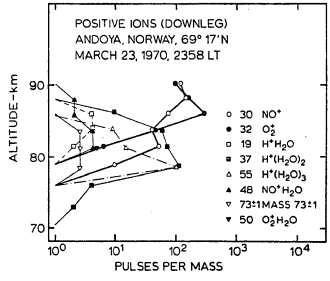

Profile 13

CHECK LIST - 14

1. Author and Ref: A. Johannessen and D. Kranskowsky, "Positive-ion composition measurement in the upper mesosphere and lower thermosphere at a high latitude during summer." JGR 77, 2888, 1972.

2. Purpose of Investigation: (+) ion at summer mesopause.

3. Equipment Flown:

   (a) Liquid helium cryopump. Quadrupole mass spectrometer 10-140 amu. 2 Electrostatic probes: Total (+) and (-) collection.

   (b) Ambient temperature, Lyα vs. height.
   Faraday rotation 1.3, 2.8, and 7.8 Mhz.

4. Date, Time, Launch site, Latitude, Rocket Equipment:

(a)	Aug. 8, 1971 NIKE-CAJUN	DAYTIME 1211GMT X=55°	Andoya, Norway 10-140 amu	69°17'N Peak alt 99.1 70.7 km to 99.1 upleg 99.1 to 68.9 downleg

   (b) .9 km between scans

5. Geophysical Conditions: Quiet, weak particle precipitation event in progress.

6. Scientific results: Set of good curves. Fig. 8 representative.

   (a) Cluster ions $H^+(H_2O)_n$ dominated below 84 km. Ceiling at 86 km.

   (b) Above 86 km, NO^+ and O_2^+ dominant w. Some Fe^+ and Mg^+

   (c) Above 86 km, $NO^+ > O_2^+$. Below 86 $NO^+ < O_2^+$.

   (d) H_3O^+ seen in diminishing amounts to 87 km.

7. Interpretation of Results? Yes.

8. Literature and theory discussed? Yes. Considers vapor phase reactions.

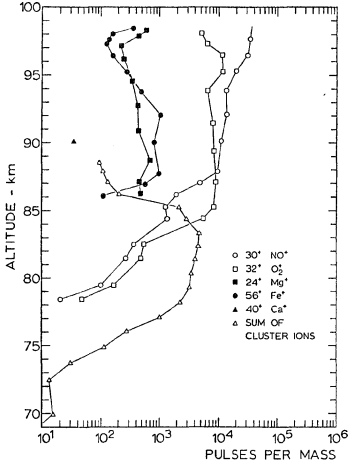

Profile 14a

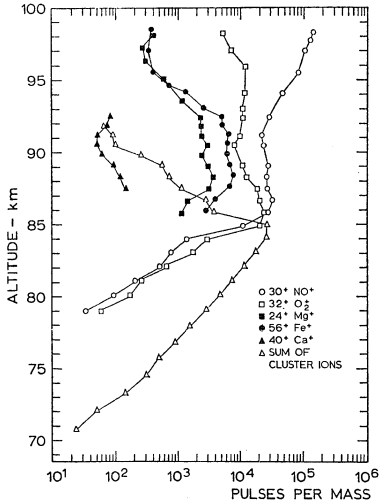

Profile 14b

CHECK LIST - 22

1. Author and Ref: Johannessen, A. and D. Krankowsky, "Daytime positive-ion composition measurement in the altitude range 73-137 km above Sardinia," JATP, 36, 1233, 1974.

2. Purpose of Investigation: Measure positive-ion concentration.

3. Equipment Flown:

   (a) Quadrupole mass filter
   Faraday Rotation at 2.3, 3.7 and 7.1 MHz.

   (b) Solar x-ray intensity 2-8 by proportional photon Lyα and EUV ionization chambers. Counters.

4. Date, Time, Launch Site, Latitude, Rocket, Equipment

   (a) July 23, 1970, 1355 UT, Sardinia
   39°6N, 9.4°E
   X = 38°
   73-137 km altitude
   10-70 amu range

5. Geophysical Conditions: Quiet

6. Scientific Results:

   (a) Cluster ions 37^+ at 78 km, 19^+ which maximized at 87 and 84.6 km, respectively, 30^+ and 32^+. 30^+ and 32^+ dominant above 85 km with sharp gradient.

   (b) E_s layers of $A\ell^+$, K^+, Ca^+ and N_i^+, M_g^+, F_e^+ and S_i^+.

7. Interpretation of Results: Collisional effects may cause lower hydrates, but $NO^+ \cdot H_2O$ was not affected. Barth (1966) [NO] used in a small model taken from Keneshea et al. (1970).

8. Literature and theory discussed? Discussion cluster and metallic ions, O_2^+ and NO^+. Sampling theory.

Ion composition measurement in the altitude range 73–137 km above Sardinia

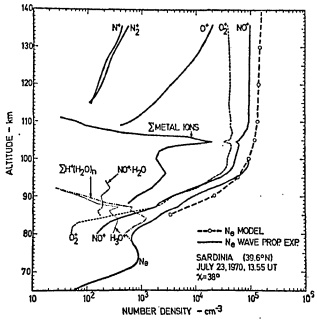

Ion composition profiles normalized to electron density.

Profile 22

Appendix II

Tabulation of neutral consitituents for winter and summer atmospheres used in the computation of ionic composition. Included are $N_2 + O_2$, T, NO, H_2O, $O(^3P)$, CO_2, KDF and JJ.

SUMMER - INVARS FILE				WINTER - INVARW FILE		
KDF	N_2+O_2	JJ	Altitude(km)	KDF	N_2+O_2	JJ
+.15E+05	+.44E+18	.1E-8	30	+.25E 05	.25E+18	.1E-08
+.30E 05	+.11E+18	.4E-8	40	+.50E 05	.64E+17	.4E-08
+.60E 05	+.26E 17	.12E-7	50	+.10E 06	.16E 17	.12E-07
+.12E 06	+.79E 16	.50E-07	60	+.20E 06	.45E 16	.50E-07
+.24E 06	+.24E 16	.40E-06	70	+.40E 06	.12E 16	.40E-06
+.50E 06	+.53E 15	.30E-05	80	+.90E 06	.31E 15	.30E-05
+.10E 07	+.72E 14	.50E-05	90	+.20E 07	.72E 14	.50E-05
+.50E 07	+.92E 13	.70E-05	100	+.60E 07	.14E 14	.70E-05
+.20E 05	+.30E+13	.90E-05	110	+.70E 07	.60E 13	.90E-05
+.10E 02	+.90E 12	.10E-04	120	+.10E 04	.17E 13	.10E-04
= 0	+.30E 12	.10E-04	130	+.10E 01	+.30E 12	
	+.12E 12	.10E-04	140	0	+.12E 12	

Profile #121

ALT	$[O(^3P)]$	$[O_2+N_2]$	$[CO_2]$
65	$.23x10^{11}$	$.45x10^{16}$	$.13x10^{13}$
70	$.25x10^{11}$	$.24x10^{16}$	$.71x10^{12}$
75	$.24x10^{11}$	$.12x10^{16}$	$.35x10^{12}$
80	$.26x10^{10}$	$.53x10^{15}$	$.16x10^{12}$
85	$.10x10^{12}$	$.20x10^{15}$	$.61x10^{11}$
90	$.50x10^{12}$	$.72x10^{14}$	$.22x10^{11}$
95	$.9x10^{12}$	$.25x10^{14}$	$.75x10^{10}$
100	$.9x10^{12}$	$.92x10^{13}$	$.28x10^{10}$

Profile #106

ALT	$[O(^3P)]$	$[O_2+N_2]$	$[CO_2]$
65	$.23x10^{11}$	$.23x10^{16}$	$.69x10^{12}$
70	$.25x10^{11}$	$.12x10^{16}$	$.35x10^{12}$
75	$.24x10^{11}$	$.62x10^{15}$	$.19x10^{12}$
80	$.26x10^{11}$	$.31x10^{15}$	$.94x10^{12}$
85	$.10x10^{12}$	$.15x10^{15}$	$.46x10^{11}$
90	$.5x10^{12}$	$.72x10^{14}$	$.22x10^{11}$
95	$.90x10^{12}$	$.31x10^{14}$	$.94x10^{10}$
100	$.90x10^{12}$	$.14x10^{14}$	$.41x10^{10}$

Appendix III

Data for computation of primary production: a) FLUX, b) absorbtion cross-sections, c) photoionization cross sections for Lyα, Lyβ, X-rays, EUV, GCR. Tabulated also is a resultant primary production of NO^+, N_2^+ and O_2^+ for 60° solar zenith angle. These data correspond to a "quiet" sun and included for comparison are graphs of

a) Solar X-ray (1Å-8Å) flux according to Swider, Nicolet and Aiken (1960) and DASA (1972) for various levels of quiet sun.

b) Plots of photoionization rate coefficients for O_2 and N_2 from DASA (1972) tabulations.

c) Plots of photoionization cross sections for O_2 and N_2.

APPENDIX IIIa

DATA FOR COMPUTATION OF PRIMARY PRODUCTIVITY

Lyman α and X-rays

A. FLUX:

Lyα $\phi_\infty = 3 \times 10^{11}$ photons sec^{-1} DNA (1972)
Quiet Sun Ackerman (1971)
Watanabe et al. (1967)

X-rays (Å)	2	3	4	5	6	7	8
Nicolet and Aiken (1960)							
Completely Quiet	1		20		300		
Quiet	10		200		300		
Lightly Disturbed	100		2×10^3		3×10^4		
DNA (1972)	.1	2	30	400	2.5×10^3	10^4	2.8×10^4
Snider (1969)							
Very Quiet		.15	2	25	250	1.5×10^3	6×10^3
Quiet	.06	1	15	25	1.3×10^3	10^4	
Barely QUiet	25			6×10^3	2×10^4		

B. ABSORBTION CROSS SECTION σ^T

Lyα: $\sigma^T(NO) = 2.4 \times 10^{-18}$ cm^2

$\sigma^T(O_2) = 1.00 \times 10^{-20}$ cm^2

$\sigma^T(O_3) = 2.32 \times 10^{-17}$ cm^2

X-rays (Å)	2	4
	1.01×10^{-21}	6.55×10^{-21}
	1.00×10^{-21}	6.98×10^{-21}

C. PHOTOIONIZATION CROSS SECTIONS

Lyα

[NO] $\sigma^i_{Ly\alpha}(NO) = 2.02 \times 10^{-18}$ cm^2

X-Rays (Å)	2Å	4Å
$\sigma^i(O_2)$	2.3×10^{-19} cm^2	9.2×10^{-19}
$\sigma^i(N_2)$	1.6×10^{-19}	5.6×10^{-19}

Nicolet and Aiken (1960)

Ackerman (1971)

Ackerman (1971)

6

2.13×10^{-20} Nicolet and Aiken (1960)

2.32×10^{-20} Snider (1969)
(referenced by DNA, 1972)

Watanabe et al. (1967)
DNA (1972)

6Å

2.0×10^{-18} DNA (1972)

1.1×10^{-18} DNA (1972)

APPENDIX IIIb

CIII AND Lyβ Data

	CIII	Lyβ
Flux (photons cm^{-2} sec^{-1}	4.4×10^{9} DNA (1972)	3.5×10^{9} DNA (1972)
	4×10^{9} Yonezawa (1966)	2.4×10^{9} Yonezawa (1966)
Energy (erg cm^{-2} sec^{-1})	.08 Yonezawa (1966)	.046 Yonezawa (1966)
σ^{T}(Air)		
O_2 σ^{T}	3.98×10^{-18} Yonezawa (1966)	1.52×10^{-18} Yonezawa (1966)
	4.0×10^{-18} DNA (1972)	1.58×10^{-18} DNA (1972)
η	.62 Yonezawa (1966)	.64 Yonezawa (1966)
σ^{i}	2.5×10^{-18} DNA (1972)	9.8×10^{-19} DNA (1972)
N_2		
$\sigma^{T}(N_2)$	8.2×10^{-20} Yonezawa (1966)	1.0×10^{-21} Yonezawa (1966)
	7×10^{-19} DNA (1972)	5×10^{-22} DNA (1972)
η	0 Yonezawa (1966)	0 Yonezawa (1966)
σ^{i} (N_2)	0 DNA (1972)	0 DNA (1972)

PRIMARY PRODUCTION OF NO^+

SUMMER

Z	X=0°	20°	40°	60°	80°	CONCENTRATION NITRIC OXIDE TEMP. MODIFIED	MEIRA (1970) EXPERIMENTAL
50	33(-19)	1.59(-19)	1.91(-24)	50.9(-40)	0	3.5(9)	8(8)
55	71(-20)	1.29(-9)	2.77(-12)	36.6(-21)	(-66)	2.3(9)	6(8)
60	62.3(-5)	2.51(-4)	9.16(-6)	50.7(-11)	(-35)	1.23(9)	3(8)
65	.209	.1313	.024	15.41(-5)	(-18)	4.64(8)	1.6(8)
70	1.11	.8902	.389	.0346	(-9)	5.9(7)	9(7)
75	1.01	.916	.638	.2169	6.71(-4)	7.8(6)	4(7)
80	.1718	.165	.142	.0921	8.86(-3)	5.3(5)	2(7)
85	.0382	.0376	.0357	.03049	.013	7.9(4)	1.7(7)
90	.302	.300	.295	.279	.207	5.4(5)	3.5(7)
95	14.9	14.87	14.77	14.48	13.047	2.5(7)	7(7)
100	12.83	12.825	12.79	12.7	12.242	2.14(7)	(8)

	PRIMARY PRODUCTION OF NO^+						CONCENTRATION NITRIC OXIDE
			WINTER				
Z	X=0°	20°	40°	60°	80°	TEMP. MODIFIED	MEIRA (1970) EXPERIMENTAL
50	4.0(-10)	8.11(-11)	9.94(-14)	2.29(-22)	1.19(-68)	1.8(9)	8(8)
55	2.3(-10)	8.96(-5)	2.73(-6)	8.787(-11)	7.51(-35)	(9)	6(8)
60	.187	.1149	.0190	9.16(-5)	3.57(-17)	6.3(8)	3(8)
65	10.7	8.34	3.36	.224	1.11(-7)	8.5(8)	1.6(8)
70	45.67	40.308	25.43	6.48	4.33(-3)	5.3(8)	9(7)
75	67.62	63.67	50.58	25.61	.665	2.96(8)	4(7)
80	53.78	52.14	46.64	33.61	5.76	1.42(8)	2(7)
85	18.22	17.97	17.06	14.64	6.45	3.74(7)	1.7(7)
90	46.22	45.97	44.89	41.94	29.15	8.41(7)	3.5(7)
95	560.8	559.63	553.77	537	457.6	9.6(8)	7(7)
100	189.83	189.64	188.867	186.5	174.36	3.(8)	(8)

PRIMARY PRODUCTION OF N_2^+ AND O_2^+

Z	SUMMER X=0°	N_2^+ (EUV and GCR) 20°	40°	60°	80°	O_2^+ (EUV, GCR, Lyβ, CIII $O_2(^1\Delta g)$ new) 60°
50	.345	.345	.345	.345	.345	.09197
55	.1901	.1904	.1904	.1904	.1904	.0504
60	.1064	.1064	.1064	.1064	.1064	.0282
65	.0698	.0598	.0598	.05984	.0598	.01587
70	.0316	.0316	.0316	.03162	.0316	.00843
75	.0166	.0157	.0157	.0157	.0157	.072
80	.0228	.01976	.00923	.00846	.007106	.281
85	.233	.2035	.1215	.0305	.00307	1.602
90	.3675	.3505	.2809	.1689	.0123	2.306
95	.2138	.2103	.2102	.1625	.0588	2.72
100	.0926	.09194	.0898	.08319	.0553	263.65

PRIMARY PRODUCTION OF N_2^+ and O_2^+

	WINTER	N_2^+ (EUV and GCR)				O_2^+ (EUV, GCR, Lyβ, CIII $O_2(^1\Delta g)$ new)
Z	X=0°	20°	40°	60°	80°	60°
50	.2147	.2147	.2147	.2147	.2147	.0567
55	.11254	.1125	.1125	.1125	.1125	.02975
60	.060	.0600	.0600	.06001	.06001	.0158
65	.020	.0200	.0200	.02006	.02006	.00821
70	.01584	.01584	.01584	.0158	.01584	.00421
75	.0126	.0117	.00985	.0085	.00829	.1
80	.0345	.025	.05132	.00676	.00418	.7012
85	.164	.144	.08534	.02147	.00246	2.19
90	.284	.2670	.2076	.1013	.00465	2.278
95	.229	.2234	.2017	.1497	.0313	25.64
100	.127	.1255	.1190	.1049	.0610	84.35

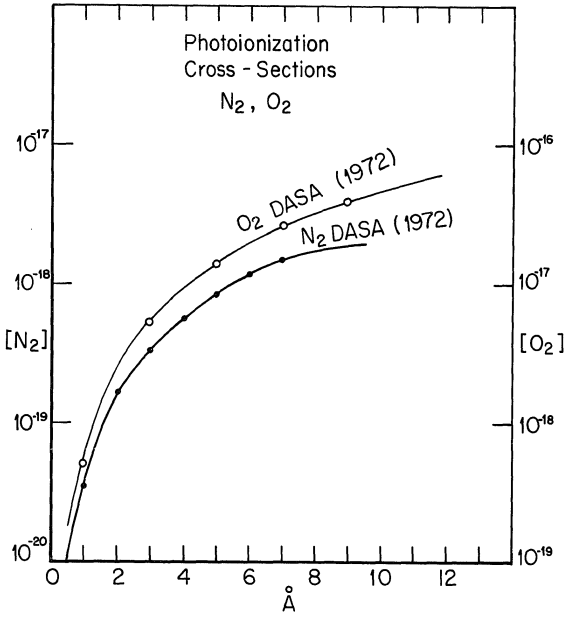

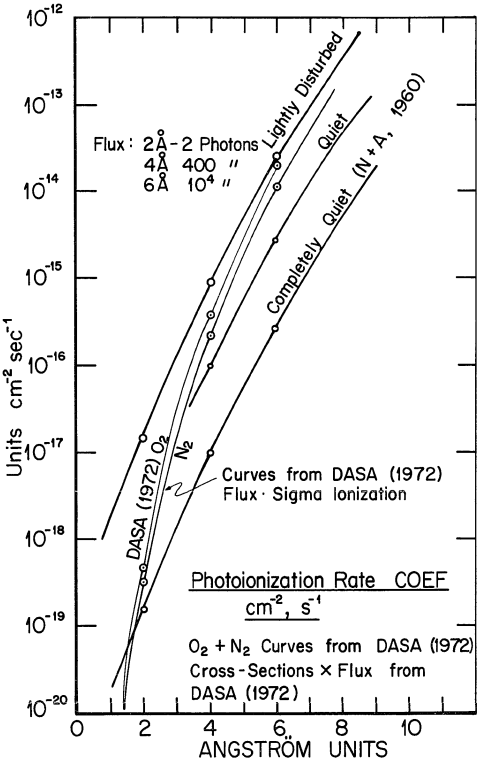

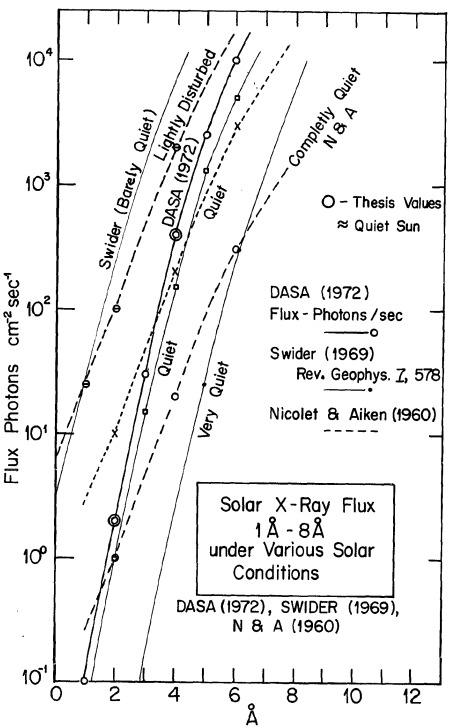

Appendix IV

Tabulation of saturation vapor pressure and number density of water over ice as a function of temperature (Smithsonion, 1965).

APPENDIX IV

NUMBER DENSITY H_2O CORRESPONDING TO SATURATION VAPOR PRESSURE WATER OVER ICE

	Torr	mb	SATURATION NUMBER DENSITY $\frac{n}{cm^3}$
100°K	8.447×10^{-15}	1.126×10^{-16}	$.81 \times 10^{+1}$
110	2.084×10^{-14}	2.778×10^{-14}	$1.83 \times 10^{+3}$
120	1.931×10^{-12}	2.575×10^{-12}	$1.55 \times 10^{+5}$
130	9.227×10^{-9}	1.23×10^{-10}	6.8×10^{6}
140	2.58×10^{-8}	3.44×10^{-9}	1.78×10^{8}
150	4.68×10^{-8}	6.248×10^{-8}	3.01×10^{9}
160	6.009×10^{-7}	8.01×10^{-7}	3.62×10^{10}
170	5.648×10^{-6}	7.53×10^{-6}	3.209×10^{11}
180	4.133×10^{-5}	5.51×10^{-5}	2.218×10^{12}
190	2.558×10^{-4}	3.41×10^{-4}	1.30×10^{13}
200	1.23×10^{-3}	1.65×10^{-3}	5.9×10^{13}
210	5.46×10^{-3}	7.28×10^{-3}	2.51×10^{14}
220	.0207	.0277	9.12×10^{14}
230	.0697	.093	2.93×10^{15}
240	.2123	.283	8.5×10^{15}
250	.5776	.770	2.2×10^{16}
260	1.485	1.98	5.51×10^{16}
270	3.57	4.76	1.27×10^{17}
280	2.355	3.14	8.1×10^{17}

Appendix V. Tabulation of additional reactions for steady state water vapor chemistry and outline of method of solution

These include reactions with the compounds CH_4, OH, H_2, H, HO_2, O('D) and O_3 which may be inserted into the vapor diffusion equation through the term which is the coefficient for n_v. The basis for the choice of these reactions is the discussion by Hunten and Strobel (1974) and Liu and Donahue (1974) and Wofsy et al. (1972). The additions include the main reactions but serve also as examples of the method whereby additional chemistry may be included in the diffusion difference equations. The pertinence to the aeronomy of these reactions is due to the possibility that the oxidation of CH_4, diffusing upward into the mesosphere, could increase the amount of H_2O.

Since these reactions have not been converted into FORTRAN and programmed into DIFRAD 13 it is not possible at this time to estimate the ease of convergence of the solutions. The resulting matrix would contain nonlinear terms, and an iterative method solution, whereby only one compound would be solved for at a time, would be the first method of solution attempted. Possible check points for the program would include

a) In situ observations in the mesosphere

b) Anderson (1971) OH data.

APPENDIX V

1. Variables CH_4, H_2O, OH, H_2 H

2. Reactions:

	k (from Hunten and Strobel, 1974)
$H_2O + h\nu \longrightarrow H_2 + O$	$J_1 = 6.1 \times 10^{-7}$ @ $\tau = 0$
$H + OH$	$J_2 = 4.7 \times 10^{-6}$ @ $\tau = 0$
$CH_4 + h\nu \longrightarrow$	$J_3 = 7 \times 10^{-6}$
$CH_4 + OH \longrightarrow H_2O + CH_3$	$k_4 = 4.7 \times 10^{-11} e^{-2500/T}$
$CH_4 + O('D) \longrightarrow OH + CH_3$	$k_5 = 1.2 \times 10^{-11} e^{-3800/T}$
$OH + HO_2 \longrightarrow H_2O + O_2$	$k_6 = 2 \times 10^{-10}$
$OH + OH \longrightarrow H_2O + O$	$k_7 = 2 \times 10^{-12}$
$H + HO_2 \longrightarrow H_2O + O$	$k_8 = 1.5 \times 10^{-12}$
$H + HO_2 \longrightarrow H_2 + O_2$	$k_9 = 1.5 \times 10^{-12}$
$H + HO_2 \longrightarrow OH + OH$	$k_{10} = 1.0 \times 10^{-11}$
$H + O_3 \longrightarrow OH + O_2$	$k_{12} = 2.6 \times 10^{-11}$
$OH + O_3 \longrightarrow HO_2 + O_2$	$k_{13} = 1.3 \times 10^{-12} e^{-950/T}$

Fixed constituents taken from standard profiles: HO_2, O_2, N_2, O_3, O('D) (all basic oxygen compounds).

3. Continuity Equations

a. $$\frac{d\phi_{CH_4}}{dz} = -J_3[CH_4] - k_4[CH_4][OH] - k_5[CH_4][O('D)]$$

b. $$\frac{d\phi_{H_2O}}{dz} = -(J_1+J_2)[H_2O] + k_4[CH_4][OH] + k_6[OH][HO_2] + k_7[OH][OH] + k_8[H][HO_2]$$

c. $$\frac{d\phi_{OH}}{dz} = -k_4[CH_4][OH] - k_5[CH_4][O('D)] - k_6[OH][HO_2] - k_7[OH]^2 + 2k_{10}[H][HO_2] - k_{13}[OH][O_3].$$

d. $\frac{d\phi_{H_2}}{dz} = J_1[H_2O] + k_9[H][HO_2]$

e. $\frac{d\phi_H}{dz} = J_2[H_2O] - (k_8 + k_9 + k_{10})[H][HO_2] - k_{12}[H][O_3]$

f. $\phi_{N_i} = -K_T \frac{dN_i}{dz} - \frac{K}{T}\frac{dT}{dz} N_i - (\frac{D}{H} - \frac{K}{H_{AV}})$

Substitute flux into a-e eqns. to get one 2nd order eqn. for each constituent and 2 boundary conditions each. Forms a set of 5 coupled eqns. for the unknowns CH_4, H_2O, OH, H_2, H.

Terms in the Eqn

$a(z) = \frac{1}{K}\frac{\partial K}{\partial z} + \frac{1}{T}\frac{\partial T}{\partial z} + \frac{1}{H_{A_V}}$

$b(z) = \frac{1}{KT}\frac{\partial K}{\partial z} \cdot \frac{\partial T}{\partial z} + \frac{1}{KH}\frac{\partial K}{\partial z} - \frac{1}{T^2}(\frac{\partial T}{\partial z})^2 - \frac{J}{K}$

$\ell(z) = \frac{n_p \pi a^2 \alpha \bar{c}}{K} = \ell' a^2 \qquad \ell' = \frac{n_p \pi \alpha \bar{c}}{K}$

$c(z) = \frac{\pi a^2 \alpha \bar{c} n_p n_s}{K} = c' a^2 \qquad c' = \frac{\pi \alpha \bar{c} n_p n_s}{K}$

$n_v'' + n_v' \cdot a + n_v(b-\ell) - c(z) = 0$

RAD = 0 No ice crystal growth of decay:

$$n_v'' + n_v' \cdot a + n_v \cdot b = 0$$

RAD $\neq$ 0 $n_v'' + n_v' \cdot a + n_v(b - \underbrace{\ell' a^2}_{\text{loss}}) - \underbrace{c' a^2}_{\text{gain}} = 0$

General Gain and Loss Processes:

Gain: $A + B \xrightarrow{k_1} N + M \qquad q = k_1[A][B]$

Loss: $N + M \xrightarrow{k_1} A + B \qquad \ell = k_1[N][M]$

$= n \cdot k_1[M]$

$$n'' + n_v' \cdot a + n \cdot b - n\ell' a^2 - n. \sum_{\substack{\text{loss}\\ \text{Reactions}}} k_1[M] - c'a^2$$

$$- \sum_{\substack{\text{gain}\\ \text{reactions}}} k[M] = 0$$

H_2O $\quad n_v'' + n_v' \cdot a + n_v \cdot \left\{ b - \ell' a^2 - \sum \text{chem loss} \right\} - c'a^2 - \sum \text{chem gain} = 0$

any other $\quad n'' + n' \cdot a + n \cdot \left\{ b - \sum \text{chem loss} \right\} - \sum \text{chem gain} = 0.$

Other: $\quad n_{m-1} + n_m \{ b - \sum \text{chem loss})(\Delta z)^2 - (\Delta z)a - 2$

$$+ n_{m+1}(1 + \Delta z \cdot a) - (\sum \text{chem gain})\Delta z^2 = 0$$

Series of Matrices for FDE for $[H_2O]$, $[CH_4]$, OH, H_2, H

H_2O

$$n(H_2O)_{m-1} + n(H_2O)_m \left\{ (b - \ell' a^2)\Delta z^2 - \Delta z \cdot a - 2 \right\} + n(H_2O)_{m+1} (1 + \Delta z \cdot a) =$$

$$= \left\{ c'a^2 + k_4[CH_4][OH] + k_6[OH][HO_2] + k_7[OH]^2 + k_8[H][HO_2] \right\} \Delta z^2$$

CH_4

$$n(CH_4)_{m-1} + n(CH_4)_m \left\{ (b - J_3 - k_4[OH] - k_5[O(^1D)])\Delta z^2 - \Delta z \cdot a - 2 \right\} + n(CH_4)_{m+1}(1 + \Delta z \cdot a) = 0$$

OH

$$n(OH)_{m-1} + n(OH)_m \left\{ (b - k_4[CH_4] - k_6[HO_2] - k_7[OH] + k_5[O('D)][CH_4] - k_{13}(O_3))\Delta z^2 - \Delta z \cdot a - 2 \right\}$$

$$+ n(CH_4)_{m+1}(1 + \Delta z \cdot a) = \left\{ 2k_{10}[H][HO_2] \right\} \Delta z^2$$

H_2

$$n(H_2)_{m-1} + n(H_2)_m \left\{ b \cdot \Delta z^2 - \Delta z \cdot a - 2 \right\} + n(H_2)_{m+1}(1 + \Delta z \cdot a) = \left\{ J_1[H_2O] + k_9[H][HO_2] \right\}$$

H

$$n(H)_{m-1}+n(H)_m\left\{(b-(k_8+k_9+k_{10})[HO_2]-k_{12}[O_3])(\Delta z)^2-\Delta z\cdot a-2\right\}+n(H)_{m+1}(1+\Delta z\cdot a) =$$

$$=\left\{J_2[H_2O]\right\}(\Delta z)^2.$$

Needed to Build

1. Invariant neutral constituent file:

   OH, O_3, $O(^1D)$, HO_2

2. Read in rate constants
3. Build Array L(I) Include in L, Build array G(I) include in BB(I)
4. Call DIFFU H_2O/HO_2, (where DIFFU is a finite difference form of a 2nd order diffusion equation expanded from DIFRAD 13).
5. Iterate
6. Test at each altitude the iterated profile.
7. Call DIFFU $H_2O/HO_2/OH$
8. Iterate
9. Test
10. Call DIFFU $H_2O/HO_2/OH/CH_4$

CH_4 L(I) = CHEML(I) = $J_3 + k_4[OH] + k_5[O(^1D)]$

I=1 G(I) = CHEMG(I)

$[H_2O]$ CHEML(I) = J

I=2 CHEMG(I) = $k_4[CH_4][OH] + k_6[OH][HO_2] + k_7[OH]^2 + k_8[H][HO_2]$

[OH] CHEML(I) = $k_4[CH_4] + k_6[HO_2] + k_7[OH] + k_{13}[O_3]$

I=3 CHEMG(I) = $2k_{10}[H][HO_2]$

$[H_2]$ CHEML(I) = 0

I=4 CHEMG(I) = $J_1[H_2O] + k_9[H][HO_2]$

$[H]$ CHEML(I) = $(k_8 + k_9 + k_{10})[HO_2] - k_{12}[O_3] - k_{10}[HO_2]$

I=5 CHEMG(I) = $J_2[H_2O]$

Appendix VI

This appendix contains a list-out of the computer programs used for computations in this thesis.

1. Computation of water vapor profile and ice crystal growth: DIFRAD 13.

Subroutines Required:

a) INTERP.O
- LINTRP
- LXNTRP
- PINTRP
- PXNTRP

These are subroutines for the linear (L) or power (P) interpolation of the files of data. For example, temperature always requires a linear interpolation and any quantity varying with the atmospheric density, such as N_2, requires a power interpolation.

b) GRDNT: This computes a gradient with respect to z of the data in file.

c) SIMQ. This is the basic program described in Chapter IV which solves the matrix formed from the linearized 2nd order water vapor diffusion equation. The vapor profile which it produces is the input for the radius growth equation NEWT2. SIMQ is taken from the Scientific Subroutine Library of IBM (1974) and is comparable to any number of other algorithms to solve sets of linear equations (e.g., SIMEQN of Scientific Subroutine of Honeywell, 1976).

d) NEWT2. This computes the growth of the ice crystal by means of an iterative scheme.

e) Files for T, K and J are assembled for altitudes of 30 to 300 km:

INVARS - J, K and $N_2 + O_2$ for summer
INVARW - J, K and $N_2 + O_2$ for winter
TEMPS - Temperature profile for summer (USSAS, 1966)
TEMPW - Temperature profile for winter (USSAS, 1966)
TEMP1 - Pt. Barrow Summer Extreme (Theon et al., 1972)
TEMP2 - Temperature profile midway between Pt. Barrow and mean summer.

2. Computation of positive ion composition including dust: DUSTCHEM

Subroutines Required:

AL316 (Brown, 1972): Solves the set of 16 continuity equations for the positive ion set.

F2 and BAKSUB: Subroutines required by AL316.

FLOPOS: Subroutine to list out the gain and loss rates for each ion due to the various interconnecting chemical reactions. This provides the data for the Flow Rate Diagrams (FRD).

3. Computation of Positive and negative ion composition excluding dust: HCO29

Subroutines:

AL316: Solves the set of 31 continuity equations.

F2 and BAKSUB: Subroutines required by AL316.

FLOPOS and FLONEG: Subroutines to list out the gain and loss rates for each ion due to the various interconnecting chemical reactions and provide data for Flow Rate Diagrams (FRD).

DIFRAD 13

```
► $LIST

$#@RUN DIFRAD13$INTERP.O$NEWT2$SIMG=@INVARS*01*$TEMPS*02*
10C  DIFRAD13
20C
30C     LAST CHANGED NOV. 24,1976,HC
40C
50       DIMENSION RP(100),DEN(100)
60      REAL LRP,LNV
70     INTEGER DIN,DTM,IER
80      REAL KA(256),N2A(256),JA(256),NVA(256),TA(256)
90      REAL LO,LV,LT,LB,MR,KT,KDF,JJ,N2,NV,NS,NDF,N2T,N2B
91      REAL ND
110       DIMENSION AA(10000),BB(100)
115       REAL L
120C
130C  GET INFORMATION FROM USER
140C
150       PRINT 1
160    1  FORMAT('DIFRAD13: TO COMPUTE WATER VAPOR NUMBER DENSITY
162   $ UNDER INFLUENCE OF'/,12X,'DIFFUSION AND ICE CRYSTAL FORMATION'/,
163    $  12X,'SET UPPER LEVEL ABOVE SATURATED LAYER'/,
164      $  12X,' MOLECULAR DIFFUSION AND VAPOR FLUX UPPER'/,
165      $    12X,' BOUNDARY CONDITION USED'///)
170    2  PRINT 3
180     3 FORMAT(' ENTER UPPER LEVEL IN KILOMETERS')
190       READ,HI
200       PRINT 4
210    4 FORMAT(' ENTER LOWER LEVEL IN KILOMETERS')
220       READ,LO
230       IF(LO.GE.HI) GO TO 2
240    5  PRINT 6
250    6  FORMAT(' ENTER STEP SIZE IN DECIMAL KILOMETERS')
260       READ,DZ
270       IF(DZ.EQ.0.) GO TO 5
280       IF(DZ.LT.0.) DZ = -DZ
290       NL = (HI - LO)/DZ + 1.
300     IF(NL.EQ.1 .OR. NL.GT.100) GO TO 5
340       PRINT 88
350    88 FORMAT(' ENTER DOWNWARD FLUX OF DUST PER CM2')
360       READ, FLO
370       PRINT 9
380      9 FORMAT(' ENTER AVERAGE CORE RADIUS IN MICRONS')
390       READ,CRM
400       CRC = CRM$1.E-4
401       PRINT 8
402     8  FORMAT(' ENTER STICKING COEFFICIENT')
403       READ,ALA
405       PRINT 40
406    40  FORMAT(' ENTER  VERTICAL DRIFT NEUTRAL ATMOSPHERE, CM/SEC.')
407      READ,DRIFT
410       PRINT 10
420    10  FORMAT(' UPPER BC FOR WATER VAPOR IS A FLUX BC, ASCENT IS +')
430     READ,FLUX
440       PRINT 11
450    11  FORMAT(' ENTER NUMBER DENSITY OF WATER VAPOR FOR LOWER BC:N SUB NL+1')
460       READ,XMP1
470       PRINT 110
480 110  FORMAT(' ENTER MAXIMUM NUMBER OF CYCLES')
490       READ,MAX
500C
510C  SET RADIUS PROFILE TO ZERO FOR FIRST DIFFU CYCLE
520C
530       RP(1) = 0.
540       RP(2) = 0.
550       NLRP = 2
560       LRP = 0.
570       DRP = 1.
```

```
580C
590C  READ DATA FROM THE INVARIANT DATA FILE
600C
610       READ(1) ICODE,NLIN,LIN,DIN
620       IF(ICODE.NE.1) GO TO 2000
630       DO 12 I = 1,NLIN
640      READ(1)KA(I),N2A(I),JA(I),NVA(I)
650   12  CONTINUE
660       NLNV = NLIN
670       LNV = LIN
680       DNV = DIN
690C
700C  READ THE TEMPERATURE FILE
710C
720       READ(2) ICODE,NLTM,LTM,DTM
730       IF(ICODE.NE.2) GO TO 2000
740       DO 13 I = 1,NLTM
750          READ(2) TA(I)
760   13  CONTINUE
770C
780C  START MAIN CYCLING LOOP AND SET RP AND DENS TO INITIAL VALUES
790C
791       DO 30 I = 1,NL
792       K = NL + 1 - I
793       RP(K) = CRC
794       DEN(K) = 3.
795       30  CONTINUE
800       SCAV = 2.904E3
801       SCV = 4.678E3
810        BETA = 6.01E20
820       ETA = 3.3E22
830       DO 20 I = 1,MAX
831        PRINT,I
840C
850C  CLEAR BUFFERS
860C
870            NL2 = NL*NL
880            DO 14 J = 1,NL2
890               AA(J) = 0.
900   14       CONTINUE
910            DO 15 J = 1,NL
920               BB(J) = 0.
930   15       CONTINUE
940C
950C  DIFFUSION CALCULATION LOOP WHICH ENDS AT STATEMENT 17.
960C
970            LV = HI
974             K = NL
975      IF(I.LT.MAX) GO TO 50
976        PRINT 305
977    305  FORMAT(5X,'LEVEL',5X,'DESCENT SPEED',5X,'UPDRAFT',
978     &  5X,'DUST CONCENTRATION,CM-3.',/)
979     50  CONTINUE
980            DO 17 J = 1,NL
1033C
1034C     CALCULATE MOLECULAR, EDDY AND TOTAL DIFFUSION COEF.
1035C
1039       LT = LV + 1
1040       LB = LV - 1
1041       CALL PINTRP(LT,N2A,NLIN,LIN,DIN,N2)
1042       N2T = N2
1043       CALL PINTRP(LB,N2A,NLIN,LIN,DIN,N2)
1044       N2B = N2
1045       CALL LINTRP(LT,TA,NLTM,LTM,DTM,TMP)
1046       TMPT = TMP
1047       CALL LINTRP(LB,TA,NLTM,LTM,DTM,TMP)
```

```
      TMPB = TMP
      D12T = .585E19*(TMPT/273.)**1.75/N2T
      D12B = .585E19*(TMPB/273.)**1.75/N2B
      DD12DZ = (D12T - D12B)/2./DZ*1.E-5
      CALL GRDNT(LV,KA,NLIN,LIN,DIN,DKDZ)
      DKDZ = DKDZ*1.E-5
      DKTDZ = DKDZ + DD12DZ
      CALL PINTRP(LV,KA,NLIN,LIN,DIN,KDF)
      CALL PINTRP(LV,N2A,NLIN,LIN,DIN,N2)
      CALL LINTRP(LV,TA,NLTM,LTM,DTM,TMP)
      D12 = .585E19*(TMP/273.)**1.75/N2
      KT = KDF + D12
C
        HAV = TMP*SCAV
        HV = TMP*SCV
        CALL GRDNT(LV,TA,NLTM,LTM,DTM,DTDZ)
        DTDZ = DTDZ*1.E-5
C
C  CALCULATION OF UPWARD DRIFT VELOCITY OF NEUTRAL ATMOSPHERE.
C    AND GRADIENT OF THE DRIFT.
C
      WW = DRIFT*.24E16/N2/KT
      IF(LV.GT.120.) WW = 0.
      IF(LV.LE.120. .AND. LV.GT.70.) WW = DRIFT*(120.-LV)/50./KT
      DWWDZ = DRIFT*(-.24E16/N2/KT-.24E16/N2B/KT)/2.E5
      IF(LV.GT.120.) DWWDZ = 0.
      IF(LV.LE.120. .AND. LV.GT.70.) DWWDZ=DRIFT*((120.-LV)/
     &  50./KT - (120.-LB)/50./KT)/2.E5
C
      L = JJ/KT
       PRINT,LV,L,WW,DWWDZ
C
C      A IS COEFFICIENT OF N PRIME
       A = 1./KT*DKTDZ + 1./TMP*DTDZ + 1./KT*(KDF/HAV + D12/HV)
     &      -WW
C
C      B IS COEFFICIENT OF N
       B = 1./KT/TMP*DKTDZ*DTDZ + 1./KT/HAV*DKDZ -
     &     1./TMP/TMP*DTDZ*DTDZ + 1./KT/HV*DD12DZ
C
            CM = 2668.92*SQRT(TMP)
            NS = -9.09718*(273.16/TMP - 1.) - 3.56654
     &      *ALOG10(273.16/TMP) + .876793*(1. - TMP/273.16)
     &      + .78584
            NS = 10.**NS/TMP/1.38E-19
            CC = 0.
       CALL PINTRP(LV,JA,NLIN,LIN,DIN,JJ)
      L = JJ/KT + DWWDZ
       RAD = RP(K)
        DENS = DEN(K)
C
C  CALCULATION OF DUST DESCENT SPEED (STOKES),RESULTANT FALL SPEED,
C  AND DUST CONCENTRATION.
C
       WD = RAD*DENS*BETA/N2
       W = WW*KT
       WDF = WD - W
       ND = FLO/WDF
       IF(WDF.LE.1.E-20) ND = 0.
       IF(I.EQ.1)  NVA(K) = N2*6.E-6
       NDF = NVA(K) - NS
C
      IF(RAD.GT.CRC)  CC = 3.1416*ALA*RAD*RAD*CM*NS*ND/KT
       IF(NDF.GT.0.)  L = L + CC/NS
 16          IND = (J - 1)*NL + J
        AA(IND) = (B - L)*DZ*DZ*1.E10 - A*DZ*1.E5 - 2.
      IF(J.EQ.1) AA(IND)= (B - L)*DZ*DZ*1.E10 - (A-WW)*DZ*1.E5-1
```

```
      IF(J.EQ.1) AA(IND)= (B - L)*DZ*DZ*1.E10 - (A-WW)*DZ*1.E5-1
      IF(J.NE.1) AA(IND - 1) = 1.
      IF(J.NE.NL) AA(IND + 1) = 1. + DZ*A*1.E5
        BB(J) = -CC*DZ*DZ*1.E10
      ZA = 1./KT*DKTDZ
      ZB = 1./TMP*DTDZ
      ZC = 1./KT*(KDF/HAV + D12/HV)
           LV = LV - DZ
         K = K - 1
      IF(I.LT.MAX) GO TO 17
      PRINT 310,LV,WDF,W,ND
  310 FORMAT(5X,F6.2,4X,F10.2,6X,F8.2,8X,F8.2)
   17    CONTINUE
      BB(1) = BB(1)  +  FLUX*DZ*1.E5/KT
        BB(NL) = BB(NL) - XNP1*(1. + DZ*A*1.E5)
      PRINT,BB(1),BB(NL)
      NLM = NL - 1
      DO 31 J = 2,NLM
        IND = (J - 1)*NL + J
   31 CONTINUE
      CALL SIMQ(AA,BB,NL,IER)
C
C  STORE CALCULATED COEFFICIENTS AS THE NEW NV ARRAY
C
           LNV = LO
           DNV = DZ
           NLNV = NL
      K = NL
        DO 18 J = 1,NL
      NVA(K) = BB(J)
    K = K - 1
   18   CONTINUE
C
C     RADIUS CALCULATION LOOP WHICH ENDS AT STATEMENT 19 AND RETURNS
C     AN ARRAY OF RP(K) AND DENS(K) TO THE DIFFUSION CALCULATION
C     LOOP FOR USE IN THE NEXT ITERATION.
C
      IF(FLO.EQ.0.) GO TO 20
        RAD = CRC
       LV = HI
      K = NL
        DO 19 J = 1,NL
           CALL PINTRP(LV,N2A,NLIN,LIN,DIN,N2)
           CALL LINTRP(LV,TA,NLTM,LTH,DTM,TMP)
           NS = -9.09718*(273.16/TMP - 1.) - 3.56654
     &     *ALOG10(273.16/TMP) + .876793*(1. - TMP/273.16)
     &     + .78584
           NS = 10.**NS/TMP/1.38E-19
           CM = 2668.92*SQRT(TMP)
        NDF = NVA(K) - NS
           IF(NDF.LE.0. .AND. RAD.LE.CRC) GO TO 181
      A = ALA*DZ*1.E5*CM*NDF*N2/BETA/ETA/2.
           CALL NEWT2(RAD,A,CRC)
  181       RP(K) = RAD
        DEN(K) = 1 + 2*((CRC/RAD)**3)
           LV = LV - DZ
      K = K - 1
   19    CONTINUE
        NLRP = NL
        LRP = LO
        DRP = DZ
   20 CONTINUE
       PRINT,BB(1),BB(NL)
C
C  PRINT OUT FINAL TMP, NV, AND RP VALUES
C
```

```
      PRINT 21,MAX
   21  FORMAT(/' DIFRAD13...FINAL PROFILES AFTER',I3,' ITERATIONS'/)
      PRINT 220,IER
  220  FORMAT(/,' IER =',I3,/)
      PRINT 22
   22 FORMAT(' LEVEL    TEMP    KDF+D12',5X,'JJ',6X,'N2+O2',
     &  6X,'MIXING RATIO',1X,'H2O',2X,  ' RADIUS'//)
      LV = HI
         K = NL
      DO 24 I = 1,NL
        CALL LINTRP(LV,TA,NLTM,LTM,DTM,TMP)
      CALL PINTRP(LV,KA,NLIN,LIN,DIN,KDF)
      CALL PINTRP(LV,JA,NLIN,LIN,DIN,JJ)
      CALL PINTRP(LV,N2A,NLIN,LIN,DIN,N2)
      MR = (NVA(K)/N2)*1.E6
         RAD = RP(K)*1.E4
      D12 = .585E19*(TMP/273.)**1.75/N2
      KT = KDF + D12
      PRINT 23,LV,TMP,KT,JJ,N2,MR,NVA(K),RAD
   23  FORMAT(1X,F6.2,F6.1,3(2X,E8.2),1X,F8.2,1X,E10.3,F8.4)
         LV = LV - DZ
         K = K - 1
   24  CONTINUE
 2000  CONTINUE
      STOP
      END
```

INTRP.O

```
#LIST INTERP

10       SUBROUTINE LINTRP(X,BUF,N,L,D,Y)
20       INTEGER D
30       DIMENSION BUF(N)
40C
50C   GET X'S POSITION IN RELATION TO INDICIES OF BUF
60C
70       I1 = (X - L)/D + 1
80       I2 = I1 + 1
90       IF(I1.GE.1) GO TO 1
100      I1 = 1
110      I2 = 2
120   1  IF(I2.LE.N) GO TO 2
130      I1 = N - 1
140      I2 = N
150C
160C  DO THE INTERPOLATION
170C
180   2  A2 = L + I1*D
190      A1 = A2 - D
200      S = (X - A1)/(A2 - A1)
210      Y = (BUF(I2) - BUF(I1))*S + BUF(I1)
220      RETURN
230      END
240      SUBROUTINE LXNTRP(X,BUF,N,L,D,Y)
250      REAL L
260      DIMENSION BUF(N)
270C
280C  GET X'S POSITION IN RELATION TO INDICIES OF BUF
290C
300      I1 = (X - L)/D + 1
310      I2 = I1 + 1
320      IF(I1.GE.1) GO TO 1
330      I1 = 1
340      I2 = 2
350   1  IF(I2.LE.N) GO TO 2
360      I1 = N - 1
370      I2 = N
380C
390C  DO THE INTERPOLATION
400C
410   2  A2 = L + I1*D
420      A1 = A2 - D
430      S = (X - A1)/(A2 - A1)
440      Y = (BUF(I2) - BUF(I1))*S + BUF(I1)
450      RETURN
460      END
470   SUBROUTINE PINTRP(X,BUF,N,L,D,Y)
480   INTEGER D
490      DIMENSION BUF(N)
500C
510C  GET X'S POSITION IN RELATION TO INDICIES OF BUF
```

```
500C
510C  GET X'S POSITION IN RELATION TO INDICIES OF BUF
520C
530  I1 = (X - L)/D + 1
540  I2 = I1 + 1
550  IF(I1.GE.1) GO TO 1
560    I1 = 1
570  I2 = 2
580   1  IF(I2.LE.N) GO TO 2
590  I1 = N - 1
600  I2 = N
610C
620C  DO THE INTERPOLATION
630C
640   2  A2 = L + I1*D
650   A1 = A2 - D
660   S = (X - A1)/(A2 - A1)
661     IF(BUF(I2).GT.0..AND.BUF(I1).GT.0.)GO TO 3
662     IF(BUF(I2).LE.0.)GO TO 4
663     Y = 0.
664     RETURN
665   4 Y = BUF(I1)*(1. - S)
666     RETURN
670   3 YL = (ALOG(BUF(I2)) - ALOG(BUF(I1)))*S + ALOG(BUF(I1))
680   Y = EXP(YL)
690   RETURN
700   END
710       SUBROUTINE PXNTRP(X,BUF,N,L,D,Y)
720       REAL L
730       DIMENSION BUF(N)
740C
750C  GET X'S POSITION IN RELATION TO INDICIES OF BUF
760C
770  I1 = (X - L)/D + 1
780  I2 = I1 + 1
790  IF(I1.GE.1) GO TO 1
800    I1 = 1
810  I2 = 2
820   1  IF(I2.LE.N) GO TO 2
830  I1 = N - 1
840  I2 = N
850C
860C  DO THE INTERPOLATION
870C
880   2  A2 = L + I1*D
890   A1 = A2 - D
900   S = (X - A1)/(A2 - A1)
901     IF(BUF(I2).GT.0..AND.BUF(I1).GT.0.)GO TO 3
902     IF(BUF(I2).LE.0.)GO TO 4
903     Y = 0.
904     RETURN
905   4 Y = BUF(I1)*(1. - S)
906     RETURN
910   3 YL = (ALOG(BUF(I2)) - ALOG(BUF(I1)))*S + ALOG(BUF(I1))
920   Y = EXP(YL)
930   RETURN
940   END
950$SUBROUTINE GRDNT(X,BUF,N,L,D,DBDX)
960$DIMENSION BUF(N)
970INTEGER D
980$NN = N
990$CALL PINTRP(X+D/50.,BUF,NN,L,D,Y1)
1000$CALL PINTRP(X-D/50.,BUF,NN,L,D,Y2)
1010$DBDX = (Y1 - Y2)/D*25.
1020$RETURN
1030$END
```

NEWT2

SIMQ

```
*LIST NEWT2

10    SUBROUTINE NEWT2(R,A,C)
20C  NEWT2 - CALCULATES RADIUS BY ITERATION
30C
40C     LAST CHANGED JUNE 8,1976,HC
50C
80      RO = R
90      RF = R
92     T = RO*RO + A/(1. + 2.*C**3/R**3)
94      IF(T.LE.0.0) GO TO 3
100    1  R = SQRT(RO*RO + A/(1. + 2.*C**3/R**3))
140     IF(ABS((R - RF)/RF) .LT. .0000001) GO TO 5
150      RF = R
160      GO TO 1
162    3 R = C
163   5  IF(R.LE.C) R = C
164  4    RETURN
170       END
```

```
*LIST SIMQ

0010*SUBROUTINE SIMQ(A,B,N,KS)
0020*DIMENSION A(1), B(1)
0030*TOL=0
0040*KS = 0
0050*JJ = -N
0060* DO 65 J= 1,N
0070*JY = J + 1
0080*JJ = JJ + N + 1
0090*BIGA = 0
0100*IT = JJ - J
0110*DO 30 I = J,N
0120* IJ = IT + I
0130*IF(ABS(BIGA) - ABS(A(IJ))) 20,30,30
0140*  20 BIGA = A(IJ)
0150*IMAX = I
0160* 30 CONTINUE
0170*IF (ABS(BIGA) - TOL) 35,35,40
0180* 35 KS = 1
0190* RETURN
0200* 40 I1 = J + N*(J - 2)
0210*IT = IMAX - J
0220* DO 50 K = J,N
0230*I1 = I1 + N
0240* I2 = I1 + IT
0250* SAVE = A(I1)
0260*A(I1) = A(I2)
0280*A(I2) = SAVE
0290* 50 A(I1) = A(I1)/BIGA
0300*SAVE = B(IMAX)
0310*B(IMAX) = B(J)
0320*B(J) = SAVE/BIGA
0330*IF(J - N) 55,70,55
0340* 55  IQS = N*(J - 1)
0350* DO 65 IX = JY,N
0360* IXJ = IQS + IX
0370*IT = J - IX
0380* DO 60 JX = JY,N
0390*IXJX = N*(JX - 1) + IX
0400*JJX = IXJX + IT
0410* 60 A(IXJX) = A(IXJX) - (A(IXJ)*A(JJX))
0420* 65 B(IX) = B(IX) - (B(J)*A(IXJ))
0430*  70  NY = N - 1
0440*IT = N*N
0450* DO 80 J = 1,NY
0460*IA = IT - J
0470* IB = N - J
0480* IC = N
0490* DO 80 K = 1,J
0500*B(IB) = B(IB) - A(IA)*B(IC)
0510* IA = IA - N
0520* 80 IC = IC - 1
0530* RETURN
0540*END
```

DUSTCHEM

```
HC001 01  07-19-74   17.612   CHEMISTRY PROGRAM TO SOLVE NON-LINEAR SYSTEMS OF EQUATIONS          LABEL ..... PAGE    1

      1        C   IONCHEMISTRY PROGRAM TO SOLVE NON-LINEAR SYSTEMS OF EQUATIONS
      2        C   W.COLE - STEVE GELLER  JULY  1973
      3        C    TO GENERATE A CHEMICAL MODEL OF THE IONOSPHERE
      4        C
      5        C
      6        C   ALGORITHM 316 FROM COMMUNICATIONS OF THE ACM IS EMPLOYED
      7              EXTERNAL F2
      8              INTEGER NVARS/16/,NK/23/,NA/16/
      9              INTEGER TITLE1(20),TITLE2(20),TITLE3(20)
     10              COMMON K(23),A(16),XX(37),KB(40),X(16),D
     11              DIMENSION FLOD(3)
     12              REAL K,DATE(2),KB
     13              REAL ND(3)
     14        C
     15        C
     16        C     READ K VALUES- REACTION RATES
     17        C
     18        C
     19              K(1)=2.5 E-10
     20              K(2)=6.0 E-11
     21              K(3)=6.3 E-10
     22              K(4)=3.3 E-10
     23              K(5)=1.6 E-28
     24              K(6)=1.1 E-27
     25              K(7)=2.0 E-27
     26              K(8)=8.0 E-11
     27              K(9)=2.8 E-30
     28              K(10)=2.2 E-9
     29              K(11)=3.0 E-10
     30              K(12)=1.9 E-9
     31              K(13)=.32 E-8
     32              K(14)=.1 E-28
     33              K(15)=.1 E-8
     34              K(16)=.1 E-8
     35              K(17)=3.4 E-27
     36              K(18)=2.3 E-27
     37              K(19)=2.4 E-27
     38              K(20)=3.0 E-29
     39              K(21)=1.0 E-9
     40              K(22)=1.9 E-28
     41              K(23)=3.0 E-10
     42              KB(17)=1.98 E-19
     43              KB(18)=4.86 E-20
     44              KB(19)=7.1 E-15
     45        C
     46        C   READ 'A' VALUES (- RECOMBINATION COEFFICIENTS - ALPHAS
     47        C
     48              A(1)=3. E-7
     49              A(2)=7.5 E-7
     50              A(3)=3.5 E-7
     51              A(4)=2.0 E-6
     52              A(5)=5.0 E-6
```

```
      A(6)=5.0 E-6
      A(7)=7.0 E-6
      A(8)=1.0 E-5
      A(9)=1.0 E-5
      A(10)=1.6 E-6
      A(11)=2.2 E-6
      A(12)=3.8 E-6
      A(13)=4.9 E-6
      A(14)=.8 E-5
      A(15)=.1 E-4
      A(16)=.1E-4
      DO 10 IX=1,16
   10 X(IX)=100.
C
C   READ IN PRESET VALUES FOR
C   PRIMARY PRODUCTION RATE, NUMBER DENSITY OF NEUTRAL CONSTITUTENTS
C   AND ELECTRON DENSITY.
C
C
C
C
C
C   PRINT THE INPUT....
C
      PRINT 901,(J,K(J),J=1,NK)
  901 FORMAT('OK - VALUES...'/(1X,I3,1X,E10.3))
      PRINT 902,(J,A(J),J=1,NA)
  902 FORMAT('OA - VALUES...'/(1X,I3,1X,E10.3))
      PRINT 904,(J,X(J),J=1,NVARS)
  904 FORMAT('OINITIAL GUESSES...'/(1X,I3,1X,G15.4))
C
C    READ IN THE XX'S WHICH VARY WITH ALTITUDE AND LIST THEM OUT. EACH
C    ALTITUDE HAS A SET OF THREE CARDS. XX(20) IS INITIAL ELECTRON DENS
C  NOTE: THE NUMBER OF TITLE CARDS MUST ALWAYS EQUAL 3 EVEN IF ONE
C    OF THEM IS BLANK. AFTER THE FIRST PROFILE AND BEFORE THE TITLE
C    OF THE SECOND, THERE MUST BE 3 BLANK CARDS. THIS PREPARES THE PROG      RAM
C    TO READ THE NEXT THREE CARDS AS TITLE INSTEAD OF DATA.
C      DUST ATTACHMENT COEFFICIENT MUST BE DESCRIBED IN TITLE
C      ONE ADDITIONAL CARD AFTER TITLE HAS COEF IN FIRST 8 COLUMNS
C
   97 READ(1,98)TITLE1
   98 FORMAT(20A4)
      PRINT 99,TITLE1
   99 FORMAT('1',20A4)
      READ(1,198)TITLE2
  198 FORMAT(20A4)
      PRINT 199,TITLE2
  199 FORMAT(20A4)
      READ(1,298)TITLE3
  298 FORMAT(20A4)
      PRINT 299,TITLE3
  299 FORMAT(20A4)
```

```
      READ(1,398)DD,FLO,DRIFT,RAD
  398 FORMAT(4E12.4)
      PRINT 399,DD,FLO,DRIFT,RAD
  399 FORMAT(/' SINGLE DUST ATTACHMENT COEFFICIENT',6X,'=',G10.4,/,
     1' DOWNWARD FLUX OF DUST',19X,'=',G10.4,/,' PEAK UPDRAFT OF NEUTRAL
     2 ATMOSPHERE       =',G10.4,/,' RADIUS OF DUST',29X,'=',G10.4,/)
C
C     SET INITIAL X(J)'S TO 100. AT THE START OF A NEW PROFILE
C
      DO 333 J=1,NA
  333 X(J)=100.
  700 ALT=0.0
      KKK=0
      READ(1,750,END=701)ALT,(XK(J),J=17,37)
  750 FORMAT(F8.1,2X,7E10.2/8E10.2/4E10.2)
      IF(ALT.EQ.0.0)GO TO 97
      PRINT 903
  903 FORMAT(//13X,'PRIMARY PRODUCTION RATES     ELECTRON'/62X,'NUMBER'/
     1 12X,'ALTITUDE    O(N2+)     O(NO+)     O(O2+)   DENSITY    O
     2O2          NO          H2O         O2+N2       CO2          N*/)
      PRINT 906,ALT,(XK(J),J=1T,27)
  906 FORMAT(3X,F9.1,2X,11(2X,E8.2)/)
      PRINT 940
  940 FORMAT(//3X'O2(DG)      O3          NO2         N2          OH          HO2
     1    N2O         CO          H2          H *)
      PRINT 941,(XK(J),J=28,37)
  941 FORMAT(10(2X,E8.2)///)
C
C     COMPUTE THE ELECTRON DENSITY, COMPARE WITH THE ORIGINAL GUESS AND
C     RECOMPUTE UNTIL THE DIFFERENCE IS LESS THAN ONE TENTH OF ONE
C     PERCENT.
C     WD IS DUST DESCENT SPEED
C     WDIF IS DUST DESCENT SPEED MINUS UPDRAFT OF NEUTRAL ATMOSPHERE
C     FLO IS DOWNWARD FLUX OF DUST
C     ND(I) IS CONCENTRATION OF DUST
C
C
  699 KKK=KKK+1
C
C     COMPUTATION OF VERTICAL VELOCITIES
C
      FLOD(1)=0.
      FLOD(2)=FLO
      FLOD(3)=10.*FLO
      WW=DRIFT*(1.24E16)/XK(25)
      IF(ALT.LE.120. .AND. ALT.GT.70.) WW=DRIFT*(120.-ALT)/50.
      WD=RAD*(13.03E20)/XK(25)
      WDIF=WD-WW
      D=DD*FLOD(KKK)/WDIF
      ND(KKK)=FLOD(KKK)/WD
      IF(WDIF.LE.1.E-20) D=0.
      IF(WDIF.LE.1.E-20)ND(KKK)=0.
```

```
NCOD1 01  07-19-76   17.612   CHEMISTRY PROGRAM TO SOLVE NON-LINEAR SYSTEMS OF EQUATIONS        LABEL ..... PAGE     4

                  157      C
                  158           MAXIT=20
                  159       500 CALL AL310(NVARS,MAXIT,3,ISING,X,F2)
                  160           DENS=X(1)
                  161           DO 908 I=2,NVARS
                  162       908 DENS=DENS+X(I)
                  163           DIFF=ABS((XX(20)-DENS)/2.)
                  164           IF(DIFF.LE.1.0)GO TO 600
                  165           XX(20)=(DENS+XX(20))/2.
                  166           GO TO 900
                  167      C
                  168      C
                  169       600 CONTINUE
                  170           CLUSNO = X(6)+X(7)+X(8)
                  171           CLUSH2O = X(10)+X(11)+X(12)+X(13)
                  172           PRINT 950,RAD,NDI(KKK),D
                  173       950 FORMAT(///' CONCENTRATION CM-3 OF',F7.3,' MICRON DUST =',F6.2,/
                  174          1' TOTAL DUST ATTACHMENT COEFFICIENT              =',G10.4,/)
                  175           PRINT 907,ISING,ALT,(J,X(J),J=1,8),CLUSNO,(J,X(J),J=9,11)
                  176       907 FORMAT(//' SOLUTION ISING=',I1,/,' ALTITUDE=',F5.1,//4X,I2,'  N2=',11
                  177          1X,'=',G15.4,/4X,I2,'  NO=',11X,'=',G15.4,/4X,I2,'  O2=',11X,'=',G15.4/
                  178          24X,I2,'  O2+(O2)=',7X,'=',G15.4/4X,I2,'  O2+(H2O)=',6X,'=',G15.4/4X,I2
                  179          3,'  NO+(H2O)=',6X,'=',G15.4/4X,I2,'  NO+(H2O)2=',5X,'=',G15.4/4X,I2,'
                  180          4NO+(H2O)3=',5X,'=',G15.4,11X,'SUM OF HYDRATED NO+ CLUSTERS =',G15.4
                  181          K/4X,I2,'  NO+(CO2)=',6X,'=',G15.4/4X,I2,'  H3O+',10X,'=',G15.4/4X,I2,
                  182          6' H3O+(H2O)=',5X,'=',G15.4)
                  183           PRINT 911,(J,X(J),J=12,13),CLUSH2O,(J,X(J),J=14,NVARS)
                  184       911 FORMAT(4X,I2,'  H3O+(H2O)2=',4X,'=',G15.4/4X,I2,'  H3O+(H2O)3=',4X,'=',
                  185          1G15.4,11X,'SUM OF HYDRATED H2O CLUSTER =',G15.4/4X,I2,
                  186          2'  H3O+(OH)=',6X,'=',G15.4/4X,I2,'  H3O+(OH)(H2O)=',1X,'=
                  187          3',G15.4/4X,I2,'  H3O+(OH)(O2)=',2X,'=',G15.4/)
                  188           PRINT 909,DENS
                  189       909 FORMAT(//'46X,'FINAL ELECTRON DENSITY (CM-3) =',G15.4/)
                  190      C
                  191      C     CALCULATION OF THE EFFECTIVE RECOMBINATION COEFFICIENTS.
                  192      C
                  193           REC=(XX(17)+XX(18)+XX(19))/(XX(20)*XX(20))
                  194           PRINT 956,REC
                  195       956 FORMAT(/,26X,'EFFECTIVE RECOMBINATION COEFFICIENT (SEC-1,CM+6) =
                  196          1,E10.4)
                  197           CALL SSWTCH(1,J)
                  198           IF(J.GE.2) GO TO 710
                  199           CALL FLOP05(ALT)
                  200       710 IF(KKK.EQ.3) GO TO 700
                  201           GO TO 699
                  202       701 STOP
                  203           END
*****W  1470 EQUALITY OR NON-EQUALITY COMPARISON MAY NOT BE MEANINGFUL IN LOGICAL IF EXPRESSIONS

 THERE WERE     1 DIAGNOSTICS IN ABOVE COMPILATION
  27K  WORDS WERE USED FOR THIS COMPILATION
```

F2 FOR DUSTCHEM

```
      1          SUBROUTINE F2(X,F,M)
      2          DIMENSION X(16)
      3          COMMON K(23),A(16),XX(37),KB(40),DUM(16),D
      4          REAL K,KB
      5          GO TO(1,2,3,4,5,6,7,8,9,10,11,12,13,14,15,16,17),M
      6        1 F=XX(17)-K(1)*X(1)*XX(21)-K(2)*X(1)*XX(27)-K(4)*X(1)*XX(23)
      7          1-A(1)*X(1)*XX(20)-D*X(1)
      8           RETURN
      9        2 F=XX(18)-K(1)*X(1)*XX(21)-K(3)*X(3)*XX(23)-K(4)*X(1)*XX(23)-
     10          1K(5)*X(2)*XX(24)*XX(25)-K(20)*X(2)*XX(26)*XX(25)-A(2)*X(2)*XX(20)
     11          2-D*X(2)
     12           RETURN
     13        3 F=XX(19)-K(2)*X(1)*XX(22)-K(3)*X(3)*XX(23)-K(9)*X(3)*XX(22)*XX(25)
     14          1-K(22)*X(3)*XX(24)*XX(25)-A(3)*X(3)*XX(20)
     15          2-K(23)*X(4)*XX(21)
     16          3-D*X(3)
     17           RETURN
     18        4   F=K(9)*X(3)*XX(22)*XX(25)-K(10)*X(4)*XX(24)-A(4)*X(4)*XX(20)
     19          1-K(23)*X(4)*XX(21)
     20          2-D*X(4)
     21           RETURN
     22        5   F=K(10)*X(4)*XX(24)-(K(11)+K(12))*X(5)*XX(24)+K(22)*X(3)*XX(25)*XX
     23          1(24)-A(5)*X(5)*XX(20)
     24          2-D*X(5)
     25           RETURN
     26        6   F=K(5)*X(2)*XX(25)*XX(24)-K(6)*X(6)*XX(24)*XX(25)+K(21)*X(9)*XX(24
     27          1)-A(6)*X(6)*XX(20)
     28          2-D*X(6)
     29           RETURN
     30        7   F=K(6)*X(6)*XX(24)*XX(25)-K(7)*X(7)*XX(24)*XX(25)-A(7)*X(7)*XX(20)
     31          1-D*X(7)
     32           RETURN
     33        8   F=K(7)*X(7)*XX(24)*XX(25)-K(8)*X(8)*XX(24)-A(8)*X(8)*XX(20)
     34          1-D*X(8)
     35           RETURN
     36        9   F=K(20)*X(2)*XX(26)*XX(25)-K(21)*X(9)*XX(24)-A(9)*X(9)*XX(20)
     37          1-D*X(9)
     38           RETURN
     39       10   F=K(11)*X(5)*XX(24)-K(17)*X(10)*XX(24)*XX(25)-A(10)*X(10)*XX(20)
     40          1+KB(17)*X(11)*XX(25)
     41          2-D*X(10)
     42           RETURN
     43       11   F=K(13)*X(14)*XX(24)+K(17)*X(10)*XX(24)*XX(25)-K(18)*X(11)*XX(25)*
     44          1XX(24)-A(11)*X(11)*XX(20)
     45          2-KB(17)*X(11)*XX(25)+KB(18)*X(12)*XX(25)
     46          3-D*X(11)
     47           RETURN
     48       12   F=K(8)*X(8)*XX(24)+K(16)*X(16)*XX(24)+K(18)*X(11)*XX(25)*XX(24)-
     49          1K(19)*X(12)*XX(25)*XX(24)-A(12)*X(12)*XX(20)
     50          2-KB(18)*X(12)*XX(25)+KB(19)*X(13)*XX(25)
     51          3-D*X(12)
     52           RETURN
```

```
                  13   F=K(1D)*X(12)*XX(24)*XX(25)-A(13)*X(13)*XX(20)
                  14   1-KB(19)*X(13)*XX(25)
                  15   2-D*X(13)
                  16    RETURN
                  17   F=K(12)*X(5)*XX(24)-K(13)*X(14)*XX(24)-K(14)*X(14)*XX(22)*XX(25)
                  18   1-A(14)*X(14)*XX(20)
                  19   2-D*X(1A)
                  20    RETURN
                  21   F=K(15)*X(16)*XX(24)-K(16)*X(15)*XX(24)-A(15)*X(15)*XX(20)
                  22   1-D*X(15)
                  23    RETURN
                  24   F=K(14)*X(14)*XX(22)*XX(25)-K(15)*X(16)*XX(24)
                  25   1-A(16)*X(16)*XX(20)
                  26   2-D*X(16)
                  27    RETURN
                  28   F=X(1)+X(2)+X(3)+X(4)+X(5)+X(6)+X(7)+X(8)+X(9)+X(10)+X(11)+
                  29   1X(12)+X(13)+X(14)+X(15)+X(16)-XX(20)
                  30   2+D*XX(20)
                  31    RETURN
                  32    END

THERE WERE NO   DIAGNOSTICS IN ABOVE COMPILATION
 26K  WORDS WERE USED FOR THIS COMPILATION
```

FLOPOS FOR DUSTCHEM

```
      SUBROUTINE FLOPOS(ALT)
      COMMON K(23),A(16),XX(37),KB(40),X(16),D
      REAL K
      WRITE (3,100)ALT
100   FORMAT('1',45X,'FLOW RATES OF POSITIVE ION REACTIONS'/59X,
     1' ALTITUDE = ',F5.1,'  KILOMETERS ')
      WRITE(3,201)
201   FORMAT('0',8X,'D(N2+)/DT =')
      WRITE(3,101)XX(17)
101   FORMAT(30X,'Q(N2+)                                    =',E10.3)
      P=-K(1)*X(1)*XX(21)
      WRITE(3,102)P
102   FORMAT(30X,'-K(1)(N2+)(O)                             =',E10.3)
      P=K(2)*X(1)*XX(22)
      WRITE(3,103)P
103   FORMAT(30X,'-K(2)(N2+)(O2)                            =',E10.3)
      P=-K(4)*X(1)*XX(23)
      WRITE(3,104)P
104   FORMAT(30X,'-K(4)(N2+)(NO)                            =',E10.3)
      P=-A(1)*X(1)*XX(20)
      WRITE(3,105)P
105   FORMAT(30X,'-A(1)(N2+)(NE)                            =',E10.3)
      P=-D*X(1)
      WRITE(3,1105)P
1105  FORMAT(30X,'-DUST*(N2+)                               =',E10.3)
      WRITE(3,202)
202   FORMAT('0',8X,'D(NO+)/DT =')
      WRITE(3,106)XX(18)
106   FORMAT(30X,'Q(NO+)                                    =',E10.3)
      P=K(1)*X(1)*XX(21)
      WRITE(3,107)P
107   FORMAT(30X,'K(1)(N2+)(O)                              =',E10.3)
      P=K(3)*X(3)*XX(23)
      WRITE(3,108)P
108   FORMAT(30X,'K(3)(O2+)(NO)                             =',E10.3)
      P=K(4)*X(1)*XX(23)
      WRITE(3,109)P
109   FORMAT(30X,'K(4)(N2+)(NO)                             =',E10.3)
      P=-K(5)*X(2)*X(24)*XX(25)
      WRITE(3,110)P
110   FORMAT(30X,'-K(5)(NO+)(H2O)(M)                        =',E10.3)
      P=-K(20)*X(2)*XX(26)*XX(25)
      WRITE(3,111)P
111   FORMAT(30X,'-K(20)(NO+)(CO2)(M)                       =',E10.3)
      P=-A(2)*X(2)*XX(20)
      WRITE(3,112)P
112   FORMAT(30X,'-A(2)(NO+)(NE)                            =',E10.3)
      P=-D*X(2)
      WRITE(3,1112)P
1112  FORMAT(30X,'-DUST*(NO+)                               =',E10.3)
      WRITE(3,203)
203   FORMAT('0',8X,'D(O2+)/DT =')
```

```
      WRITE(3,113)XX(19)
113   FORMAT(30X,'Q(O2+)                                    =',E10.3)
      P=K(2)*X(11)*XX(22)
      WRITE(3,114)P
114   FORMAT(30X,'K(2) (N2+) (O2)                           =',E10.3)
      P=-K(3)*X(3)*XX(23)
      WRITE(3,115)P
115   FORMAT(30X,'-K(3) (O2+) (NO)                          =',E10.3)
      P=-K(9)*X(3)*XX(22)*XX(25)
      WRITE(3,116)P
116   FORMAT(30X,'-K(9) (O2+) (O2) (M)                      =',E10.3)
      P=-K(22)*X(3)*XX(24)*XX(25)
      WRITE(3,117)P
117   FORMAT(30X,'-K(22) (O2+) (H2O) (M)                    =',E10.3)
      P=-A(3)*X(3)*XX(20)
      WRITE(3,118)P
118   FORMAT(30X,'-A(3) (O2+) (NE)                          =',E10.3)
      P=-DMX(3)
      WRITE(3,1118)P
1118  FORMAT(30X,'-DUST*(O2+)                               =',E10.3)
      P=K(23)*X(4)*XX(21)
      WRITE(3,119)K(23),P
119   FORMAT(30X,'K(23) (O4+) (O)                           =',E10.3)
      WRITE(3,204)
204   FORMAT('0',8X,'D(O4+)/DT =')
      P=K(9)*K(3)*XX(22)*XX(25)
      WRITE(3,120)P
120   FORMAT(30X,'K(9) (O2+) (O2) (M)                       =',E10.3)
      P=-K(10)*X(5)*XX(24)
      WRITE(3,121)P
121   FORMAT(30X,'-K(10) (O4+) (H2O)                        =',E10.3)
      P=+K(23)*X(4)*XX(21)
      WRITE(3,123)P
123   FORMAT(30X,'-K(23) (O4+) (O)                          =',E10.4)
      P=-A(4)*X(5)*XX(20)
      WRITE(3,122)P
122   FORMAT(30X,'-A(4) (O4+)NE                             =',E10.4)
      P=-DMX(4)
      WRITE(3,1122)P
1122  FORMAT(30X,'-DUST*(O4+)                               =',E10.3)
      WRITE(3,205)
205   FORMAT('0',8X,' D(O2+H2O)/DT =')
      P=K(10)*X(4)*XX(24)
      WRITE(3,124)P
124   FORMAT(30X,'K(10) (O4+) (H2O)                         =',E10.4)
      P=K(22)*X(3)*XX(24)*XX(25)
      WRITE(3,125)P
125   FORMAT(30X,'K(22) (O2+) (H2O) (M)                     =',E10.3)
      P=-(K(11)*K(12))*X(5)*XX(24)
      WRITE(3,126)P
126   FORMAT(30X,'-(K(11)*K(12)) (O2+H2O) (H2O)             =',E10.3)
      P=-A(5)*X(5)*XX(20)
```

```
      105          WRITE(3,127)P
      106      127 FORMAT(30X,*-A(5)(O2+H2O)(NE)                =*,E10.3)
      107          P=-D*X(5)
      108          WRITE(3,1127)P
      109     1127 FORMAT(30X,*-DUST*(O2+H2O)                   =*,E10.3)
      110          WRITE(3,206)
      111      206 FORMAT(*0*,8X,*D(NO+H2O)/DT =*)
      112          P=K(5)*X(2)*XX(24)*XX(25)
      113          WRITE(3,128)P
      114      128 FORMAT(30X,*K(5)(NO+)(H2O)(M)                =*,E10.3)
      115          P=K(21)*X(9)*XX(24)
      116          WRITE(3,129)P
      117      129 FORMAT(30X,*K(21)(NO+CO2)(H2O)               =*,E10.3)
      118          P=-K(6)*X(6)*XX(24)*XX(25)
      119          WRITE(3,130)P
      120      130 FORMAT(30X,*-K(6)(NO+H2O)(H2O)(M)            =*,E10.3)
      121          P=-A(6)*X(6)*XX(20)
      122          WRITE(3,131)P
      123      131 FORMAT(30X,*-A(6)(NO+H2O)(NE)                =*,E10.3)
      124          P=-D*X(6)
      125          WRITE(3,1131)P
      126     1131 FORMAT(30X,*-DUST*(NO+H2O                    =*,E10.3)
      127          WRITE(3,207)
      128      207 FORMAT(*0*,8X,*D(NO+(H2O)2)/DT =*)
      129          P=K(6)*X(6)*XX(24)*XX(25)
      130          WRITE(3,132)P
      131      132 FORMAT(30X,*K(6)(NO+H2O)(H2O)(M)             =*,E10.3)
      132          P=-K(7)*X(7)*XX(24)*XX(25)
      133          WRITE(3,133)P
      134      133 FORMAT(30X,*-K(7)(NO+(H2O)2)(H2O)(M)         =*,E10.3)
      135          P=-A(7)*X(7)*XX(20)
      136          WRITE(3,134)P
      137      134 FORMAT(30X,*-A(7)(NO+(H2O)2)(NE)             =*,E10.3)
      138          P=-D*X(7)
      139          WRITE(3,1134)P
      140     1134 FORMAT(30X,*-DUST*(NO+(H2O)2)                =*,E10.3)
      141          WRITE(3,208)
      142      208 FORMAT(*0*,8X,*D(NO+(H2O)3)/DT =*)
      143          P=K(7)*X(7)*XX(24)*XX(25)
      144          WRITE(3,434)P
      145      434 FORMAT(30X,*K(7)(NO+(H2O)2)(H2O)(M)           =*,E10.3)
      146          P=-K(8)*X(8)*XX(24)
      147          WRITE(3,135)P
      148      135 FORMAT(30X,*-K(8)(NO+(H2O)3)(H2O)             =*,E10.3)
      149          P=-A(8)*X(8)*XX(20)
      150          WRITE(3,136)P
      151      136 FORMAT(30X,*-A(8)(NO+(H2O)3)(NE)              =*,E10.3)
      152          P=-D*X(8)
      153          WRITE(3,1136)P
      154     1136 FORMAT(30X,*-DUST*(NO+(H2O)3                  =*,E10.3)
      155          WRITE(3,209)
      156      209 FORMAT(*0*,8X,*D(NO+CO2)/DT =*)
```

```
      P=K(20)*K(2)*XX(26)*XX(25)
      WRITE(3,137)P
  137 FORMAT(30X,'K(20)(NO+)(CO2)(M)                    =',E10.3)
      P=-K(21)*X(9)*XX(24)
      WRITE(3,138)P
  138 FORMAT(30X,'-K(21)(NO+CO2)(H2O)                   =',E10.3)
      P=-A(9)*X(9)*XX(20)
      WRITE(3,139)P
  139 FORMAT(30X,'-A(9)(NO+CO2)(NE)                     =',E10.3)
      P=-D*X(9)
      WRITE(3,1139)P
 1139 FORMAT(30X,'-DUST*(NO+CO2                         =',E10.3)
      WRITE(3,210)
  210 FORMAT('0',8X,'D(H3O+)/DT =')
      P=K(11)*X(5)*XX(24)
      WRITE(3,140)P
  140 FORMAT(30X,'K(11)(O2+H2O)(H2O)                    =',E10.3)
      P=-K(17)*X(10)*XX(24)*XX(25)
      WRITE(3,141)P
  141 FORMAT(30X,'-K(17)(H3O+)(H2O)(M)                  =',E10.3)
      P=-A(10)*X(10)*XX(20)
      WRITE(3,142)P
  142 FORMAT(30X,'-A(10)(H3O+)(NE)                      =',E10.3)
      P=-D*X(10)
      WRITE(3,1142)P
 1142 FORMAT(30X,'-DUST*(H3O+)                          =',E10.3)
      WRITE(3,211)
  211 FORMAT('0',8X,'D(H3O+H2O)/DT =')
      P=K(13)*K(14)*XX(24)
      WRITE(3,143)P
  143 FORMAT(30X,'K(13)(H3O+OH)(H2O)                    =',E10.3)
      P=K(17)*K(10)*XX(24)*XX(25)
      WRITE(3,144)P
  144 FORMAT(30X,'K(17)(H3O+)(H2O)(M)                   =',E10.3)
      P=-K(18)*X(11)*XX(24)*XX(25)
      WRITE(3,145)P
  145 FORMAT(30X,'-K(18)(H3O+H2O)(H2O)(M)               =',E10.3)
      P=-A(11)*X(11)*XX(20)
      WRITE(3,146)P
  146 FORMAT(30X,'-A(11)(H3O+H2O)(NE)                   =',E10.3)
      P=-D*X(11)
      WRITE(3,1146)P
 1146 FORMAT(30X,'-DUST*(H3O+H2O)                       =',E10.3)
      WRITE(3,212)
  212 FORMAT('0',8X,'D(H3O+(H2O)2)/DT =')
      P=K(8)*X(8)*XX(24)
      WRITE(3,147)P
  147 FORMAT(30X,'K(8)(NO+(H2O)3)(H2O)                  =',E10.3)
      P=K(16)*X(15)*XX(24)
      WRITE(3,148)P
  148 FORMAT(30X,'K(16)(H3O+OH H2O)(H2O)                =',E10.3)
      P=K(18)*X(11)*XX(24)*XX(25)
```

```
      WRITE(3,1149)P
  149 FORMAT(30X,'K(18) (H3O+H2O) (H2O) (M)                =',E10.3)
      P=K(19)*X(12)*XX(24)*XX(25)
      WRITE(3,150)P
  150 FORMAT(30X,'-K(19) (H3O+(H2O)2) (H2O) (M)            =',E10.3)
      P=-A(12)*X(12)*XX(20)
      WRITE(3,151)P
  151 FORMAT(30X,'-A(12) (H3O+(H2O)2) (NE)                 =',E10.3)
      P=-D*X(12)
      WRITE(3,1151)P
 1151 FORMAT(30X,'-DUST*(H3O+(H2O)2)                       =',E10.3)
      WRITE(3,213)
  213 FORMAT('0',.8X,'D(H3O+(H2O)3)/DT =')
      P=K(19)*X(12)*XX(24)*XX(25)
      WRITE(3,152)P
  152 FORMAT(30X,'K(19) (H3O+(H2O)2) (H2O) (M)             =',E10.3)
      P=-A(13)*X(13)*XX(20)
      WRITE(3,153)P
  153 FORMAT(30X,'-A(13) (H3O+(H2O)3) (NE)                 =',E10.3)
      P=-D*X(13)
      WRITE(3,1153)P
 1153 FORMAT(30X,'-DUST*(H3O+(H2O)3)                       =',E10.3)
      WRITE(3,214)
  214 FORMAT('0',.8X,'D(H3O+OH)/DT =')
      P=K(12)*X(5)*XX(24)
      WRITE(3,154)P
  154 FORMAT(30X,'K(12) (O2+H2O) (H2O)                     =',E10.3)
      P=-K(13)*X(14)*XX(24)
      WRITE(3,155)P
  155 FORMAT(30X,'-K(13) (H3O+OH) (H2O)                    =',E10.3)
      P=-K(14)*X(14)*X(3)*XX(25)
      WRITE(3,156)P
  156 FORMAT(30X,'-K(14) (H3O+OH) (O2) (M)                 =',E10.3)
      P=-A(14)*X(14)*XX(22)
      WRITE(3,157)P
  157 FORMAT(30X,'-A(14) (H3O+OH) (NE)                     =',E10.3)
      P=-D*X(14)
      WRITE(3,1157)P
 1157 FORMAT(30X,'-DUST*(H3O+OH)                           =',E10.3)
      WRITE(3,215)
  215 FORMAT('0',.8X,'D(H3O+OH.H2O)/DT =')
      P=K(15)*X(16)*XX(24)
      WRITE(3,158)P
  158 FORMAT(30X,'K(15) (H3O+OH O2) (H2O)                  =',E10.3)
      P=-K(16)*X(15)*XX(24)
      WRITE(3,159)P
  159 FORMAT(30X,'-K(16) (H3O+OH H2O) (H2O)                =',E10.3)
      P=-A(15)*X(15)*XX(20)
      WRITE(3,160)P
  160 FORMAT(30X,'-A(15) (H3O+OH H2O) (NE)                 =',E10.3)
      P=-D*X(15)
      WRITE(3,1160)P
```

```
                261        1160 FORMAT(30X,'-DUST*(H3O+OH H2O)                    *',E10.3)
                262             WRITE(3,216)
                263         216 FORMAT('0',8X,'D(H3O+OH,O2)/DT =')
                264             P=K(14)*X(14)*XX(22)*XX(25)
                265             WRITE(3,161)P
                266         161 FORMAT(30X,'K(14)(H3O+OH)(O2)(M)                   *',E10.3)
                267             P=-K(15)*X(16)*XX(24)
                268             WRITE(3,162)P
                269         162 FORMAT(30X,'-K(15)(H3O+OH O2)(H2O)                 *',E10.3)
                270             P=-A(16)*X(16)*XX(20)
                271             WRITE(3,163)P
                272         163 FORMAT(30X,'-A(16)(H3O+OH O2)(NE)                  *',E10.3)
                273             P=-DPX(16)
                274             WRITE(3,1163)P
                275        1163 FORMAT(30X,'-DUST*(H3O+OH O2)                      *',E10.3)
                276             RETURN
                277             END

THERE WERE  NO   DIAGNOSTICS IN ABOVE COMPILATION
 28K  WORDS WERE USED FOR THIS COMPILATION
```

AL316

AND

BAKSUB

```
                1              SUBROUTINE AL316(N,MAXIT,NUMSIG,SING,K,EVALFN)
                2        C ALGORITHM 316
                3        C     SOLUTION OF SYSTEMS OF NON-LINEAR EQUATIONS
                4        C
                5              INTEGER SING,CONVG
                6              REAL X(N)
                7              REAL COE(50,51),TEMP(50)
                8              REAL PART(50)
                9              INTEGER TALLY
               10              INTEGER POINT(50,50)
               11              INTEGER ISUB(49)
               12        C
               13              CONVG=1
               14              SING=1
               15              RELCVG=10.**(-NUMSIG)
               16              DO 2 M=1,MAXIT
               17        C
               18              DO 1 J=1,N
               19            1 POINT(1,J)=J
               20              DO 3 K=1,N
               21              IF(K.GT.1) CALL BAKSUB(K,N,X,ISUB,COE,POINT)
*****W  1457 DO LOOP INDEX K MAY NOT BE REDEFINED IN CALL OR ABNORMAL FUNCTION
*****W  1457 DO PARAMETER 4 MAY NOT BE REDEFINED IN CALL OR ABNORMAL FUNCTION
               22                   CALL EVALFN(X,F,K)
*****W  1457 DO LOOP INDEX K MAY NOT BE REDEFINED IN CALL OR ABNORMAL FUNCTION
               23                   FACTOR=.001
               24        C AAA.
               25              300  TALLY=0
               26                   DO 4 I=K,N
               27                   ITEMP=POINT(K,I)
               28                   HOLD= X(ITEMP)
               29                   H= FACTOR*HOLD
               30                   IF(H.EQ.0.0) H=.001
               31                   X(ITEMP)= HOLD+H
               32                   IF(K.GT.1) CALL BAKSUB(K,N,X,ISUB,COE,POINT)
*****W  1457 DO LOOP INDEX K MAY NOT BE REDEFINED IN CALL OR ABNORMAL FUNCTION
*****W  1457 DO PARAMETER N MAY NOT BE REDEFINED IN CALL OR ABNORMAL FUNCTION
               33                   CALL EVALFN(X,FPLUS,K)
*****W  1457 DO LOOP INDEX K MAY NOT BE REDEFINED IN CALL OR ABNORMAL FUNCTION
               34                   PART(ITEMP)= (FPLUS-F)/H
               35                   X(ITEMP)=HOLD
               36        C  FIX TO AVOID ZERO DIVISION
               37                   PTEST= PART(ITEMP)
               38                   IF(ABS(PTEST).EQ.0.0) GO TO 44
               39                   IF(ABS(F/PTEST).LE. 1.E20) GO TO 4
               40              44   TALLY=TALLY+1
               41              4    CONTINUE
               42                   IF(TALLY.LE.N-K) GO TO 200
               43                   FACTOR=FACTOR*10.
               44                   IF(FACTOR.GT. .5) GO TO 600
               45                   GO TO 300
               46        C AA.
```

```
                47          200   IF(K.LT.N1) GO TO 100
                48                IF(ABS(PART(ITEMP)).EQ. 0.) GO TO 600
                49                COE(K+N+1)=0.
                50                KMAX=ITEMP
                51                GO TO 3
                52          C  A.
                53           100  KMAX=POINT(K+K)
                54                DERMAX=ABS(PART(KMAX))
                55                KPLUS=K+1
                56                DO 6 I=KPLUS+N
                57                JSUB= POINT(K+I)
                58                TEST= ABS(PART(JSUB))
                59                IF(TEST.LT.DERMAX) GO TO 800
                60                DERMAX=TEST
                61                POINT(KPLUS+I)=KMAX
                62                KMAX=JSUB
                63                GO TO 6
                64          C  A.
                65           800  POINT(KPLUS+I)=JSUB
                66          C ENDI.
                67            6   CONTINUE
                68                IF(ABS(PART(KMAX)).EQ. 0.) GO TO 600
                69                ISUB(K)=KMAX
                70                COE(K+N+1)=0.
                71                DO 9 J=KPLUS+N
                72                JSUB= POINT(KPLUS+J)
                73                COE(K+JSUB)= - PART(JSUB)/PART(KMAX)
                74            9   COE(K+N+1)= COE(K+N+1)+PART(JSUB)*X(JSUB)
                75          C ENDK.
                76            3   COE(K+N+1)=(COE(K+N+1)-F)/PART(KMAX) + X(KMAX)
                77                X(KMAX)= COE(N+N+1)
                78                IF(N+GT+1) CALL BACSUB(N+N+X+ISUB+COE+POINT)
*****W  1457 ADJUSTABLE DIMENSION N MAY NOT BE REDEFINED IN CALL OR ABNORMAL FUNCTION
*****W  1457 ADJUSTABLE DIMENSION N MAY NOT BE REDEFINED IN CALL OR ABNORMAL FUNCTION
                79                IF(M.EQ+1) GO TO 13
                80                DO 10 I=1+N
                81                IF(ABS((ITEMP(I)-X(I))/X(I)) .GT. RELCVG) GO TO 12
                82           10   CONTINUE
                83                CONVG=CONVG+1
                84                IF(CONVG.GE.3) GO TO 999
                85                GO TO 13
                86           12   CONVG=1
                87           13   DO 20 I=1+N
                88           20   TEMP(I)=X(I)
                89            2   CONTINUE
                90                RETURN
                91          999   MAXIT=M
                92                RETURN
                93          600   SING=0
                94                RETURN
                95                END
*****W  1470 EQUALITY OR NON-EQUALITY COMPARISON MAY NOT BE MEANINGFUL IN LOGICAL IF EXPRESSIONS

  THERE WERE     9 DIAGNOSTICS IN ABOVE COMPILATION
   26K  WORDS WERE USED FOR THIS COMPILATION
```

```
                1           SUBROUTINE BAKSUB(K,N,X,ISUB,COE,P)
                2           DIMENSION X(N),COE(150,51),ISUB(49),P(150,50)
                3           INTEGER P
                4           KM=K
                5       10  IF(KM.LT.2) RETURN
                6           KMAX=ISUB(KM-1)
                7           X(KMAX)=0.0
                8           DO 2 J=KM,N
                9           JSUB=P(KM,J)
               10       2  X(KMAX)=X(KMAX) + COE(KM-1,JSUB)*X(JSUB)
               11           X(KMAX)= X(KMAX) + COE(KM-1,N+1)
               12           K=KM-1
               13           GO TO 10
               14           END

THERE WERE  NO   DIAGNOSTICS IN ABOVE COMPILATION
 25K  WORDS WERE USED FOR THIS COMPILATION
```

HC029

```
OS FORTRAN IV 360N-FO-479 3-5          MAINPGM          DATE  01/27/75     TIME    03.03.39      PAGE 0001

      C     IONCHEMISTRY PROGRAM TO SOLVE A NON-LINEAR SYSTEM OF EQUATIONS
      C     TO GENERATE A POSITIVE AND NEGATIVE ION MODEL OF THE D REGION.
      C     THE INPUTS ARE  1) THE POSITIVE RATE CONSTANTS, K( 1, 2), THE NEGATIVE
      C     RATE CONSTANTS, KN( 1,3), POSITIVE BACKWARD RATE CONSTANTS,K(2,
      C     4),NEUTRAL CONSTITUENTS, RX, 5),POSITIVE IONS, X, AND 5), NEGATIVE
      C     IONS, XN.
      C       A IS RECOMBINATION COEFFICIENT.
      C     W.COLF - STEVE GELLER  JULY  1973
      C
      C
      C     ALGORITHM 316 FROM COMMUNICATIONS OF THE ACM IS EMPLOYED
0001            EXTERNAL F2
0002            INTEGER NVARS/31/,NK/23/,NA/16/
0003            INTEGER TITLE(20),TITLE2(20),TITLE3(20)
0004            DIMENSION XN(5)
0005            COMMON K(23),AF(16),XX(37),K9(40),X(31),XN(75),SUMP,ALT
0006            REAL K,DATE(2),K8,KK
0007            EQUIVALENCE(X(17),XN(1))
      C
      C
      C
      C     READ K VALUES- REACTION RATES
      C
0008            K(1)=1.4 E-10
0009            K(2)=5.0 E-11
0010            K(3)=6.3 E-10
0011            K(4)=3.3 E-10
0012            K(5)=1.6 E-28
0013            K(6)=1.1 E-27
0014            K(7)=2.0 E-27
0015            K(8)=8.0 E-11
0016            K(9)=2.8 E-30
0017            K(10)=2.2 E-9
0018            K(11)=3.0 E-10
0019            K(12)=1.9 E-9
0020            K(13)=3.2 E-9
0021            K(14)=1.0 E-29
0022            K(15)=1.0 E-9
0023            K(16)=1.0 E-9
0024            K(17)=3.4 E-27
0025            K(18)=2.2 E-27
0026            K(19)=2.4 E-27
0027            K(20)=3.0 E-29
0028            K(21)=5.0 E-10
0029            K(22)=2.8 E-28
0030            K(23)=3.0 E-10
0031            KA(17)=1.58 E-10
0032            KA(18)=4.86 E-20
0033            KA(19)=7.1 E-15
      C
      C     READ KN VALUES - NEGATIVE ION REACTION RATE CONSTANTS.
      C
0034            KN(1)=1.3 E-15
0035            KN(2)=9.20 E-10
0036            KN(3)=1.0 E-11
0037            KN(4)=1.44
0038            KN(5)=6.0 E-10
0039            KN(6)=1.0 E-12
0040            KN(7)=2.0 E-10
0041            KN(8)= 6.0 E-10
```

```
0042          KN(9)=5.66 E-1C
0043          KN(10)=5.0 E-10
0044          KN(11)=1.2 E-30
0045          KN(12)=9.0 E-26
0046          KN(13)=1.0 E-29
0047          KN(14)=2.2 E-28
0048          KN(15)=8.9 E-10
0049          KN(16)=1.52 E-30
0050          KN(17)=1.0 E-31
0051          KN(18)=1.7 E-14
0052          KN(19)=1.0 E-1C
0053          KN(20)=9.0 E-1C
0054          KN(21)=8.0 E-11
0055          KN(22)=.33
0056          KN(23)=3.0 E-1C
0057          KN(24)=2.1 E-18
0058          KN(25)=4.0 E-31
0059          KN(26)=2.17 E-10
0060          KN(27)=2.0 E-29
0061          KN(28)=9.0 E-3C
0062          KN(29)=4.0 E-10
0063          KN(30)=.2
0064          KN(31)=4.0 E-1C
0065          KN(32)=1.5 E-29
0066          KN(33)=1.C E-16
0067          KN(35)=5.0 E-15
0068          KN(36)=1.0 E-11
0069          KN(37)=1.0 E-1C
0070          KN(38)=6.5 E-2C
0071          KN(39)=1.5 E-11
0072          KN(40)=2.0 E-1C
0073          KN(41)=2.3 E-14
0074          KN(42)=2.2 E-1C
0075          KN(43)=4.3 E-1C
0076          KN(44)=2.5 E-10
0077          KN(45)=1.5 E-1C
0078          KN(46)=.2
0079          KN(47)=6.0 E-12
0080          KN(48)=8.0 E-11
0081          KN(49)=5.8 E-10
0082          KN(50)=1.0 E-10
0083          KN(51)=4. E-30
0084          KN(52)=1.6 E-22
0085          KN(54)=9.0 E-10
0086          KN(55)=1.2 E-9
0087          KN(56)=.34
0088          KN(57)=1.8 E-28
0089          KN(59)=1.8 E-11
0090          KN(60)=4.8 E-11
0091          KN(61)=.03
0092          KN(62)=1.3 E-10
0093          KN(63)=4.0 E-12
0094          KN(64)=3.8 E-29
0095          KN(65)=2. E-18
0096          KN(66)=1.0 E-9
0097          KN(67)=1.0 E-7
0098          KN(68)=1.4 E-9
0099          KN(69)=9.4 E-28
0100          KN(70)=7.5 E-29
0101          KN(71)=3.4 E-25
```

```
0102            KN(72)=2.0 E-10
0103            KN(73)=1.5 E-31
                C
                C  READ 'A' VALUES (- RECOMBINATION COEFFICIENTS - ALPHAS
                C
0104            A(1)=3. E-7
0105            A(2)=2.5 E-7
0106            A(3)=3.5 E-7
0107            A(4)=2.0 E-6
0108            A(5)=5.0 E-6
0109            A(6)=5.0 E-6
0110            A(7)=7.0 E-6
0111            A(8)=1.0 E-5
0112            A(9)=1.0 E-5
0113            A(10)=3.6 E-6
0114            A(11)=8.0 E-6
0115            A(12)=1.3 E-5
0116            A(13)=3.0 E-5
0117            A(14)=5.0 E-6
0118            A(15)=1.0 E-5
0119            A(16)=1.9 E-5
                C
                C   READ IN PRESET VALUES FOR
                C   PRIMARY PRODUCTION RATE, NUMBER DENSITY OF NEUTRAL CONSTITUTENTS
                C   AND ELECTRON DENSITY.
                C
                C
                C
                C   PRINT THE INPUT....
0120                CALL GETDAT(DATE)
                C
0121                PRINT 900,DATE
0122              900 FORMAT('0RUN  DATE.....',2A4)
0123                PRINT 901,(J,X(J),J=1,NX)
0124              901 FORMAT('0X - VALUES...'/(1X,I3,1X,E10.3))
0125                PRINT 905,(J,XN(J),J=1,35)
0126              905 FORMAT('0XN - VALUES...'/(1X,I3,1X,E10.3))
0127                PRINT 902,(J,A(J),J=1,NA)
0128              902 FORMAT('0A - VALUES...'/(1X,I3,1X,E10.3))
                C     SET INITIAL X(J)'S TO 100. AT THE START OF A NEW PROFILE
0129                DO 10 I=1,16
0130             10 X(I)=100.
0131                DO 11 I=17,31
0132             11 X(I)=1.
0133                X(2)=100.
0134                X(6)=100.
0135                X(7)=100.
0136                X(12)=100.
0137                PRINT 904,(J,X(J),J=1,NVARS)
0138              904 FORMAT('0INITIAL GUESSES...'/(1X,I3,1X,G15.4))
                C
                C    READ IN THE X'S WHICH VARY WITH ALTITUDE AND LIST THEM OUT. EACH
                C    ALTITUDE HAS A SET OF THREE CARDS. XN(20) IS INITIAL ELECTRON DENS
                C  NOTE  THE NUMBER OF TITLE CARDS MUST ALWAYS EQUAL 3 EVEN IF ONE
                C    OF THEM IS BLANK. AFTER THE FIRST PROFILE AND BEFORE THE TITLE
                C    OF THE SECOND, THERE MUST BE 3 BLANK CARDS. THIS PREPARES THE PROGRAM
                C   TO READ THE NEXT THREE CARDS AS TITLE INSTEAD OF DATA.
                C
0139              97 READ(1,98)TITLE1
0140              98 FORMAT(20A4)
```

```
OOS FORTRAN IV 360N-FO-479 3-5        MAINPGM          DATE   01/07/75     TIME    03.03.39     PAGE 0004

0141                PRINT 99,TITLE1
0142            99  FORMAT('1',20A4)
0143                READ(1,198)TITLE2
0144           198  FORMAT(20A4)
0145                PRINT 199,TITLE2
0146           199  FORMAT(20A4)
0147                READ(1,298)TITLE3
0148           298  FORMAT(20A4)
0149                PRINT 299,TITLE3
0150           299  FORMAT(20A4)
0151           300 ALT=0.0
0152                TS=0
0153                TBZ=0
0154                I=0
0155                JA=0
0156                II=0
0157                JJ=0
0158                READ(1,350,END=7011)ALT,(XX(J),J=17,37)
0159           350 FORMAT(F8.1,2X,7E10.2/8E10.2/6E10.2)
0160                IF(ALT.EQ.0.0)GO TO 97
0161                PRINT 903
0162           903 FORMAT(//13X,'PRIMARY PRODUCTION RATES      ELECTRON'/42X,'NUMBER'/
                   12X,'ALTITUDE    QEN2+1      QEN0+1      QO2+1      DENSITY      Q
                   2D2          N0          H2O         O2+N2       CO2          N'/)
0163                PRINT 906,ALT,(XX(J),J=17,27)
0164           906 FORMAT(3X,F5.1,2X,11(2X,F8.2)/)
0165                PRINT 940
0166           940 FORMAT(33X'O2+DO3      O3          NO2         N2          OH          HO2
                   1    N2O         CO          H2          H *)
0167                PRINT 941,(XX(J),J=28,37)
0168           941 FORMAT(10(2X,E8.2)/)
               C
               C    COMPUTE THE ELECTRON DENSITY, COMPARE WITH THE ORIGINAL GUESS AND
               C     RECOMPUTE UNTIL THE DIFFERENCE IS LESS THAN ONE TENTH OF ONE
               C    PERCENT.
               C   SOLVE THE SYSTEM
               C
0169                MAXIT=6
0170           500 CALL AL316(NVARS,MAXIT,3,ISING,X,F2)
0171                MAXIT=1
               C   COMPUTE THE ELECTRON DENSITY
0172          1001 SUMP=RK(1)*XE(2)*RK(3)*XE(4)*X(5)*X(6)*X(7)*X(8)
                   **X(9)*RK(10)*XE(11)*XE(12)*XE(13)*X(14)*X(15)*X(16)
0173                SUMN=RK(1)*XN(2)*XN(3)*XN(4)*XN(5)*XN(6)*XN(7)*XN(8)*XN(9)*
                   1XN(10)*XN(11)*XN(12)*XN(13)*XN(14)*XN(15)
0174           908 DENS=SUMP-SUMN
0175                PRINT 4000,XX(20),DENS,SUMP,SUMN
0176          4000 FORMAT(//10X,' XX(20) =',G19.4,10X,' DENS =',G19.4,10X,' SUMP =',
                   1G19.4,10X,' SUMN =',G19.4///)
0177                DIFF=ABS(XX(20)-DENS)
0178                IF(DIFF.LE.2.3GO TO 800
0179                IF(XX(20),GT.DENS)GO TO 8001
0180          8000 TSX=XX(20)
0181                PRINT 8010,TSX
0182          8010 FORMAT(//10X,' TSX =',G15.4/)
0183                I=I+1
0184                IF(I.GF.1111=1
0185                IF(II+JJ.GE.2)GO TO 9003
0186                XX(20)=XX(20)*2.
0187                GO TO 900
```

```
DOS FORTRAN IV 360N-FO-479 3-5        MAINPGM          DATE  01/07/75      TIME     03.03.39      PAGE 0005

0188          8001 TBX=XX(20)
0189               PRINT 8070,TBX
0190          8070 FORMAT(//50X,* TBX =*,G15.4/)
0191               JA=JA+1
0192               IF(JA.GE.11)JA=1
0193               IF(JA+11.GE.JIGC TO 8003
0194               XX(20)=XX(20)*.5
0195               GO TO 500
0196          8003 XX(20)=(TSX+TBX)/2.
0197               GO TO 500
              C
0198           600 PRINT 907,ISING,ALT,(J,XI(J),J=1,11)
0199           907 FORMAT('0SOLUTION   ISING=',II/,'0ALTITUDE=',F9.1/ 4X,I2,' N2=',1
                   1X,'=',G15.4/4X,I2,' NO=',11X,'=',G15.4/4X,I2,' O2=',11X,'=',G15.4/
                   24X,I2,' O2+(O2)',7X,'=',G15.4/4X,I2,' O2+(H2O)',6X,'=',G15.4/4X,I2
                   3,' NO+(H2O)',6X,'=',G15.4/4X,I2,' NO+(H2O)2',5X,'=',G15.4/4X,I2,'
                   4NO+(H2O)3',5X,'=',G15.4/4X,I2,' NO+(CO2)',6X,'=',G15.4/4X,I2,' H3O
                   5+',10X,'=',G15.4/4X,I2,' H3O+(H2O)',5X,'=',G15.4)
                   PRINT 911,(J,XI(J),J=12,16)
0200
0201           911 FORMAT(4X,I2,' H3O+(H2O)2',4X,'=',G15.4/4X,I2,' H3O+(H2O)3',4X,'=
                   1,G15.4/4X,I2,' H3O+(OH)',6X,'=',G15.4/4X,I2,' H3O+(OH)(H2O)',1X,'=
                   2',G15.4/4X,I2,' H3O+(OH)(O2)',2X,'=',G15.4/)
0202           650 PRINT 651,(J,XN(J),J=1,9),XN(10),XN(11),XN(13),XN(15)
0203           651 FORMAT(/4X,I2,' O-  ',11X,'=',G15.4/4X,I2,' O2-',11X,'=',G15.4/
                   14X,I2,' O3-',11X,'=',G15.4/4X,I2,' O4-',11X,'=',G15.4/4X,I2,' NO-
                   2',10X,'=',G15.4/4X,I2,' NO3-',10X,'=',G15.4/4X,I2,' NO3-.(H2O',10X,'=',
                   3G15.4/4X,I2,' CO3-',10X,'=',G15.4/4X,I2,' CO4-',10X,'=',G15.4/4X,
                   3*13',1X,
                   4NO2-.H2O',7X,'=',G15.4/4X,'14 O2-.(H2O)2    =',G15.4/4X,' 17',1X,'
                   5NO2-.H2O',6X,'=',G15.4/4X,'20 NO2-.(H2O)2   =',G15.4)
0204          1300 PRINT 652,XN(12),XN(14)
0205           652 FORMAT(4X,'15 NO3-.H2O',6X,'=',G15.4/4X,'18 NO3-.(H2O)2   =',G15.4
                   1//)
0206               SNOC=X(6)+X(7)+X(8)
0207               SWATE=X(10)+X(11)+X(12)+X(13)
0208               SNEGC=XN(10)+XN(11)+XN(12)+XN(14)+XN(15)
0209               PRINT 8080,SNOC,SWATE,SNEGC
0210          8080 FORMAT(/5X,'SUM OF NITRIC OXIDE CLUSTER IONS          =',G15.4/
                   15X,       'SUM OF WATER CLUSTER IONS              =',G15.4/
                   25X,       'SUM OF HYDRATED NEGATIVE IONS          =',G15.4//)
0211               PRINT 909,DENS
0212           909 FORMAT(' ENP WHICH THE FINAL ELECTRON DENSITY              =',G15.4/)
              C    CALCULATION OF THE EFFECTIVE RECOMBINATION COEFFICIENTS.
0213               REC=(XX(17)+XX(18)+XX(19))/DENS*DENS
0214               PRINT 956,REC
0215           956 FORMAT(' VALUE OF EFFECTIVE RECOMBINATION COEFFICIENT   =',F10.3/)
0216               PLAMB=SUMN/DENS
0217               PRINT 777,PLAMB
0218           777 FORMAT(' VALUE OF LAMBDA',32X,'=',F10.3//)
0219               CALL FLOPOS
0220               CALL FLCNEG
0221               GO TO 703
0222           701 STOP
0223               END
```

F2 FOR HCO29

```
DOS FORTRAN IV 360H-F0-479 3-5          F2                    DATE   01/26/79      TIME     17.40.02      PAGE 0331

0001            SUBROUTINE F2(X,F,M)
0002            DIMENSION X(9)
0003            COMMON X(73),A(16),B(37),H(63),DUMMY(1),K(75),SUMP
0004            REAL K,M,KK
0005            GO TO(1,2,3,4,5,6,7,8,9,10,11,12,13,14,15,16,101,102,103,104,105,
               1106,107,108,109,110,111,112,113,114,1159,M
                C
                C   VARIABLE NAMES IN F2 MUST ALL BE SUBSCRIPTED AS NOT ANS.
                C
0006                1 F=X(17)-K(1)**X(1)*X(21)-K(2)*X(1)*X(22)-K(4)*X(1)*X(24)
                   1-K(1)*X(1)*X(20)
0007                RETURN
0008               2 F=X(18)+K(1)*X(1)*X(21)+K(3)*X(3)*X(23)+K(4)*X(1)*X(23)-
                   1K(5)*X(2)*X(24)+X(25)-A(20)*X(2)*X(26)*X(25)-A(21)*X(23)*X(20)
0009                RETURN
0010               3 F=X(19)+K(2)*X(1)*X(27)-K(3)*X(3)*X(23)-K(9)*X(3)*X(22)*X(25)
                   1-K(22)*X(1)*X(24)*X(25)-A(3)*X(3)*X(20)
                   2+X(23)*X(4)*X(21)
0011                RETURN
0012               4 F=X(5)*X(3)*X(27)*X(25)-K(10)*X(6)*X(26)-A(6)*X(6)*X(20)
                   1-K(23)*X(4)*X(21)
0013                RETURN
0014               5 F=X(10)*X(6)*X(24)-(K(11)*K(23)*X(5)*X(24)*X(22)*X(3)*X(25)*X
                   1(24)-A(5)*X(5)*X(20)
0015                RETURN
0016               6 F=X(9)*X(2)*X(25)*X(24)-X(6)*X(6)*X(24)*X(25)*X(21)*X(9)*X(24
                   1)-A(6)*X(6)*X(20)
0017                RETURN
0018               7 F=X(6)*X(6)*X(24)*X(25)-K(7)*X(7)*X(24)*X(25)-A(7)*X(7)*X(20)
0019                RETURN
0020               8 F=X(7)*X(7)*X(24)*X(25)-K(8)*X(8)*X(24)-A(8)*X(8)*X(20)
0021                RETURN
0022               9 F=K(20)*X(2)*X(26)*X(25)-K(21)*X(9)*X(24)-A(9)*X(9)*X(20)
0023                RETURN
0024              10 F=K(11)*X(5)*X(24)-K(17)*X(10)*X(24)*X(25)-A(10)*X(10)*X(23)
                   1+K(17)*X(11)*X(25)
0025                RETURN
0026              11 F=K(13)*X(14)*X(24)+K(17)*X(13)*X(24)*X(25)-K(18)*X(11)*X(25)*
                   1X(24)-A(11)*X(11)*X(20)
                   2-K(17)*X(11)*X(25)*K(18)*X(12)*X(25)
0027                RETURN
0028              12 F=K(9)*X(8)*X(24)+K(16)*X(15)*X(24)*X(10)*X(11)*X(25)*X(24)-
                   1K(19)*X(12)*X(25)*X(24)-A(12)*X(12)*X(20)
                   2-K(18)*X(13)*X(25)*K(19)*X(13)*X(25)
0029                RETURN
0030              13 F=K(19)*X(12)*X(24)*X(25)-A(13)*X(13)*X(20)
                   1-K(19)*X(13)*X(25)
0031                RETURN
0032              14 F=K(12)*X(5)*X(24)-K(13)*X(16)*X(24)-K(16)*X(16)*X(22)*X(25)
                   1-A(14)*X(14)*X(20)
0033                RETURN
0034              15 F=X(15)*X(16)*X(24)-K(16)*X(15)*X(24)-A(15)*X(15)*X(23)
0035                RETURN
0036              16 F=K(14)*X(14)*X(22)*X(25)-K(15)*X(16)*X(24)
                   1-A(16)*X(16)*X(20)
0037                RETURN
0038             101 F=-K(14)*X(17)-K(5)*X(17)*X(35)-K(6)*X(17)*X(31)-K(7)*X(17)*
                   1K(21)-K(8)*X(17)*X(36)-K(9)*X(17)*X(29)-K(10)*X(17)*X(21)-
                   2K(11)*X(17)*X(22)*X(25)-K(12)*X(17)*X(26)*X(25)+K(13)*X(24)*
                   3X(21)*X(25)-K(53)*X(17)*X(34)-K(55)*X(17)*X(33)+K(33)*X(2
```

```
      490)*X(20)+KN(1)*X(20)*X(21)+KN(33)*X(20)*X(22)-KN(35)*X(17)*X2
     5(22)-KN(37)*X(17)*X(20)-KN(42)*X(17)*X(17)-1.,F-7)*X(17)*X(1)*
     6X(2)*X(3)*X(5)*X(6)*X(7)*X(8)*X(9)*X(10)*X(11)*X(12)*X(13)*
     7X(14)*X(15)*X(16))*X(N)*X(21)-KN(13)*X(17)*X(21)*X(25)
0039      RETURN
0040  102 F=-KN(2)*X(18)*X(21)-KN(14)*X(19)*X(24)*X(25)-KN(15)*X(18)*X(23
     1)+KN(16)*X(20)*X(22)*X(23)+KN(17)*X(22)*X(20)*X(23)+KN(18)*X(
     2)*X(23)+KN(19)*X(21)-KN(20)*X(23)*X(22)*X(20)*X(21)-KN(24)*X(
     3)*X(21)-KN(23)*X(18)-KN(23)*X(24)*X(18)*X(23)-KN(25)*X(18)*X(23
     4)+X(25)-KN(26)*X(18)*X(29)-KN(28)*X(18)*X(26)*X(23)-KN(27)*X(18)*
     5X(26)*X(23)-1.,F-7)*X(18)*X(1)*X(2)*X(3)*X(6)*X(7)*X(8)*X(9)*X
     6(10)*X(11)*X(12)*X(13)*X(14)*X(15)*X(16))*X(N)*X(21)*X(25)
     7)*X(22)*X(20)-KN(72)*X(18)*X(28)-KN(56)*X(18)*X(27)
0041      RETURN
0042  103 F=KN(19)*X(17)*X(25)*KN(11)*X(17)*X(22)*X(22)-KN(19)*X(19)*X(21
     1)*X(21)*X(18)*X(29)*KN(79)*X(20)*X(21)-KN(30)*X(19)-KN(31)*
     2X(19)*X(23)-
     3(KN(36)+KN(37))*X(15)*X(23)-(KN(39)+KN(40))*X(19)*X(3)*
     4KN(42)*X(25)*X(29)-1.,F-7)*X(19)*X(1)*X(2)*X(3)*X(5)*X(6)*
     5X(7)*X(8)*X(9)*X(10)*X(11)*X(12)*X(13)*X(14)*X(15)*X(16))
0043      RETURN
0044  104 F=-KN(25)*X(20)*X(21)
     1-KN(43)*X(20)*X(26)-KN(44)*X(20)*X(23)-KN(48)*X(20)*X(24)
     2-KN(10)*X(20)*X(22)*KN(25)*X(10)*X(22)*X(25)
     3*KN(41)*X(25)*X(22)-(1.0E-7)*X(20)*
     4(X(1)*X(2)*X(3)*X(4)+X(5)*X(6)*X(7)*X(8)*X(9)*X(10)*X(11)*X(12)
     7*X(13)*X(14)*X(15)*X(16))
0045      RETURN
0046  105 F=-KN(20)*X(21)*X(22)*KN(53)*X(17)*X(34)
     1*KN(73)*KN(25)*X(23)*X(23)-(1.0 E-7)*X(21)*
     6(X(1)*X(2)*X(3)*X(4)*X(5)*X(6)*X(7)*X(8)*X(9)*X(10)*X(11)*X(12)
     7*X(13)*X(14)*X(15)*X(16))
0047      RETURN
0048  106 F=PN(36)*X(19)*X(23)*KN(47)*X(24)*X(23)*KN(51)*X(30)*X(20)*
     1X(25)*KN(13)*X(17)*X(23)*X(25)
     2      +KN(39)*X(15)*X(30)-KN(59)*X(22)*X(25)*KN(63)*X(22)*
     3X(30)*KN(15)*X(18)*X(30)*KN(55)*X(17)*X(30)-KN(46)*X(23)-
     4KN(57)*X(23)*X(26)*X(25)-(1.E-7)*X(22)*
     6(X(1)*X(2)*X(3)*X(4)*X(5)*X(6)*X(7)*X(8)*X(9)*X(10)*X(11)*X(12)
     7*X(13)*X(14)*X(15)*X(16))
0049      RETURN
0050  107 F=                  +KN(40)*X(19)*X(30)*KN(44)*X(22)*X(23)
     *                       +KN(48)*X(24)*X(33)
     1*KN(59)*X(22)*X(29)*KN(62)*X(25)*X(23)- KN(61)*X(23)
     2-KN(70)*X(23)*X(24)*KN(25)*X(1)-(1.0 E-7)*X(25)*
     6(X(1)*X(2)*X(3)*X(4)*X(5)*X(6)*X(7)*X(8)*X(9)*X(10)*X(11)*X(12)
     7*X(13)*X(14)*X(15)*X(16))*KN(6)*X(22)*X(30)
0051      RETURN
0052  108 F=KN(12)*X(17)*X(22)*X(25)-KN(21)*X(24)*X(23)
     1*KN(31)*X(19)*X(26)*KN(45)*X(25)*X(21)- KN(46)*X(26)
     2-X(47)*X(26)*X(23)-KN(48)*X(24)*X(30)-(1.0 E-7)*X(24)*
     6(X(1)*X(2)*X(3)*X(4)*X(5)*X(6)*X(7)*X(8)*X(9)*X(10)*X(11)*X(12)
     7*X(13)*X(14)*X(15)*X(16))
0053      RETURN
0054  109 F=KN(27)*X(18)*X(26)*KN(22)*X(28)*X(18)*X(26)*X(26)
     1-X(14)*X(25)*X(22)*KN(43)*X(20)*X(26)-KN(45)*X(25)*X(21)
     2*KN(49)* X(26)*X(26)-KN(60)*X(25)*X(23)
     4-X(62)*X(25)*X(29)-(1.0 E-7)*X(25)*
     6(X(1)*X(2)*X(3)*X(4)*X(5)*X(6)*X(7)*X(8)*X(9)*X(10)*X(11)*X(12)
     7*X(13)*X(14)*X(15)*X(16))
```

```
      RETURN
  110 F=KN(14)*X(18)*XX(24)*XX(22)+KN(68)*X(20)*XX(24)
     *-KN(69)* X(26)*XX(24)*XX(22)-KN(49)* X(26)*XX(26)
     *-(1.0 E-7)*X(26)*
     6(X(1)+X(2)+X(3)+X(4)+X(5)+X(6)+X(7)+X(8)+X(9)+X(10)+X(11)+X(12)
     7+X(13)+X(14)+X(15)+X(16))
      RETURN
  111 F=KN(69)* X(26)*XX(24)*XX(22)-(1.0 E-7)* X(27)*
     6(X(1)+X(2)+X(3)+X(4)+X(5)+X(6)+X(7)+X(8)+X(9)+X(10)+X(11)+X(12)
     7+X(13)+X(14)+X(15)+X(16))
      RETURN
  112 F=KN(57)*X(22)*XX(24)*XX(23)- KN(64)*X(29)*XX(24)*XX(22)
     *-(1.0 E-7)*X(29)*
     6(X(1)+X(2)+X(3)+X(4)+X(5)+X(6)+X(7)+X(8)+X(9)+X(10)+X(11)+X(12)
     7+X(13)+X(14)+X(15)+X(16))
      RETURN
  113 F=KN(70)*X(23)*XX(24)*XX(25)-KN(71)* X(28)*XX(24)*XX(25)
     *-(1.0 E-7)* X(28)*
     6(X(1)+X(2)+X(3)+X(4)+X(5)+X(6)+X(7)+X(8)+X(9)+X(10)+X(11)+X(12)
     7+X(13)+X(14)+X(15)+X(16))
      RETURN
  114 F=KN(71)* X(28)*XX(24)*XX(25)-(1.0 E-7)* X(30)*
     6(X(1)+X(2)+X(3)+X(4)+X(5)+X(6)+X(7)+X(8)+X(9)+X(10)+X(11)+X(12)
     7+X(13)+X(14)+X(15)+X(16))
      RETURN
  115 F=+KN(64)*X(29)*XX(24)*XX(22)-(1.E-7)*X(31)*(X(1)+X(2)+X(3)+X(4)+
     1X(5)+X(6)+X(7)+X(8)+X(9)+X(10)+X(11)+X(12)+X(13)+X(14)+X(15)+
     2X(16))
      RETURN
      END
```

FLOPOS FOR HC029

```
OS FORTRAN IV 360N-FO-479 3-5        FLOFOS          DATE  01/02/75      TIME     10.28.43      PAGE 0001

0001          SUBROUTINE FLOFOS
0002          REAL K,KB,KN
0003          COMMON K(33),B(16),KK(37),KB(40),X(31),KN(79),SUMP,ALT
0004          WRITE (3,100)ALT
0005      100 FORMAT('1',45X,'FLOW RATES OF POSITIVE ION REACTIONS'//99X,
             *'ALTITUDE=',F8.2,' KILOMETERS')
0006          WRITE(3,201)
0007      201 FORMAT('0',8X,'D(N2+)/DT =')
0008          WRITE(3,101)KK(17)
0009      101 FORMAT(30X,'-K(32)*(N2+)*(O)                              =',E10.3)
0010          P=-K(32)*X(31)*KK(21)
0011          WRITE(3,1023)P
0012      102 FORMAT(30X,'-K(33)*(N2+)*(O)                              =',E10.3)
0013          P=-K(33)*X(31)*KK(22)
0014          WRITE(3,1031)P
0015      103 FORMAT(30X,'-K(28)*(N2+)*(O2)                             =',E10.3)
0016          P=-K(28)*X(31)*KK(20)
0017          WRITE(3,1041)P
0018      104 FORMAT(30X,'-K(6)*(N2+)*(NO)                              =',E10.3)
0019          P=-A(1)*X(11)*KK(20)
0020          WRITE(3,1051)P
0021      105 FORMAT(30X,'-K(1)*(N2+)*(NE)                              =',E10.3)
0022          WRITE(3,202)
0023      202 FORMAT('0',8X,'D(NO+)/DT =')
0024          WRITE(3,106)KK(18)
0025      106 FORMAT(30X,'(NO+)                                         =',E10.3)
0026          P=K(18)*X(11)*KK(21)
0027          WRITE(3,1071)P
0028      107 FORMAT(30X,'K(1)*(N2+)*(O)                                =',E10.3)
0029          P=K(33)*X(31)*KK(23)
0030          WRITE(3,1081)P
0031      108 FORMAT(30X,'K(3)*(O2+)*(NO)                               =',E10.3)
0032          P=K(4)*X(11)*KK(25)
0033          WRITE(3,1091)P
0034      109 FORMAT(30X,'K(4)*(N2+)*(NO)                               =',E10.3)
0035          P=-K(33)*X(31)*KK(24)*KK(25)
0036          WRITE(3,1101)P
0037      110 FORMAT(30X,'-K(5)*(NO+)*(NO)*(M)                          =',E10.3)
0038          P=-K(20)*X(29)*KK(26)*KK(25)
0039          WRITE(3,1111)P
0040      111 FORMAT(30X,'-K(22)*(NO+)*(CO2)*(M)                        =',E10.3)
0041          P=-A(2)*X(29)*KK(20)
0042          WRITE(3,1121)P
0043      112 FORMAT(30X,'-A(2)*(NO+)*(NE)                              =',E10.3)
0044          WRITE(3,203)
0045      203 FORMAT('0',8X,'D(O2+)/DT =')
0046          WRITE(3,1131)KK(19)
0047      113 FORMAT(30X,'(O2+)                                         =',E10.3)
0048          P=K(29)*X(11)*KK(22)
0049          WRITE(3,1141)P
0050      114 FORMAT(30X,'K(2)*(N2+)*(O2)                               =',E10.3)
0051          P= K(29)*X(4)*KK(21)
0052          WRITE(3,2000)P
0053     2000 FORMAT(30X,'K(28)*(O+)*(O)                                =',E10.3)
0054          P=-K(9)*X(3)*KK(23)
0055          WRITE(3,1151)P
0056      115 FORMAT(30X,'-K(3)*(O2+)*(NO)                              =',E10.3)
0057          P=-K(9)*X(3)*KK(22)*KK(25)
0058          WRITE(3,1161)P
0059      116 FORMAT(30X,'-K(9)*(O2+)*(O2)*(M)                          =',E10.3)
```

```
0060          P=-K(22)*K(3)*EXP(26)*EXP(25)
0061          WRITE(3,117)P
0062      117 FORMAT(30X,'-K(22)(O2+)(H2O)(M)                    =',E10.3)
0063          P=-A(3)*K(3)*EXP(20)
0064          WRITE(3,118)P
0065      118 FORMAT(30X,'-A(3)(O2+)(NE)                         =',E10.3)
0066          WRITE(3,204)
0067      204 FORMAT('0',8X,'D(O4+)/DT =')
0068          P=K(9)*K(3)*EXP(22)*EXP(25)
0069          WRITE(3,120)P
0070      120 FORMAT(30X,'K(9)(O2+)(O2)(M)                       =',E10.3)
0071          P=-A(4)*K(3)*EXP(20)
0072          WRITE(3,122)P
0073      122 FORMAT(30X,'-A(4)(O4+)(NE)                         =',E10.3)
0074          P=-K(10)*K(3)*EXP(24)
0075          WRITE(3,121)P
0076      121 FORMAT(30X,'-K(10)(O4+)(H2O)                       =',E10.3)
0077          P=-K(25)*K(4)*EXP(21)
0078          WRITE(3,123)P
0079      123 FORMAT(30X,'-K(25)(O4+)(O)                         =',E10.3)
0080          WRITE(3,209)
0081      209 FORMAT('0',8X,' D(O2+H2O)/DT =')
0082          P=K(10)*K(4)*EXP(24)
0083          WRITE(3,124)P
0084      124 FORMAT(30X,'K(10)(O4+)(H2O)                        =',E10.3)
0085          P=K(22)*K(3)*EXP(24)*EXP(25)
0086          WRITE(3,125)P
0087      125 FORMAT(30X,'K(22)(O2+)(H2O)(M)                     =',E10.3)
0088          P=-(K(11)*K(12)*K(5)*EXP(26)
0089          WRITE(3,126)P
0090      126 FORMAT(30X,'-(K(11)*K(12)(O2+H2O)(H2O)             =',E10.3)
0091          P=-A(5)*K(5)*EXP(20)
0092          WRITE(3,127)P
0093      127 FORMAT(30X,'-A(5)(O2+H2O)(NE)                      =',E10.3)
0094          WRITE(3,206)
0095      206 FORMAT('0',8X,'D(NO+H2O)/DT =')
0096          P=K(5)*K(2)*EXP(26)*EXP(25)
0097          WRITE(3,128)P
0098      128 FORMAT(30X,'K(5)(NO+)(H2O)(M)                      =',E10.3)
0099          P=K(21)*K(19)*EXP(26)
0100          WRITE(3,129)P
0101      129 FORMAT(30X,'K(21)(NO+CO2)(H2O)                     =',E10.3)
0102          P=-K(6)*K(6)*EXP(26)*EXP(25)
0103          WRITE(3,130)P
0104      130 FORMAT(30X,'-K(6)(NO+H2O)(H2O)(M)                  =',E10.3)
0105          P=-A(6)*K(6)*EXP(20)
0106          WRITE(3,131)P
0107      131 FORMAT(30X,'-A(6)(NO+H2O)(NE)                      =',E10.3)
0108          WRITE(3,207)
0109      207 FORMAT('0',8X,'D(NO+(H2O)2)/DT =')
0110          P=K(6)*K(6)*EXP(24)*EXP(25)
0111          WRITE(3,132)P
0112      132 FORMAT(30X,'K(6)(NO+H2O)(H2O)(M)                   =',E10.3)
0113          P=-K(7)*K(7)*EXP(26)*EXP(25)
0114          WRITE(3,133)P
0115      133 FORMAT(30X,'-K(7)(NO+(H2O)2)(H2O)(M)               =',E10.3)
0116          P=-A(7)*K(7)*EXP(20)
0117          WRITE(3,134)P
0118      134 FORMAT(30X,'-A(7)(NO+(H2O)2)(NE)                   =',E10.3)
0119          WRITE(3,208)
```

```
0120      208 FORMAT('0',8X,'D(NO+(H2O))/DT =')
0121          P=K(7)*X(7)*XX(24)*XX(25)
0122          WRITE(3,4941)P
0123      434 FORMAT(30X,'+K(7)(NO+(H2O)2)(H2O)(M)                    =',E10.3)
0124          P=-K(8)*X(8)*XX(24)
0125          WRITE(3,1939)P
0126      135 FORMAT(30X,'-K(8)(NO+(H2O)3)(H2O)                       =',E10.3)
0127          P=-K(8)*X(8)*XX(20)
0128          WRITE(3,1369)P
0129      136 FORMAT(30X,'-K(8)(NO+(H2O)3)(NE)                        =',E10.3)
0130          WRITE(3,209)
0131      209 FORMAT('0',8X,'D(NO+CO2)/DT =')
0132          P=K(20)*X(2)*XX(26)*XX(25)
0133          WRITE(3,1379)P
0134      137 FORMAT(30X,'K(20)(NO+)(CO2)(M)                          =',E10.3)
0135          P=-K(2)*X(9)*XX(24)
0136          WRITE(3,1381)P
0137      138 FORMAT(30X,'-K(21)(NO+CO2)(H2O)                         =',E10.3)
0138          P=-A(9)*X(9)*XX(20)
0139          WRITE(3,1399)P
0140      139 FORMAT(30X,'-A(9)(NO+CO2)(NE)                           =',E10.3)
0141          WRITE(3,210)
0142      210 FORMAT('0',8X,'D(H3O+)/DT =')
0143          P=K(11)*X(9)*XX(24)
0144          WRITE(3,1403)P
0145      140 FORMAT(30X,'K(11)(O2+H2O)(H2O)                          =',E10.3)
0146          P=K(7)*X(10)*XX(24)*XX(25)
0147          WRITE(3,1431)P
0148      141 FORMAT(30X,'-K(17)(H3O+)(H2O)(M)                        =',E10.3)
0149          P=-A(10)*X(10)*XX(20)
0150          WRITE(3,1421)P
0151      142 FORMAT(30X,'-A(10)(H3O+)(NE)                            =',E10.3)
0152          WRITE(3,211)
0153      211 FORMAT('0',8X,'D(H3O+H2O)/DT =')
0154          P=K(13)*X(14)*XX(24)
0155          WRITE(3,1433)P
0156      143 FORMAT(30X,'K(13)(H3O+OH)(H2O)                          =',E10.3)
0157          P=K(17)*X(10)*XX(24)*XX(25)
0158          WRITE(3,1441)P
0159      144 FORMAT(30X,'K(17)(H3O+)(H2O)(M)                         =',E10.3)
0160          P=-K(18)*X(11)*XX(24)*XX(25)
0161          WRITE(3,1493)P
0162      145 FORMAT(30X,'-K(18)(H3O+H2O)(H2O)(M)                     =',E10.3)
0163          P=-A(11)*X(11)*XX(20)
0164          WRITE(3,1441)P
0165      146 FORMAT(30X,'-A(11)(H3O+)(NE)                            =',E10.3)
0166          WRITE(3,212)
0167      212 FORMAT('0',8X,'D(H3O+(H2O)2)/DT =')
0168          P=K(18)*X(11)*XX(24)
0169          WRITE(3,1493)P
0170      147 FORMAT(30X,'K(18)(NO+(H2O)3)(H2O)                       =',E10.3)
0171          P=K(16)*X(15)*XX(24)
0172          WRITE(3,1483)P
0173      148 FORMAT(30X,'K(16)(H3O+OH H2O)(H2O)                      =',E10.3)
0174          P=K(18)*X(11)*XX(24)*XX(25)
0175          WRITE(3,1491)P
0176      149 FORMAT(30X,'K(18)(H3O+H2O)(H2O)(M)                      =',E10.3)
0177          P=-K(19)*X(12)*XX(24)*XX(25)
0178          WRITE(3,1503)P
0179      150 FORMAT(30X,'-K(19)(H3O+(H2O)2)(H2O)(M)                  =',E10.3)
```

```
305 FORTRAN IV 360M-PO-479 3-5        PLOPOS          DATE   01/02/75      TIME     18.28.43      PAGE 0004

0180            P=-A(12)*K(12)*XX(20)
0181            WRITE(3,151)P
0182        151 FORMAT(30X,'-A(12)(H3O+(H2O)2(NE)                    =',E10.3)
0183            WRITE(3,215)
0184        213 FORMAT('O',8X,'D(H3O+(H2O)3)/DT =')
0185            P=K(19)*K(21)*XX(24)*XX(25)
0186            WRITE(3,152)P
0187        152 FORMAT(30X,'K(19)(H3O+(H2O)2(H2O)(M)                 =',E10.3)
0188            P=-A(13)*K(13)*XX(20)
0189            WRITE(3,153)P
0190        153 FORMAT(30X,'-A(13)(H3O+(H2O)3(NE)                    =',E10.3)
0191            WRITE(3,214)
0192        214 FORMAT('O',8X,'D(H3O+OH)/DT =')
0193            P=K(12)*K(5)*XX(24)
0194            WRITE(3,154)P
0195        154 FORMAT(30X,'K(12)(O2+H2O)(H2O)                       =',E10.3)
0196            P=-K(13)*K(16)*XX(24)
0197            WRITE(3,155)P
0198        155 FORMAT(30X,'-K(13)(H3O+OH)(H2O)                      =',E10.3)
0199            P=-K(16)*K(16)*K(3)*XX(25)
0200            WRITE(3,156)P
0201        156 FORMAT(30X,'-K(16)(H3O+OH)(O2)(M)                    =',E10.3)
0202            P=-A(14)*K(16)*XX(22)
0203            WRITE(3,157)P
0204        157 FORMAT(30X,'-A(14)(H3O+OH)(NE)                       =',E10.3)
0205            WRITE(3,215)
0206        215 FORMAT('O',8X,'D(H3O+OH,H2O)/DT =')
0207            P=K(15)*K(16)*XX(24)
0208            WRITE(3,158)P
0209        158 FORMAT(30X,'K(15)(H3O+OH O2)(H2O)                    =',E10.3)
0210            P=-K(16)*K(15)*XX(24)
0211            WRITE(3,159)P
0212        159 FORMAT(30X,'-K(16)(H3O+OH H2O)(H2O)                  =',E10.3)
0213            P=-A(15)*K(15)*XX(20)
0214            WRITE(3,160)P
0215        160 FORMAT(30X,'-A(15)(H3O+OH H2O)(NE)                   =',E10.3)
0216            WRITE(3,216)
0217        216 FORMAT('O',8X,'D(H3O+OH,O2)/DT =')
0218            P=K(14)*K(16)*XX(22)*XX(25)
0219            WRITE(3,161)P
0220        161 FORMAT(30X,'K(14)(H3O+OH)(O2)(M)                     =',E10.3)
0221            P=-K(15)*K(16)*XX(24)
0222            WRITE(3,162)P
0223        162 FORMAT(30X,'-K(15)(H3O+OH O2)(H2O)                   =',E10.3)
0224            P=-A(16)*K(16)*XX(20)
0225            WRITE(3,163)P
0226        163 FORMAT(30X,'-A(16)(H3O+OH O2(NE)                     =',E10.3)
0227            RETURN
0228            END
```

FLONEG FOR HCO29

```
005 FORTRAN IV 360H-FO-479 3-S        FLOWCG          DATE  01/02/75      TIME    16.29.59      PAGE 0001

0001            SUBROUTINE FLOWCG
0002            DIMENSION RN(15)
0003            COMMON RR(33),AI(6),RX(33),RB(40),RI(31),RN(75),SUMP,ALT
0004            EQUIVALENCE(RI(17),RN(1))
0005            REAL K,KB,KR
0006            WRITE (3,1000)ALT
0007         1000 FORMAT('1',45X,'FLOW RATES OF NEGATIVE ION REACTIONS'//55X,
               1'ALTITUDE=',F9.1,' KILOMETERS')
0008            WRITE(3,300)
0009          300 FORMAT('0',8X, 'D(O-)/DT =')
0010            P=RN(1)*RR(20)*RX(21)
0011            WRITE(3,110)P
0012          110 FORMAT(30X, '+RN(1)*RE(10-)                              =',E10.3)
0013            P=RN(2)*RR(21)*RI(10)
0014            WRITE(3,3010)P
0015         3010 FORMAT(30X,'RN(2)*RI(O2-1(O)                             =',E10.3)
0016            P = RN(3)*RI(29)*RN(20)
0017            WRITE(3,113)P
0018          113 FORMAT(30X, '+RN(3)*RI(O2)*(NE)                          =',E10.3)
0019            P=RN(3)*RR(20)*RX(22)
0020            WRITE(3,3011)P
0021         3011 FORMAT(30X,'+RN(3)*(NE)*(O2)                             =',E10.3)
0022            P=RN(8)*RI(20)*RX(21)*RX(25)
0023            WRITE(3,54321)P
0024         54321 FORMAT(30X,'+RN(8)*(NE)*(O)*(M)                         =',E10.3)
0025            P=RN(4)*RI(1)
0026            WRITE(3,100)P
0027          100 FORMAT(30X, '+RN(4)*(O-)                                 =',E10.3)
0028            P=RN(5)*RR(1)*RX(19)
0029            WRITE(3,101)P
0030          101 FORMAT(30X, '+RN(5)*(O-)*(CO)                            =',E10.3)
0031            P=RN(6)*RR(1)*RX(31)
0032            WRITE(3,102)P
0033          102 FORMAT(30X, '+RN(6)*(O-)*(N2)                            =',E10.3)
0034            P=RN(7)*RR(1)*RX(21)
0035            WRITE(3,103)P
0036          103 FORMAT(30X, '+RN(7)*(O-)*(O)                             =',E10.3)
0037            P=RN(8)*RR(1)*RX(26)
0038            WRITE(3,104)P
0039          104 FORMAT(30X, '+RN(8)*(O-)*(H2)                            =',E10.3)
0040            P=RN(9)*RR(1)*RX(29)
0041            WRITE(3,1099)P
0042          105 FORMAT(30X, '+RN(9)*(O-)*(O3)                            =',E10.3)
0043            P=RN(10)*RN(1)*RX(23)
0044            WRITE(3,1049)P
0045          106 FORMAT(30X, '+RN(10)*(O-)*(NO)                           =',E10.3)
0046            P=RN(11)*RN(1)*RX(22)*RX(22)
0047            WRITE(3,107)P
0048          107 FORMAT(30X, '+RN(11)*(O-)*(O2)*(O2)                      =',E10.3)
0049            P=RN(12)*RN(1)*RX(26)*RX(29)
0050            WRITE(3,1089)P
0051          108 FORMAT(30X, '+RN(12)*(O-)*(O2)*(M)                       =',E10.3)
0052            P=RN(13)*RN(1)*RX(29)*RX(29)
0053            WRITE(3,1099)P
0054          109 FORMAT(30X, '+RN(13)*(O-)*(NO)*(M)                       =',E10.3)
0055            P=RN(35)*RI(1)*RX(22)
0056            WRITE(3,3012)P
0057         3012 FORMAT(30X,'+RN(35)*(O-)*(O2)                            =',E10.3)
0058            P=RN(37)*RI(1)*RX(26)
0059            WRITE(3,3013)P
```

```
905 FORTRAN IV 360N-FO-479 3-5        FLONEG          DATE  01/02/75      TIME    18.29.59      PAGE 0002

0060          3013 FORMAT(30X,'-KN(37)(O-3(O2(10G))                    ',E10.3)
0061               P=-KN(42)*X(17)*XX(27)
0062               WRITE(3,3014)P
0063          3014 FORMAT(30X,'-KN(42)(O-3(N)                          ',E10.3)
0064               P=-KN(50)*XN(13)*XX(36)
0065               WRITE(3,111)P
0066           111 FORMAT(30X, '-KN(50)(O-3(N2O)                       ',E10.3)
0067               P=-KN(55)*XN(1)*XX(30)
0068               WRITE(3,112)P
0069           112 FORMAT(30X, '-KN(55)(O-3(NO2)                       ',E10.3)
0070               P=-11.0 E-7*XN(1)*SUMP
0071               WRITE(3,114)P
0072           114 FORMAT(30X, '-1.(-7)(O-1(SUMP)                      ',E10.3)
0073               WRITE(5,301)
0074           301 FORMAT('0',88, '0(O2-3/DT ='
0075               P=KN(16)*XX(22)*XX(22)*XX(20)
0076               WRITE(3,1181)P
0077           118 FORMAT(30X,'KN(16)(O2)(O2)(NE)                      ',E10.3)
0078               P=KN(17)*XN(22)*XX(20)*XX(31)
0079               WRITE(5,1191)P
0080           119 FORMAT(30X,'KN(17)(O2)(N2)(NE)                      ',E10.3)
0081               P=KN(18)*XN(4)*XX(22)
0082               WRITE(3,120)P
0083           120 FORMAT(30X,'KN(18)(O-3(O2)                          ',E10.3)
0084               P=KN(19)*XN(3)*XX(21)
0085               WRITE(3,121)P
0086           121 FORMAT(30X,'KN(19)(O3-3(O)                          ',E10.3)
0087               P=KN(20)*XN(5)*XX(22)
0088               WRITE(3,122)P
0089           122 FORMAT(30X,'KN(20)(NO-3(O2)                         ',E10.3)
0090               P=KN(21)*XN(3)*XX(21)
0091               WRITE(3,123)P
0092           123 FORMAT(30X,'KN(21)(O3-3(O)                          ',E10.3)
0093               P=KN(32)*X(20)*XX(22)*XX(24)
0094               WRITE(3,54322)P
0095         54322 FORMAT(30X,'KN(32)(NE)(O2)(N2O)                     ',E10.3)
0096               P=KN(45)*XX(22)*XX(20)
0097               WRITE(3,3015)P
0098          3015 FORMAT(30X,'KN(45)(NE)(O2)                          ',E10.3)
0099               P=-KN(2)*XN(2)*XX(21)
0100               WRITE(3,1183)P
0101           119 FORMAT(30X,'-KN(2)(O2-3(O)                          ',E10.3)
0102               P=-KN(14)*XN(2)*XX(24)*XX(25)
0103               WRITE(3,1161)P
0104           116 FORMAT(30X,'-KN(14)(O2-3(H2O)(M)                    ',E10.3)
0105               P=-KN(15)*XN(2)*XX(30)
0106               WRITE(5,1171)P
0107           117 FORMAT(30X,'-KN(15)(O2-3(NO2)                       ',E10.3)
0108               P=-KN(22)*XN(2)
0109               WRITE(3,1241)P
0110           124 FORMAT(30X,'-KN(22)(O2-1                            ',E10.3)
0111               P=-(KN(23)*XN(24))*XN(2)*XX(21)
0112               WRITE(3,1231)P
0113           125 FORMAT(30X,'-(KN(23)*KN(24))(O2-1(O                 ',E10.3)
0114               P=-KN(25)*XN(2)*XX(22)*XX(29)
0115               WRITE(5,1261)P
0116           126 FORMAT(30X,'-KN(25)(O2-1(O2)(M)                     ',E10.3)
0117               P=-KN(26)*XN(2)*XX(29)
0118               WRITE(5,1271)P
0119           127 FORMAT(30X,'-KN(26)(O2-3(O3)                        ',E10.3)
```

```
OS/3 FORTRAN IV 360N-FO-479 3.5          FLONEG                    DATE  01/02/75      TIME     18.29.59      PAGE 0003

0120                P=-RN(27)*RN(2)*RX(26)*RX(22)
0121                WRITE(3,1299)P
0122           129  FORMAT(30X,'-RN(27)(02-1(C02)(02)                    =',E10.3)
0123                P=-RN(28)*RN(2)*RX(26)*RX(26)
0124                WRITE(3,1288)P
0125           128  FORMAT(30X,'-RN(28)(02-1(C02)(C02)                   =',E10.3)
0126                P=-RN(9)*RE(8)*RX(22)
0127                WRITE(3,3017)P
0128          3017  FORMAT(30X,'-RN(92)(02-1(02)                         =',E10.3)
0129                P=-RN(54)*RE(8)*RX(27)
0130                WRITE(3,3018)P
0131          3018  FORMAT(30X,'-RN(54)(02-1(N)                          =',E10.3)
0132                P=-RN(72)*RE(8)*RX(28)
0133                WRITE(3,3016)P
0134          3016  FORMAT(30X,'-RN(72)(02-1(02)(LOG)                    =',E10.3)
0135                P=-(1.0 E-7)*RN(2)*SUMP
0136                WRITE(3,2600)P
0137          2600  FORMAT(30X,'-1.0(-7)(02-1(SUMP)                      =',E10.3)
0138                WRITE(3,902)
0139           302  FORMAT('0',8X,'0(03-1/DT =')
0140                P=RN(9)*RN(1)*RX(29)
0141                WRITE(3,1301)P
0142           130  FORMAT(30X,'RN(9)(0-1(03)                            =',E10.3)
0143                P=RN(1)*RN(1)*RX(22)*RX(22)
0144                WRITE(3,1313)P
0145           131  FORMAT(30X,'RN(1)(0-1(02)(02)                        =',E10.3)
0146                P=RN(26)*RN(2)*RX(29)
0147                WRITE(3,1331)P
0148           193  FORMAT(30X,'RN(26)(02-1(03)                          =',E10.3)
0149                P=RN(29)*RN(4)*RX(21)
0150                WRITE(3,1341)P
0151           134  FORMAT(30X,'RN(29)(04-1(0)                           =',E10.3)
0152                P=RN(62)*RX(25)*RX(29)
0153                WRITE(3,330181)P
0154         33018  FORMAT(30X,'RN(62)(C04-1(03)                         =',E10.3)
0155                P=-RN(93)*RN(3)*RX(23)
0156                WRITE(3,1321)P
0157           137  FORMAT(30X,'-RN(1)(03-1(0)                           =',E10.3)
0158                P=-RN(30)*RN(3)
0159                WRITE(3,1351)P
0160           135  FORMAT(30X,'-RN(30)(03-1                             =',E10.3)
0161                P=-RN(31)*RN(3)*RX(26)
0162                WRITE(3,1361)P
0163           136  FORMAT(30X,'-RN(31)(03-1(C02)                        =',E10.3)
0164                P=-(RN(36)+RN(37))*RN(3)*RX(23)
0165                WRITE(3,1411)P
0166           141  FORMAT(30X,'-(RN(36)+RN(37))(03-1(NO)                =',E10.3)
0167                P=-(RN(90)+RN(40))*RN(3)*RX(30)
0168                WRITE(3,1493)P
0169           143  FORMAT(30X,'-(RN(90)+RN(40))(03-1(NO2)               =',E10.3)
0170                P=-(1.0 E-7)*RN(3)*SUMP
0171                WRITE(3,1571)P
0172           157  FORMAT(30X,'-1.0(-7)(03-1(SUMP)                      =',E10.3)
0173                WRITE(3,903)
0174           303  FORMAT('0',8X,'0(04-1/DT =')
0175                P=RN(29)*RN(2)*RX(22)*RX(25)
0176                WRITE(3,1513)P
0177           151  FORMAT(30X,'RN(29)(02-1(02)(N)                       =',E10.3)
0178                P=RN(41)*RN(9)*RX(22)
0179                WRITE(3,1621)P
```

```
0180      152 FORMAT(30X,*RN(4)*(CO4-)(NO)
0181          P=-RN(29)*RN(20)*RX(21)
0182          WRITE(3,1493)P
0183      144 FORMAT(30X,* -RN(29)*(O4-)(NO)
0184          P=-RN(43)*RN(44)*RX(26)
0185          WRITE(3,1492)P
0186      147 FORMAT(30X,*-RN(43)*(CO2)
0187          P=-RN(44)*RN(4)*RX(23)
0188          WRITE(3,1493)P
0189      148 FORMAT(33X,*-RN(44)*(O4-)(NO)
0190          P=-RN(48)*RN(4)*RX(26)
0191          WRITE(3,1493)P
0192      149 FORMAT(30X,*-RN(48)*(O4-)(HZO)
0193          P=-RN(18)*RN(4)*RX(22)
0194          WRITE(3,1501)P
0195      150 FORMAT(30X,*-RN(18)*(O4-)(O2)
0196          P=-(1.0 0-7)*RN(4)*SUMP
0197          WRITE(3,2700)P
0198     2700 FORMAT(30X,*-1.0(-7)*(O4-)(SUMP)
0199          WRITE(3,304)
0200      304 FORMAT('0',8X,'D(NO-)/DT =')
0201          P=RN(50)*RN(1)*RX(34)
0202          WRITE(3,154)P
0203      154 FORMAT(30X,*RN(30)*(O-)(NZO)
0204          P=RN(33)*RX(20)*RX(23)*RX(23)
0205          WRITE(3,3030)P
0206     3030 FORMAT(30X,*RN(7))*(AE)*(NO)(NO)
0207          P=-RN(20)*RN(5)*RX(22)
0208          WRITE(3,1493)P
0209      153 FORMAT(30X,*-RN(20)*(NO-)(O2)
0210          P=-(1.0E-7)*RN(5)*SUMP
0211          WRITE(3,1591)P
0212      155 FORMAT(30X,*-1.0(-7)*(NO-)(SUMP)
0213          WRITE(3,305)
0214      305 FORMAT('0',8X,'D(NO2-)/DT =')
0215          P=RN(3)*RN(1)*RX(25)*RX(25)
0216          WRITE(3,1613)P
0217      161 FORMAT(30X,*RN(1))*(NO)(NO)
0218          P=RN(15)*RN(2)*RX(30)
0219          WRITE(3,1693)P
0220      165 FORMAT(30X,*RN(15)*(O2-)(NO2)
0221          P=RN(36)*RN(3)*RX(23)
0222          WRITE(3,1901)P
0223      158 FORMAT(30X,*RN(36)*(O3-)(NO)
0224          P=RN(39)*RX(19)*RX(30)
0225          WRITE(3,3019)P
0226     3019 FORMAT(30X,*RN(39)*(O3-)(NO2)
0227          P=RN(47)*RN(8)*RX(23)
0228          WRITE(3,1593)P
0229      159 FORMAT(30X,*RN(47)*(O3-)(NO)
0230          P=RN(51)*RX(30)*RX(20)*RX(25)
0231          WRITE(3,1601)P
0232      160 FORMAT(30X,*RN(51)*(NO2)(N)(NE)
0233          P=RN(55)*RN(1)*RX(30)
0234          WRITE(3,1661)P
0235      166 FORMAT(30X,*RN(55)*(N-)(NO2)
0236          P=-RN(56)*RN(6)
0237          WRITE(3,1673)P
0238      167 FORMAT(33X,*-RN(56)*(NO2-)
0239          P=-RN(57)*RN(6)*RX(24)*RX(25)
```

```
FORTRAN IV 360M-PO-479 3-5        FLOWEG                DATE  01/02/75      TIME    18.29.59      PAGE 0009

      WRITE(3,1688)P
  168 FORMAT(30X,'-KN(9)(NO2-)(H2O)(M)                          =',E10.3)
      P=-RN(9)*RE(22)*RE(29)
      WRITE(3,3021)P
 3021 FORMAT(30X,'-KN(59)(NO2-)(O3)                             =',E10.3)
      P=-RN(63)*RE(22)*RE(30)
      WRITE(3,3020)P
 3020 FORMAT(30X,'-KN(63)(NO2-)(NO2)                            =',E10.3)
      P=-1.0 P-T3*RN(6)*SUMP
      WRITE(3,1713)P
  171 FORMAT(30X,'-1.0(-T3(NO2-)(SUMP)                          =',E10.3)
      WRITE(3,3063)
  306 FORMAT('0',,8X,'DI(NO3-)/DT =')
      P=RN(40)*RN(5)*RE(30)
      WRITE(3,1719)P
  173 FORMAT(30X,'RN(40)(O3-)(NO2)                              =',E10.3)
      P=RN(44)*RE(6)*RE(25)
      WRITE(3,1741)P
  174 FORMAT(30X,'RN(44)(OH-)(NO)                               =',E10.3)
      P=RN(68)*RN(8)*RE(30)
      WRITE(3,1761)P
  176 FORMAT(30X,'RN(68)(CO3-)(NO2)                             =',E10.3)
      P=RN(59)*RN(6)*RE(29)
      WRITE(3,1781)P
  178 FORMAT(30X,'RN(59)(NO2-)(O3)                              =',E10.3)
      P=RN(60)*RN(9)*RE(28)
      WRITE(3,1791)P
  179 FORMAT(30X,'RN(60)(CO4-)(NO)                              =',E10.3)
      P=RN(63)*RE(22)*RE(30)
      WRITE(3,3021)P
 3021 FORMAT(30X,'RN(63)(NO2-)(NO2)                             =',E10.3)
      P=-RN(61)*RN(7)
      WRITE(3,1809)P
  180 FORMAT(30X,'-RN(61)(NO3-)                                  =',E10.3)
      P=-RN(70)*RN(7)*RE(26)*RE(25)
      WRITE(3,1813)P
  181 FORMAT(30X,'-RN(70)(NO3-)(H2O)(M)                          =',E10.3)
      P=-1.0 P-T3*RN(7)*SUMP
      WRITE(3,1871)P
  182 FORMAT(30X,'-1.0(-T3(NO3-)(SUMP)                          =',E10.3)
      WRITE(3,3072
  307 FORMAT('0',,8X,'DI(CO3-)/DT =')
      P=RN(12)*RN(1)*RE(26)*RE(25)
      WRITE(3,1831)P
  183 FORMAT(30X,'RN(12)(O-)(CO2)(M)                            =',E10.3)
      P=RN(31)*RN(5)*RE(26)
      WRITE(3,1853)P
  184 FORMAT(30X,'RN(31)(O3-)(CO2)                              =',E10.3)
      P=RN(69)*RN(9)*RE(28)
      WRITE(3,1869)P
  186 FORMAT(30X,'RN(69)(CO4-)(O)                               =',E10.3)
      P=-RN(21)*RN(10)*RE(21)
      WRITE(3,1843)P
  184 FORMAT(30X,'-RN(21)(CO3-)(O)                              =',E10.3)
      P=-RN(69)*RN(8)
      WRITE(3,1879)
  187 FORMAT(30X,'-RN(46)(CO3-)                                  =',E10.3)
      P=-RN(47)*RN(8)*RE(23)
      WRITE(3,1889)P
  188 FORMAT(30X,'-RN(47)(CO3-)(NO)                              =',E10.3)
```

```
0300          P=-RN(48)*RN(8)*RX(30)
0301          WRITE(3,189)P
0302      189 FORMAT(30X,'-RN(48)(CO3-)(NO2)                    **,E10.3)
0303          P=-(1.0 E-7)*RN(8)*SUMP
0304          WRITE(3,191)P
0305      191 FORMAT(30X,'-1.0(-7)(CO3-)(SUMP)                  **,E10.3)
0306          WRITE(3,308)
0307      308 FORMAT('0',8X,'D(CO4-)/DT =')
0308          P=RN(27)*RN(2)*RX(26)*RX(22)
0309          WRITE(3,192)P
0310      192 FORMAT(30X,'RN(27)(O2-)(CO2)(O2)                  **,E10.3)
0311          P=RN(28)*RN(2)*RX(26)*RX(26)
0312          WRITE(3,193)P
0313      193 FORMAT(30X,'RN(28)(O2-)(CO2)(CO2)                 **,E10.3)
0314          P=RN(4)*RN(4)*RX(26)
0315          WRITE(3,195)P
0316      195 FORMAT(30X,'RN(4)(O4-)(CO2)                       **,E10.3)
0317          P=RN(49)*RN(10)*RX(26)
0318          WRITE(3,197)P
0319      197 FORMAT(30X,'RN(49)(O2-H2O)(CO2)                   **,E10.3)
0320          P=-RN(41)*RN(9)*RX(22)
0321          WRITE(3,194)P
0322      194 FORMAT(30X,'-RN(41)(CO4-)(O2)                     **,E10.3)
0323          P=-RN(45)*RN(9)*RX(21)
0324          WRITE(3,196)P
0325      196 FORMAT(30X,'-RN(65)(CO4-)(O)                      **,E10.3)
0326          P=-RN(60)*RN(9)*RX(23)
0327          WRITE(3,198)P
0328      198 FORMAT(30X,'-RN(60)(CO4-)(NO)                     **,E10.3)
0329          P=-RN(62)*RX(25)*RX(29)
0330          WRITE(3,3022)P
0331     3022 FORMAT(30X,'-RN(62)(CO4-)(O3)                     **,E10.3)
0332          P=-(1.0 E-7)*RN(9)*SUMP
0333          WRITE(3,200)P
0334      200 FORMAT(30X,'-(1.0(-7)(CO4-)(SUMP)                 **,E10.3)
0335          WRITE(3,309)
0336      309 FORMAT('0',8X,'D(O2-H2O)/DT =')
0337          P=RN(49)*RN(2)*RX(26)*RX(22)
0338          WRITE(3,210)P
0339      210 FORMAT(30X,'RN(49)(O2-)(H2O)(O2)                  **,E10.3)
0340          P=RN(68)*RN(4)*RX(26)
0341          WRITE(3,211)P
0342      211 FORMAT(30X,'RN(68)(O4-)(H2O)                      **,E10.3)
0343          P=-RN(49)*RN(10)*RX(26)
0344          WRITE(3,213)P
0345      213 FORMAT(30X,'-RN(49)(O2-H2O)(O2)                   **,E10.3)
0346          P=-RN(69)*RN(10)*RX(24)*RX(22)
0347          WRITE(3,212)P
0348      212 FORMAT(30X,'-RN(69)(O2-H2O)(H2O)(O2)              **,E10.3)
0349          P=-(1.0 E-7)*RN(10)*SUMP
0350          WRITE(3,215)P
0351      215 FORMAT(30X,'-1.0(-7)(O2-H2O)(SUMP)                **,E10.3)
0352          WRITE(3,310)
0353      310 FORMAT('0',8X,'D(O2-(H2O)2)/DT =')
0354          P=RN(69)*RN(10)*RX(24)*RX(22)
0355          WRITE(3,216)P
0356      216 FORMAT(30X,'RN(69)(O2-H2O)(H2O)(O2)               **,E10.3)
0357          P=-(1.0 E-7)*RN(11)*SUMP
0358          WRITE(3,217)P
0359      217 FORMAT(30X,'-1.0(-7)(O2-(H2O)2)(SUMP)             **,E10.3)
```

```
305 FORTRAN IV 360N-FO-479 3-5          FLOWFG                  DATE  01/02/75      TIME    18.29.59      PAGE 0007

0360            WRITE(3,311)
0361        311 FORMAT('0',8X,'D(NO2-H2O)/DT =')
0362            P=KN(57)*KN(6)*XX(26)*XX(23)
0363            WRITE(3,2181)P
0364        218 FORMAT(30X,'KN(57)(NO2-)(H2O)(N3)                    =',E10.3)
0365            P=-KN(64)*X(29)*XX(26)*XX(22)
0366            WRITE(3,330221)P
0367     330221 FORMAT(30X,'-KN(64)(NO2-,H2O)(H2O)(O2)                =',E10.3)
0368            P=-(1.0 E-7)*XN(13)*SUMP
0369            WRITE(3,2191)P
0370        219 FORMAT(30X,'-1.0(-7)(NO2-H2O)(SUMP)                  =',E10.3)
0371            WRITE(3,3312)
0372       3312 FORMAT('0',8X,'D(NO2-(H2O)2)/DT =')
0373            P=KN(64)*X(29)*XX(26)*XX(22)
0374            WRITE(3,3023)P
0375       3023 FORMAT(30X,'KN(64)(NO2-,H2O)(H2O)(O2)                =',E10.3)
0376            P=-(1.0 E-7)*X(29)*SUMP
0377            WRITE(3,302519
0378       3025 FORMAT(30X,'-1.0(-7)(NO2-,(H2O)2)(SUMP)              =',E10.3)
0379            WRITE(3,312)
0380        312 FORMAT('0',8X,'D(NO3-H2O)/DT =')
0381            P=KN(70)*XN(7)*XX(26)*XX(25)
0382            WRITE(3,2201)P
0383        220 FORMAT(30X,'KN(70)(NO3-)(H2O)(M)                     =',E10.3)
0384            P=-KN(71)*XN(12)*XX(26)*XX(25)
0385            WRITE(3,2211)P
0386        221 FORMAT(30X,'-KN(71)(NO3-H2O)(H2O)(M)                 =',E10.3)
0387            P=-(1.0 E-7)*XN(12)*SUMP
0388            WRITE(3,2221)P
0389        222 FORMAT(30X,'-1.0(-7)(NO3-H2O)(SUMP)                  =',E10.3)
0390            WRITE(3,313)
0391        313 FORMAT('0',8X,'D(NO3-(H2O)2)/DT =')
0392            P=KN(71)*XN(12)*XX(26)*XX(25)
0393            WRITE(3,2231)P
0394        223 FORMAT(30X,'KN(71)(NO3-H2O)(H2O)(M)                  =',E10.3)
0395            P=-(1.0 E-7)*XN(14)*SUMP
0396            WRITE(3,2241)P
0397        224 FORMAT(30X,'-1.0(-7)(NO3-(H2O)2)(SUMP)               =',E10.3)
0398            RETURN
0399            END
```

REFERENCES

Ackerman, M., Ultraviolet Solar Radiation Related to Mesospheric Processes, in Mesospheric Models and Related Experiments, D. Reidel Publ. Co., Dordrecht, Holland, 1971.

Anderson, J. G., Rocket-Bourne Ultraviolet Spectrometer Measurement of OH Resonance Fluorescence with a Diffusive Transport Model for Mesospheric Photochemistry, J. Geophys. Res., 76, 4634, 1971.

Appleton, E. V., R. Naismith and G. Builder, Ionospheric Investigations in High Latitudes, Nature, 132, 340, 1933.

Arnold, F., J. Kissel, D. Krankowsky, H. Wieder, J. Zahringer, Negative Ions in the Lower Ionosphere: A Mass-spectrometric Measurement, J Atmos. Terr. Phys., 33, 1169, 1971.

Baker, K., T. Tsang, R. Olsen and J. Randhawa, Measurement of Nitric Oxide in the Midlatitude Mesosphere, Paper at Fall Annual Meeting AGU, San Francisco, December 11, 1975.

Banks, Peter M. and G. Kockarts, Aeronomy, Part A and Part B. Academic Press, New York and London, 1973.

Barth, C. A., Nitrogen and Oxygen Atomic Reactions in the Chemosphere, in Chemical Reactions in the Lower and Upper Atmosphere, J. Wiley, and Sons, New York, 1961.

Barth, C. A., Rocket Measurement of the Nitric Oxide Dayglow, J. Geophys. Res., 69, 3301, 1964.

Bauer, S. J., L. J. Blumle, J. L. Donley, R. J. Fitzeureiter and J. E. Jackson, Simultaneous Rocket and Satellite Measurements of the Topside Ionosphere, J. Geophys. Res., 69, 186, 1964.

Biondi, M. A., Atomic Collisions and Plasma Physics, Reaction Rate Data; DASIAC-DNA Supplement No. 44, January 1974a.

Biondi, M. A., Electron-Ion Recombination Rates at Elevated Temperatures and Studies of Cluster Ions, in DASIAC-Reaction Rate Data No. 44, January 1974, Supp. Resume of FY 74 DNA Sponsored Programs, 1976b.

Bourdeau, R. E., A. C. Aiken and J. L. Donley, Lower Ionosphere at Solar Minimum, J. Geophys. Res., 71, 727, 1966.

Bowling, T. S., K. Norman and A. P. Willmore, D-Region Measurements during a Solar Eclipse, Planet. Space Sci., 15, 1035, 1967.

Bowman, M. R., L. Thomas and J. E. Geisler, The Effect of Diffusion Processes on the Hydrogen and Oxygen Constituents in the Mesophere and Lower Thermosphere, J. Atmos. Terr. Phys., 32, 1661, 1970.

Branscomb, L. M., A Review of Photodetachment and Related Negative Ion Processes Relevant to Aeronomy, Ann. Geophysik, 20, 88, 1964.

Brown, K. M., Algorithm 316, Solution of Simultaneous Non-Linear Equations in Collected Algorithms of the Communications of the ACM, 10, 728,1967.

Brown, R. P., On the Influence of Energetic Electron Precipitation on the Water Cluster Ion Population in the Upper D-Region, J. Atmos. Terr. Phys., 32, 1747, 1970.

Burke, Rudolf R., Hydrogen Atom Participation in D-Region Ion Chemistry, J. Geophys. Res., 75(7), 1345, 1970.

Burke, Rudolf R., Private Communication, AeroChem Res. Lab, Inc., Princeton, New Jersey, 1970.

Burke, Rudolf R., Comments on a Letter by W. Swider, "Sources for $H^+(H_2O)_n$ in Ions in the D-Region, J. Geophys. Res., 77(10), 1998, 1972.

Byuro, E. D. and G. M. Martynkevich, Relative Concentrations of Water Vapor in the Mesosphere and Lower Thermosphere of Arctic and Temperate Latitudes of the USSR Measured by Radio-Frequency Mass Spectrometers, in Physics of Noctilucent Clouds, J. Ikaunieks, ed., from Proceedings of the Conference on Mesospheric Clouds, Riga, 20-23, November 1968, Isreal Program for Scientific Translation, Jerusalem, Keter Press, 1973.

Chanin, L. M., and M. A. Biondi, Mobilities of Mercury Ions in Helium, Neon and Argon, Phys. Rev. 107, 1219, 1957.

Chanin, L. M., A. V. Phelps and M. A. Biondi, Measurements of the Attachment of Low Energy Electrons to Oxygen Molecules, Phys. Rev., 128, 219, 1962.

Chapman, S. and T. G. Cowling, The Mathematical Theory of Non-Uniform Gases, Cambridge University Press, Cambridge, England, 1970.

Chapman, S. and P. C. Kendall, Noctilucent Clouds and Thermospheric Dust: Their Diffusion and Height Distribution, Quart. J. Royal Met. Soc., 91, 115, 1965.

Charlson, R. J., Noctilucent Clouds: A Steady State Model, Quart. J. Royal Met. Soc., 91, 517, 1965.

Chesworth, E. T. and L. C. Hale, Ice Particulates in the Mesosphere, Geophys. Res. Lett., 1, 347, 1974.

Clyne, M. A. A. and B. A. Thrush, Kinetics of the Reactions of Active Nitrogen with Oxygen and Nitric Oxide, Proc. R. Soc., A261, 159, 1961.

Colegrove, F. D., W. B. Hanson and F. S. Johnson, Eddy Diffusion and Oxygen Transport in the Lower Thermosphere, J. Geophys. Res., 70, 4931, 1965.

Colegrove, F. D., F. S. Johnson and W. B. Hanson, Atmospheric Composition in the Lower Thermosphere, J. Geophys. Res., 71, 2227, 1966.

COSPAR International Reference Atmosphere (CIRA), North-Holland Publ. Co., Amsterdam, 1965.

Crutzen, Paul J., Energy Conversions and Mean Vertical Motions in the High Latitude Summer Mesosphere and Lower Thermosphere, in Mesospheric Models and Related Experiments, G. Fiocco, ed., D. Reidel Publ. Co., Holland, 1971.

Dachs, J., On Nightglow Intensity Variations Connected with Vertical Movements in the Upper Atmosphere, in Atmospheric Emissions, B. M. McCormac and A. Omholt (eds.), Van Nostrand-Reinhold Co., New York, 1969.

Davies, Kenneth, Ionospheric Radio Waves, Blaisdell Publ. Co., Waltham, Mass., 1969.

Defense Nuclear Agency, Reaction Rate Handbook, Second Edition, Published by DASIAC, DOD Nuclear Information and Analysis Center, General Electric, TEMPO, Santa Barbara, Calif., 1972.

Dellinger, J. H., Sudden Ionospheric Disturbances, Terr. Mag. Atmos. Elect., 42, 49, 1937.

Divari, N. B., The Dust Concentration in the Upper Layers of the Earth's Atmosphere, Geomag. and Aeron., 4, 688, 1964.

Donahue, T. M., B. Guenther and J. E. Blamont, Noctilucent Clouds in the Daytime: Circumpolar Particulate Layers Near the Summer Mesopause, J. Atmos. Sci., 29, 1205, 1972.

Dunkin, D. B., F. C. Fehsenfeld, A. L. Schmeltekopf, and E. E. Ferguson, Three Body Association Reactions of NO+ with O_2, N_2 and CO_2, J. Chem. Phys. 54, 3817, 1971.

Evans, W. F. J. and E. J. Llewellyn, Measurements of Mesospheric Ozone from Observations of the 1.27μ Band, Radio Science, 7, 45, 1972.

Fedynsky, A. V., Measurement of Water Vapor Concentration at 71-87 km Heights, International Symposium on Noctilucent Clouds, Tallinn, 1966.

Fehsenfeld, F. C. and E. E. Ferguson, Origin of Water Cluster Ions in the D-Region, J. Geophys. Res., 74, 2217, 1969.

Fehsenfeld, F. C. and E. E. Ferguson, Recent Laboratory Measurements of D and E Region Ion-Neutral Reactions, Radio Sci., 7, 113, 1972.

Fehsenfeld, F. C. and E. E. Ferguson, Laboratory Studies of Negative Ion Reactions with Atmospheric Trace Constituents, J. Chem. Phys., 61, 3181, 1974.

Ferguson, E. E., Laboratory Measurements of D-Region Ion-Molecule Reactions, Mesospheric Models and Related Experiments, D. Reidel Publ. Co., Dordrecht-Holland, 1971a.

Ferguson, E. E., D-Region Ion Chemistry, Rev. Geo. and Space Phys, 9, 997, 1971b.

Ferguson, E. E. and F. C. Fehsenfeld, Water Vapor Ion Cluster Concentrations in the D-Region, J. Geophys. Res., 74, 5743, 1969.

Fiocco, G. and G. Grams, On the Origin of Noctilucent Clouds: Extraterrestrial Dust and Trapped Water Molecules, J. Atmos. Terr. Phys., 33, 815, 1971.

Fleagle, R. G. and J. A. Businger, An Introduction to Atmospheric Physics, Academic Press, New York and London, 1963.

Fogle, B., Noctilucent Clouds, Ph.D. Thesis, University of Alaska, 1966a.

Fogle, B., Recent Advances in Research on Noctilucent Clouds, Bull. Amer. Met. Soc., 47, 781, 1966b.

Fogle, B., Noctilucent Clouds - Their Characteristics and Interpretation, in Thermospheric Circulation, W. Webb, MIT Press, Cambridge, 1972.

Fogle, B. and B. Haurwitz, Noctilucent Clouds, Space Sci. Rev., 6, 277, 1966.

Fogle, B. and M. Rees, Spectral Measurements of Noctilucent Clouds, J. Geophys. Res., 77, 720, 1972.

Fuchs, N. A., The Mechanics of Aerosols, Pergamon Press, Oxford, 1964.

Geistler, J. E., Vertical Motions and Nitric Oxide in the Upper Mesosphere, in Meteorological and Chemical Factors in D-Region Aeronomy, Record of 3rd Aeronomy Conference, ed. C. F. Sechrist, Jr., Sept. 1968, University of Illinois, Urbana, Ill., 1969.

Geistler, J. E. and R. E. Dickenson, Vertical Motions and Nitric Oxide in the Upper Mesosphere, J. Atmos. Terr. Phys., 30, 1505, 1968.

Good, A., D. A. Durden and P. Kebarle, Ion-Molecule Reactions in Pure Nitrogen and Nitrogen Containing Traces of Water at Total Pressures .5-4 Torr. Kinetics of Clustering Reactions Forming $H^+(H_2O)_n$, J. Chem. Phys., 32(1), 212, 1970a.

Good, A., D. A. Durden and P. Kebarle, Mechanism and Formation of Ion Molecule Reactions Leading to Formation of $H^+(H_2O)_n$ in Moist Oxygen and Air, J. Chem. Phys., 32, 222, 1970b.

Goldberg, R. A. and A. C. Aiken, Studies of Positive Ion Composition in the Equatorial D-Region Ionosphere, J. Geophys. Res., 76, 8352, 1971.

Goldberg, R. A. and L. J. Blumle, Positive Ion Composition from a Rocket-Bourne Mass Spectrometer, J. Geophys. Res., 75, 133, 1970.

Gregory, J. B., Radio Wave Reflections from the Mesosphere. 1. Heights of Occurrence, J. Geophys. Res., 66, 429, 1961.

Gregory, J. B., The Influence of Atmospheric Circulation on the Mesosphere Electron Densities in Winter, J. Atmos. Sci., 22, 18, 1965.

Gutnick, M., Mean Annual Mid-Latitude Moisture Profiles to 31 km, Air Force Surveys in Geophysics No. 147, July 1962.

Heimerl, J. M. and John A. Vanderhoff, N_2 Clustering to NO^+, Trans. AGU, 52, 870, 1971.

Hemenway, C. L., R. K. Soberman and G. Witt, Sampling of Noctilucent Cloud Particles, Tellus 16, 84, 1964a.

Hemenway, C. L., E. F. Fullam, R. A. Skrinanek, R. K. Soberman and G. Witt, Electron Microscope Studies of Noctilucent Clouds Particles, Tellus 16, 96, 1964.

Hesstvedt, E., On the Effect of Vertical Eddy Transport on Atmospheric Composition in the Mesosphere and Lower Thermosphere, Geofysiske Publikas-Joner, 27, 1968.

Hesstvedt, E., The Effect of Vertical Eddy Transport on the Composition of the Mesosphere and Lower Thermosphere, in Stratospheric Circulation, ed. W. Webb, Academic Press, New York, London, 1969.

Hesstvedt, E., A Meridional Model for the Oxygen-Hydrogen Atmosphere, in Mesospheric Models and Related Experiments, ed. G. Fiocco D. Reidel Publ. Co., Dordrecht-Holland, 1971.

Hoult, D. P., D-Region Probe Theory, J. Geophys. Res., 70, 3183, 1965.

Howard, C. J., H. W. Rundle and F. Kaufman, Rates of Formation of Water Clusters for O_2^+ and NO^+, Bull. Amer. Phys. Soc., 16, 213, 1971.

Huffman, R. E., D. E. Paulsen, J. C. Larabee and R. B. Cairns, Decrease in D-Region $O_2(^1\Delta g)$ Photoionization Rates Resulting from CO_2 Absorbtion, J. Geophys. Res., 76, 1028, 1971.

Hunt, B. G., Cluster Ions and Nitric Oxide in the D-Region, J. Atmos. Terr. Phys., 33, 929, 1971a.

Hunt, B. G., A Diffusive-Photochemical Study of the Mesosphere and Lower Thermosphere and Associated Conservation Mechanisms, J. Atmos. Terr. Phys., 33, 1869, 1971b.

Hunt, B. G., A Generalized Aeronomic Model of the Mesosphere and Lower Thermosphere Including Ionospheric Processes, J. Atmos. Terr. Phys., 35, 1755, 1973.

Hunten, D. M., The Escape of Light Gases from Planetary Atmospheres, J. Atmos. Sci., 30, 1481-1494, 1973.

Hunten, Donald M. and Michael B. McElroy, Metastable $O_2(^1\Delta g)$ as a Major Source of Ions in the D-Region, J. Geophys. Res., 73, 2421, 1968.

Hunten, Don M. and D. F. Strobel, Production and Escape of Terrestrial Hydrogen, J. Atmos. Sci., 31, 305, 1974.

Johannessen, A. and D. Krankowsky, Positive-Ion Composition Measurement in the Upper Mesosphere and Lower Thermosphere at a High Latitude during Summer, J. Geophys. Res., 77(16), 2888, 1972.

Johannessen, A. and D. Krankowsky, Daytime Positive Ion Composition Measurement in the Altitude Range 73-137 km above Sardinia, J. Atmos. Terr. Phys., 36, 1233, 1974.

Kantorovich, L. V. and V. I. Krylov, Approximate Methods of Higher Analysis, Interscience Pub. N.Y. and P. Noordhoff Ltd., Groningen, The Netherlands 1964.

Kaplan, Joseph, Nitric Oxide in the Earth's Upper Atmosphere, Nature, 144, 152, 1939.

Kaufman, F., Aeronomic Reactions Involving Hydrogen: A Review of Recent Laboratory Studies, Ann. Geo., 20, 106, 1964.

Kebarle, P., S. K. Seales, A. Zolla, J. Scarborough and M. Arshadi, The Solution of Hydrogen Ion by Water Molecules in the Gas Phase: Heats and Entropies of Solution of Individual Reactions: $H^+(H_2O)_{n-1}+H\ O$ $H^+(H_2O)_n$, J. Amer. Chem. Soc., 89, 6393, 1967.

Keneshea, Thomas J., A Solution to the Reaction Rate Equations in the Atmosphere below 150 km, AFCRL Report 63-711, 1963.

Krankowsky, D., F. Arnold, H. Wider, J. Kissel and J. Zahringer, Positive Ion Composition in the Lower Ionosphere, Radio Sci., 7, 93, 1972b.

Kreysig, Erwin, Advanced Engineering Mathematics, John Wiley and Sons, Inc. New York, London, Sydney, Toronto, Third Ed., 1972.

Labitzke, K., Temperature Changes in the Mesosphere and Stratosphere Associated with Circulation Changes in Winter, J. Atmos. Sci., 29, 756, 1972.

Latham, J., Cloud Physics, Reports on Progress in Physics, 32, 69, 1969.

Lelevier, R. E. and L. M. Branscomb, Ion Chemistry Governing Mesospheric Electron Concentrations, J. Geophys. Res., 73, 27, 1968.

Leu, M. T., Manfred A. Biondi and R. Johnsen, Measurements of the Recombination of Electrons with $H_3O^+\cdot(H_2O)_n$ -Series Ions, Phys. Rev., A7, 292, 1973.

Lineburger, W. C. and L. J. Puckett, Hydrated Positive Ions in Nitric-Oxide-Water Afterglows, Phys. Rev., 187, 286, 1969.

Liu, S. C. and T. M. Donahue, The Aeronomy of Hydrogen in the Atmosphere of the Earth, J. Atmos. Sci., 31, 1118, 1974.

Loevy, C., Simple Models of Thermally Driven Mesospheric Circulation, J. Atmos. Sci., 21, 327, 1964.

Ludlam, F. H., Noctilucent Clouds, Tellus, 9, 341, 1957.

MacDonald, J. E., Use of the Electrostatic Analogy in Studies of Ice Crystal Growth, Z. Angew. Math. Phys., 14, 610-619, 1963.

MacDonald, J. E., Atmospheric Exclusion Limits for Clouds of Water and Other Substances, J. Geophys. Res., 69, 3669, 1964.

Mastenbrook, H. J., Water Vapor Distribution in the Stratosphere and High Troposphere, J. Atmos. Sci., 25, 299, 1968.

Mason, C. J. and J. J. Horvath, The Direct Measurement of Nitric Oxide Concentration in the Upper Atmosphere by a Rocket-Bourne Chemiluminescent Detector, Geophys. Res. Lett., 3, 391, 1976.

Meira, L. G. Jr., Rocket Measurments of Upper Atmosphere Nitric Oxide and Their Consequences to the Lower Ionosphere, University of Colorado Ph.D. Geophysics, 1970, 1971.

Mechtly, E. A., C. F. Sechrist,Jr. and L. G. Smith, Electron Loss Coefficients for the D-Region of the Ionosphere from Rocket Measurements during the Eclipses of March 1970 and November 1966, J. Terr. Atmos. Phys., 34, 641, 1972.

Mechtly, E. A., K. Seino and L. G. Smith, Lower Ionosphere Electron Densities Measured during the Solar Eclipse of November 12, 1966, Radio Sci., 4, 371, 1969.

Mechtly, E. A. and L. G. Smith, Seasonal Variation of the Lower Ionosphere at Wallops Is. during the IQSY, J. Atmos. Terr. Phys., 30, 1555, 1968.

Mitra, A. P., A Review of D-Region Processes in Non-Polar Latitudes, J. Atmos. Terr. Phys., 30, 1065, 1968.

Murgatroyd, R. J. and R. M. Goody, Sources and Sinks of Radiative Energy from 30 to 90 km, Quart. J. Roy. Met. Soc., 84(361), 225, 1958.

Murgatroyd, R. J. and F. Singleton, Possible Meridional Circulation in the Stratosphere and Mesosphere, Quart. J. Roy. Met. Soc., 87, 125; 88, 105, 1961.

Narcisi, R. S., Ion Composition Measurements and Related Ionospheric Processes in the D and E Regions, Ann. Geophys., 22, 224, 1966.

Narcisi, R. S., Composition Studies of the Lower Ionosphere, in Physics of the Upper Atmosphere, ed. Franco Verniani, International School of Atmospheric Physics, Proceedings of 1st Course, Erice, June 15-29, 1970, Editrice Compositori-Bologna, 1970a.

Narcisi, R. S., Measurements of Positive and Negative Ions in the Lower Ionosphere, An Abstract of April 28, 1970 Meeting, Bull. Amer. Phys. Soc., 15, 518, 1970b.

Narcisi, R. S., Shock Wave and Electric Field Effects in D-Region Water Cluster Ion Measurements, Trans. AGU, 51, 366, 1970c.

Narcisi, R. S. and A. D. Bailey, Mass Spectrometer Measurements of Positive Ions at Altitudes from 64 to 112 kilometers, J. Geophys. Res., 70, 3687, 1965.

Narcisi, R. S. and W. Roth, The Formation of Cluster Ions in Laboratory Sources and in the Ionosphere, in Advances in Electronics and Electron Physics, 29, 79, 1970.

Narcisi, R. S., A. D. Bailey, L. DellaLucca, C. Sherman, D. M. Thomas, Mass Spectrometric Measurements of Negative Ions in the D- and Lower E-Regions, J. Atmos. Terr. Phys., 33, 1147, 1971.

Narcisi, R. S., C. Sherman, C. R. Philbrick, D. M. Thomas, A. D. Bailey, L. E. Wlodyka, R. A. Wlodyka, D. Baker and G. Federico, Negative Ion Composition of the D and E Regions during a PCA, in Proc. COSPAR Symp. of Solar Particle Event of November 1969, AFCRL, 411, 1972.

Narcisi, R. S., C. R. Philbrick, D. M. Thomas, A. D. Bailey, L. E. Wlodyka, D. Baker, G. Federico, R. Wlodyka, M. E. Gardner, Positive Ion Composition Measurements of the D and E Regions during a PCA, in Proc. COSPAR Symp. on Solar Particle Event of Nov. 1969, AFCRL, 421, 1972.

Narcisi, R. S., A. D. Bailey, L. E. Wlodyka and C. R. Philbrick, Ion Composition Measurements in the Lower Ionosphere during the November 1966 and March 1970 Solar Eclipses, J. Atmos. Terr. Phys., 34, 647, 1972.

Narcisi, R. S., C. R. Philbrick, J. C. Ulwick and M. E. Gardner, Mesospheric Nitric Oxide Concentrations during a PCA, J. Geophys. Res., 77, 1332, 1972.

Narcisi, R. S., Mass Spectrometer Measurements in the Ionosphere, in Physics and Chemistry of the Upper Atmosphere, ed., B. M. McCormac, D. Reidel Publ. Co., Dordrecht-Holland, 1973.

Narcisi, R. S. and W. Swider, Mesospheric Neutral Constituents Deduced from PCA Ion Composition Measurements, EOS Trans. AGU, 54, 382, 1973, abstract only.

Natanson, G. L., On the Theory of the Charging of Amicroscopic Aerosol Particles as a Result of the Capture of Gas Ions, Sov. Phys. Tech. Phys., Engl. Transl., 5, 538, 1960.

Nicolet, M., Contribution a l'Etude de la Structure de l'Ionosphere, Mem. Inst. Roy. Met. Belg., 19, 162, 1945.

Nicolet, M., Aeronomic Chemical Reactions, in Physics and Medicine of the Atmosphere and Space, in 2nd Int'l. Symp. of the Atmosphere and Space held at San Antonio, November 1958, John Wiley and Sons, 1960.

Nicolet, Marcel, Ionospheric Processes and Nitric Oxide, J. Geophys. Res., 70, 691, 1965.

Nicolet, M., Aeronomic Reactions of Hydrogen and Ozone, in Mesospheric Models and Related Experiments, D. Reidel Publ. Co., 1971.

Nicolet, M. and A. C. Aiken, The Formation of the D-Region of the Ionosphere, J. Geophys. Res., 65, 1469, 1960.

Niles, F. E., Personal Communication, 1975a,b.

Niles, F. E., J. M. Heimerl, G. E. Keller, L. J. Puckett, Reactions involving cluster ions, Radio Sci., 7, 117, 1972.

Norton, R. B. and C. A. Barth, Theory of Nitric Oxide in the Earth's Atmosphere, J. Geophys. Res., 75, 3903, 1970.

Oran, E. S., P. S. Julienne and D. F. Strobel, The Aeronomy of Odd Nitrogen in the Thermosphere, J. Geophys. Res., 80, 3068, 1975.

Parthasarathy, R., Personal Communication, 1974.

Parthasarathy, R., Personal Communication, 1975.

Parthasarathy, R., Personal Communication, 1976.

Parthasarathy, R., Mesopause Dust as a Sink for Ionization, J. Geophys. Res., 81, 2392, 1976.

Parthasarathy, R. and D. B. Rai, Effect of Meteoric Dust on the Effective Recombination Coefficient in the Lower Ionosphere, Radio Sci., 1, 1401, 1966.

Paton, J., Noctilucent Clouds, Met. Magazine, 93, 161, 1964.

Patterson, T. N. L., Atomic and Molecular Hydrogen in the Thermosphere, Planet. Space Sci., 14, 417, 1966.

Paul, W., H. P. Rheinhard and V. von Zahn, Das Elektrische Massenfilter als Massenspektrometer und Isotopentrenner, Z. Physik, 152, 143, 1958.

Paulsen, D. E., R. E. Huffman and J. C. Larrabee, Improved Photoionization rates of $O_2(^1\Delta g)$ in the D Region, Radio Sci., 7, 51, 1972.

Pedersen, A., J. A. Kane and J. Troim, Rocket Measurement Showing Removal of Electrons above the Mesosphere in Summer at High Latitude, Planet. Space Sci., 18, 945, 1970.

Peterson, J. R. and J. T. Moseley, CO_2^- and $CO_3^- \cdot H_2O$ Photodissociation and its Possible Importance in the D-Region at Sunrise and in Daytime, AGU Fall Annual Meeting, 1974.

Phelps, A. V., Laboratory Studies of Electron Attachment and Detachment Processes of Aeronomic Interest. Can. J. Chem., 47, 1783, 1969.

Piggott, W. R. and E. V. Thrane, The Electron Densities in the E- and D-Regions above Kjeller, J. Atmos. Terr. Phys., 28, 467, 1966.

Puckett, L. J. and M. W. Teague, Reactions of NO^+ in $NO \cdot H_2O$ and $NO\text{-}NH_3$ Gas Mixtures, J. Chem. Phys., 54, 2564, 1971.

Reid, George C., Production and Loss of Electrons in the Quiet Daytime D-Region of the Ionosphere, J. Geophys. Res., 75, 2551, 1970.

Reid, George C., The Roles of Water Vapor and Nitric Oxide in Determining Electron Densities in the D-Region, in Mesospheric Models and Related Experiments, ed., G. Fiocco, D. Reidel Publ. Co., Dordrecht, Holland, 1971a.

Reid, G. C., The D-Region during PCA Conditions, J. Atmos. Terr. Phys., 33, 1147, 1971b.

Reid, G. C., Ice Clouds at the Summer Polar Mesopause, J. Atmos. Sci., 32, 523, 1974.

Reid, George C., Personal Communication, 1975.

Reiter, E., Atmospheric Transport Processes. Part 2: Chemical Tracers, United States A.E.C., Division of Tech. Information, Washington, D. C., 1971.

Riga, The Physics of Mesospheric (Noctilucent) Clouds, Israel Program for Scientific Translation, Jeruselam, 1973.

Romanelli, Michael J., Runge-Kutta Methods for the Solution of Ordinary Differential Equations, in Mathematical Methods for Digital Computers, ed. A. Ralston, H. S. Wilf, John Wiley and Sons (1960), New York-London, 110, 1960.

Rusch, D., Satellite Ultraviolet Measurements of Nitric Oxide Fluorescence with a Diffusive Transport Model, J. Geophys. Res., 78, 5676, 1973.

Sayers, J., In-Situ Probes for Ionospheric Investigations, J. Atmos. Terr. Phys., 32, 663, 1970.

Schilling, G. F., Forbidden Regions for the Formation of Clouds in a Planetary Atmosphere, J. Geophys. Res., 69, 3663, 1964.

Scholz, T. G., D. H. Enhalt, L. E. Heidt and E. A. Martell, Water Vapor Molecular Hydrogen, Methane and Tritium Concentrations near the Stratopause, J. Geophys. Res., 75, 3049, 1970.

Sechrist, C. F., ed., Meteorological and Chemical Factors in D-Region Aeronomy, Third Aeronomy Conference, Sept. 1968, University of Illinois, Urbana, Ill.

Shimazaki, T., Dynamic Effects on Height Distributions of Neutral Constituents of Earth's Vapor Atmosphere: A Calculation of the Atmospheric Model Between 70 and 500 km, J. Atmos. Terr. Phys., 30, 1279, 1967.

Shimazaki, T., A. R. Laird, A Model Calculation of the Diurnal Variation in Minor Neutral Constituents in the Mesosphere and Lower Thermosphere including Transport Processes, J. Geophys. Res., 75, 3221, 1970.

Shimazaki, T. and A. R. Laird, Seasonal Effects on Distributions of Minor Neutral Constituents in Mesosphere and Lower Thermosphere, Radio Sci., 7, 23, 1972.

Sissenwine, N., D. D. Grantham and H. A. Salmela, Mid-Latitude Humidity to 32 km, J. Atmos. Sci., 25, 1129, 1968.

Smith, L. G., Ionization by Lyman-α in the E Region at Sunrise, J. Atmos. Terr. Phys., 28, 1195, 1966.

Smith, W. S., J. S. Theon, P. C. Swartz, L. B. Kotchen and J. J. Horvath, Temperature, Pressure, Density and Wind Measurements in the Stratosphere and Mesosphere, 1966, NASA Tech. Rep. TR-R-288, NASA, Washington, D. C., August 1968.

Smithsonian Meteorological Tables, 6th Revision, Smithsonian Institution, Washington, D. C., 1963.

Snider, W., Sources for $H_2O^+ \cdot (H_2O)_n$ Ions in the D-Region, J. Geophys. Res., 75, 7299, 1970.

Soberman, R. K., S. A. Chrest, J. J. Manning, L. Rey, T. G. Ryan, R. A. Skrivanek and N. Wilhelm, Techniques for Rocket Sampling of Noctilucent Cloud Particles, Tellus 16, 89, 1964.

Sonin, A. A., Theory of Ion Collection by a Supersonic Atmospheric Sounding Rocket, J. Geophys. Res., 72, 4547, 1967.

Stanford, J. L., Possible Long-Term Variations in Stratospheric Water-Vapor Content, Weather, March 1974, 107, 1974.

Strobel, D. F., Diurnal Variation of Nitric Oxide in the Upper Atmosphere, J. Geophys. Res., 76, 2441, 1971a.

Strobel, D. F., Odd Nitrogen in the Mesosphere, J. Geophys. Res., 76, 8384, 1971b.

Strobel, D. F., Minor Neutral Constituents in the Mesosphere and Lower Thermosphere, Radio Sci., 7, 1, 1972.

Strobel, D. F., D. M. Hunten and M. B. McElroy, Production and Diffusion of Nitric Oxide, J. Geophys. Res., 75, 4307, 1970.

Strobel, D. F., E. S. Oran and P. D. Feldman, The Aeronomy of Odd Nitrogen in the Thermosphere. 2. Twilight Emissions, J. Geophys. Res., 81, 3745, 1976.

Swider, W. Jr., Ionization Rates due to the Attenuation of 1-100Å Non-Flare Solar X-rays in the Terrestrial Atmosphere, Revs. Geophys., 7, 573, 1969.

Theon, J. S., W. Nordberg, L. B. Katchen, and J. J. Hornoth, Some Observations on the Thermal Behavior of the Mesosphere, J. Atmos. Sci., 24, 428-438, 1967.

Theon, J. S., W. Smith, J. Casey and B. R. Kirkwood, The Mean Observed Meteorological Structure and Circulation of the Stratosphere and Mesosphere, NASA Tech. Rep. R-375, Washington, D. C., March 1972.

Thomas, L., P. M. Gondhalekar and M. R. Bowman, The Negative-Ion Composition of the Daytime D-Region, J. Atmos. Terr. Phys., 35, 397, 1973.

Tinsley, B. A., Reinterpretation of Geocoronal Observations with Increased High/Low Altitude Hydrogen Ratio, Planet. Space Sci., 17, 769, 1969.

Tisone, G., Measurements of NO densities during Sunrise at Kauai, J. Geophys. Res., 78, 746, 1973.

Tohmatsu, T. and T. Nagata, Dynamical Studies of the Oxygen Green Line in Airglow, Planet. Space Sci., 10, 103, 1963.

Tollinn, Noctilucent Clouds, International Symposium at Tollinn, 1966, eds. I. A. Khvostikov and G. Witt, Moscow, 1967.

Turco, R. P., A Discussion of Possible Negative Ion Detachment Mechanisms in the Sunrise D-Region, Radio Sci., 9, 655, 1974.

Turco, R. P. and C. F. Sechrist, An Investigation of the Ionospheric D Region at Sunrise, 2. Estimation of some Photodetachment Rates, Radio Sci., 7, 717, 1972a.

Turco, R. P. and C. F. Sechrist, An Investigation of the Ionospheric D Region at Sunrise, 3. Time Variations of Negative-Ion and Electron Densities, Radio Sci., 7, 725, 1972b.

U. S. Standard Atmosphere: Supplements, U. S. Government Printing Office, Washington, D. C., 1966.

Vestine, E. H., Noctilucent Clouds, J. Roy. Astron. Soc. Can., Toronto, 28, 249, 1934.

Volland, H., A Simplified Model of the Geomagnetic Sq-Current System and Electric Fields within the Ionosphere, Cosmic Electrodynamics, 1, 428, 1971.

Wallace, L. and M. B. McElroy, The Visual Dayglow, Planet. Space Sci., 14, 677, 1966.

Wantanabe, K., F. M. Matsunga and H. Sakai, Absorbtion Coefficient and Photoionization Yield of NO in the Region 580-1350Å, Appl. Optics, 6, 391, 1967.

Webber, W., The Production of Free Electrons in the Ionosphere D Layer by Solar Galactic Cosmic Rays and the Resultant Absorbtion of Radio Waves, J. Geophys. Res., 67, 5091, 1962.

Whipple, F. L., The Dust Cloud about the Earth, Nature, 189, 127, 1961.

Whitten, R. C. and I. G. Poppoff, Fundamentals of Aeronomy, John Wiley and Sons, Inc., New York, London, Sydney, Toronto, 1971.

Willman, Ch., Some Problems of Noctilucent Cloud Climalology, p. 19-27 in Noctilucent Clouds, International Symposium at Tollinn, 1966, ed. I. A. Khvostikov and G. Witt, Moscow, 1967.

Witt, G., C. L. Hemenway, N. Lange, S. Modin and R. K. Soberman, Composition Analysis of Particles from Noctilucent Clouds, Tellus, 16, 103, 1964.

Wofsy, Steve C., John C. McConnell and Michael B. McElroy, Atmospheric CH_4, CO and CO_2, J. Geophys. Res., 77, 4477, 1972.

Wright, P. G., On the Discontinuity Involved in Diffusion Across an Interface (the Δ of Fuchs), in The Physical Chemistry of Aerosols, Discussion of the Faraday Society November 30, 1960. The Faraday Society, Aberdeen University Press Ltd., 6 Upper Kirkgate, Aberdeen, Scotland, 1961.

Yonezawa, T., Theory of Formation of the Ionosphere, Space Sci. Rev., 5, 3, 1966.

Young, C. and E. S. Epstein, Atomic Oxygen in the Polar Winter Mesosphere, J. Atmos. Sci., 19, 435, 1962.